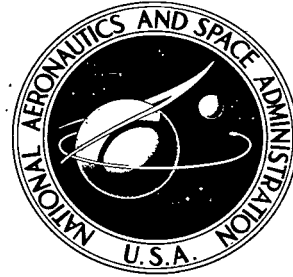


NASA TECHNICAL NOTE



NASA TN D-6460

C.1

NASA TN D-6460

LOAN COPY: RE
AFWL (DO
KIRTLAND AF



PERFORMANCE CHARACTERISTICS OF
A SINGLE-ENGINE FIGHTER MODEL FITTED
WITH AN IN-FLIGHT THRUST REVERSER

by Donald L. Maiden and Charles E. Mercer

Langley Research Center

Hampton, Va. 23365



0133301

1. Report No. NASA TN D-6460		2. Government Accession No.		0133301	
4. Title and Subtitle PERFORMANCE CHARACTERISTICS OF A SINGLE-ENGINE FIGHTER MODEL FITTED WITH AN IN-FLIGHT THRUST REVERSER		5. Report Date September 1971		6. Performing Organization Code	
		8. Performing Organization Report No. L-7824		10. Work Unit No. 126-63-11-45	
7. Author(s) Donald L. Maiden and Charles E. Mercer		11. Contract or Grant No.		13. Type of Report and Period Covered Technical Note	
9. Performing Organization Name and Address NASA Langley Research Center Hampton, Va. 23365		14. Sponsoring Agency Code		15. Supplementary Notes	
		12. Sponsoring Agency Name and Address National Aeronautics and Space Administration Washington, D.C. 20546		16. Abstract This investigation was conducted at the Langley 16-foot transonic tunnel at Mach numbers up to 1.30. The purpose of the investigation was to establish changes in thrust-minus-drag performance as well as longitudinal and directional stability and control characteristics attributable to an in-flight thrust reverser. The performance results and the effects of the thrust reverser on local surface temperatures and pressures are presented in this report. Test conditions simulated landing-approach conditions as well as high-speed maneuvering such as may be required for combat or steep descent from high altitude. The results indicate that the developed thrust control unit will produce reverse thrust up to 52 percent of forward thrust at static conditions and that reverse-thrust effectiveness increased with an increase in Mach number over the speed range investigated. Secondary cooling during reverse thrust and local tail temperatures may require further design considerations.	
17. Key Words (Suggested by Author(s)) In-flight thrust reverser		18. Distribution Statement Unclassified - Unlimited			
19. Security Classif. (of this report) Unclassified	20. Security Classif. (of this page) Unclassified	21. No. of Pages 129	22. Price* \$3.00		

PERFORMANCE CHARACTERISTICS OF A SINGLE-ENGINE FIGHTER
MODEL FITTED WITH AN IN-FLIGHT THRUST REVERSER

By Donald L. Maiden and Charles E. Mercer
Langley Research Center

SUMMARY

A wind-tunnel investigation has been conducted in the Langley 16-foot transonic tunnel on a 1/7.5-scale, powered, single-engine fighter-airplane model retrofitted with an in-flight thrust control unit (TCU). The purpose of the investigation was to determine the changes in propulsion performance characteristics as well as changes in stability and control attributed to the installation of the TCU. This report presents the results of the performance analysis only. The investigation was conducted statically and through a Mach number range of 0.23 to 1.30 at angles of attack from -3° to 12° . The primary-nozzle jet-total-pressure ratio was varied from 1.0 (jet off) to approximately 5. The model wings were configured for the cruise and the landing-approach conditions. Several exhaust-deflector-door configurations and six progressive blocker-door positions from stowed to fully deployed conditions were tested.

The results of the investigation indicate that the drag penalty attributed to the TCU modification in the stowed position was small; that with the modification, forward take-off thrust performance can be increased by 4 percent for military power with the upper deflector doors set at 32.5° and the lower at 52.5° but is reduced by 1.3 percent for after-burning power with both upper and lower deflector doors set at 43.5° ; that a maximum reverse thrust of 52-percent forward thrust was produced by the selected TCU configuration at static conditions and that reverse-thrust effectiveness increased with an increase in Mach number; that engine-operating characteristics should be only slightly degraded, but secondary cooling air during reverse-thrust operation may have to be supplemented; and that maximum local temperatures (70 percent of primary-nozzle-jet total temperature) appear to occur at 90-percent blocker-door closure for the selected TCU configuration.

INTRODUCTION

The concept of a fully modulating thrust reverser for in-flight thrust control on jet-powered fighter airplanes has been investigated periodically for about 20 years. During this time, the complexity of the hardware, adverse stability and control influences, and

engine-operating limitations have made the use of in-flight thrust reversers impractical. (See refs. 1 to 8.) However, continued increases in the thrust-to-weight ratio of modern air-superiority fighters, combined with advances in thrust-reverser technology, have renewed interest in the use of in-flight thrust reversers. (See refs. 9 and 10.) With the apparent success of the Saab-37 Viggen, which incorporates a thrust reverser with both blocker and deflector doors, the feasibility of thrust-reverser operation for STOL capabilities for a fighter airplane has been demonstrated. (See refs. 11 to 13.) The anticipated operational improvements for tactical aircraft which may be achieved by use of thrust modulation have resulted in a program for the development of an in-flight thrust reverser for tactical or attack aircraft. As part of this program, an investigation has been conducted in the Langley 16-foot transonic tunnel on a thrust control unit (TCU) with blocker and deflector doors retrofitted to an existing single-engine fighter model. (See ref. 3.) The investigation was conducted statically and through a Mach number range of 0.23 to 1.30 at angles of attack from -3° to 12° . A hydrogen peroxide gas generator was used to provide hot exhaust gas, and the primary-nozzle-jet total-pressure ratio was varied from 1.0 (jet off) to approximately 5.

The purpose of this investigation was to determine the influence of the TCU on performance, stability, and control of a single-engine fighter airplane. This report presents the performance results of the investigation and the effects of the thrust reverser on local surface temperatures and pressures.

SYMBOLS AND ABBREVIATIONS

Symbols

A	area, meters ²
AR	aspect ratio
C_D	fuselage-tail drag coefficient, D/qS
$C_{(F-D)}$	thrust-minus-drag coefficient, $\frac{F - D}{qS}$
C_p	pressure coefficient, $\frac{p_l - p_{\infty}}{q}$
$C_{p,b}$	base pressure coefficient, $\frac{p_b - p_{\infty}}{q}$
$C_{p,f}$	local fuselage pressure coefficient, $\frac{p_f - p_{\infty}}{q}$

- c wing chord, meters
- c_r root wing chord, meters
- c_t tip wing chord, meters
- D fuselage-tail aerodynamic drag, newtons
- d diameter, meters
- F jet (gross) thrust, positive toward nose, newtons

F_i ideal isentropic thrust, $\dot{m}_p \sqrt{\frac{2\gamma}{\gamma-1} R_p T_{t,p} \left[1 - \left(\frac{p_\infty}{p_{t,p}} \right)^{\frac{\gamma-1}{\gamma}} \right]}$, newtons

- M free-stream Mach number
- \dot{m}_p primary-nozzle-jet mass-flow rate, kg/sec
- \dot{m}_s secondary-cooling-air mass-flow rate, kg/sec
- p_a ambient pressure, N/m²
- p_b base pressure, N/m²
- p_f local fuselage pressure, N/m²
- p_l local pressure, N/m²
- $p_{t,p}$ primary-nozzle-jet total pressure, N/m²
- $p_{t,s}$ secondary-cooling-air total pressure, N/m²
- p_∞ free-stream static pressure, N/m²
- q free-stream dynamic pressure, N/m²

R_p	gas constant (primary-nozzle jet), 376.7 N-m/kg-K
R_s	gas constant (secondary cooling air), 287.3 N-m/kg-K
r	radius, meters
S	wing (reference) area, 0.4125 meter ²
T_f	local fuselage temperature, kelvins
T_h	local horizontal-tail temperature, kelvins
T_S	local skog and tail-hook temperature, kelvins
T_{tc}	local TCU temperature, kelvins
$T_{t,p}$	primary-nozzle-jet total temperature, kelvins
$T_{t,s}$	secondary-cooling-air total temperature, kelvins
T_v	local vertical-tail temperature, kelvins
T_∞	free-stream static temperature, kelvins
α	angle of attack, degrees
γ	ratio of specific heats
δ_b	blocker-door position of TCU, percent blockage
δ_{dl}	lower-deflector-door angle of TCU, degrees
δ_{du}	upper-deflector-door angle of TCU, degrees
δ_h	horizontal-tail deflection angle, degrees
Λ	sweep angle, degrees

Subscripts:

F	forward-thrust mode
R	reverse-thrust mode

Abbreviations

A/B	afterburning
NPR	nominal primary-nozzle-jet total-pressure ratio
TCU	thrust control unit

APPARATUS AND METHODS

Wind Tunnel

The Langley 16-foot transonic tunnel is a single-return atmospheric wind tunnel with an octagonal slotted-throat test section and continuous air exchange. The tunnel has a continuously variable speed range from Mach 0.20 to 1.30. A description of the 16-foot transonic tunnel is given in references 14 and 15.

Model and Support System

The test model was a 1/7.5-scale model of a single-engine fighter airplane. Except where noted, the model was in a clean configuration; that is, wing-flap and slat deflection angles were 0° , horizontal-tail deflection angle was -1.5° , and rudder deflection angle was 0° . For a Mach number of 0.23, a landing-approach configuration was simulated, where wing-flap and slat deflection angles were -30° and -20° , respectively, horizontal-tail deflection angle was -10° , and rudder deflection angle was 0° . Figure 1 shows the basic unmodified airplane configuration installed in the Langley 16-foot transonic tunnel. Corresponding views of the model modified with a retrofit thrust control unit (TCU) are presented in figure 2.

The model was wing-tip supported by a bifurcated sting-support system as shown in figure 3. Geometric characteristics of the model are also given in the figure. The wing formed an integral part of the support system and provided a fixture for the six-component balance. The fuselage was mounted on the balance so that all fuselage-tail and thrust-drag forces could be measured. Since the wing was part of the support system, wing forces were not measured.

Except for a fiber glass nose section, the model was constructed principally of steel and was powered by a hydrogen peroxide turbojet-engine simulator, similar to that described in references 16 and 17. Two engine simulators, one representing a convergent nozzle at the military-power setting and the other representing a convergent nozzle at the afterburning-power setting, were used to produce a hot jet exhaust with physical characteristics closely matching the exhaust of a turbojet engine.

The jet-engine simulator was enveloped by a secondary-cooling-air ejector. Metered air, simulating secondary cooling air, was supplied through high-pressure air lines inside the right wing. (See fig. 3.) Two afterbody-ejector configurations were used in the investigation: one was the basic airplane configuration, and the second was the airplane modified to incorporate an in-flight TCU. (See fig. 4.)

The in-flight TCU used in this investigation was a shrouded blocker-door type combined with a tertiary-air ejector and was fitted aft of the convergent nozzle. The tertiary-air inlets also serve as reverse-thrust exhaust ports. Three external deflection doors in a Y-orientation were utilized to vary the exhaust-port area from that required for the optimum thrust-minus-drag performance in the forward-thrust mode to the larger port area required for exhaust during the reverse-thrust mode. (See figs. 4 and 5.) Six sets of fixed brackets were utilized to provide deflector-door angular positions of (1) fully closed (however, a small clearance exists on either side of the deflector doors); (2) faired ($\delta_{du} = 2^\circ$, $\delta_{dl} = 2^\circ$); (3) $\delta_{du} = 28.5^\circ$, $\delta_{dl} = 60^\circ$; (4) $\delta_{du} = 32.5^\circ$, $\delta_{dl} = 52.5^\circ$; (5) $\delta_{du} = 43.5^\circ$, $\delta_{dl} = 43.5^\circ$; and (6) $\delta_{du} = 60^\circ$, $\delta_{dl} = 60^\circ$. Six sets of exhaust-gas blocker doors were used to represent six blocker-door positions simulating a deployment sequence from fully stowed to fully deployed. (See fig. 6.)

Thrust-Reverser Operating Procedure

The in-flight thrust-control system has been designed to operate in the following manner: During forward-thrust operation, deflector doors located on the ejector can be set in the closed, faired, or open position. The open deflector-door setting provides three tertiary-air inlets intended to improve low-speed thrust-minus-drag performance. In the modulating and reverse-thrust mode, the three deflector doors on the side of the ejector shroud open outwardly to provide forward-facing outlets for the exhaust gases. A set of three blocker doors then intrude into the exhaust stream behind the nozzle to block and turn the flow forward and out of the deflector-door ports.

Instrumentation

A six-component strain-gage balance was used to measure forces and moments on the fuselage and tail of the model. (See fig. 3.) As explained in the previous section, forces and moments on the wing were not measured.

Pressure transducers were used to measure primary-nozzle-jet total pressure, secondary-cooling-air static and total pressure, TCU base pressures and fuselage-afterbody static pressures in front of a deflector-door opening. (See figs. 4 and 7.)

Thermocouples were used to measure primary-nozzle-jet total temperature, secondary-cooling-air total temperature, and internal-skin temperature at the exit. In addition, thermocouples were used to survey skin temperatures on the horizontal and vertical tails and on the fuselage forward of a reverse-thrust exhaust port. (See figs. 4 and 7.)

The angle of attack of the fuselage was measured by a calibrated attitude indicator mounted in the canopy. Two electronic turbine flowmeters were used to measure the mass-flow rate of hydrogen peroxide to the primary nozzle and the average value was used. A calibrated venturi was used to measure the secondary-cooling-air flow rate.

Tests

Tests were conducted in the Langley 16-foot transonic tunnel at Mach numbers from 0 to 1.30 with the angle of attack varied from approximately -3° to 12° . The primary-nozzle-jet total-pressure ratio was varied from 1.0 (jet off) to approximately 5, depending on Mach number. Secondary-cooling-air mass-flow rate remained constant during variations of the primary total-pressure ratio but was changed with Mach number from approximately 0.054 kg/sec to 0.099 kg/sec.

RESULTS AND DISCUSSION

The performance of an in-flight thrust control unit (TCU) is evaluated by determining: (1) the transonic and supersonic drag penalty or thrust reduction incurred; (2) the efficiency of the reverse thrust; and (3) any adverse effect on engine characteristics by the addition of the TCU. Data obtained for each of these factors are discussed in the following sections.

Jet-Off Fuselage-Tail Drag

The variation of jet-off fuselage-tail drag coefficient for various configurations at zero angle of attack is presented in figure 8. The drag coefficient also includes the base (ejector annulus) drag, which was not removed for this presentation. A drag level has been shown at Mach numbers from 1.0 to 1.2 only to show the anticipated drag characteristics through this range. Two in-flight TCU configurations ($\delta_{du} = \delta_{dl} = \text{Faired}$ and $\delta_{du} = \delta_{dl} = \text{Closed}$) are compared with the basic model for both military and afterburning power. For each configuration, the faired line represents results obtained with the basic configuration. The agreement of data obtained with the TCU configurations with the faired

line indicates that installation of the TCU did not result in any significant drag penalty. However, no consideration has been made for an increase in trim drag as a result of a shift in airplane center of gravity due to the weight addition of the TCU.

The variation of jet-off, fuselage-tail drag coefficient for various TCU configurations at zero angle of attack and military power is presented in figure 9. For all configurations, the blocker door is deployed 100 percent; for figure 9(c), data for $\delta_b = 0$ percent are included which indicate that for jet-off conditions the fuselage-tail drag is not appreciably changed with blocker-door position. A summary of figures 8 and 9, shown in figure 10, indicates a general increase in drag with deployment of the three deflector doors with the highest drag (approximately 125-percent increase subsonically) attributed to the deflector-door angular setting of $\delta_{du} = 60^\circ$, $\delta_{dl} = 60^\circ$. These data exhibit the deflector-door-drag contribution to the reverse-thrust efficiency of the TCU.

Jet Operating Performance

The variation of the estimated engine-operating pressure ratio $p_{t,p}/p_\infty$ with Mach number for a typical turbojet engine is presented in figure 11. For discussion purposes, comparisons between the various configurations will generally be made at these operating pressure ratios.

Static forward-thrust performance.- Figure 12 is a comparison of the static forward-thrust coefficient $F/p_a S$ for the basic configuration with those of the in-flight TCU configuration at several pressure ratios and two engine-power settings. The ideal isentropic thrust coefficient $F_i/p_a S$ is also included in this figure. Figure 13 is a comparison of the static thrust ratios F/F_i of the basic and the TCU configurations. At the scheduled engine-operating pressure ratio for static take-off conditions, the TCU configuration with the deflector doors in the open position ($\delta_{du} = 32.5^\circ$, $\delta_{dl} = 52.5^\circ$, $\delta_b = 0$ percent) shows a 4-percent increase in performance over the basic configuration for military power and a 1.3-percent loss in performance for afterburning power ($\delta_{du} = 43.5^\circ$, $\delta_{dl} = 43.5^\circ$, $\delta_b = 0$ percent). The TCU configuration with the deflector doors in the faired position reveals a 3.5- to 4-percent loss in performance compared with the basic configuration for both power settings. The increase in performance at military power for the TCU configuration with the deflector doors open is probably due to the fact that the open deflector doors allow tertiary air to flow into the ejector similar to a blow-in-door ejector. The tertiary air enters aft of the secondary-cooling-air ejector annulus counteracting jet aspiration of the annulus region between the jet plume and the TCU shroud. This tertiary flow prevents overexpansion of the jet and produces thrust augmentation. Thrust augmentation of this type can be obtained at static conditions and at low forward speeds because of lowered pressures on the forward-facing surfaces of the deflector doors which act in part as a bellmouthed thrust augments. (See ref. 18.) For after-

burning power, combined primary-nozzle and secondary-cooling-air flows fill the TCU shroud inducing little or no tertiary air and consequently producing little thrust augmentation. The loss in performance encountered by the TCU configuration with the deflector doors in the faired position could be attributed to the jet exhaust aspirating the larger TCU annular region between the jet plume to the TCU shroud with only a small amount of tertiary air entering the ejector.

Thrust-minus-drag coefficient.- The variation of thrust-minus-drag coefficient with primary-nozzle-jet total-pressure ratio for the military-power nozzle at several angles of attack and Mach numbers is given in figure 14. The same variation is shown in figure 15 for the afterburning-power nozzle at 0° angle of attack. These figures present the fundamental data for the basic and several TCU configurations.

Effect of deflector-door setting on forward-thrust performance.- Figure 16 gives a comparison of the thrust-minus-drag coefficient for the basic configuration with those of the TCU configurations at several Mach numbers for both power settings. Generally, the thrust-minus-drag coefficient is more adversely affected by the TCU modification when operating at military power except at low subsonic Mach numbers. Figure 17 presents a summary of these data in the form of a comparison between the basic and TCU forward thrust-minus-drag performance. For afterburning power at low Mach numbers, a loss in performance of up to about 4 percent was contributed by the TCU configuration with deflector doors open. Above a Mach number of 0.60, equivalent performance is indicated for all TCU configurations. For military power, improved performance (a maximum of about 4 percent) is indicated up to a Mach number of 0.29 for the TCU configuration with deflector doors open ($\delta_{du} = 32.5^\circ$, $\delta_{dl} = 52.5^\circ$). Above a Mach number of 0.29, the open deflector doors act as speed brakes and contribute drag which increases rapidly with Mach number. With the deflector doors closed, a large loss in performance (up to 8 percent subsonically decreasing to 0 percent at $M = 1.30$) is indicated. With the deflector doors faired, the performance of the TCU configuration is less detrimental than that of the other configurations above a Mach number of 0.29 with the loss of performance of about 3 percent diminishing with increased Mach number until performance equal to that of the basic configuration is achieved at supersonic speeds. At military power, an operation technique may be to keep the deflector doors deployed in the open position until a Mach number of 0.29 is reached and then change to the faired position for higher speeds.

Effect of deflector-door setting on reverse-thrust performance.- A comparison of the effect of deflector-door angular settings on reverse-thrust performance for several Mach numbers is presented in figure 18. This figure indicates that reverse-thrust efficiency is lower for the equal deflector-door angular settings ($\delta_{du} = \delta_{dl} = 43.5^\circ$ or 60°) than for the asymmetrical settings with the largest decrease occurring with the maximum deflector-door opening ($\delta_{du} = \delta_{dl} = 60^\circ$). This trend is opposite to the results presented

earlier in the jet-off drag comparisons (see fig. 10), where the most effective speed brakes were shown to be the TCU with the maximum and equal deflector-door openings. These data indicate, as expected, that the reverse-thrust vectors have a greater influence on performance than the speed brakes. Based on these data and stability considerations, the deflector-door angular setting of $\delta_{du} = 32.5^\circ$ and $\delta_{dl} = 52.5^\circ$ appears to be one of the best door-setting combinations tested and was therefore selected for use in the study of blocker-door deployment.

Effect of blocker-door position on reverse-thrust performance.- Reverse and modulated thrust performance are presented in figures 19 to 21 for the TCU configuration with the upper deflector doors set at 32.5° and the lower doors at 52.5° . Figure 19 presents the variation of static-thrust coefficient with primary-nozzle-jet total-pressure ratio and blocker-door position. Static-thrust modulation appears to be nearly linear with pressure ratio. Both blocker-door closures of 90 and 100 percent indicate a reverse-thrust coefficient. The variation of thrust-minus-drag coefficient with primary-nozzle-jet total-pressure ratio and blocker-door position for several Mach numbers is shown in figure 20. With external, free-stream airflow, the effect of primary total-pressure ratio on forward thrust becomes nonlinear at some conditions with blocker-door closure especially at $M = 0.60$ and $\delta_b = 50$ percent. (See fig. 20(c).)

Static-thrust-modulation performance as a function of blocker-door setting at the estimated engine-operating pressure ratio is given in figure 21(a). Zero static thrust occurs at a blocker-door closure of $\delta_b = 82$ percent with a maximum static reverse thrust of 52 percent of the forward thrust attained at 100-percent blocker-door closure. Thrust-modulation performance for the landing-approach configuration (flaps and slats deployed) at $M = 0.23$ is given in figure 21(b). These data show that zero thrust-minus-drag occurs at a blocker-door setting of about 77 percent or a decrease of about 5 percent from the static condition. This zero point would shift for the full-scale condition since the aerodynamic forces on the wing and ram or induced drag resulting from taking inlet airflow on board was not measured and, therefore, has not been considered in this investigation. It should be noted that in figures 21(a) and 21(b), the forward-thrust term in the denominator has the deflection doors at the selected open position ($\delta_{du} = 32.5^\circ$, $\delta_{dl} = 52.5^\circ$) since figure 17 shows that the highest performance with the blocker doors stowed was achieved at this condition. A similar plot of thrust-modulation performance as a function of blocker-door position at the estimated engine-operating pressure ratio for Mach numbers from 0.34 to 1.30 is given in figure 21(c); however, the forward-thrust term in the denominator of the performance ratio, $\left(\frac{C_{(F-D)}_R}{C_{(F-D)}_F}\right)$ was obtained with the deflector doors in the faired position. The zero thrust-minus-drag point continues to occur at lower values of δ_b with increased Mach number; this continued occurrence is attributed to an increase in fuselage-tail drag at higher speeds. At a Mach num-

ber of 1.30, zero thrust-minus-drag occurs at 56-percent blocker-door closure or about 26 percent lower than static conditions. At any Mach number under combat conditions, deploying the blocker and deflector doors would result in a considerable reduction in air-speed and would provide greater maneuverability.

TCU Effect on Engine Characteristics

Primary-nozzle-jet mass flow.- The ratio of the primary-nozzle-jet mass flow for various TCU configurations to that for the basic configuration is presented in figures 22 and 23 for forward-thrust conditions and for full-reverse thrust $\delta_b = 100$ percent in figure 24. This ratio is a measure of the effect of the TCU on steady-state engine performance. If the magnitude of the ratio $\dot{m}_{p,TCU}/\dot{m}_{p,basic}$ is not unity, then engine controls will be forced to change operating conditions to accommodate the change in such a manner that for ratios greater than unity, the primary-nozzle-jet total pressure for the TCU configurations will be less than that for the basic configuration, and vice versa. For the TCU operating in the forward-thrust mode at military power, deflector-door operation tends to reduce the primary flow slightly. (See fig. 22.) With the deflector doors closed, an increase in primary mass flow of about 1 percent is noted for the Mach number range; however, with the doors deflected to $\delta_{du} = 32.5^\circ$ and $\delta_{dl} = 52.5^\circ$, a 3-percent maximum flow reduction at $M = 0.34$ is indicated at the estimated engine-operating pressure ratio. For afterburning power, the primary mass flow for the TCU configurations is increased from that of the basic configuration by as much as 1 percent at the estimated engine-operating pressure ratio, depending on deflector-door setting. Again deployment of the deflector doors slightly reduces primary mass flow. (See fig. 23.) In the reverse-thrust mode ($\delta_b = 100$ percent), the primary flow for the TCU configurations is increased from that of the basic configuration by as much as 1 percent for the three deflector-door settings. Since these effects are small and the time spent in reverse thrust limited, the effect of the TCU on primary flow rate is probably satisfactory.

Ejector pumping characteristics.- The ejector pumping characteristics of various configurations for several Mach numbers at 0° angle of attack are given in figure 25 for military power and in figure 26 for afterburning power. For all configurations, the ratio of secondary-cooling-air mass flow to primary-nozzle-jet mass flow (entrainment ratio) was kept constant for a given estimated engine-operating pressure ratio and Mach number

$$\left(\text{for example, at } M = 0.35 \text{ and } \frac{p_{t,p}}{p_\infty} = 2.35, \frac{\dot{m}_s}{\dot{m}_p} \sqrt{\frac{R_s T_{t,s}}{R_p T_{t,p}}} \approx 0.036 \text{ for all configurations} \right)$$

as shown in figure 27. With the TCU in the stowed position ($\delta_{du} = \delta_{dl} = \text{Faired}$), a slight increase is indicated in secondary flow rate at military power (fig. 25) with essentially no change at afterburning power (fig. 26). However, for the reverse-thrust mode, the

secondary flow for the TCU configuration is slightly degraded compared with that for the basic configuration. Increased secondary flow is indicated by achieving the same entrainment ratio $\dot{m}_s/\dot{m}_p\sqrt{R_s T_{t,s}/R_p T_{t,p}}$ at a lower secondary-cooling-air total-pressure ratio $(p_{t,s}/p_{t,p})$. The increase in the secondary flow rate for the TCU in the forward-thrust mode is small and probably within the accuracy of measurement; however, operation in reverse thrust indicates a restriction in secondary flow which could cause concern for full-scale installation. For example, for the TCU configuration with $\delta_{du} = 32.5^\circ$ and $\delta_{dl} = 52.5^\circ$ in the reverse-thrust mode, $p_{t,s}/p_{t,p} = 0.52$ at $M = 0.60$; and for the basic configuration, $p_{t,s}/p_{t,p} = 0.38$ at $M = 0.60$. This increase in secondary total-pressure ratio indicates a restriction in secondary airflow and could create an increase in local aft-end temperatures.

Secondary-cooling-air total temperatures.- A comparison of secondary-cooling-air total temperatures for forward- and reverse-thrust operation is given in figure 28. The data indicate a general increase in the temperature of secondary cooling air with primary-nozzle-jet total-pressure ratio; this increase is because the heat efflux from the primary tailpipe is greater than that which the conductive mass flow of secondary air can remove. In the reverse-thrust mode, the secondary-air temperature is lower than that in the forward-thrust mode; this lower temperature indicates that reverse thrust has a beneficial effect on secondary-air temperatures at the lower pressure ratios; however, with an increase in the primary total-pressure ratio, a more rapid increase is shown in the secondary-air temperature which would probably exceed that in the forward-thrust mode as the hot reverse-exhaust gas is forced back into the secondary-air passage in reverse-thrust mode.

TCU Effect on External-Surface Temperatures

Fuselage temperatures.- The variation of local fuselage temperatures with primary-nozzle-jet total-pressure ratio for various blocker-door positions is presented for several Mach numbers for the selected TCU configuration ($\delta_{du} = 32.5^\circ$, $\delta_{dl} = 52.5^\circ$) in figure 29, with the exception of figure 29(a) which gives data for the TCU configuration with the deflector doors faired. The local fuselage temperatures ($T_{f,1}$ and $T_{f,2}$) forward of the reverse ports generally show an increase with primary total-pressure ratio for most Mach numbers. These data indicate that the fuselage skin could be subjected to temperatures of approximately 70-percent primary-nozzle-jet total temperatures. (See fig. 29(c), $M = 0.60$, $\alpha = 6^\circ$.) Figure 30 presents the variation of local fuselage temperature with angle of attack for the greater blocker-door deployments. These data indicate that angle of attack had little effect on the level of temperature; however, the general trend was a

slight reduction in temperature with angle of attack. Figure 31 displays the variation of local fuselage temperatures with blocker-door position. This figure indicates that a rapid temperature increase occurs for the blocker-door closures above 50 percent with the maximum local fuselage temperatures occurring at approximately 90-percent blocker-door closure and then decreasing at the 100-percent full-reverse-thrust condition.

Tail and tail-hook temperatures.- Local temperature variations on the skeg, tail hook, and horizontal- and vertical-tail surfaces for the landing-approach configuration with reverse-thrust modulation are given in figure 32. A maximum increase in the skeg and tail-hook temperatures, similar to the increase in fuselage temperatures, occurs at 90-percent blocker-door closure. Both the horizontal and vertical tails encountered an increase in temperature near their base regions with blocker-door position. These data indicate that the surfaces at the base of the tails may require shielding from the exhaust gases, especially for full-scale hot-day operation. In addition, it should be noted that tail deflection may cause even higher temperatures in the base region of the tails during reverse-thrust operation, especially on the rudder of the vertical tail where temperatures were not obtained in this investigation.

TCU Effect on Cooling-Film and Inner-Skin Temperatures

Figure 33 presents the variation of TCU cooling-film temperature (air temperatures near the shroud wall) and inner-skin temperature with primary-nozzle-jet total-pressure ratio for various configurations at several Mach numbers. These data indicate that a temperature gradient exists around the TCU shroud circumference. During the forward-thrust mode (figs. 33(a) and 33(b)), tertiary air, introduced with the deflector doors faired and open, cools the shroud only in the vicinity of the deflector doors. Generally, tertiary air creates a significant difference in shroud temperature with the area directly behind the tertiary-air inlets being cooler than that in the region between the inlets. The opposite trend is shown for the reverse-thrust mode (fig. 33(c)) with the region behind the reverse-thrust exhaust ports (the same as the tertiary-air inlets except with $\delta_p = 100$ percent) being hotter than the region between the ports. At this condition, the wall (skin) temperature increases to approximately 50 percent of that of the primary-nozzle exhaust gas. This increase is probably a result of heat conducted through the TCU shroud from the exhaust ports and the hot exhaust gas from the reverse-thrust flowing around the shroud into the low-pressure TCU base cavity.

TCU Effect on External Aft-End Pressures

Fuselage pressures.- Figure 34 shows the variation of fuselage pressure coefficient with primary-nozzle-jet total-pressure ratio for several TCU configurations. For the TCU configuration with deflector doors faired and blocker doors stowed for military power (fig. 34(a)), the flow along the fuselage is accelerated as it enters the deflector door with

an increase in primary total-pressure ratio. This acceleration is observed up to a pressure ratio of about 3, after which the flow begins to decelerate. This trend is common up to $M = 0.90$, but at $M = 1.30$ the variation of primary total-pressure ratio had little effect on the pressure field ahead of the deflector door. At the jet-off condition ($p_{t,p}/p_{\infty} = 1.0$), a pressure recovery is indicated as the air flows downstream on the fuselage toward the deflector door. For afterburning power, the jet effects are not as pronounced as those for military power with the variation of Mach number having a larger effect. This Mach number effect is probably because the primary-nozzle flow prevents tertiary air from entering the ejector above $M = 0.35$, which results in undisturbed external flow over the deflector doors and fuselage. (See fig. 34(b).) This same effect is observed with the deflector doors in the closed position. (See figs. 34(c) and 34(d).) With the deflector doors deployed in the selected open position ($\delta_{du} = 32.5^{\circ}$, $\delta_{dl} = 52.5^{\circ}$) and for forward thrust, similar results are obtained as for the faired deflector-door configuration. (See fig. 34(e).) For full reverse thrust with the deflector doors set at the selected open position for military power (fig. 34(f)), no consistent pattern for the external pressures is indicated, with increased primary total-pressure ratio causing mixed reaction on the fuselage pressures.

TCU base pressures.- The variation in TCU base pressure coefficient with primary-nozzle-jet total-pressure ratio is given in figure 35. The base pressure field is significantly affected with increased primary total pressure in the full-reverse-thrust mode, and at all Mach numbers the base pressures are reduced by jet operation. This reduced base pressure may account for the higher temperatures observed in the TCU during full reverse thrust in the same plane of the exhaust ports. The low base pressure causes recirculation of the exhaust into the base causing that section to have somewhat higher temperatures.

CONCLUSIONS

A wind-tunnel investigation has been conducted in the Langley 16-foot transonic tunnel on a thrust control unit (TCU) with blocker and deflector doors retrofitted to a single-engine fighter model. The investigation was conducted statically and through the 0.23 to 1.30 Mach number range at angles of attack from -3° to 12° . The primary-nozzle-jet total-pressure ratio was varied from 1.0 (jet off) to approximately 5.

The results of the investigation indicate the following:

1. The drag penalty attributed to the TCU modification in the stowed position was small.
2. With the TCU modification, forward take-off thrust performance can be increased by 4 percent for military power with the upper deflector doors set at 32.5° and the lower

door set at 52.5° with 0-percent blocker-door closure but is reduced by 1.3 percent for afterburning power with the upper and lower deflector doors set at 43.5° with 0-percent blocker-door closure.

3. The highest reverse-thrust performance was achieved with deflector-door angular positions of 32.5° for the upper doors and 52.5° for the lower door.

4. With deflector-door angular positions of 32.5° for the upper doors and 52.5° for the lower door and with 100-percent blocker-door closure, a maximum reverse thrust of 52 percent of forward thrust was achieved under static conditions, and reverse-thrust performance increased with increasing Mach number.

5. Engine-operation characteristics should be only slightly degraded during reverse-thrust operation, but secondary cooling air during reverse-thrust operation may have to be supplemented.

6. Maximum local temperatures (70 percent of primary-nozzle-jet total temperature) appear to occur at 90-percent blocker-door closure for the selected TCU configuration (upper deflector doors set at 32.5° and lower door set at 52.5°).

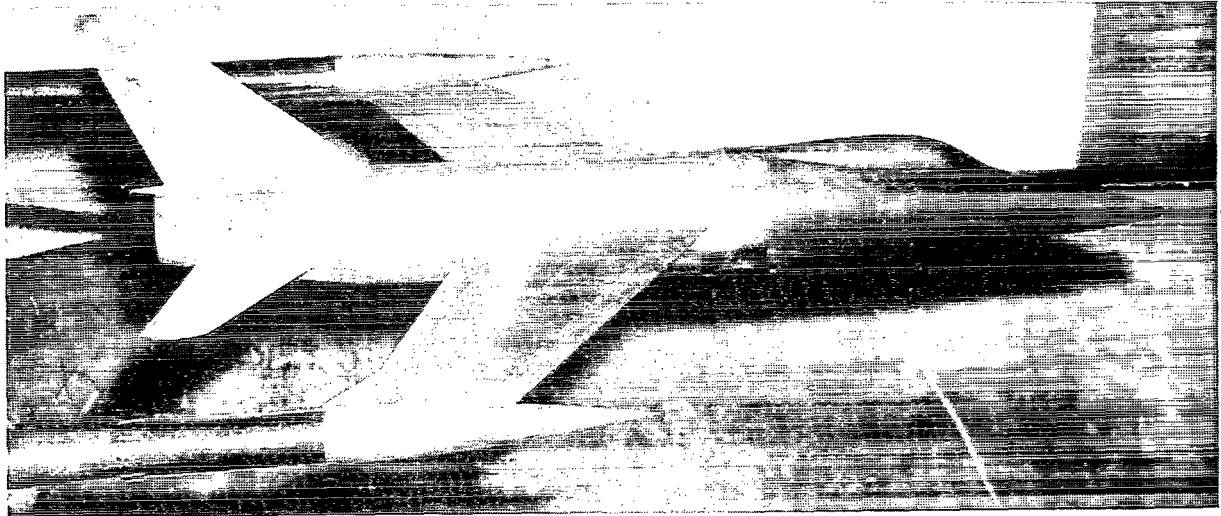
Langley Research Center,
National Aeronautics and Space Administration,
Hampton, Va., August 12, 1971.

REFERENCES

1. Polak, I. P.: Development of Turbo-Jet Engine Thrust Destroying and Reversing Nozzle No. AEL 102. Rep. No. AEL-1108, 1950. (Project TED Nos. NAM-PP-375 and NAM-04614), Naval Air Material Center, NAES (Philadelphia), Jan. 13, 1950.
2. Povolny, John H.; Steffen, Fred W.; and McArdle, Jack G.: Summary of Scale-Model Thrust-Reverser Investigation. NACA Rep. 1314, 1957. (Supersedes NACA TN 3664.)
3. Swihart, John M.: Effect of Target-Type Thrust Reverser on Transonic Aerodynamic Characteristics of a Single-Engine Fighter Model. NACA RM L57J16, 1958.
4. Kohl, Robert C.; and Algranti, Joseph S.: Investigation of a Full-Scale, Cascade-Type Thrust Reverser. NACA TN 3975, 1957.
5. Kohl, Robert C.: Performance and Operation Studies of a Full-Scale Jet-Engine Thrust Reverser. NACA TN 3665, 1956.
6. Tolhurst, William H., Jr.; Kelly, Mark W.; and Greif, Richard K.: Full-Scale Wind-Tunnel Investigation of the Effects of a Target-Type Thrust Reverser on the Low-Speed Aerodynamic Characteristics of a Single-Engine Jet Airplane. NASA TN D-72, 1959.
7. Kelly, Mark W.; Greif, Richard K.; and Tolhurst, William H., Jr.: Full-Scale Wind-Tunnel Tests of a Swept-Wing Airplane With a Cascade-Type Thrust Reverser. NASA TN D-311, 1960.
8. Falarski, Michael D.; and Mort, Kenneth W.: Full-Scale Wind-Tunnel Investigation of a Target-Type Thrust Reverser on the A-37B Airplane. NASA TM X-1985, 1970.
9. Weiss, D. C.; and McGuigan, W. M.: Inflight Thrust Control for Fighter Aircraft. AIAA Paper No. 70-513, Mar. 1970.
10. Linderman, D. L.; and Mount, J. S.: Development of an In-Flight Thrust Reverser for Tactical/Attack Aircraft. AIAA Paper No. 70-699, June 1970.
11. Taylor, John W. R., ed.: Jane's All The World's Aircraft, 1969-1970. McGraw-Hill Book Co., Inc., c.1969.
12. Bruner, Georges: Les Avions Etrangers, Autre que Soviétiques, au Salon de Bourget. L'Aéronautique et L'Astronautique, vol. 1970-1, no. 17, 1970, pp.39-49.
13. Aronson, Robert, ed.: European Fighter Aircraft. Mach. Des., vol. 41, no. 24, Oct. 16, 1969, pp. 44-50.

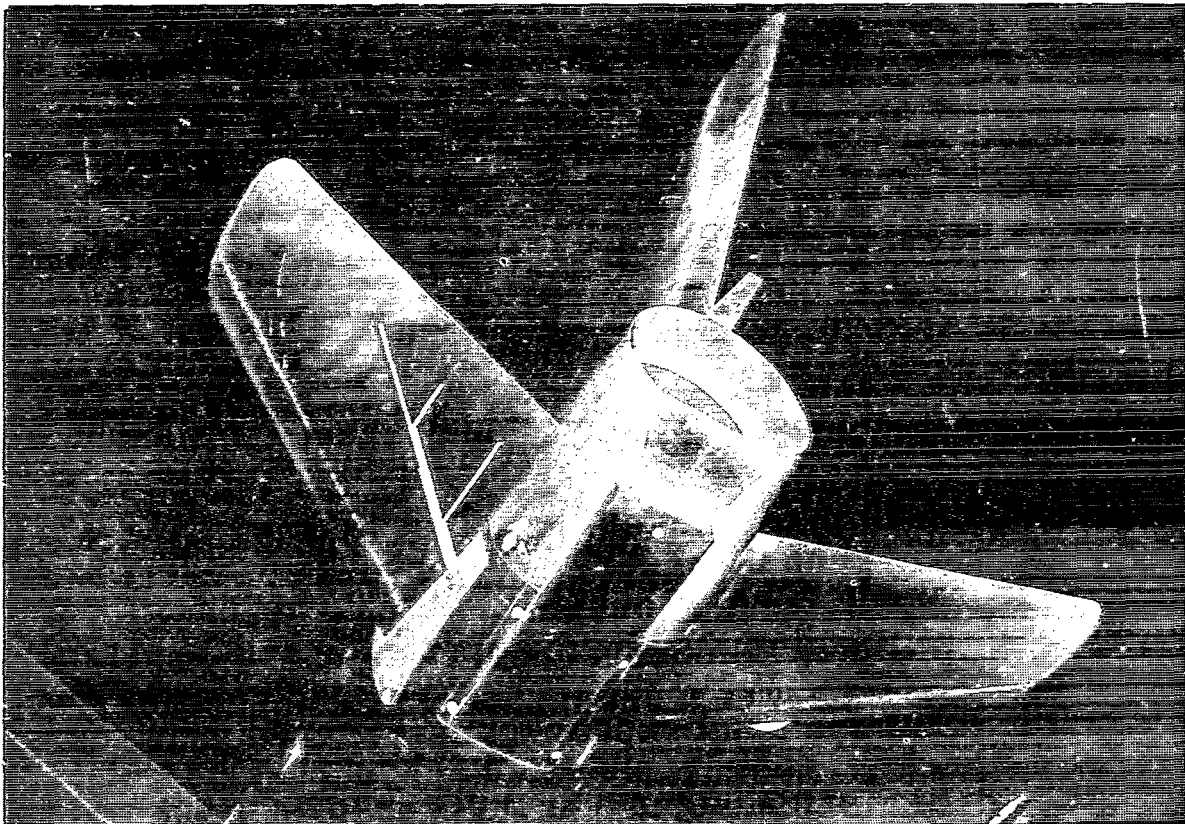


14. Schaefer, William T., Jr.: Characteristics of Major Active Wind Tunnels at the Langley Research Center. NASA TM X-1130, 1965.
15. Ward, Vernon G.; Whitcomb, Charles F.; and Pearson, Merwin D.: Air-Flow and Power Characteristics of the Langley 16-Foot Transonic Tunnel With Slotted Test Section. NACA RM L52E01, 1952.
16. Runckel, Jack F.; and Swihart, John M.: A Hydrogen Peroxide Hot-Jet Simulator for Wind-Tunnel Tests of Turbojet-Exit Models. NASA MEMO 1-10-59L, 1959.
17. Salters, Leland B., Jr.; and Chamales, Nicholas C.: Studies of Flow Distortion in the Tailpipes of Hydrogen Peroxide Gas Generators Used for Jet-Engine Simulation. NASA TM X-1671, 1968.
18. Simonson, Albert J.; and Schmeer, James W.: Static Thrust Augmentation of a Rocket-Ejector System With a Heated Supersonic Primary Jet. NASA TN D-1261, 1962.



L-69-6345

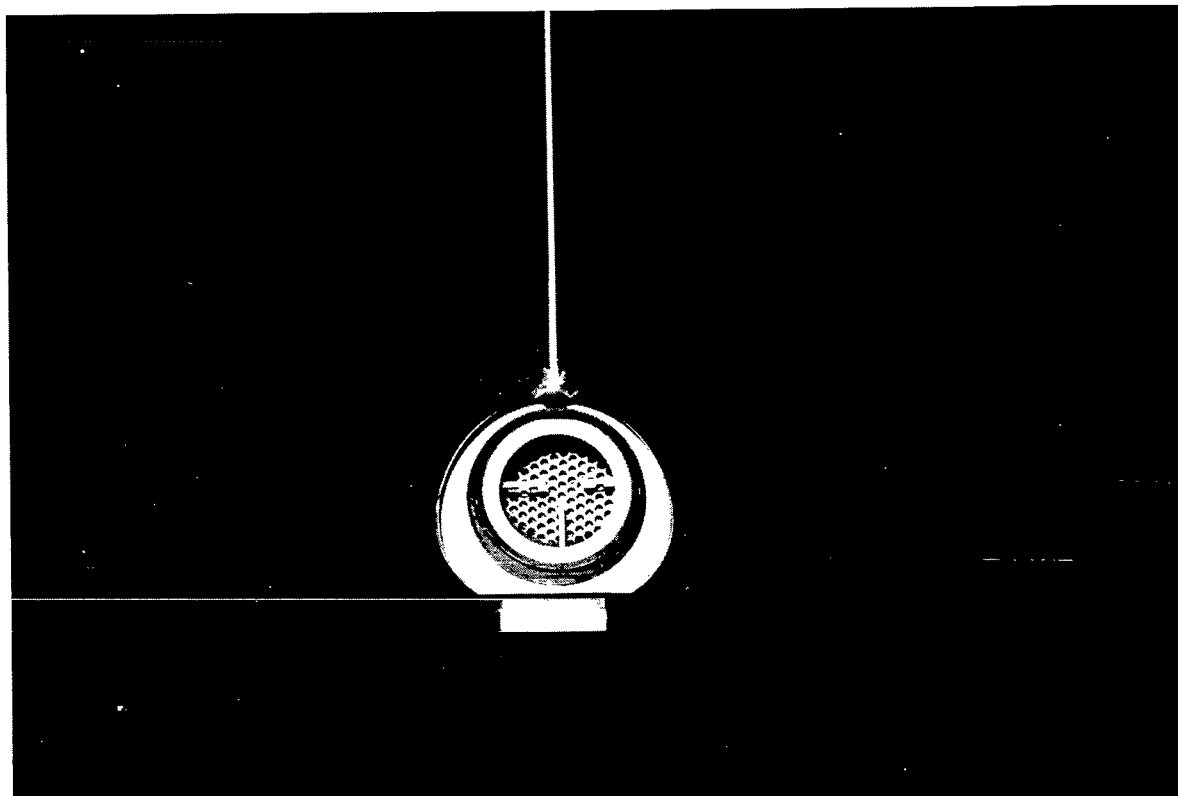
(a) Side view of model with basic afterbody.



L-71-683

(b) Rear view of basic afterbody.

Figure 1.- Single-engine fighter model installed in the Langley 16-foot transonic tunnel.



L-71-684

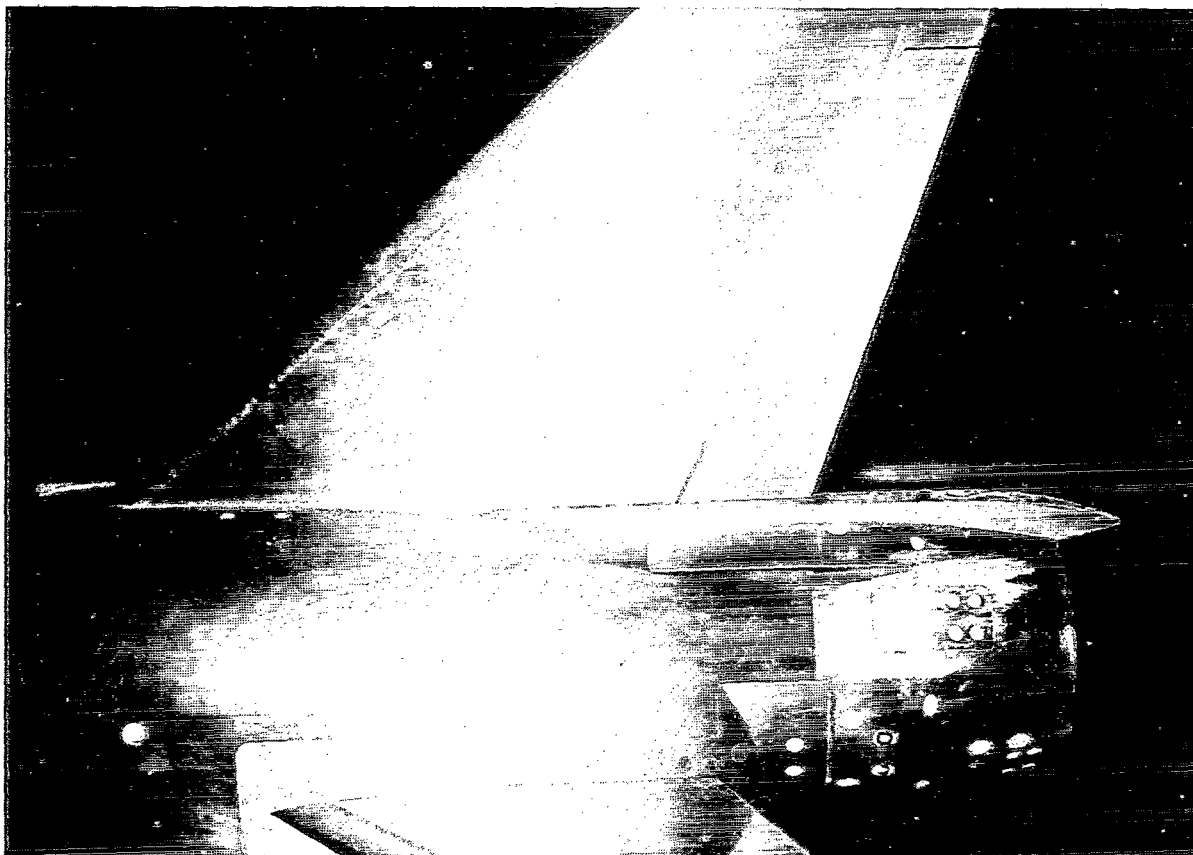
(c) Aft-end view of basic-afterbody nozzle arrangement.

Figure 1.- Concluded.



L-69-6920

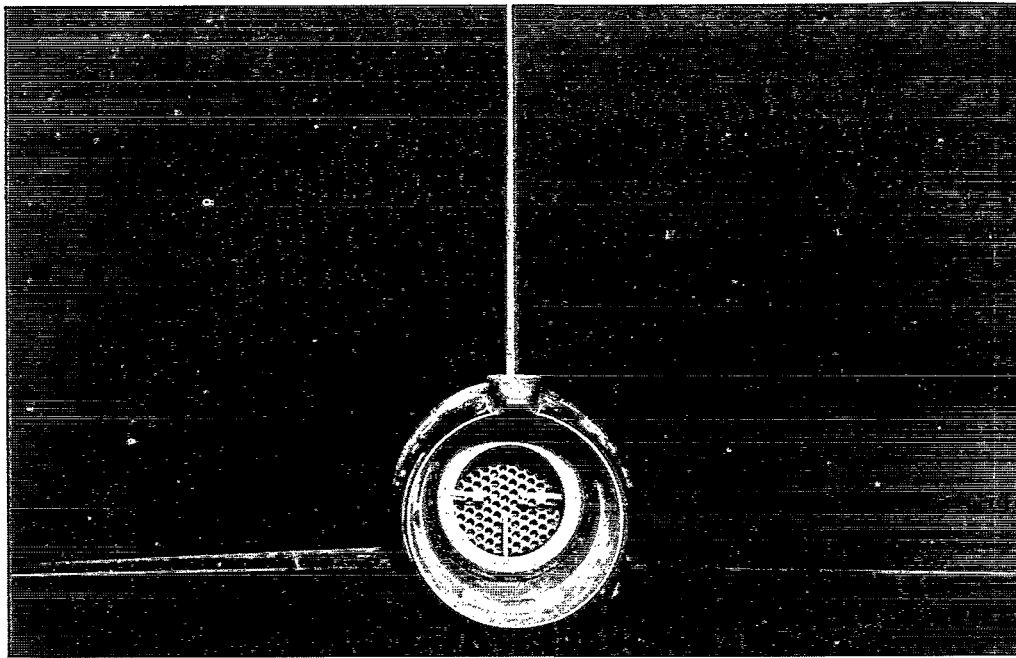
(a) Approach configuration with thrust control unit deployed.



L-71-685

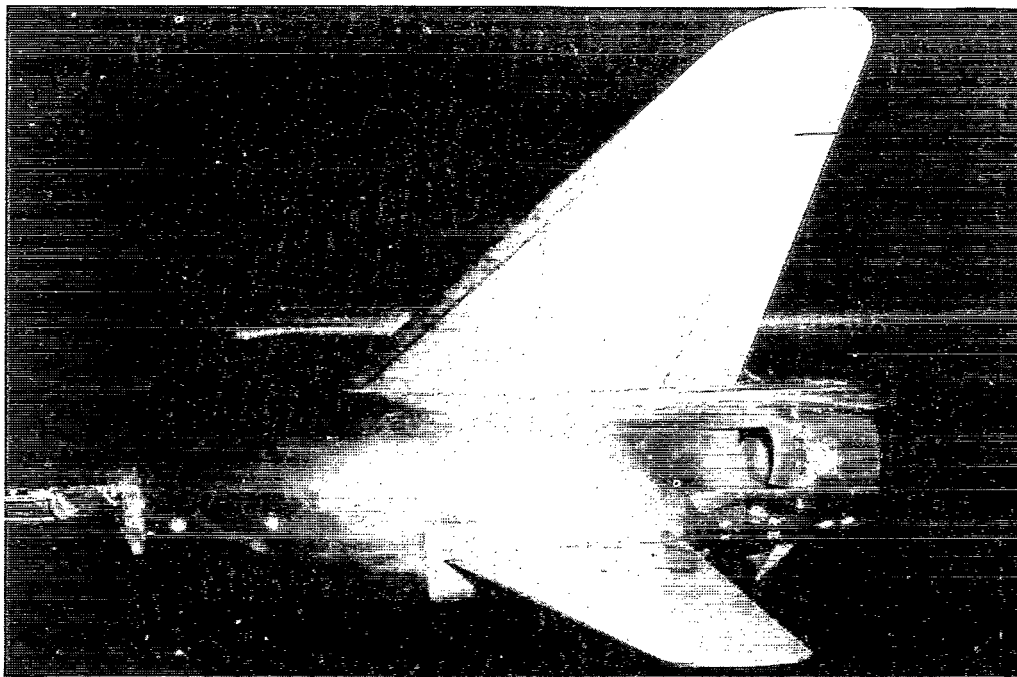
(b) Stowed configuration ($\delta_{du} = \delta_{dl} = \text{Closed}$) of thrust control unit.

Figure 2.- Retrofit thrust control unit mounted on a single-engine fighter model installed in the Langley 16-foot transonic tunnel.



L-71-686

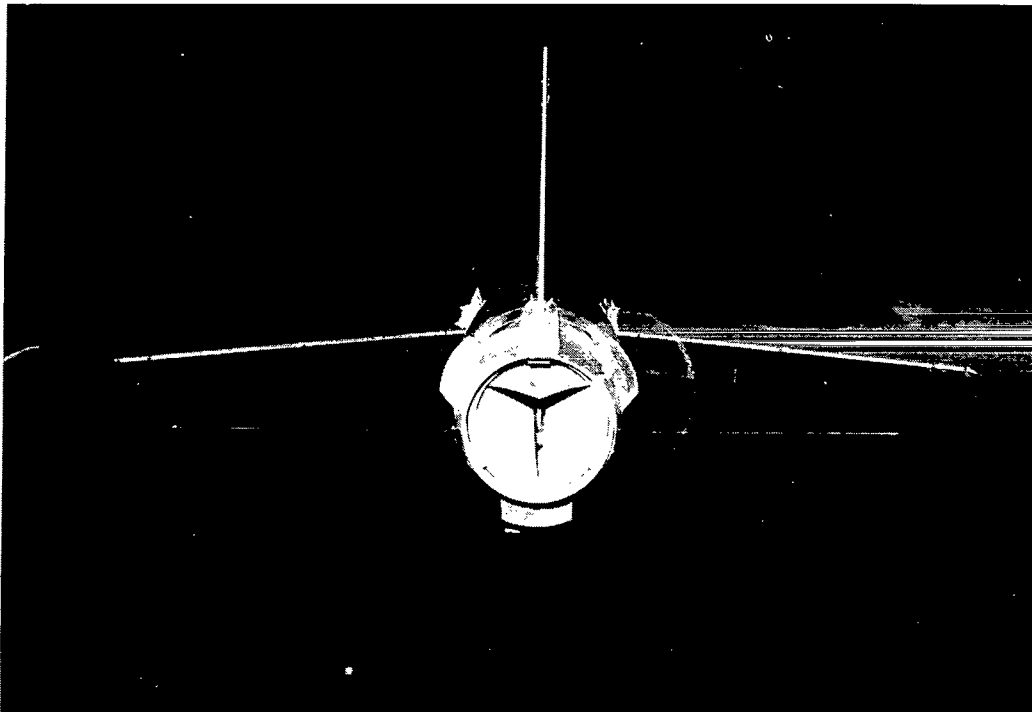
(c) Aft-end view of nozzle arrangement of stowed thrust control unit.



L-69-6398

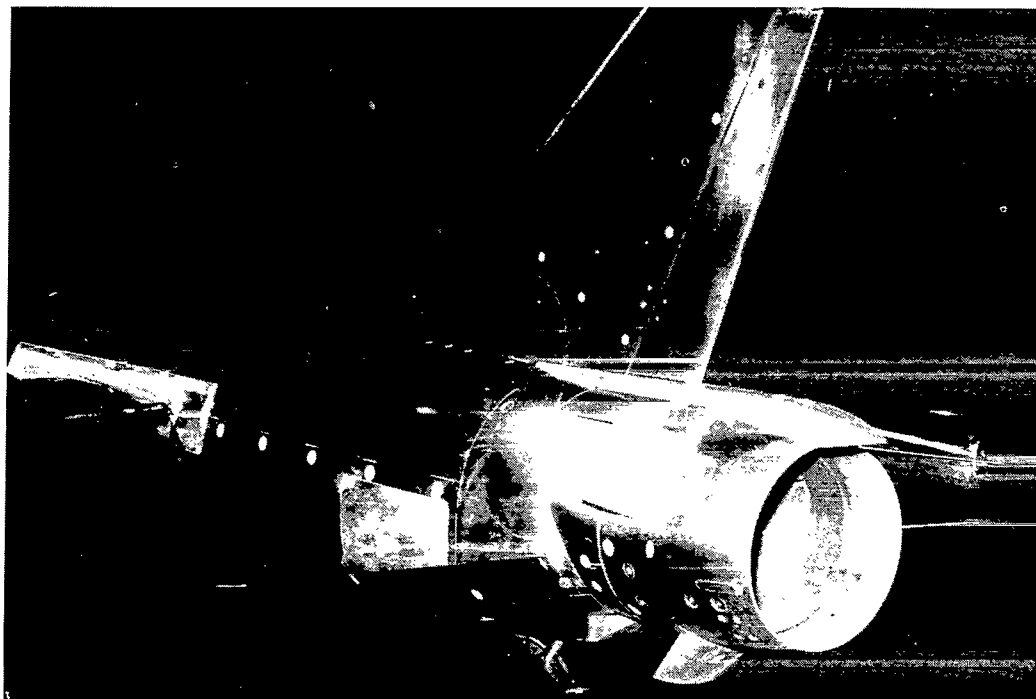
(d) Deployed configuration of thrust control unit; $\delta_b = 100\%$; $\delta_{du} = 32.5^\circ$;
 $\delta_{dl} = 52.5^\circ$.

Figure 2.- Continued.



L-71-687

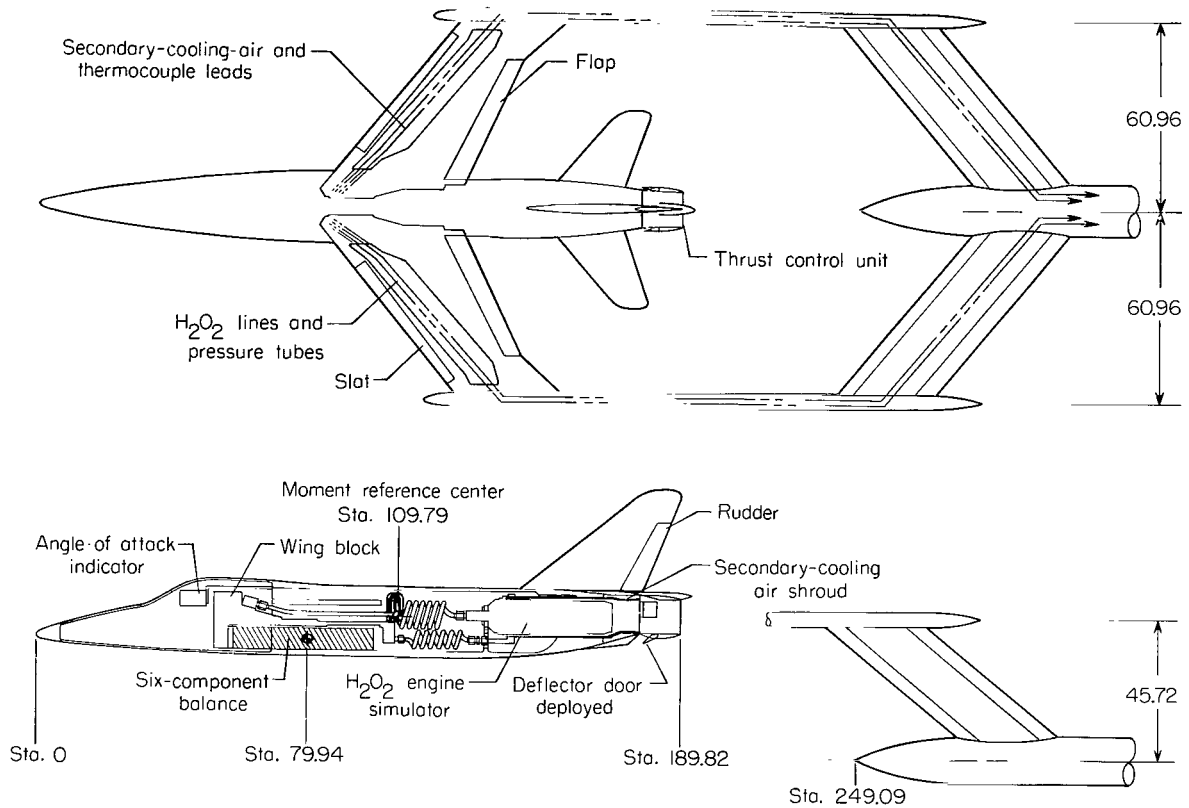
(e) Aft-end view of deployed thrust control unit; $\delta_b = 90\%$.



L-71-688

(f) Landing-approach configuration with thrust control unit and tail hook deployed.

Figure 2.- Concluded.



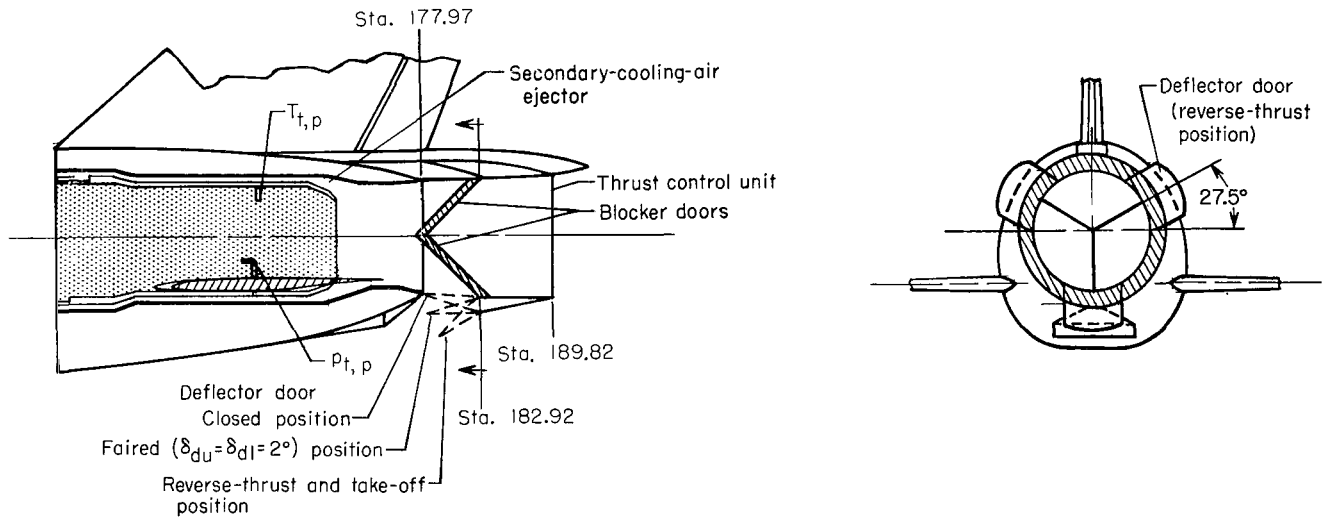
Wing	
Area (nominal)	0.4125 m ²
AR	4.00
Δ at c/4	35°
Cathedral	2.50°
Root section	NACA 65A006 modified
Tip section	NACA 65A006 modified
c _r	43.87 cm
c _t	21.94 cm
Taper ratio	0.50

Horizontal tail	
Area (total exposed)	0.0720 m ²
AR	3.50
Δ at c/4	35°
Root section	NACA 65A006
Tip section	NACA 65A004
c _r	25.13 cm
c _t	10.06 cm
Taper ratio	0.40

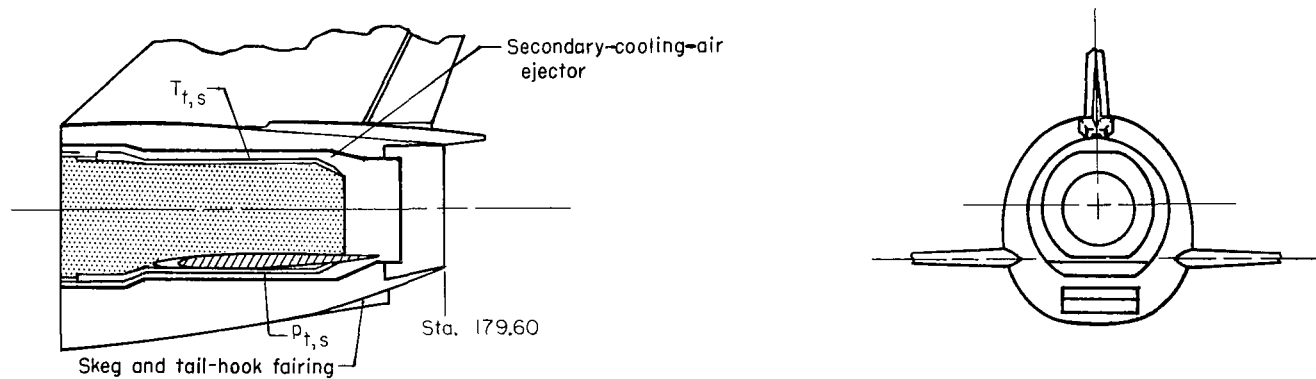
Engine	
Dry nozzle diameter	7.15 cm
A/B nozzle diameter	8.89 cm
Dry nozzle area	0.0040 m ²
A/B nozzle area	0.0062 m ²

Vertical tail	
Fin area (including rudder)	0.0729 m ²
Rudder area	0.0110 m ²
Δ at c/4	45°35'
Root section	NACA 0006
Tip section	NACA 0006

Figure 3.- Schematic of modified model with retrofit thrust control unit and bifurcated sting support. All dimensions are in centimeters unless otherwise noted.

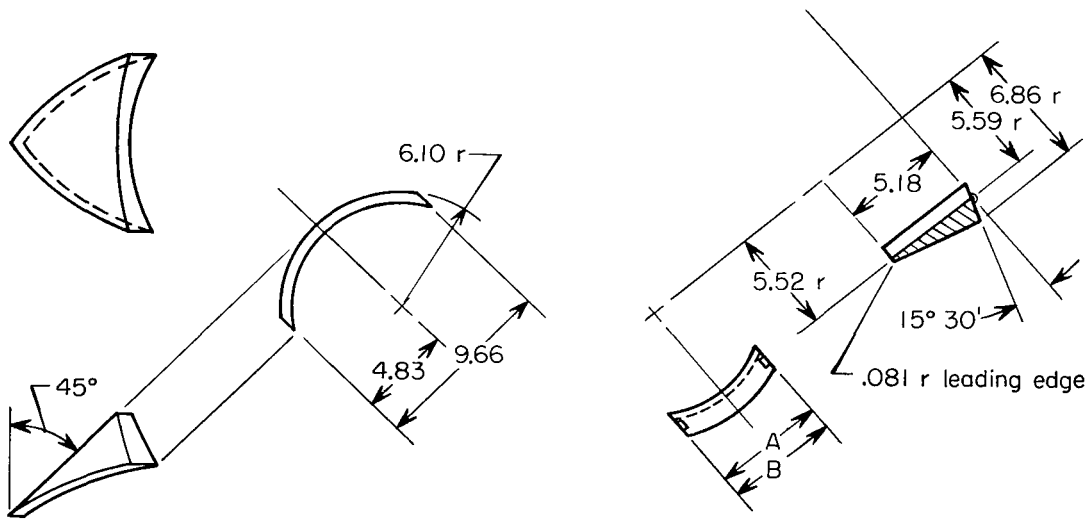
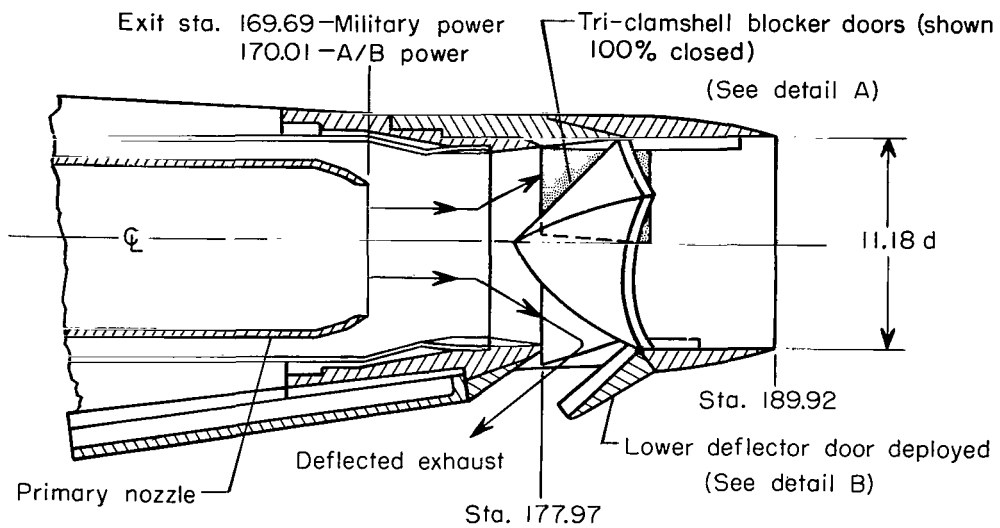


(a) Modified afterbody and ejector with thrust control unit (TCU).



(b) Reference afterbody and ejector (basic).

Figure 4.- Schematic showing basic afterbody and modified afterbody with retrofit thrust control unit.



A=5.31 cm —Upper deflector door
B=5.89 cm —Lower deflector door

Detail A—Typical clamshell geometry

Detail B—Deflector-door details

Figure 5.- Schematic of aft fuselage cutaway showing tri-clamshell in 100-percent-closed position. $\delta_b = 100\%$.

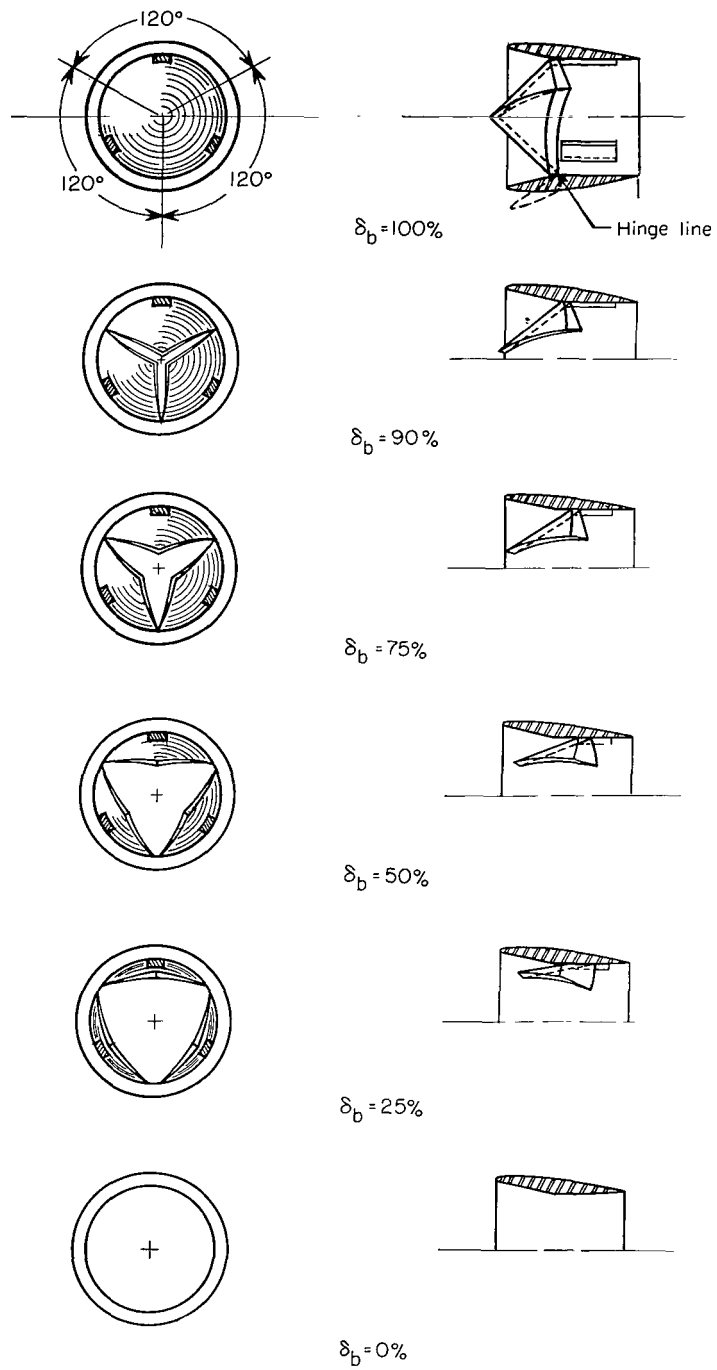


Figure 6.- Blocker-door configurations of thrust control unit.

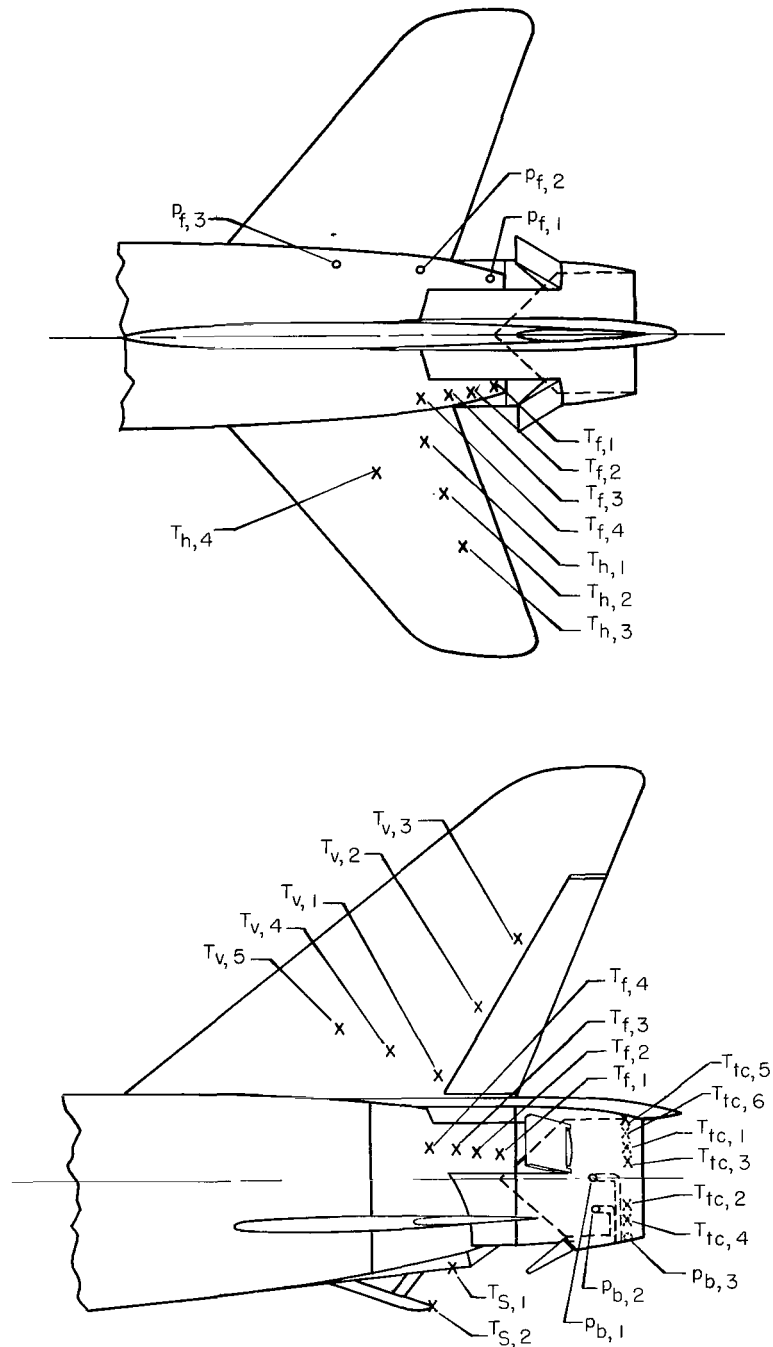


Figure 7.- Schematic showing static-pressure-orifice and thermocouple locations on fuselage.

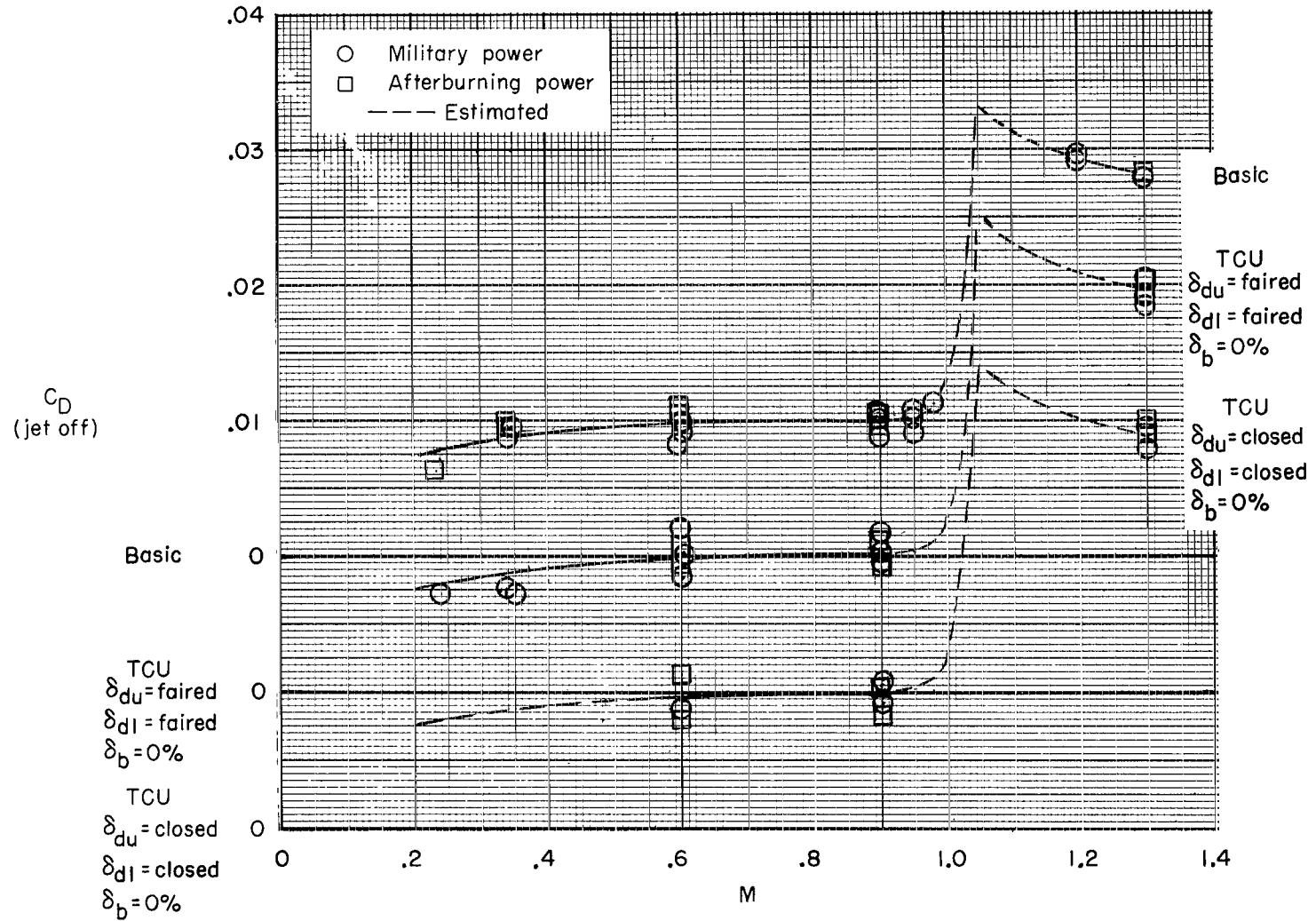
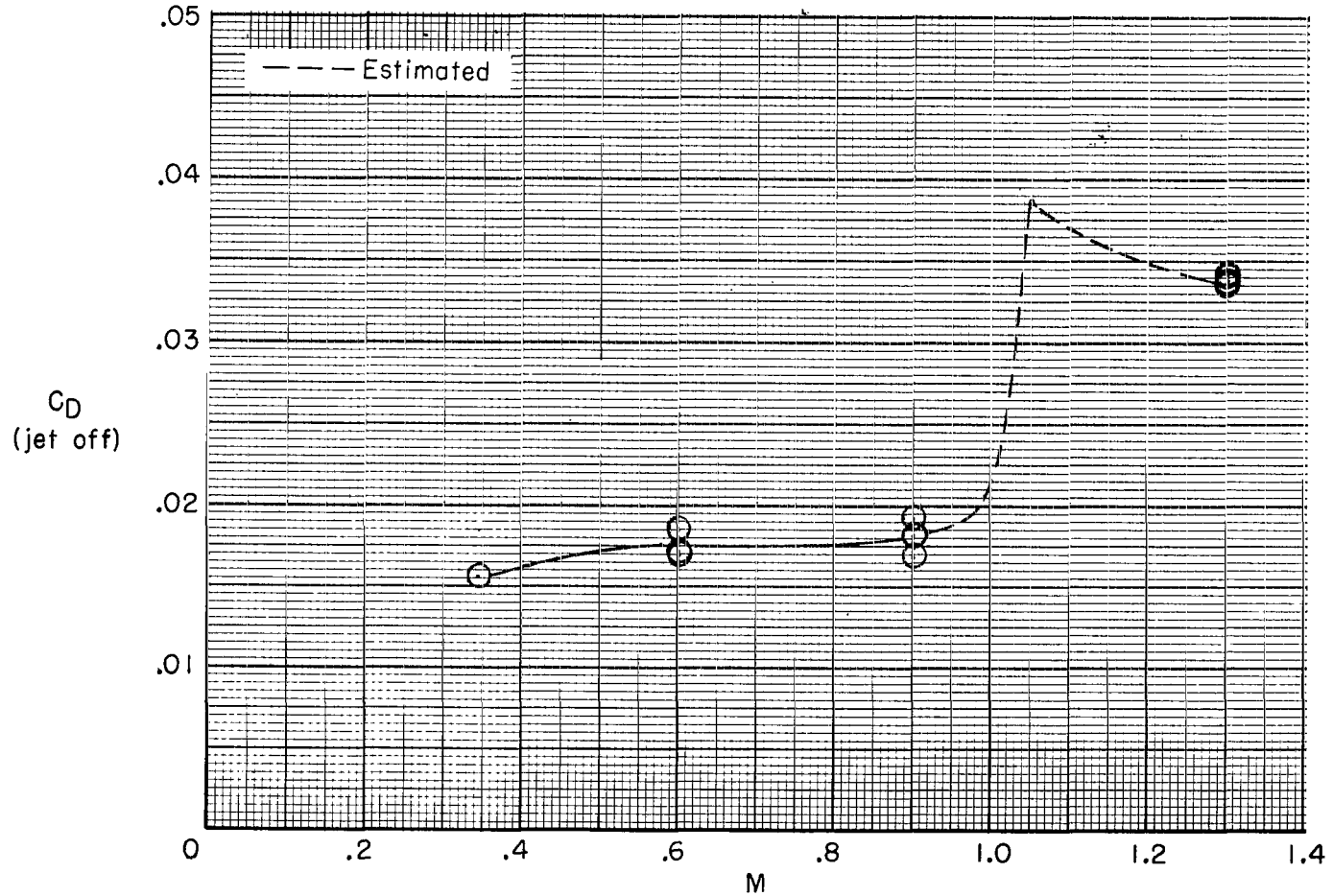
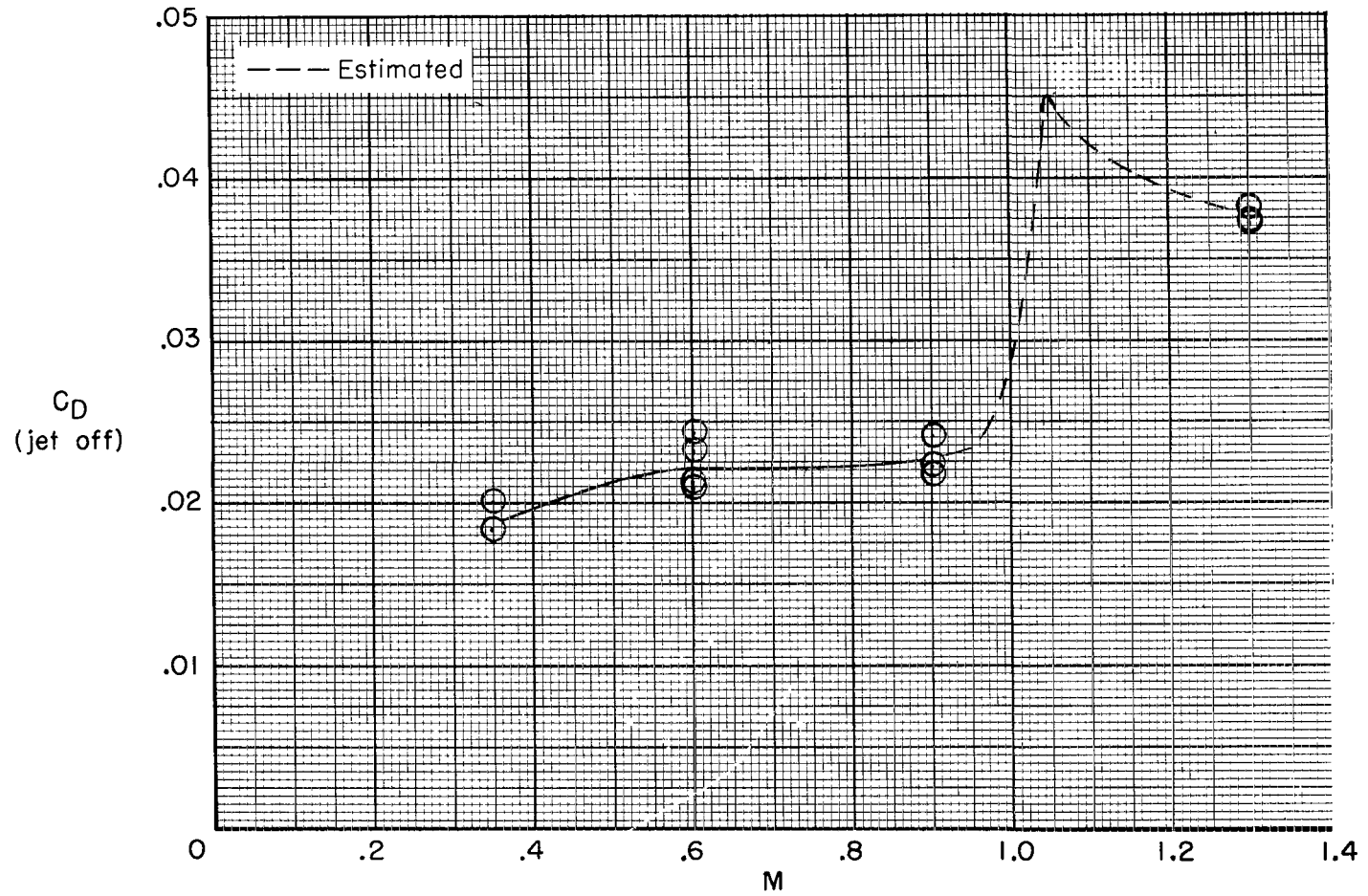


Figure 8.- Variation of jet-off fuselage-tail drag coefficient for various configurations at zero angle of attack. (Faired line represents basic configuration.)



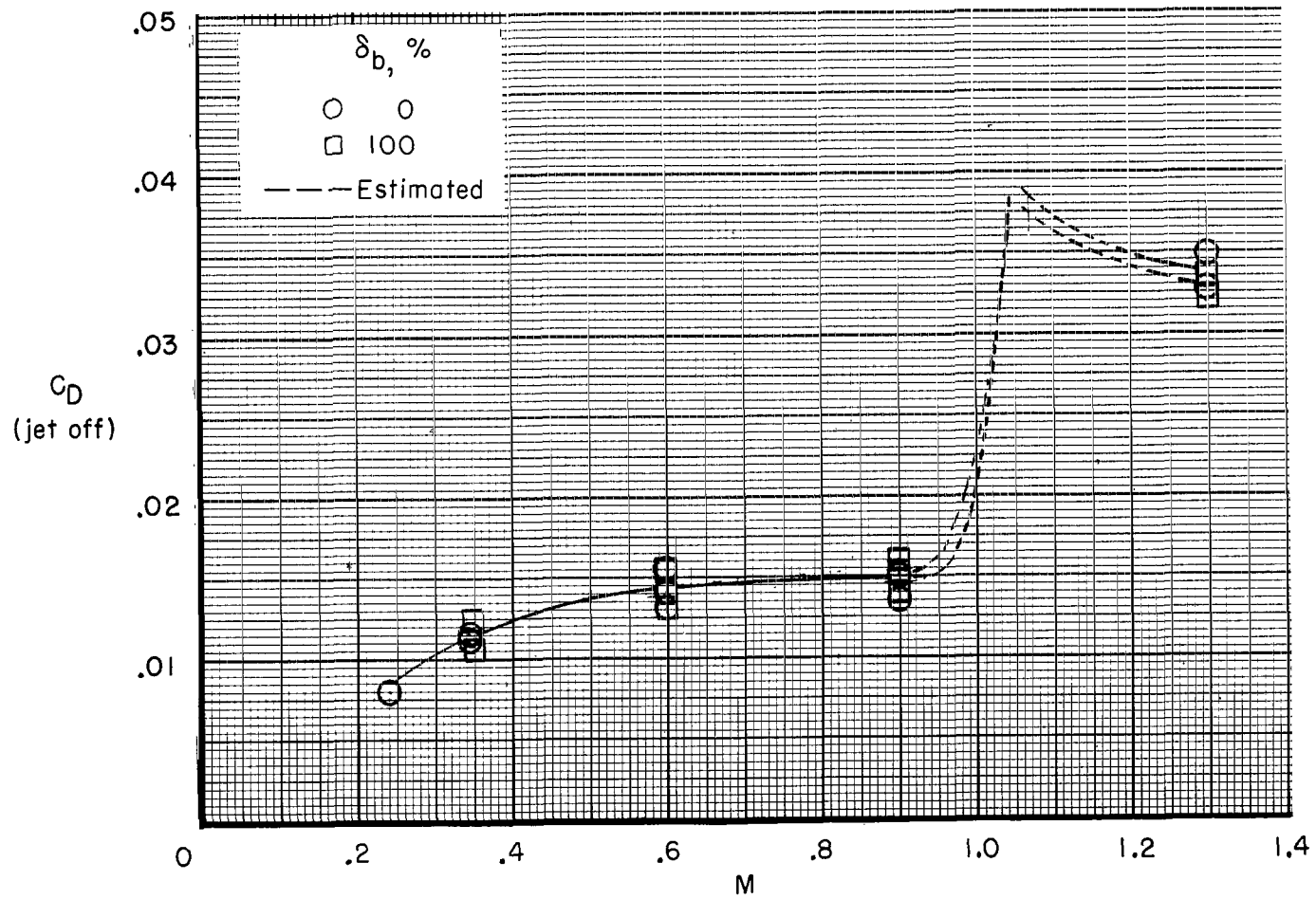
(a) $\delta_{du} = 43.5^\circ$; $\delta_{dl} = 43.5^\circ$; $\delta_b = 100\%$.

Figure 9.- Variation of jet-off, fuselage-tail drag coefficient for various TCU configurations at zero angle of attack and military power.



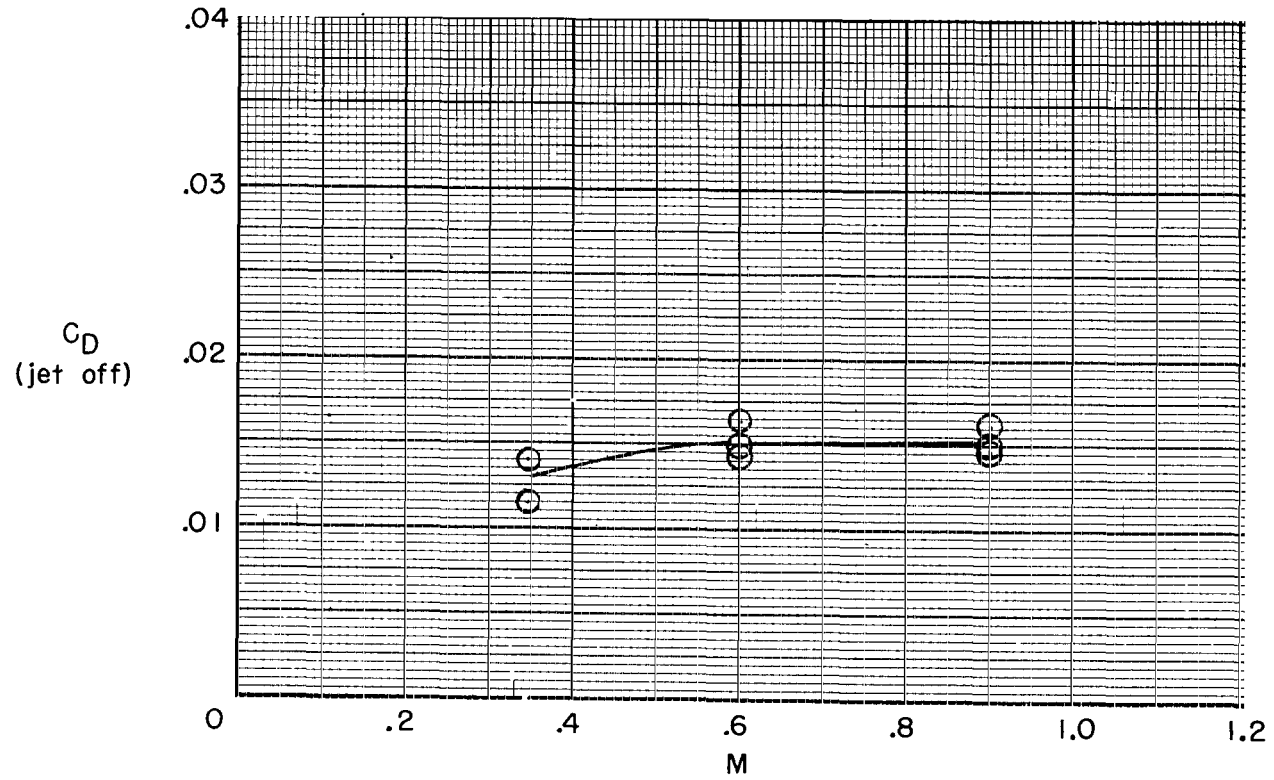
(b) $\delta_{du} = 60^\circ$; $\delta_{dl} = 60^\circ$; $\delta_b = 100\%$.

Figure 9.- Continued.



(c) $\delta_{du} = 32.5^\circ$; $\delta_{dl} = 52.5^\circ$.

Figure 9.- Continued.



(d) $\delta_{du} = 28.5^\circ$; $\delta_{dl} = 60^\circ$; $\delta_b = 100\%$.

Figure 9.- Concluded.

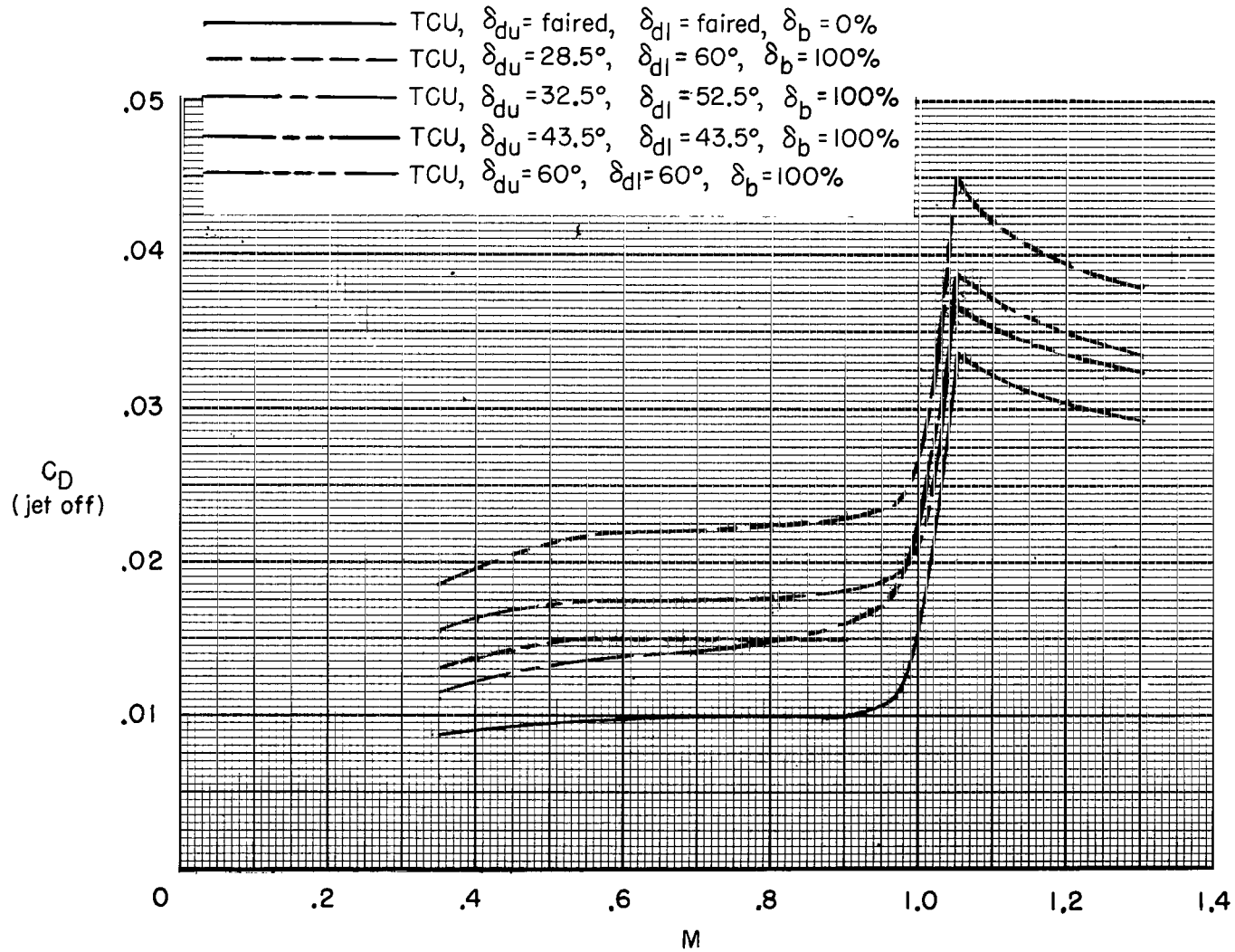


Figure 10.- Comparison of jet-off, fuselage-tail drag coefficient for various TCU configurations at zero angle of attack and military power.

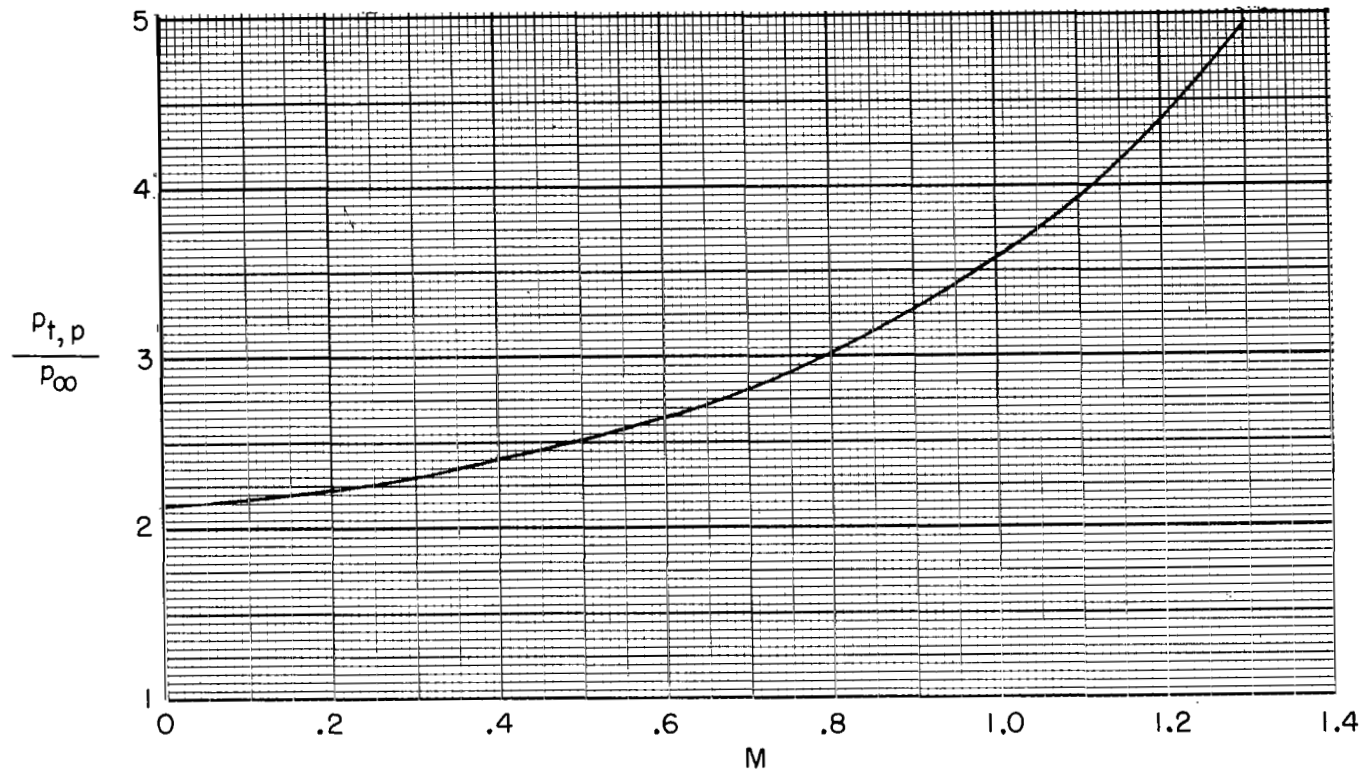


Figure 11.- Estimated engine-operating pressure-ratio schedule with Mach number for a turbojet engine for military and afterburning power.

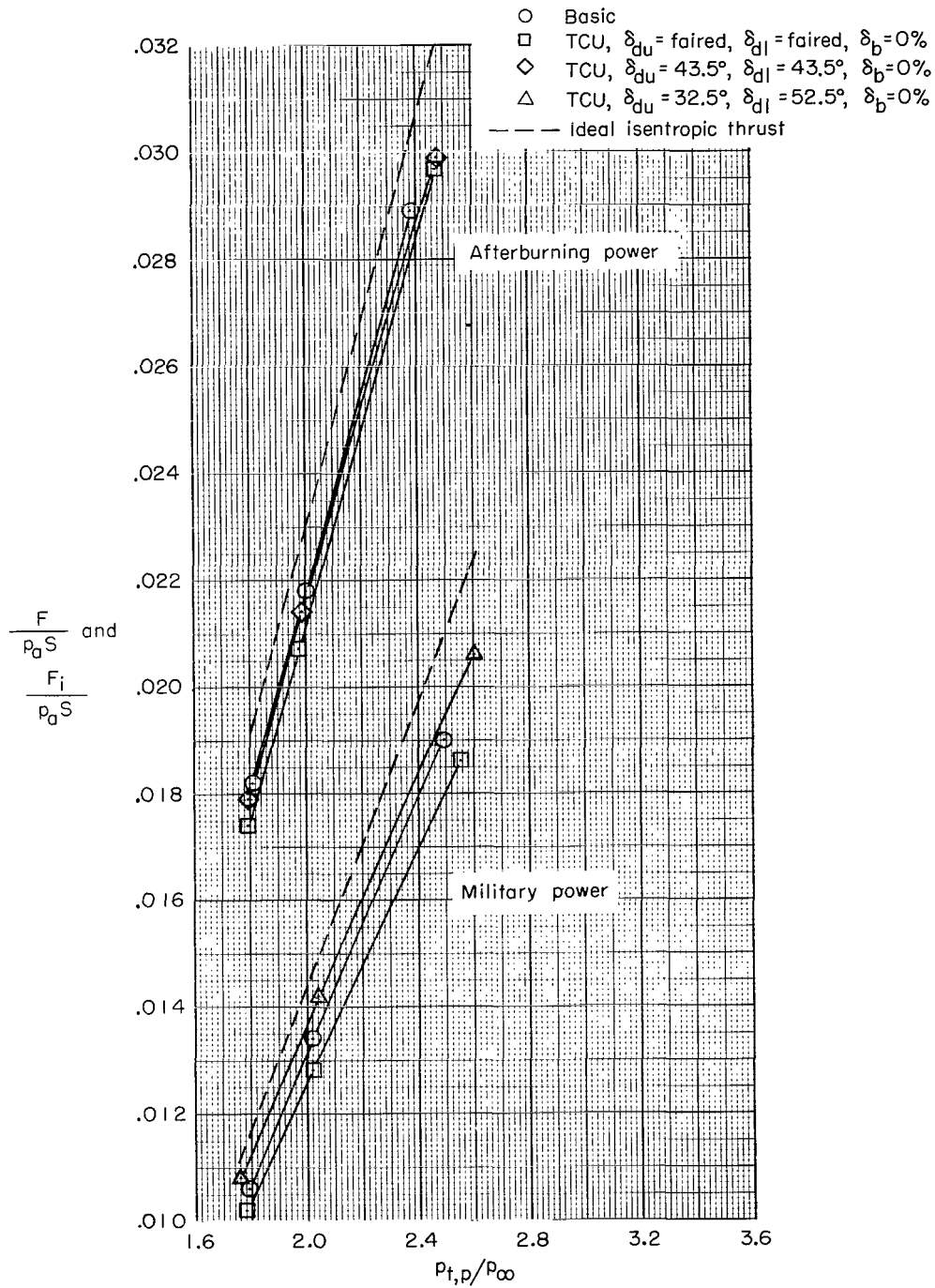


Figure 12.- A comparison of static forward-thrust coefficient for the TCU configuration and the basic configuration at several primary-nozzle-jet total-pressure ratios.

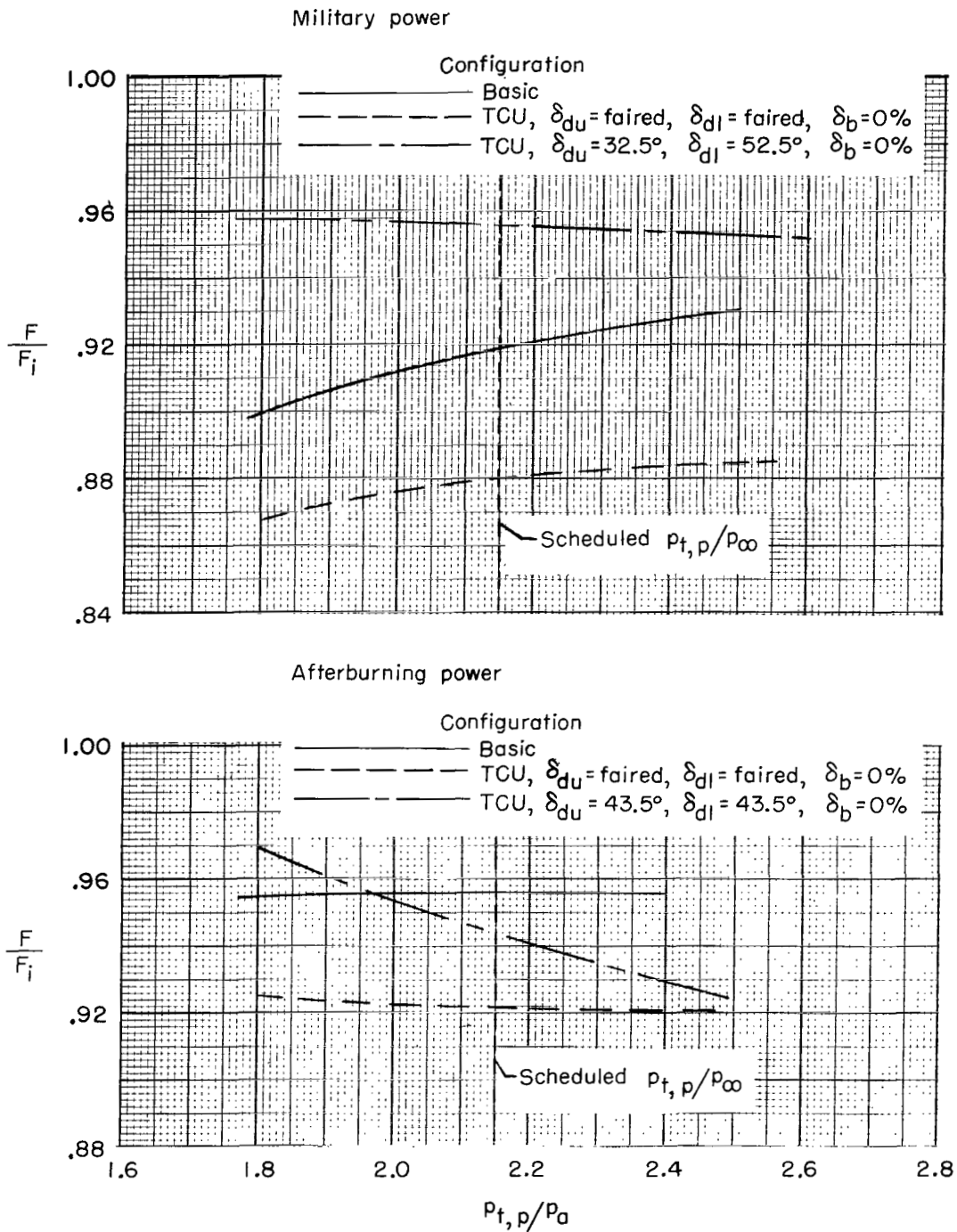
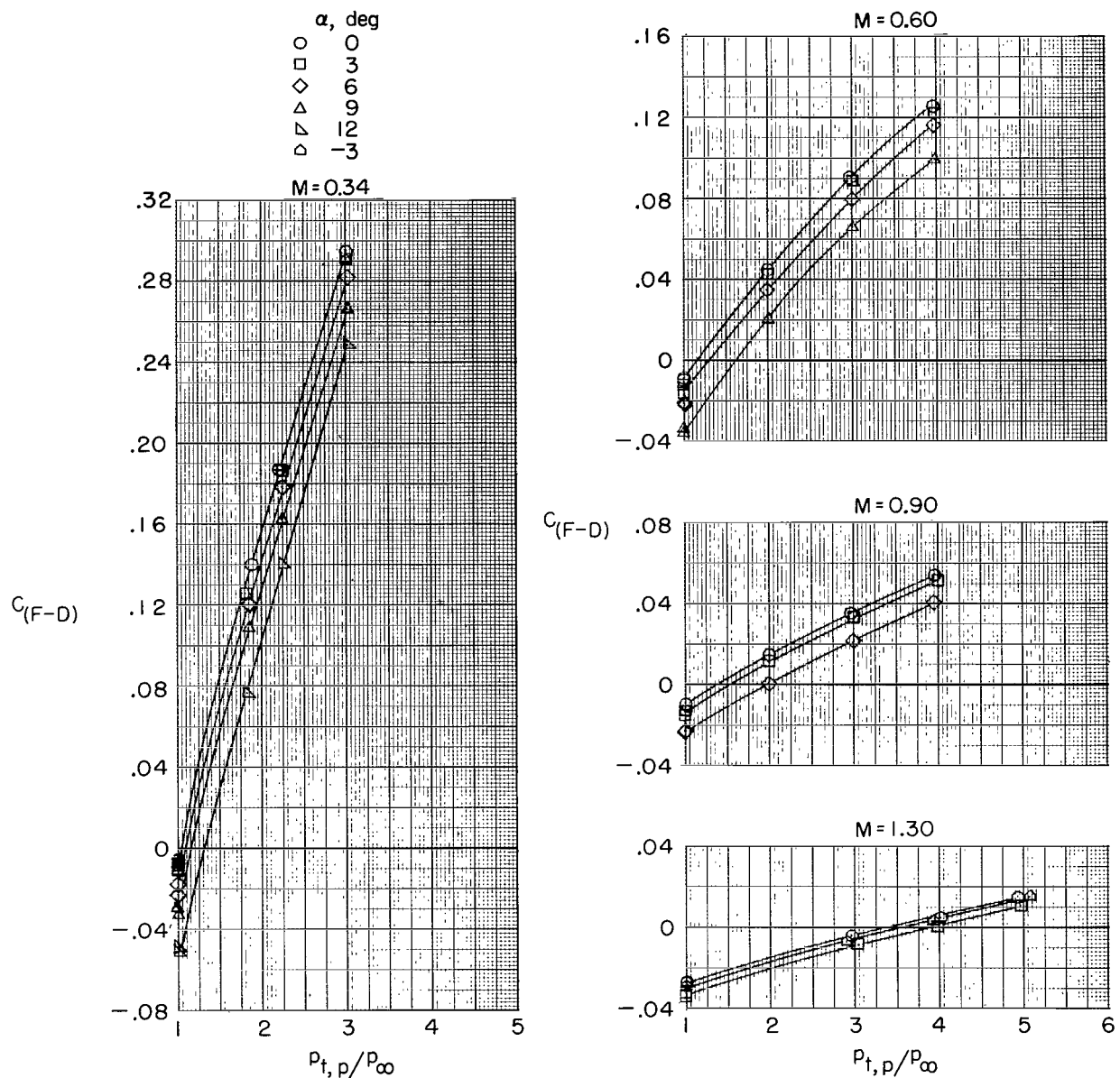
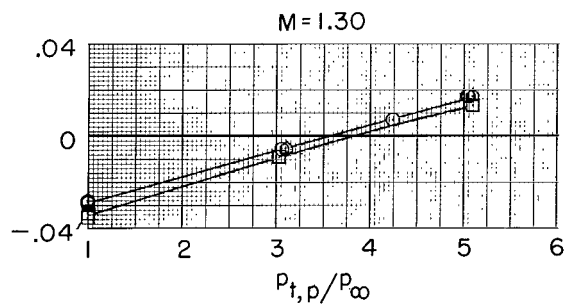
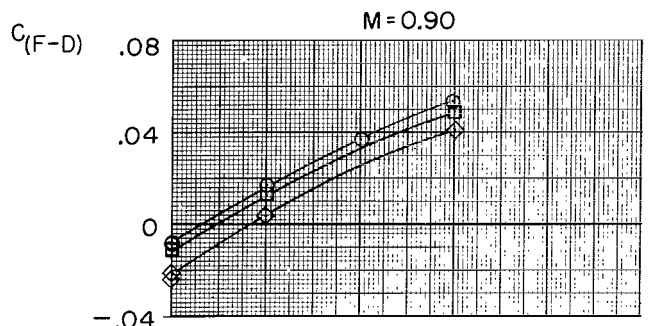
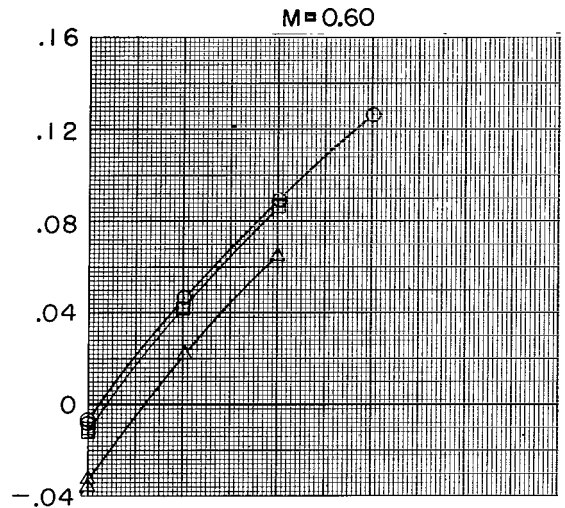
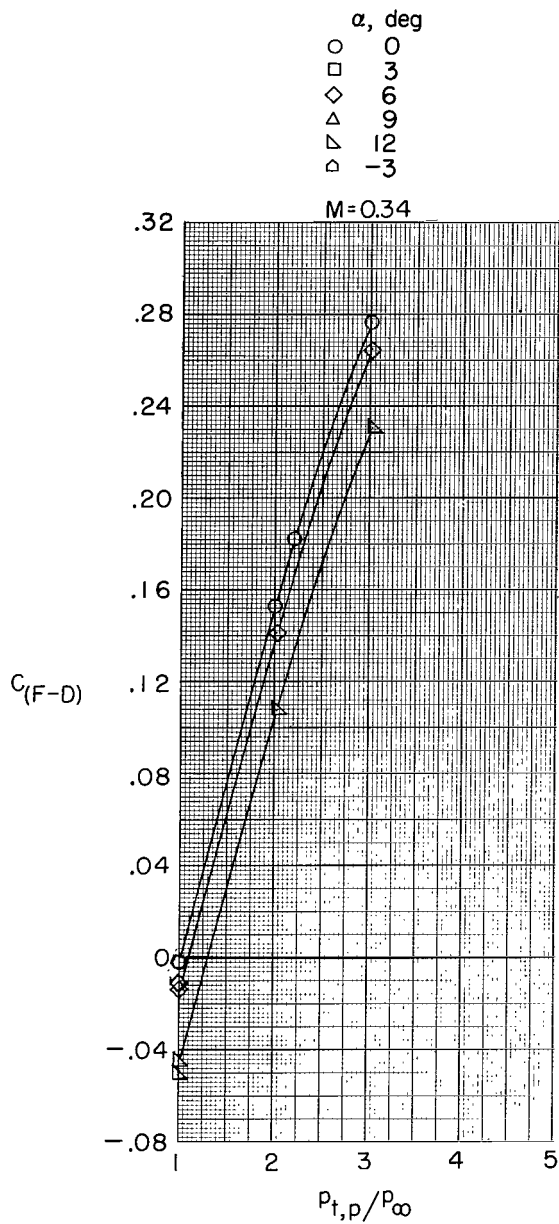


Figure 13.- Comparison of static thrust ratios of the basic and TCU configurations.



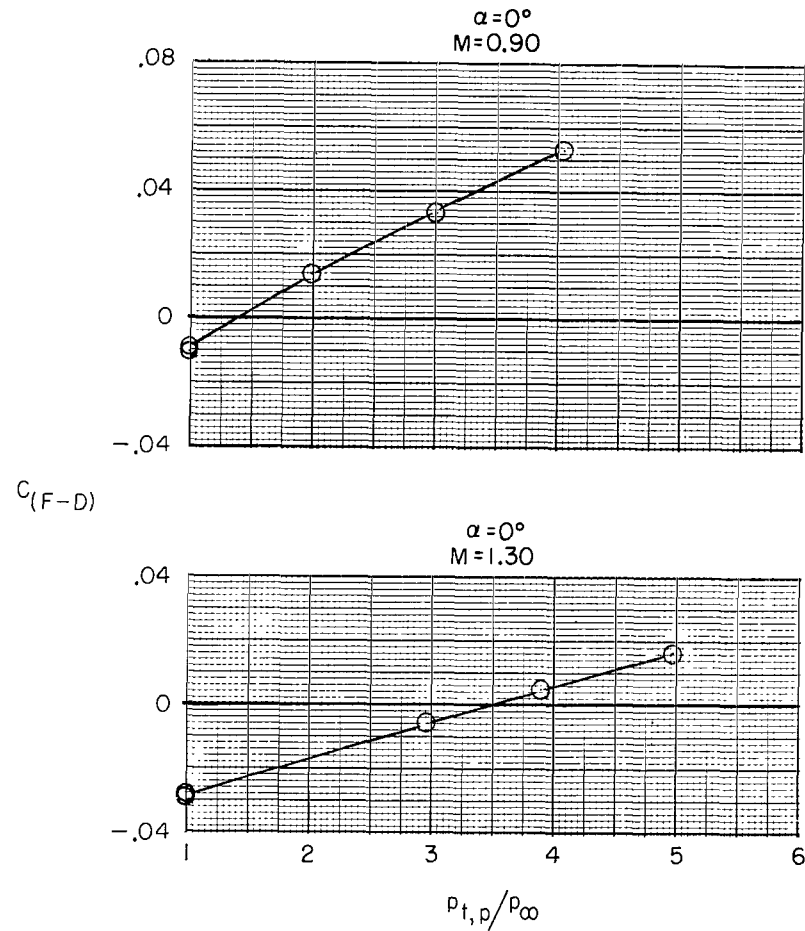
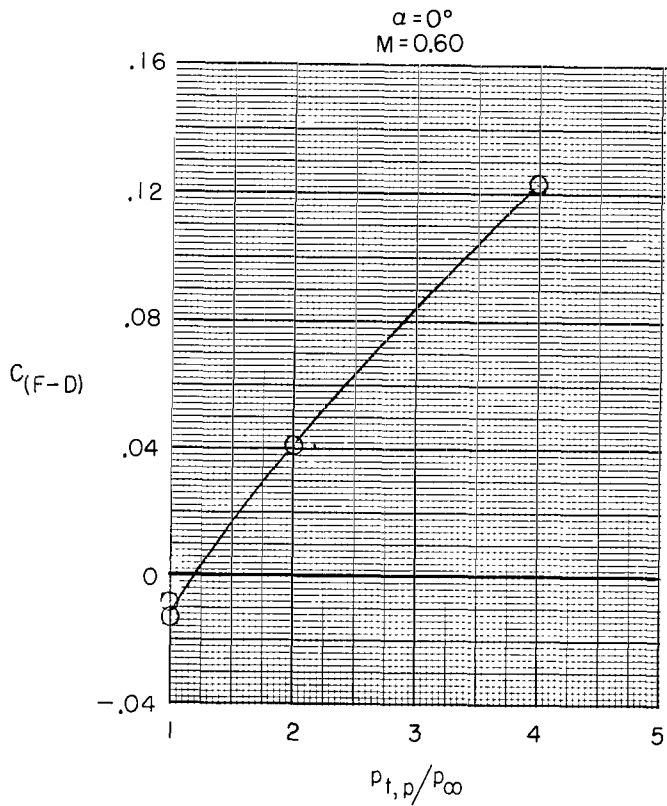
(a) Basic.

Figure 14.- Variation of thrust-minus-drag coefficient with primary-nozzle-jet total-pressure ratio for several angles of attack with military power.



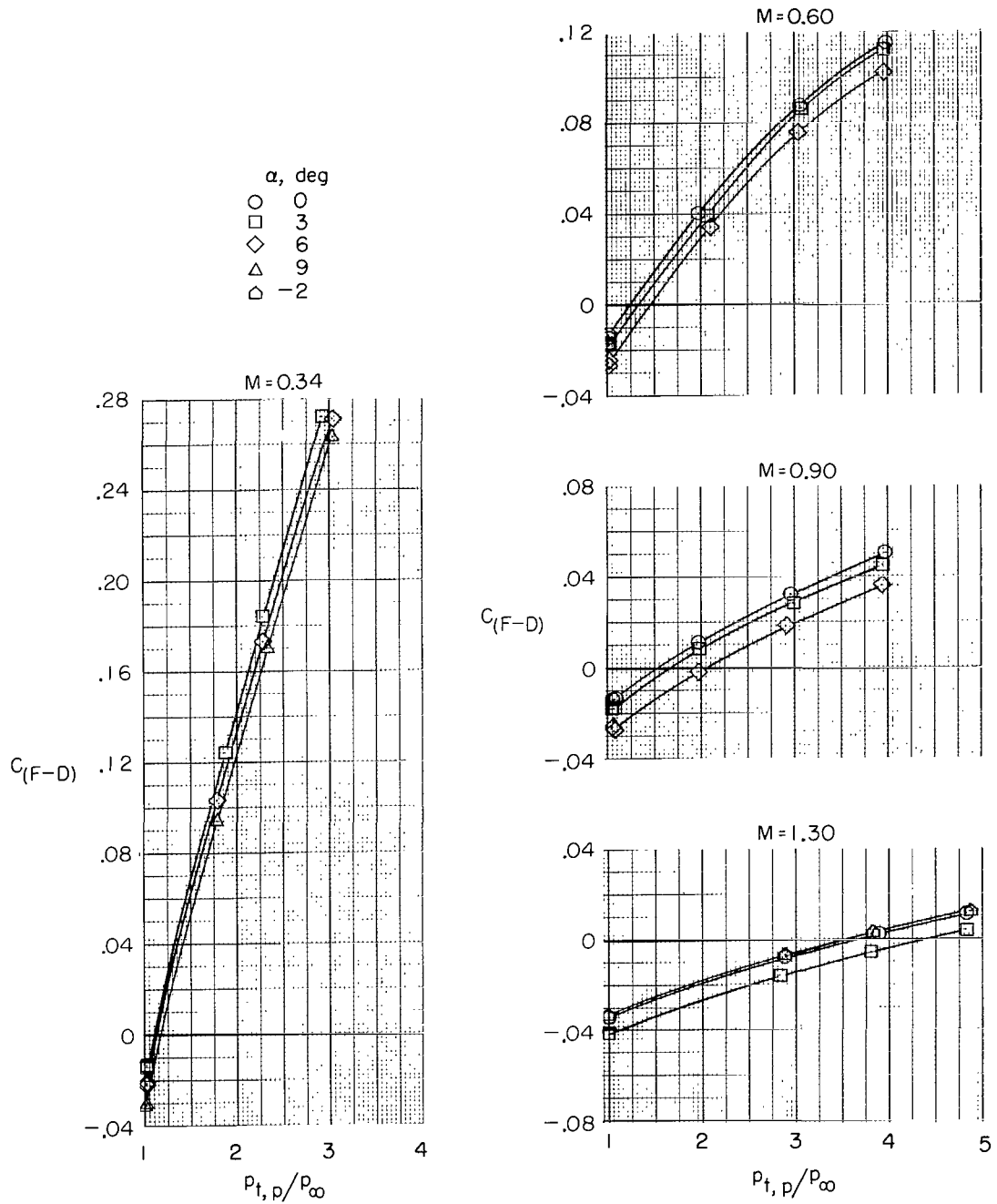
(b) TCU; $\delta_{du} = \text{Faired}$; $\delta_{dl} = \text{Faired}$; $\delta_b = 0\%$.

Figure 14.- Continued.



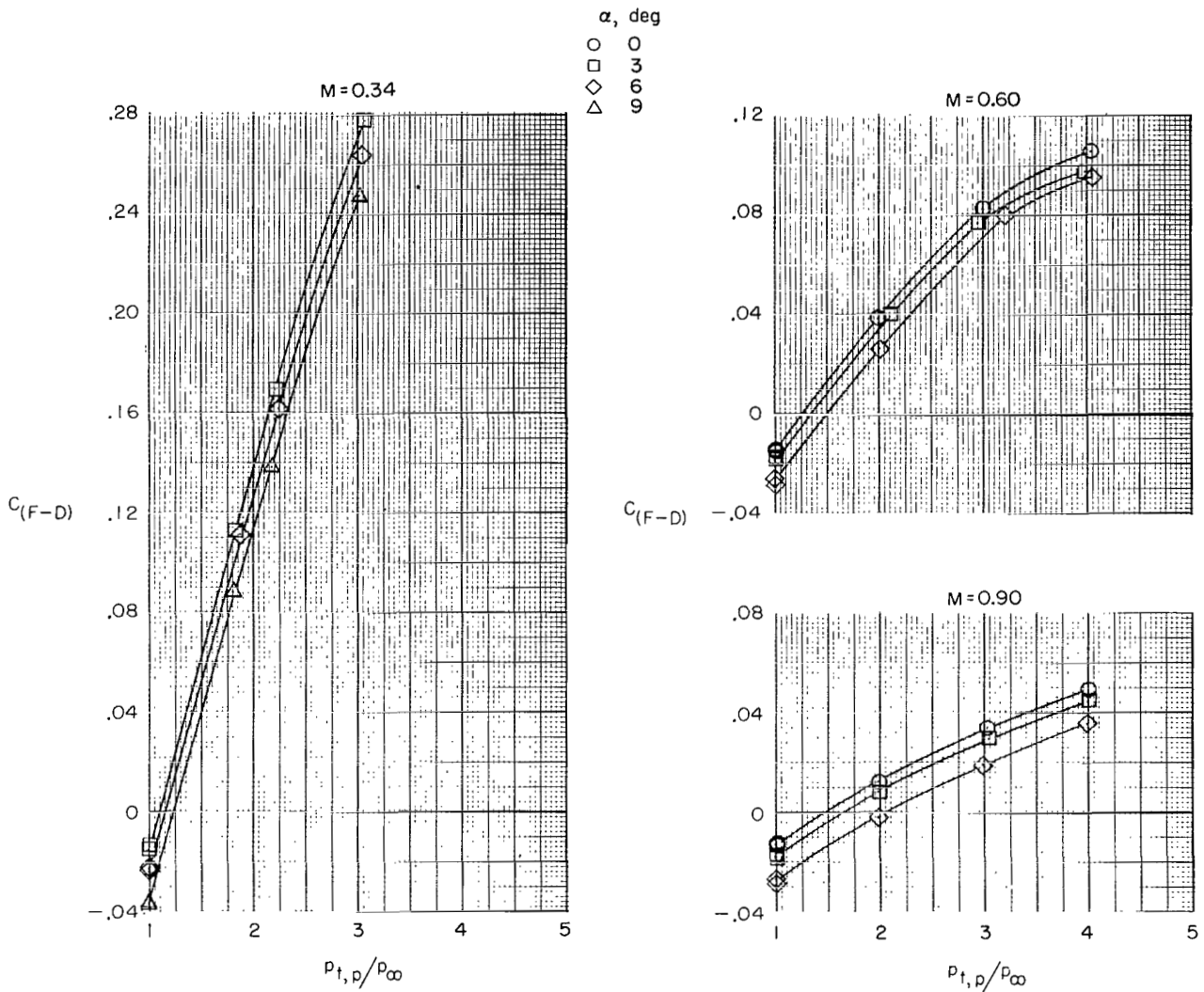
(c) TCU; $\delta_{du} = \text{Closed}$; $\delta_{dl} = \text{Closed}$; $\delta_b = 0\%$.

Figure 14.- Continued.



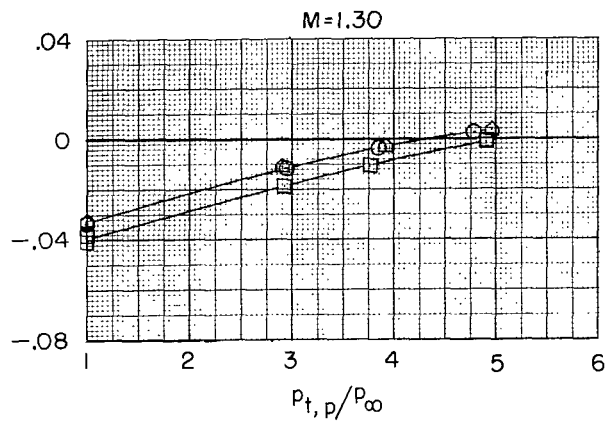
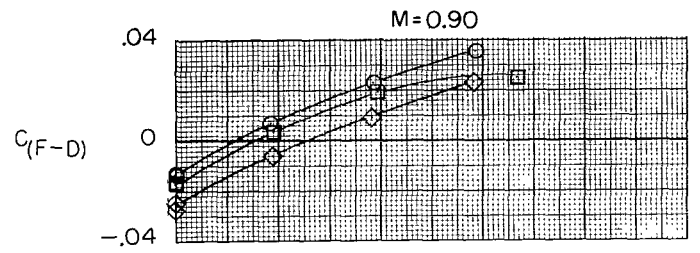
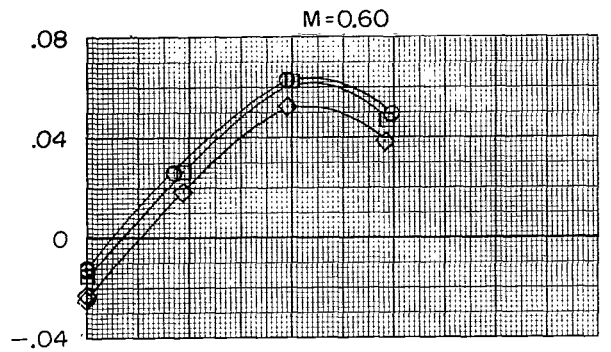
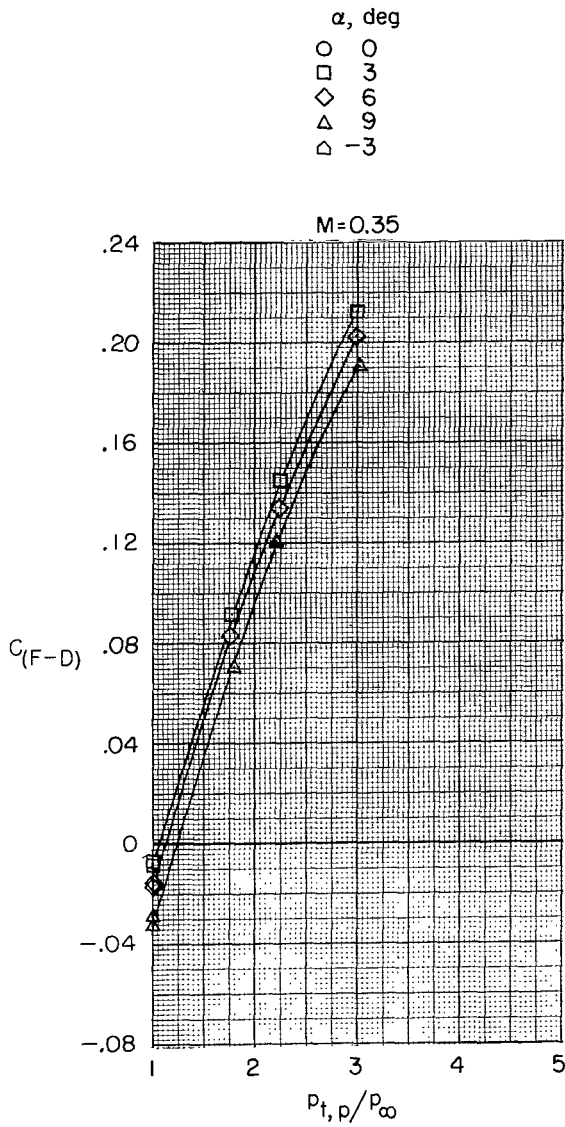
(d) TCU; $\delta_{du} = 32.5^\circ$; $\delta_{dl} = 52.5^\circ$; $\delta_b = 0\%$.

Figure 14.- Continued.



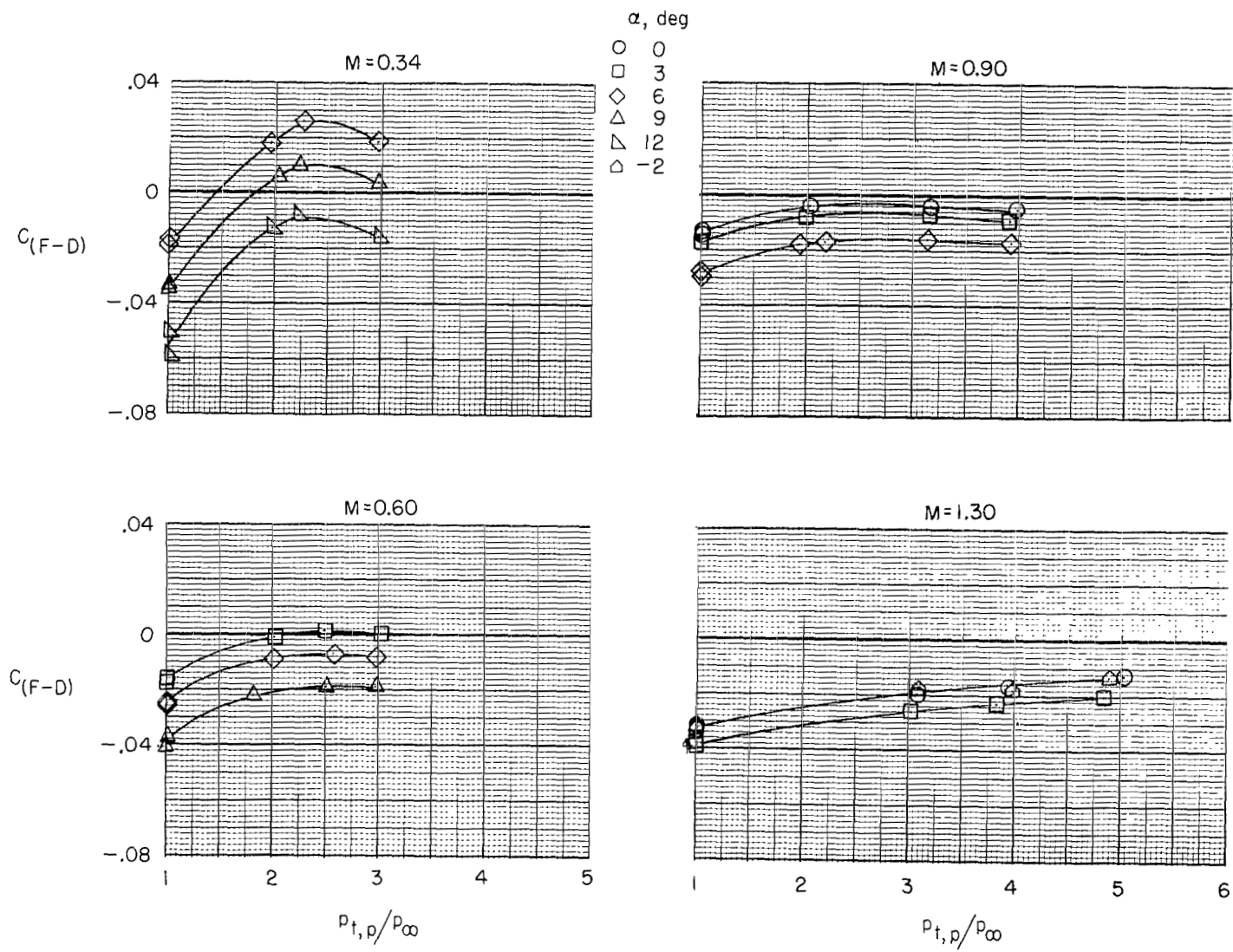
(e) TCU; $\delta_{du} = 32.5^\circ$; $\delta_{dl} = 52.5^\circ$; $\delta_b = 25\%$.

Figure 14.- Continued.



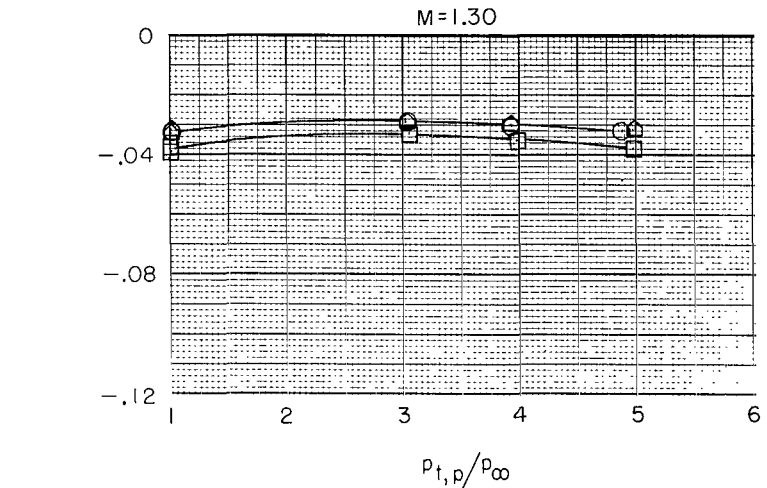
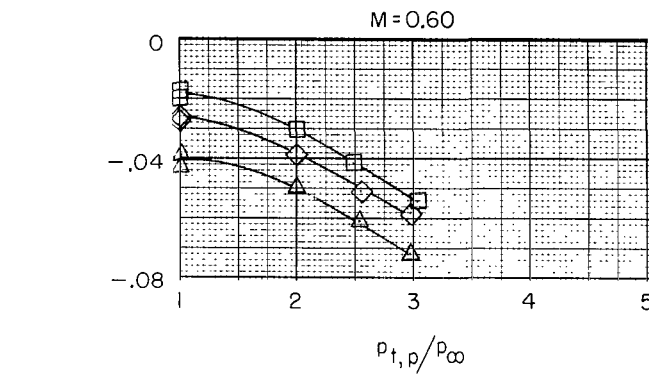
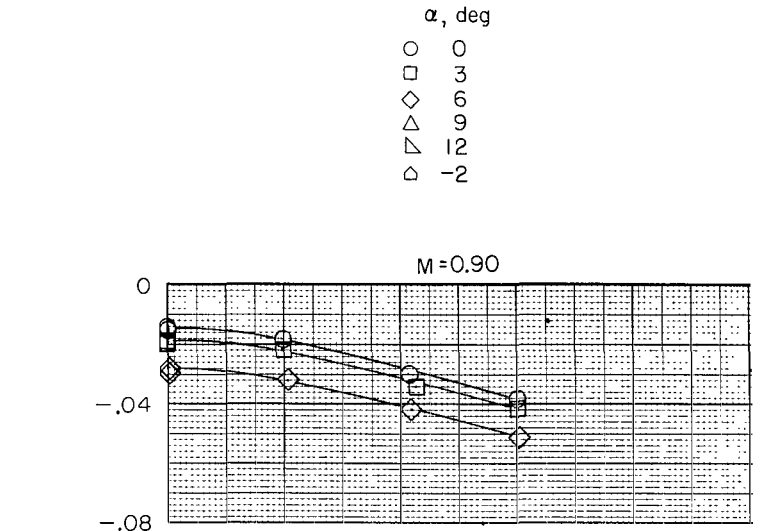
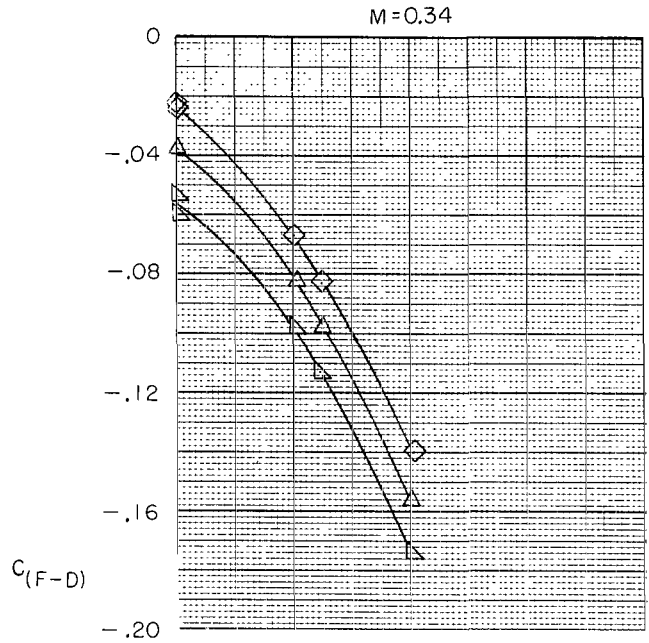
(f) TCU; $\delta_{du} = 32.5^\circ$; $\delta_{dl} = 52.5^\circ$; $\delta_b = 50\%$.

Figure 14.- Continued.



(g) TCU; $\delta_{du} = 32.5^{\circ}$; $\delta_{dl} = 52.5^{\circ}$; $\delta_b = 75\%$.

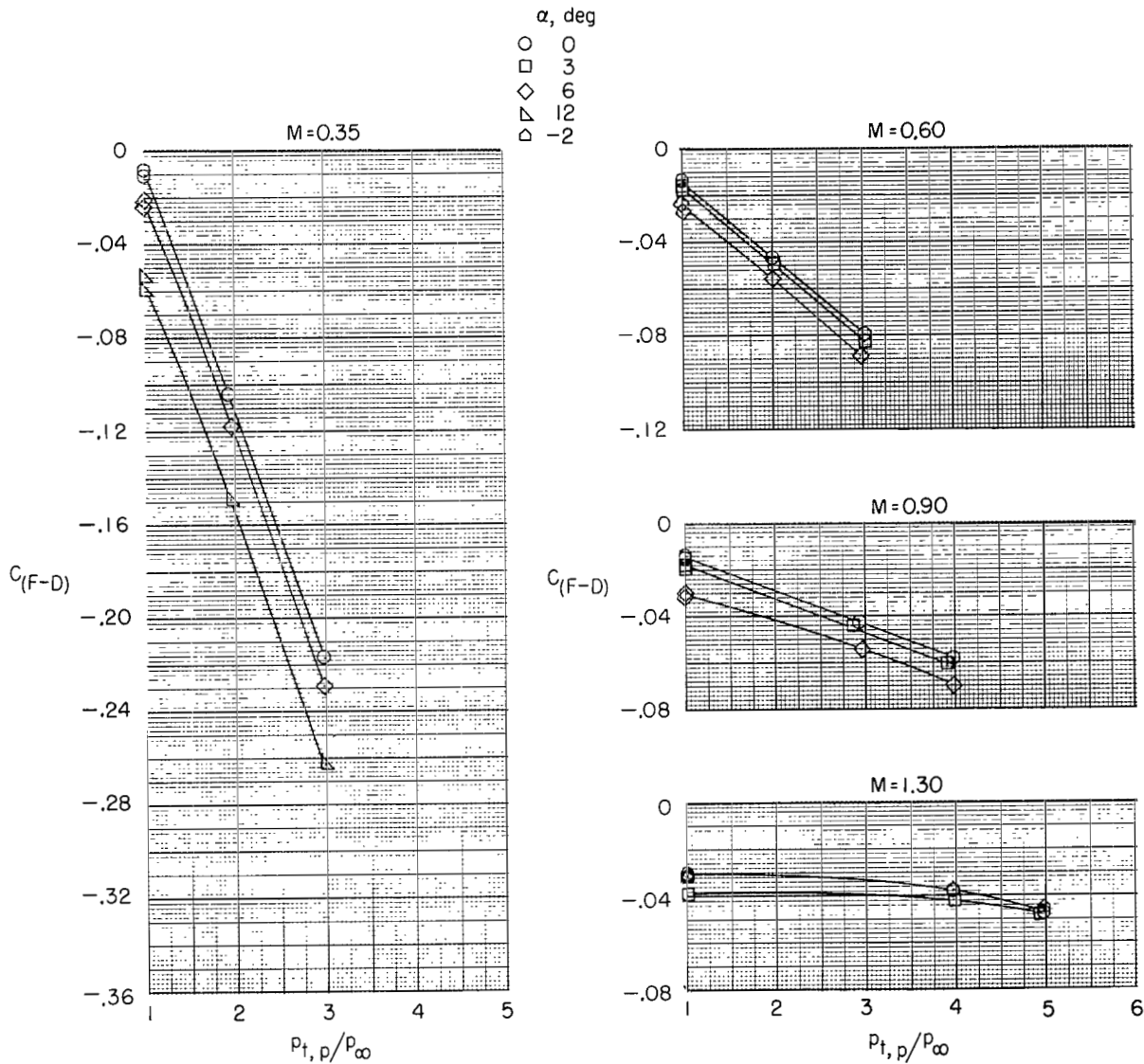
Figure 14.- Continued.



- α , deg
- 0
 - 3
 - ◇ 6
 - △ 9
 - ▽ 12
 - ◁ -2

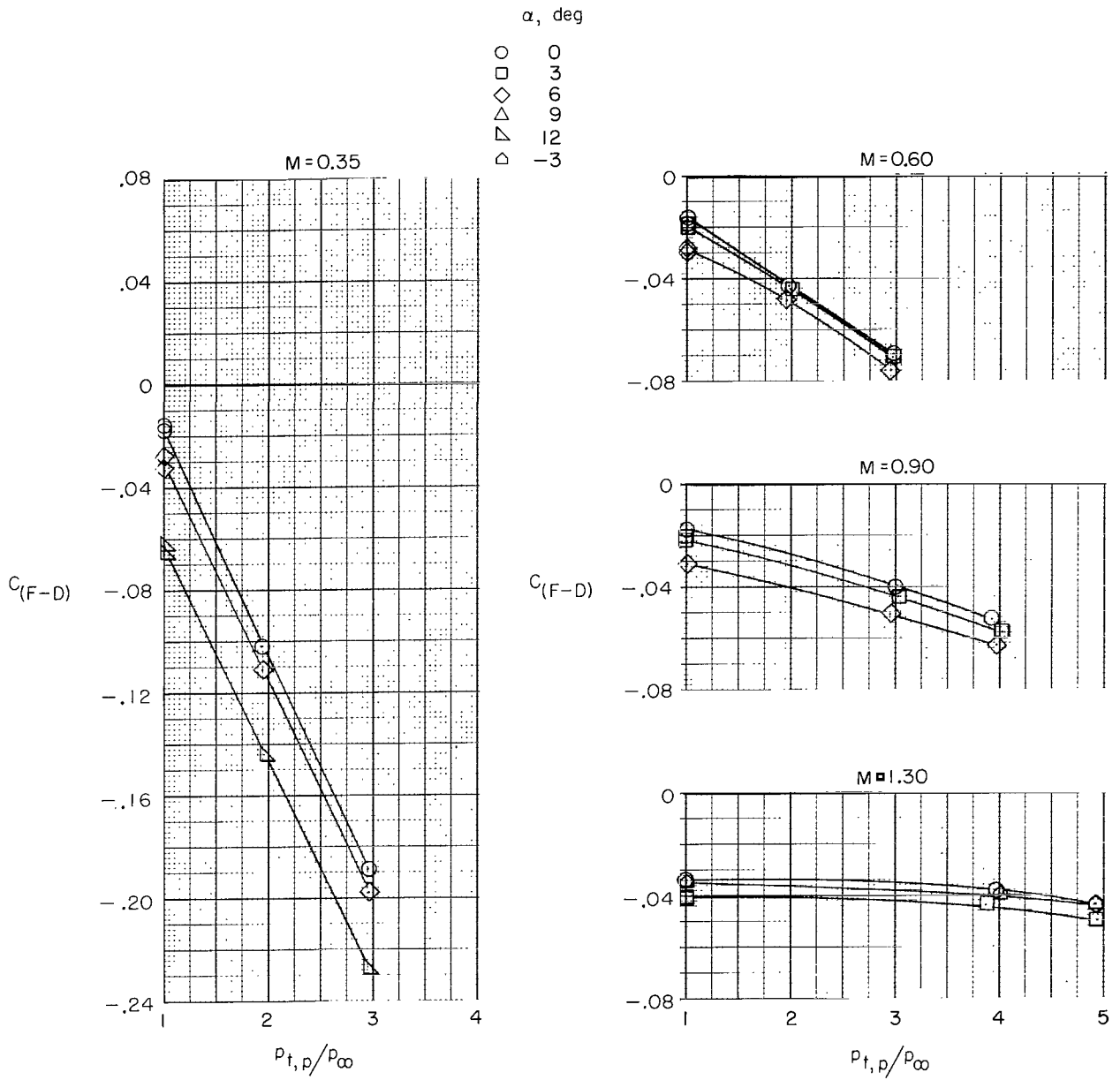
(h) TCU; $\delta_{du} = 32.5^\circ$; $\delta_{dl} = 52.5^\circ$; $\delta_b = 90\%$.

Figure 14.- Continued.



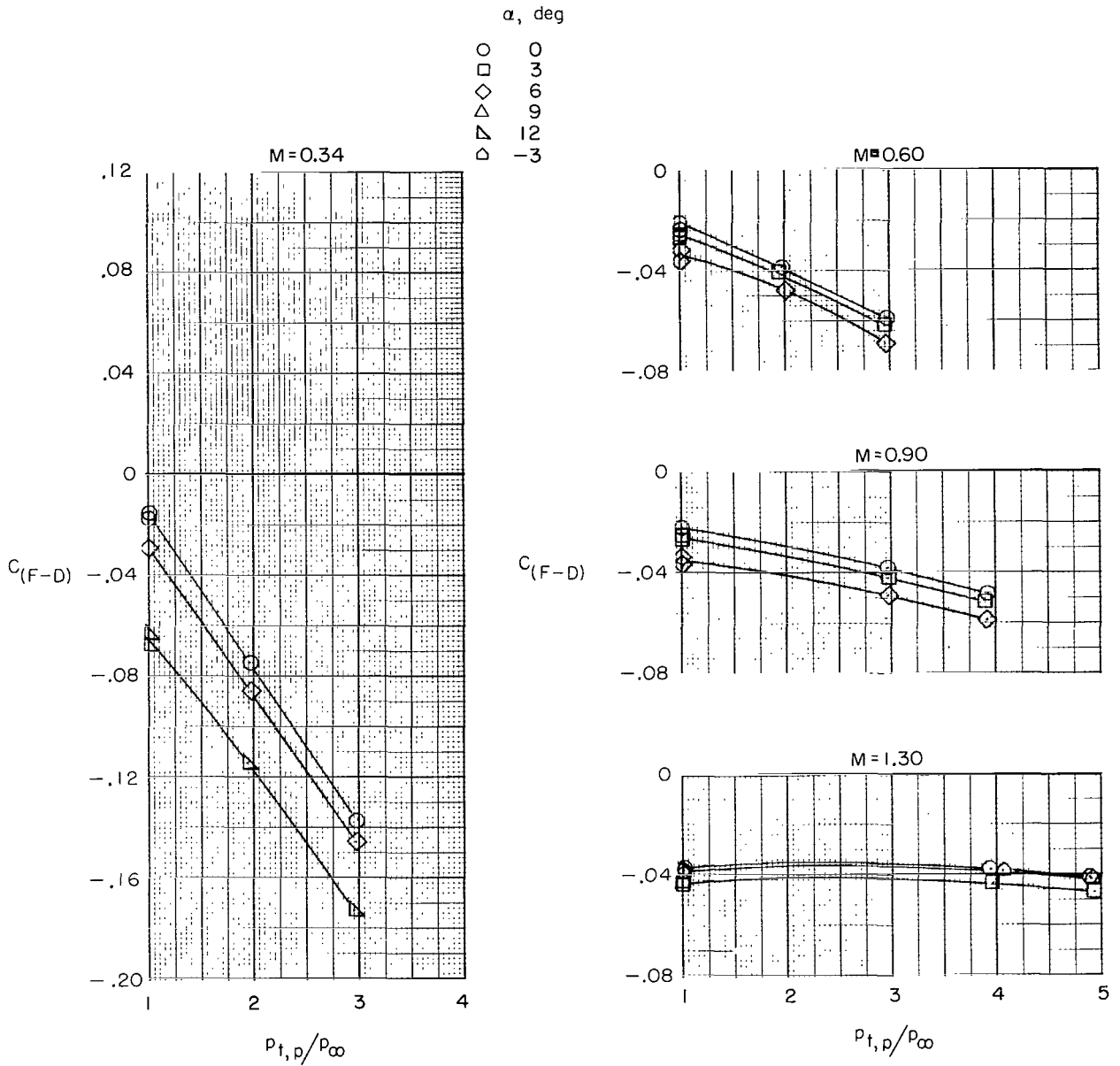
(i) TCU; $\delta_{du} = 32.5^\circ$; $\delta_{dl} = 52.5^\circ$; $\delta_b = 100\%$.

Figure 14.- Continued.



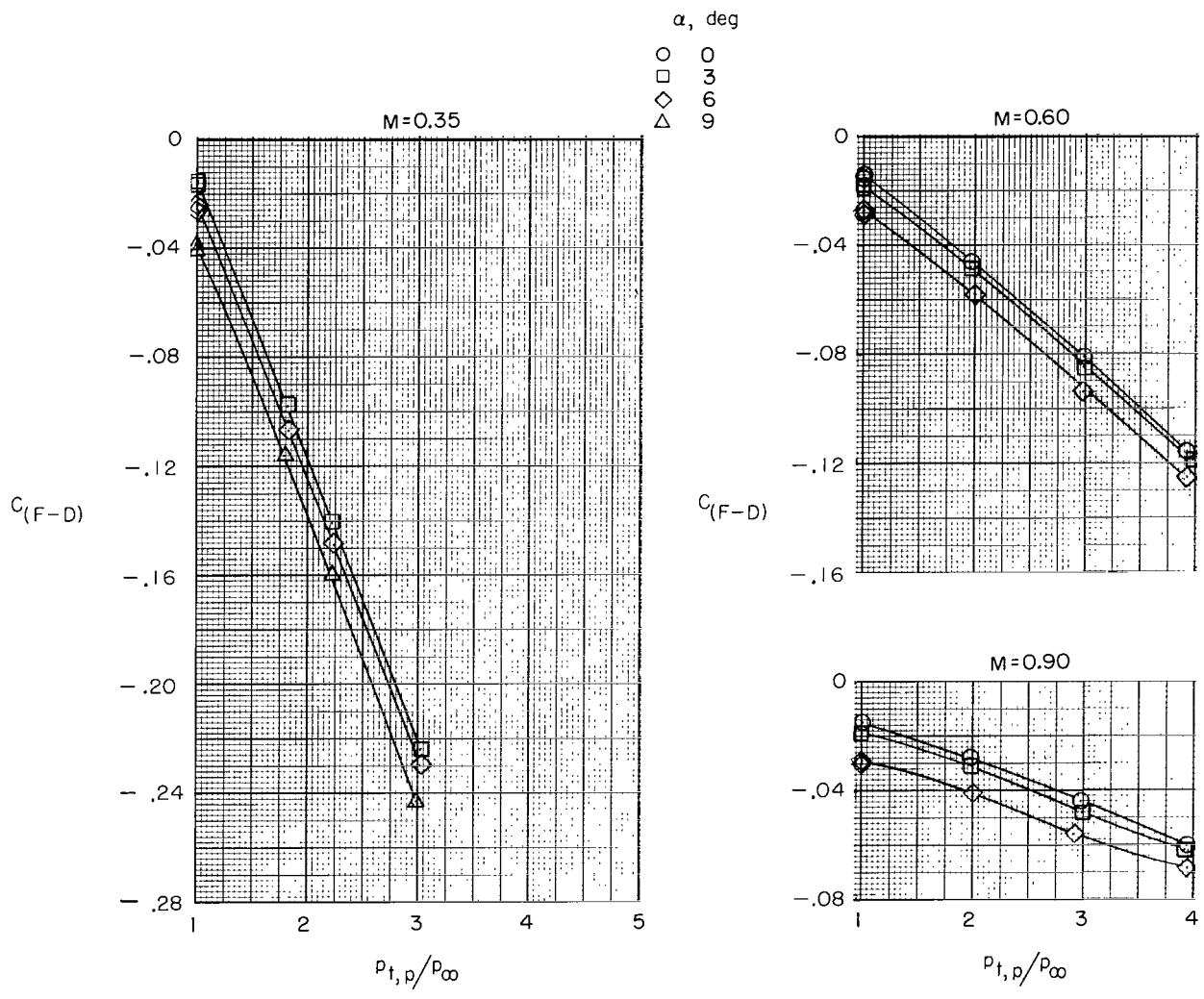
(j) TCU; $\delta_{du} = 43.5^{\circ}$; $\delta_{dl} = 43.5^{\circ}$; $\delta_b = 100\%$.

Figure 14.- Continued.



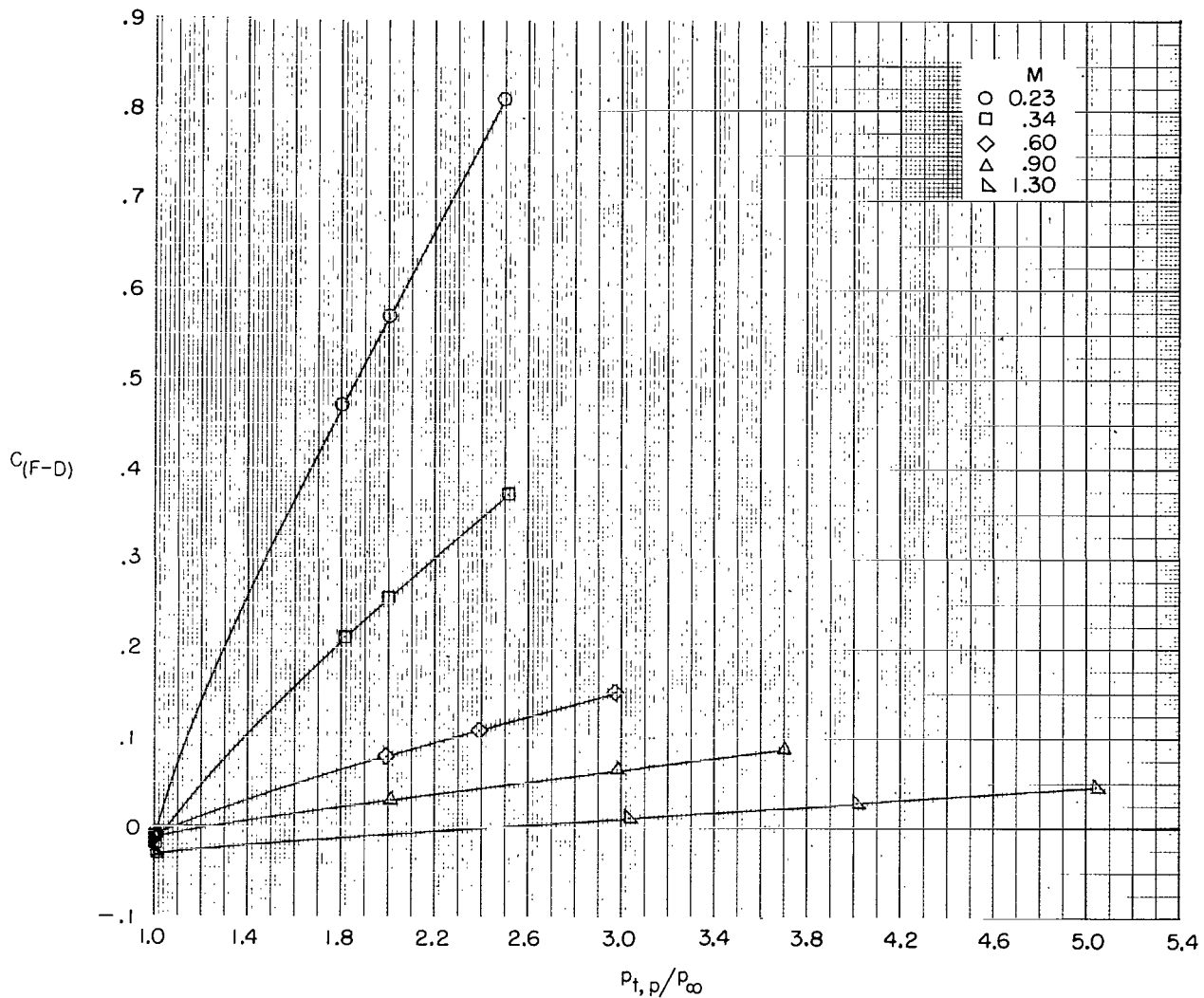
(k) TCU; $\delta_{du} = 60^\circ$; $\delta_{dl} = 60^\circ$; $\delta_b = 100\%$.

Figure 14.- Continued.



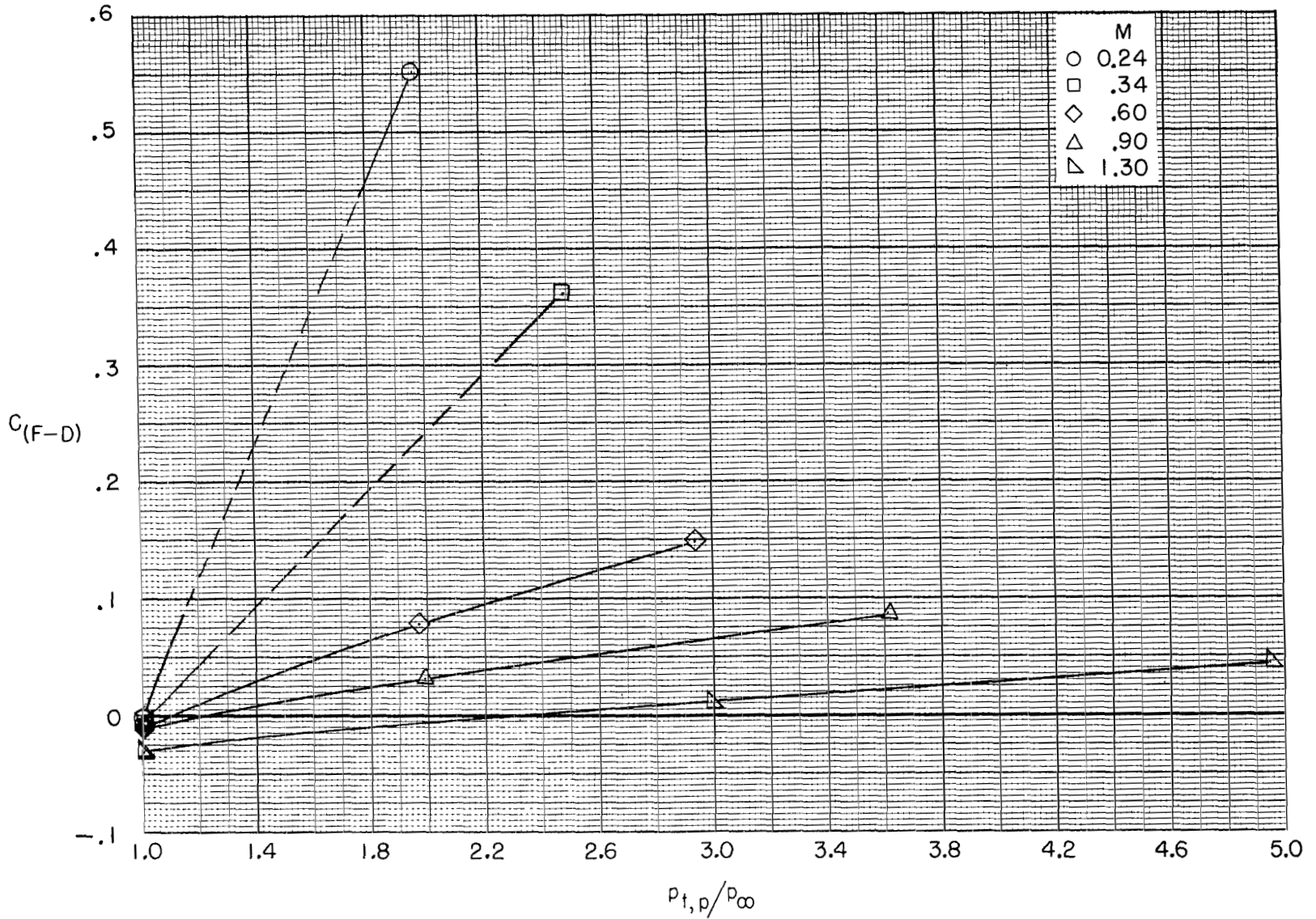
(1) $\delta_{du} = 28.5^\circ$; $\delta_{dl} = 60^\circ$; $\delta_b = 100\%$.

Figure 14.- Concluded.



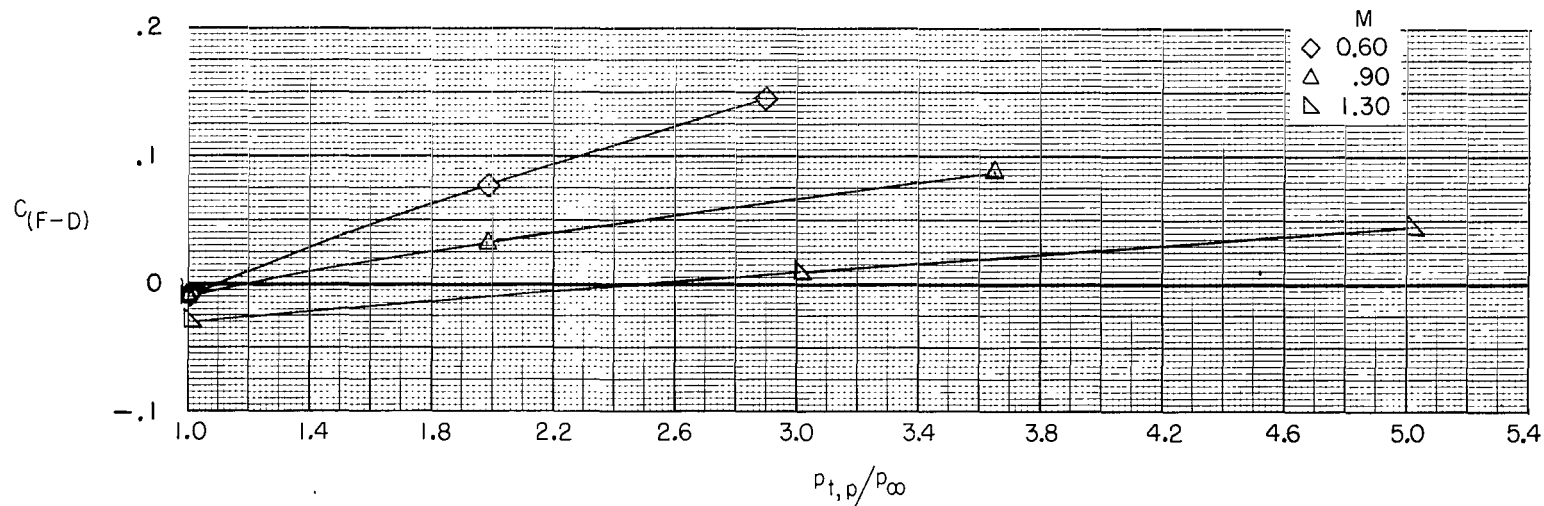
(a) Basic.

Figure 15.- Variation of thrust-minus-drag coefficient with primary-nozzle-jet total-pressure ratio for zero angle of attack and with afterburning power.



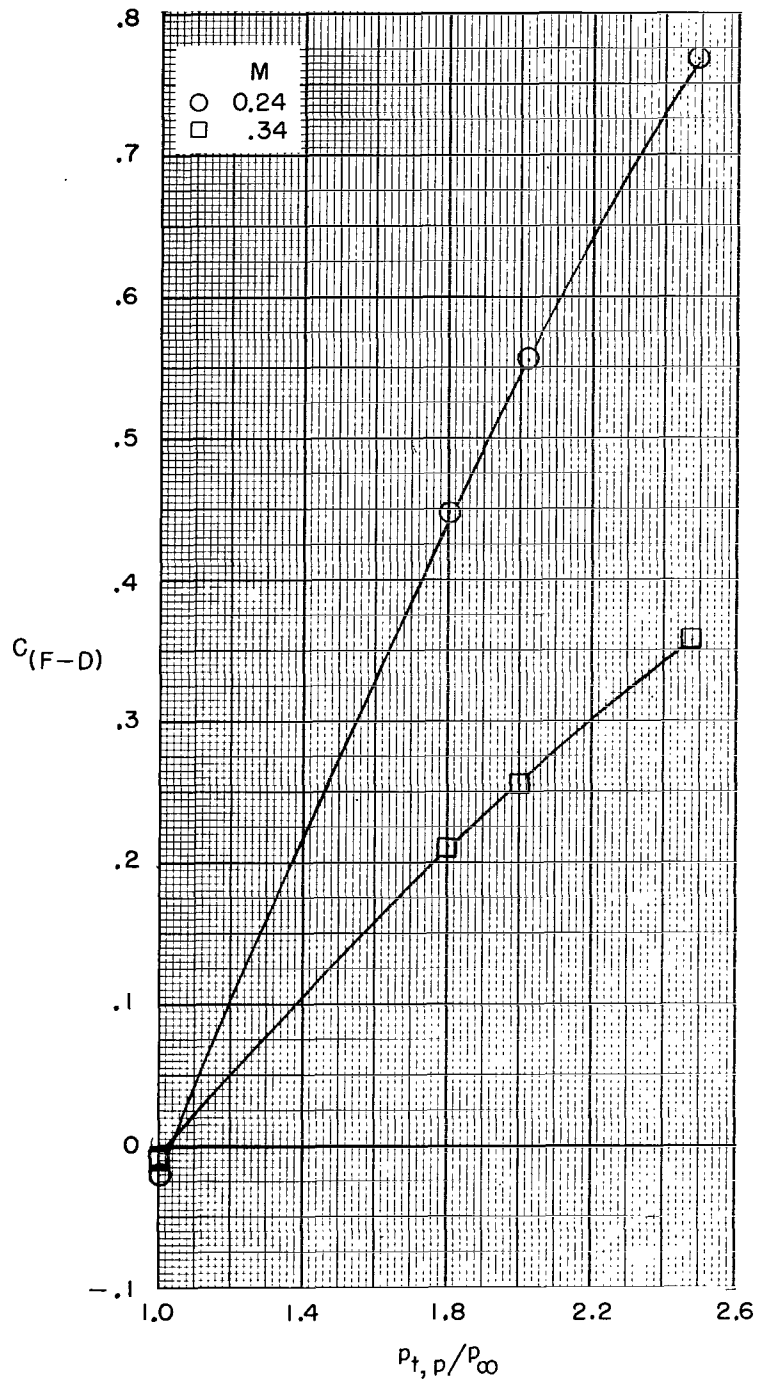
(b) TCU; $\delta_{du} = \text{Faired}$; $\delta_{dl} = \text{Faired}$; $\delta_b = 0\%$.

Figure 15.- Continued.



(c) $\delta_{du} = \text{Closed}$; $\delta_{dl} = \text{Closed}$; $\delta_b = 0\%$.

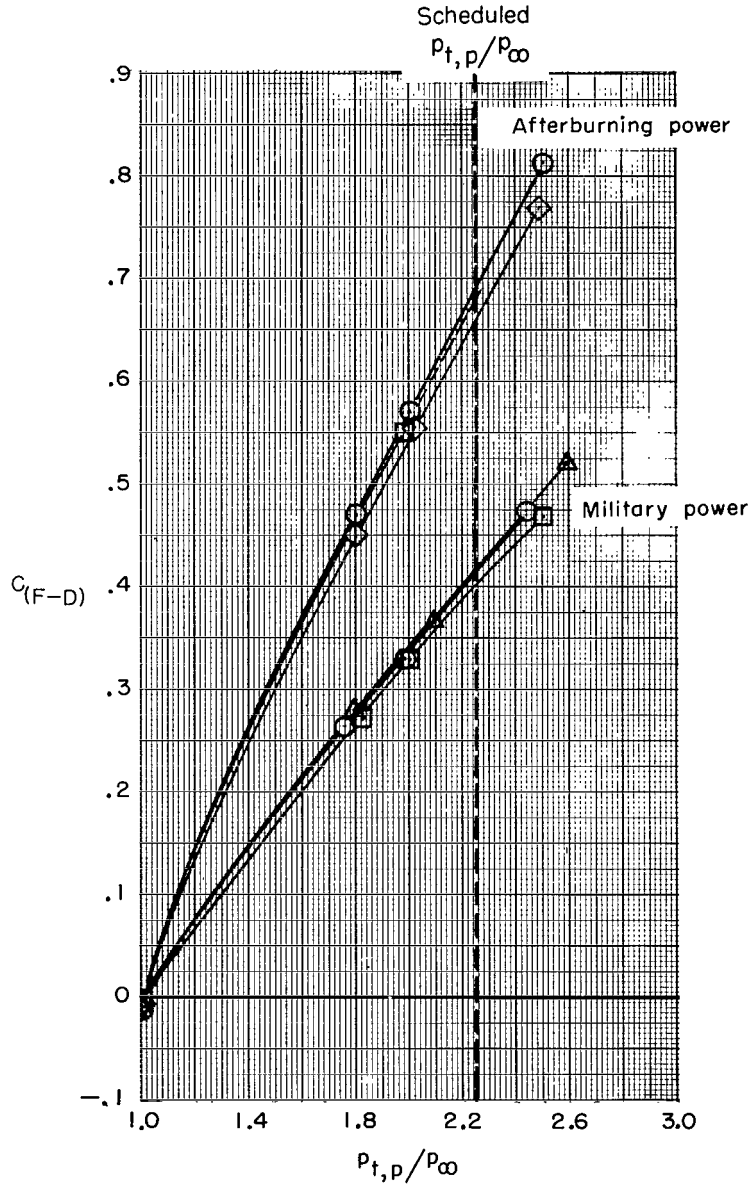
Figure 15.- Continued.



(d) $\delta_{du} = 43.5^{\circ}$; $\delta_{dl} = 43.5^{\circ}$; $\delta_b = 0\%$.

Figure 15.- Concluded.

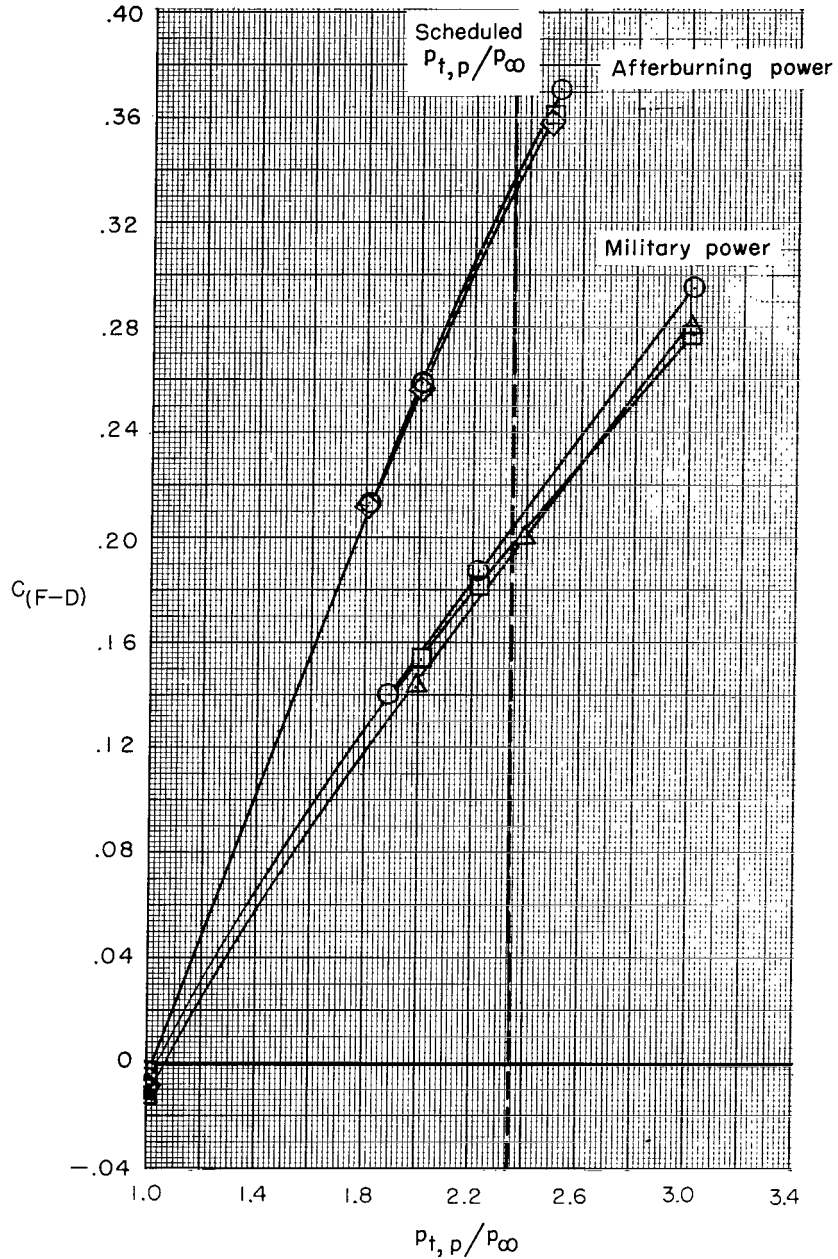
- Basic
- TCU, δ_{du} and δ_{dl} = faired
- ◇ TCU, $\delta_{du} = 43.5^\circ$ and $\delta_{dl} = 43.5^\circ$
- △ TCU, $\delta_{du} = 32.5^\circ$ and $\delta_{dl} = 52.5^\circ$



(a) $M = 0.23$.

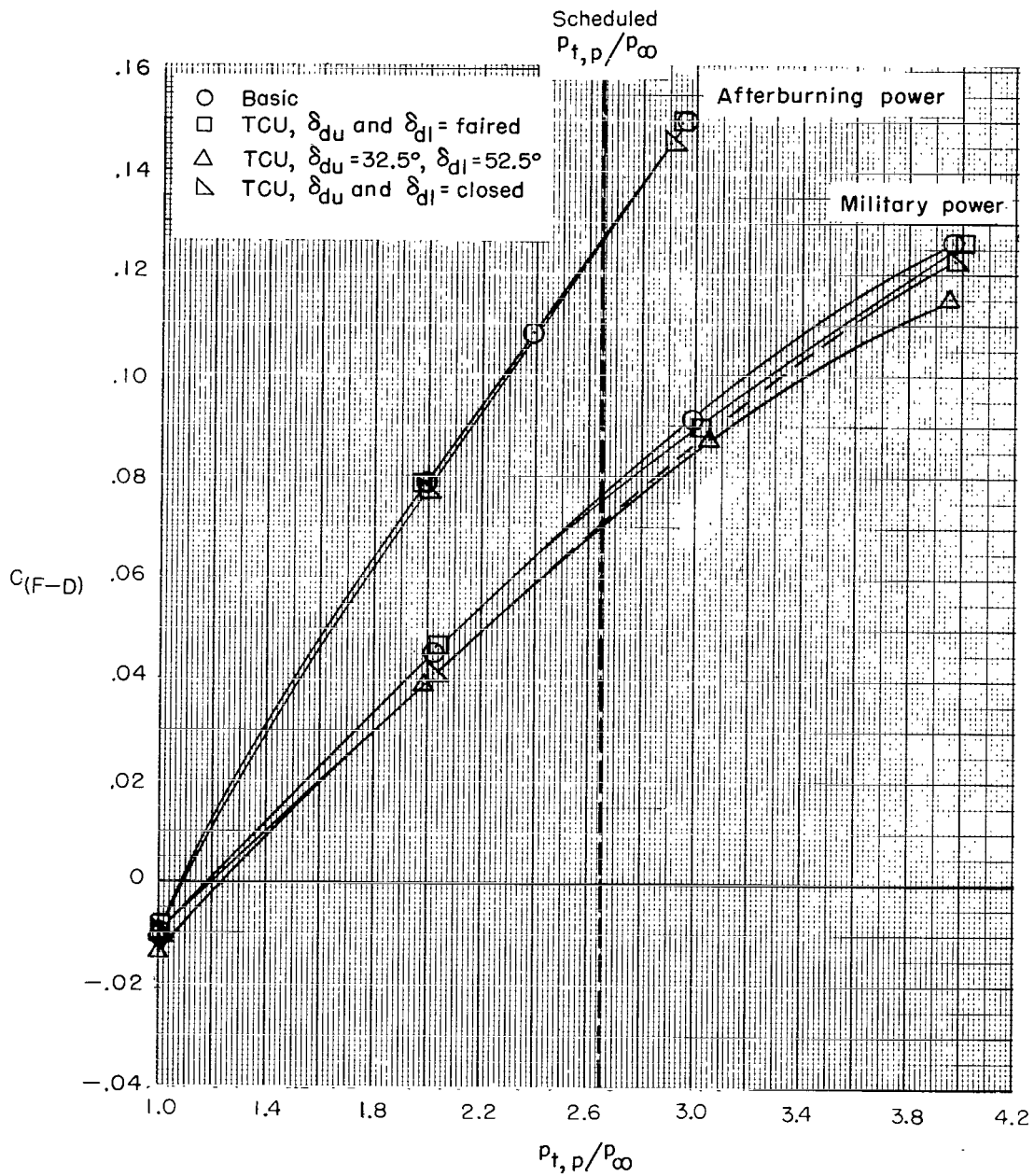
Figure 16.- A comparison of the thrust-minus-drag coefficient for the basic configuration with that for the TCU configuration in the forward-thrust mode. $\delta_b = 0^\circ$; $\alpha = 0^\circ$.

- Basic
- TCU, δ_{du} and δ_{dl} = faired
- ◇ TCU, $\delta_{du} = 43.5^\circ$ and $\delta_{dl} = 43.5^\circ$
- △ TCU, $\delta_{du} = 32.5^\circ$ and $\delta_{dl} = 52.5^\circ$



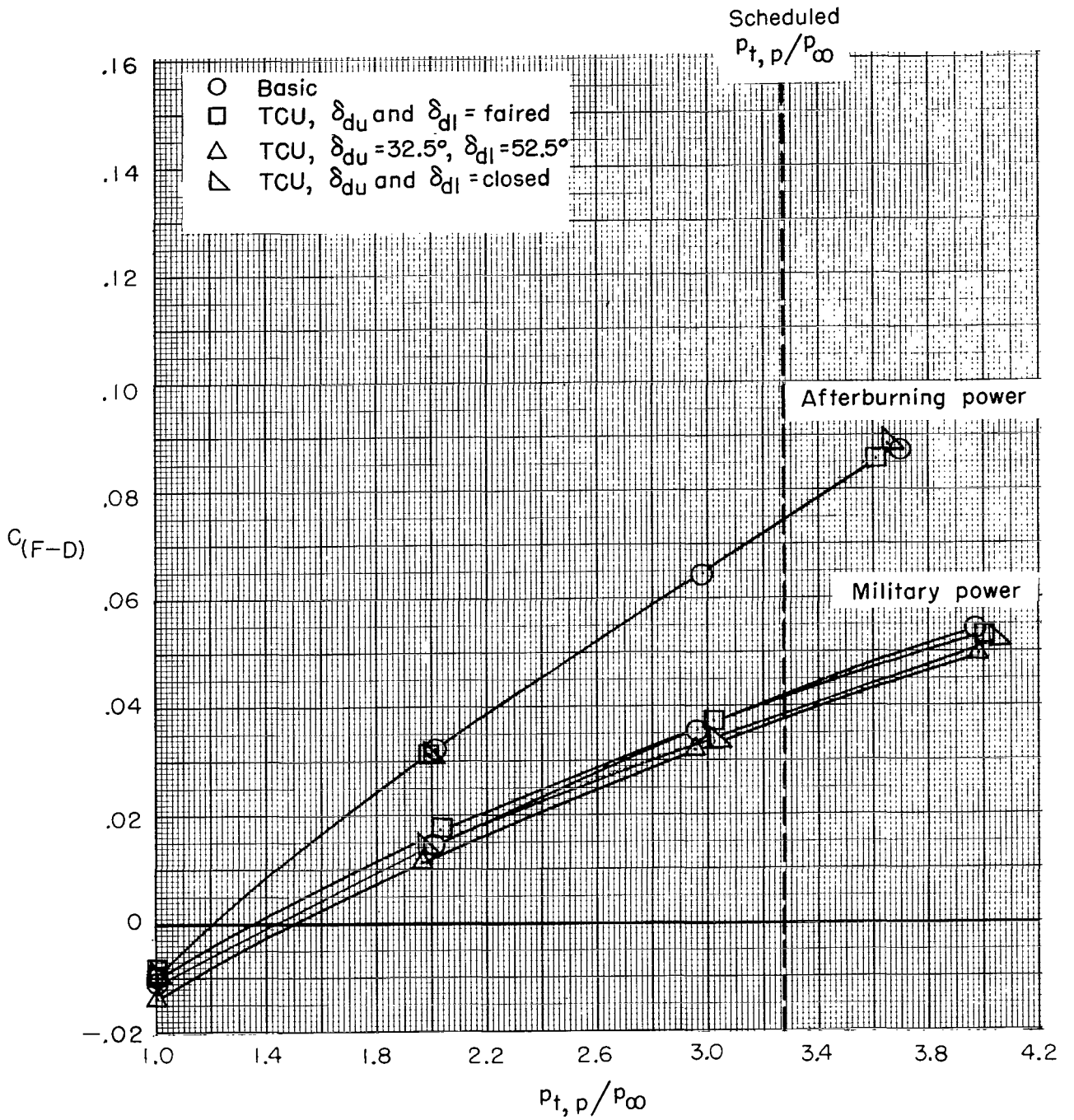
(b) $M = 0.34$.

Figure 16.- Continued.



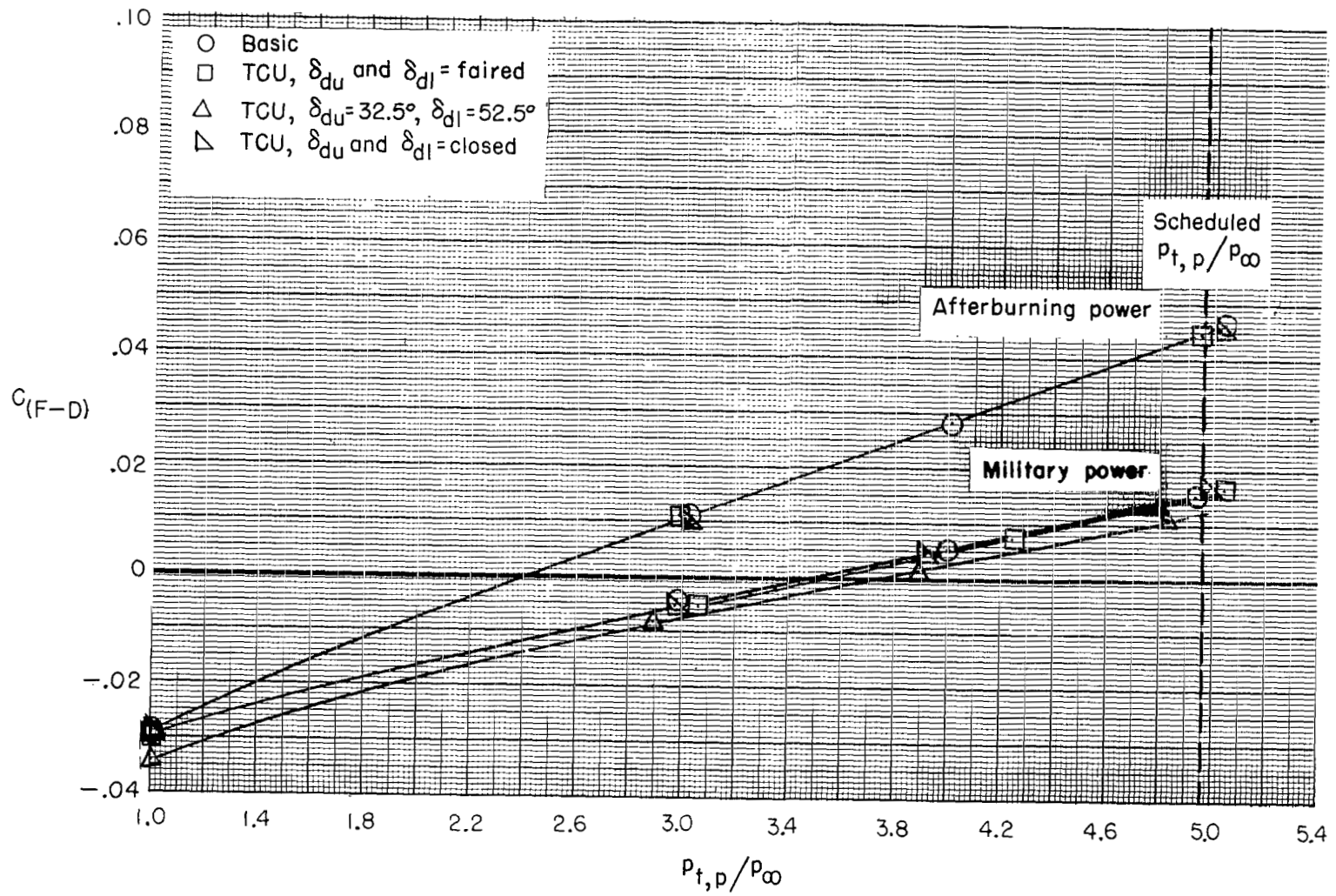
(c) $M = 0.60$.

Figure 16.- Continued.



(d) $M = 0.90$.

Figure 16.- Continued.



(e) $M = 1.30$.

Figure 16.- Concluded.

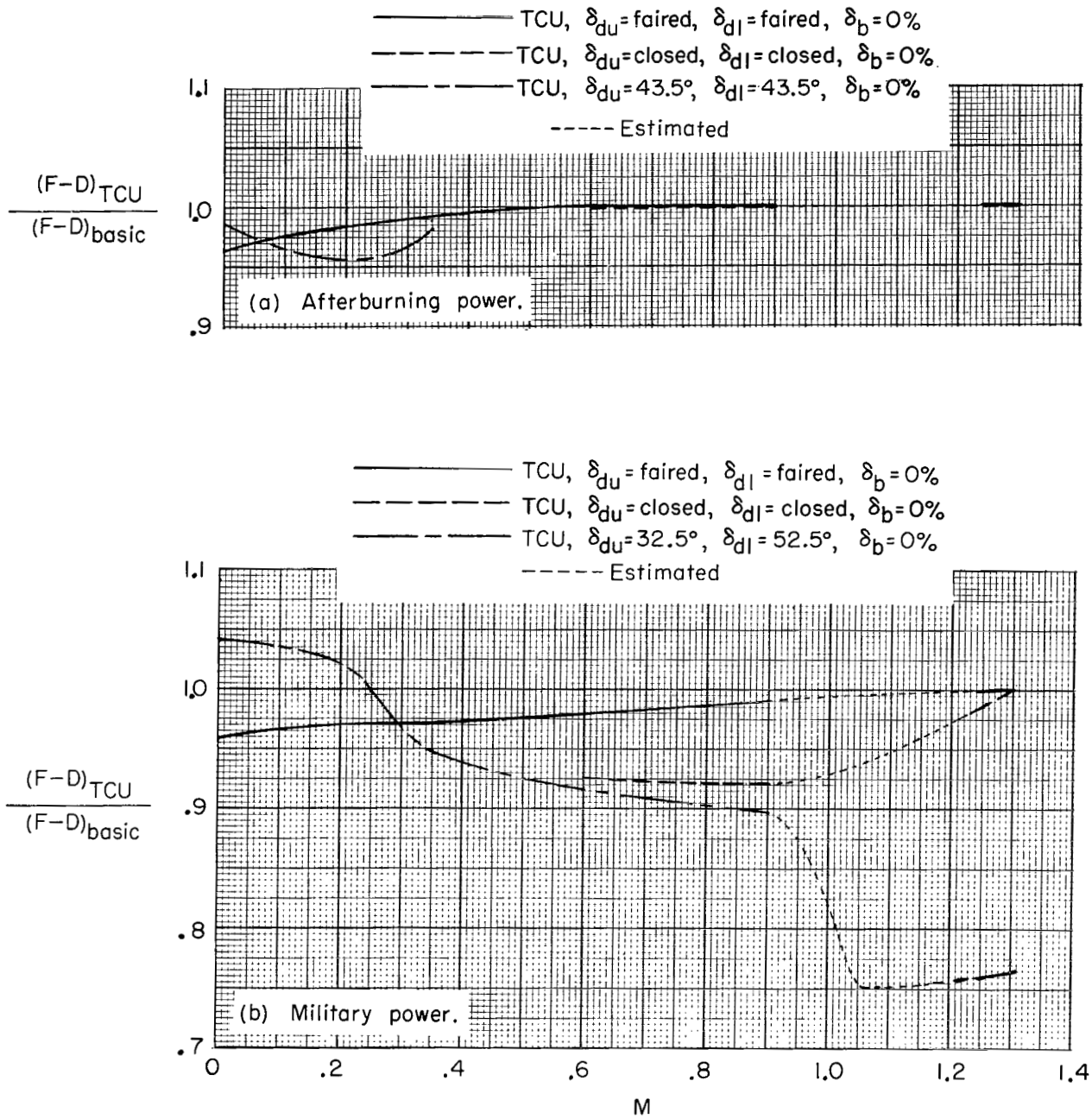


Figure 17.- Comparison of the ratio of thrust-minus-drag coefficient for the TCU configurations to that for the basic configuration at the estimated engine-operating pressure-ratio schedule. $\alpha = 0^\circ$.

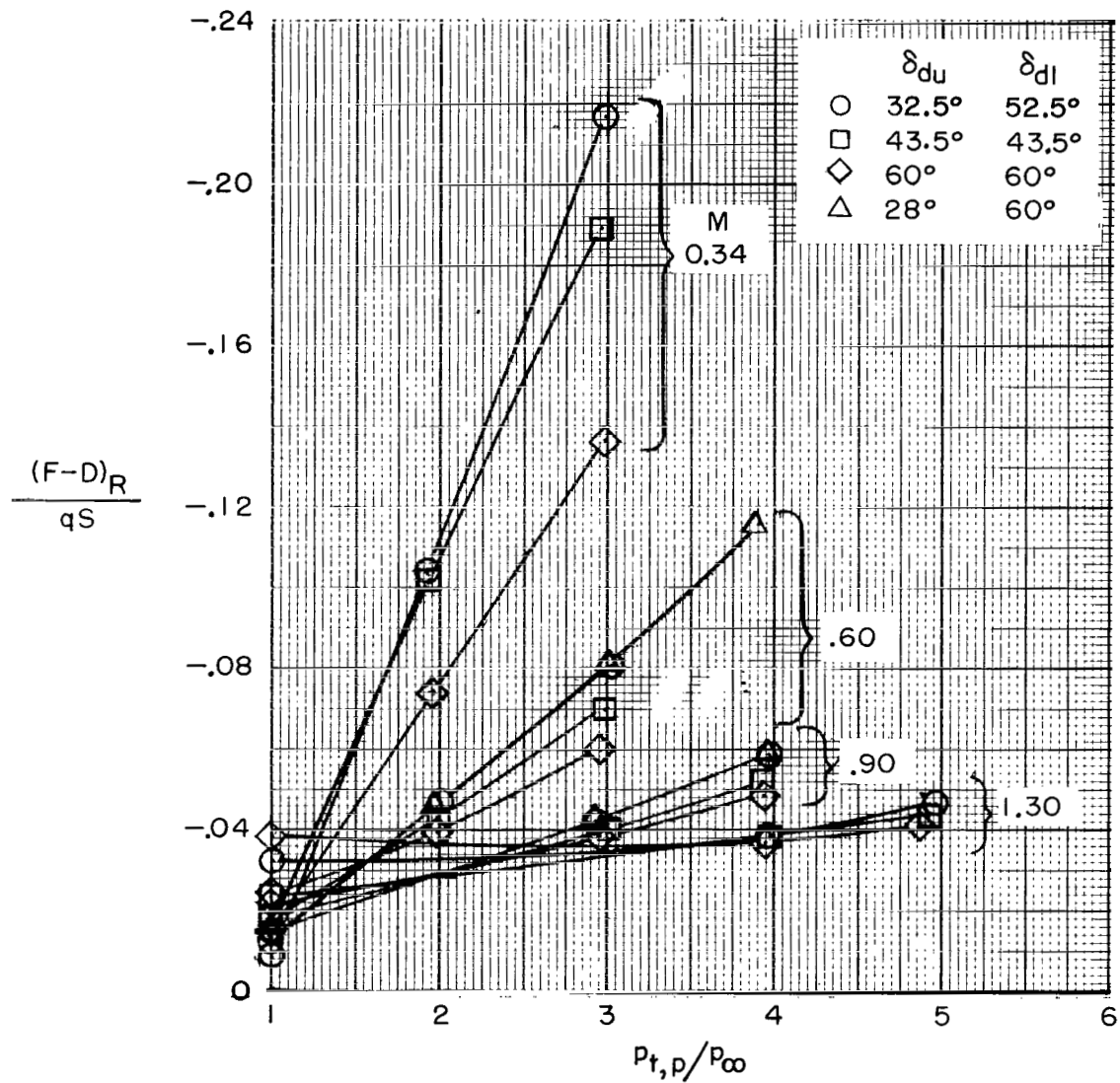


Figure 18.- A comparison of the effect of deflector-door angular settings on reverse-thrust performance. $\alpha = 0^\circ$; $\delta_D = 100\%$; military power.

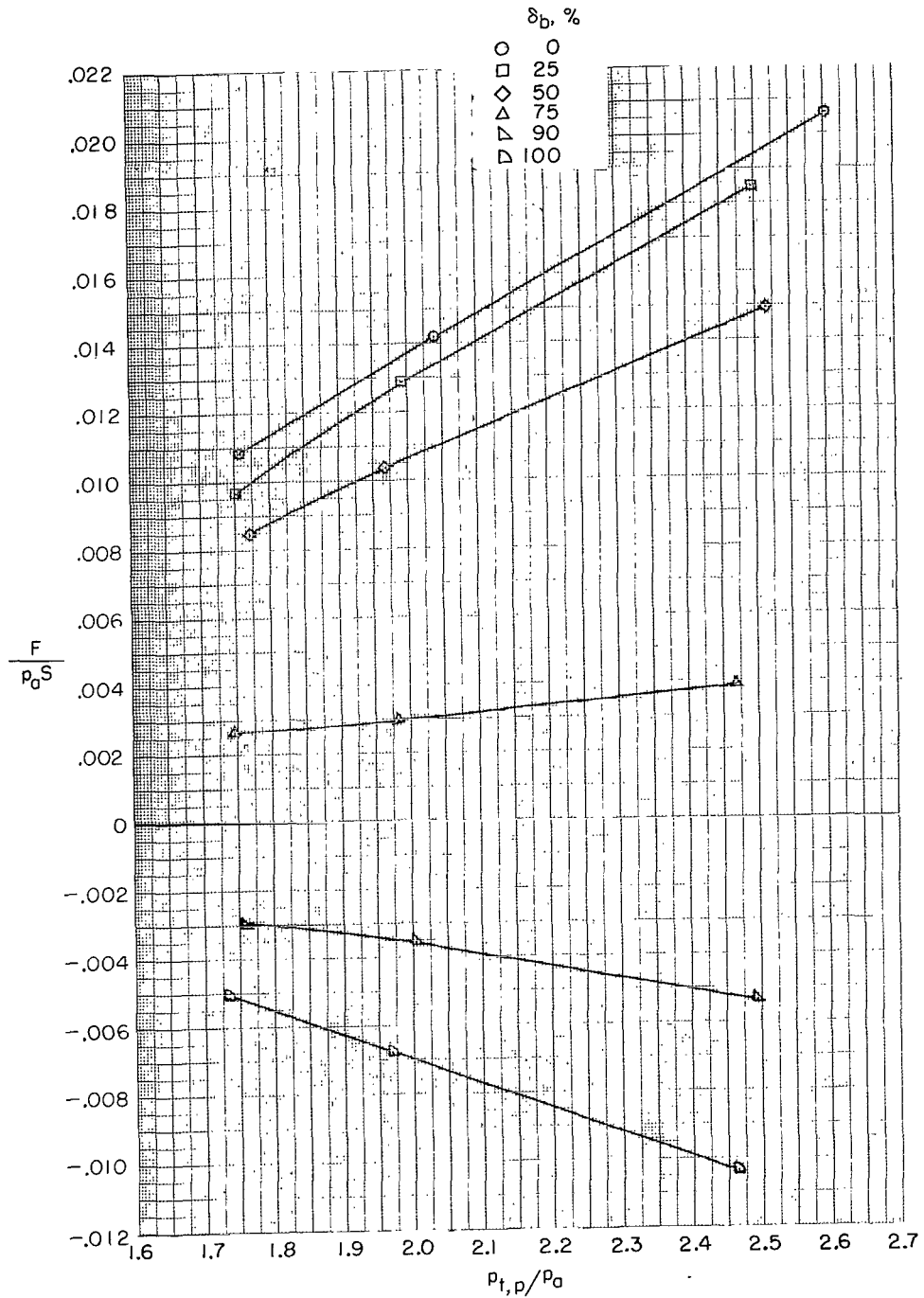
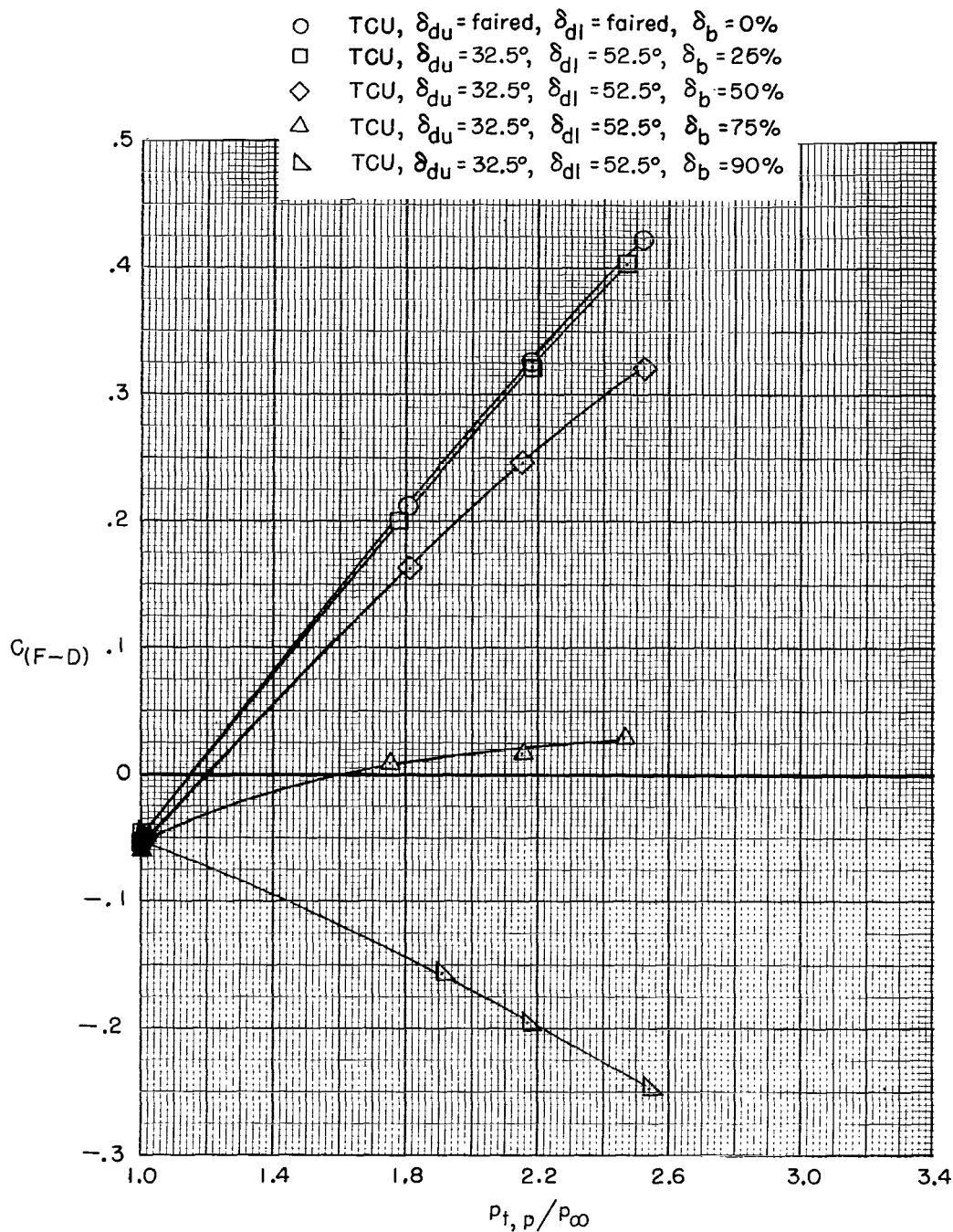


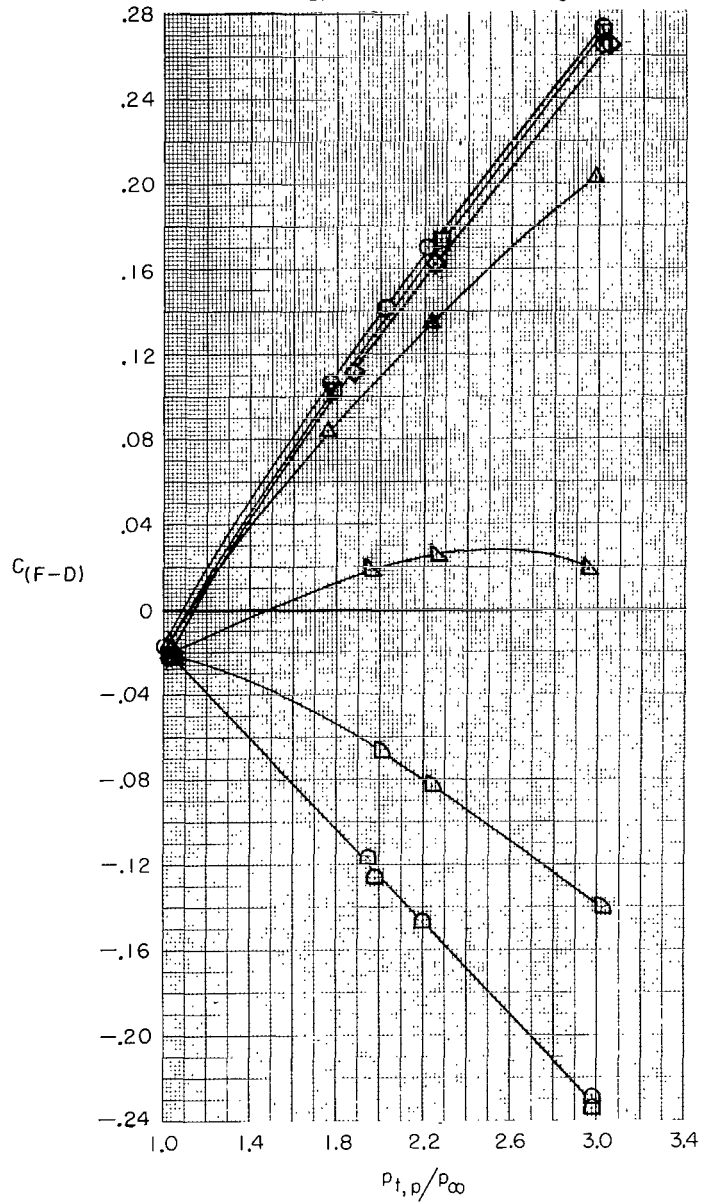
Figure 19.- Variation of static-thrust coefficient with primary-nozzle-jet total-pressure ratio and blocker-door position. $\delta_{du} = 32.5^\circ$; $\delta_{dl} = 52.5^\circ$.



(a) $M = 0.23$; $\alpha = 12^\circ$; approach configuration.

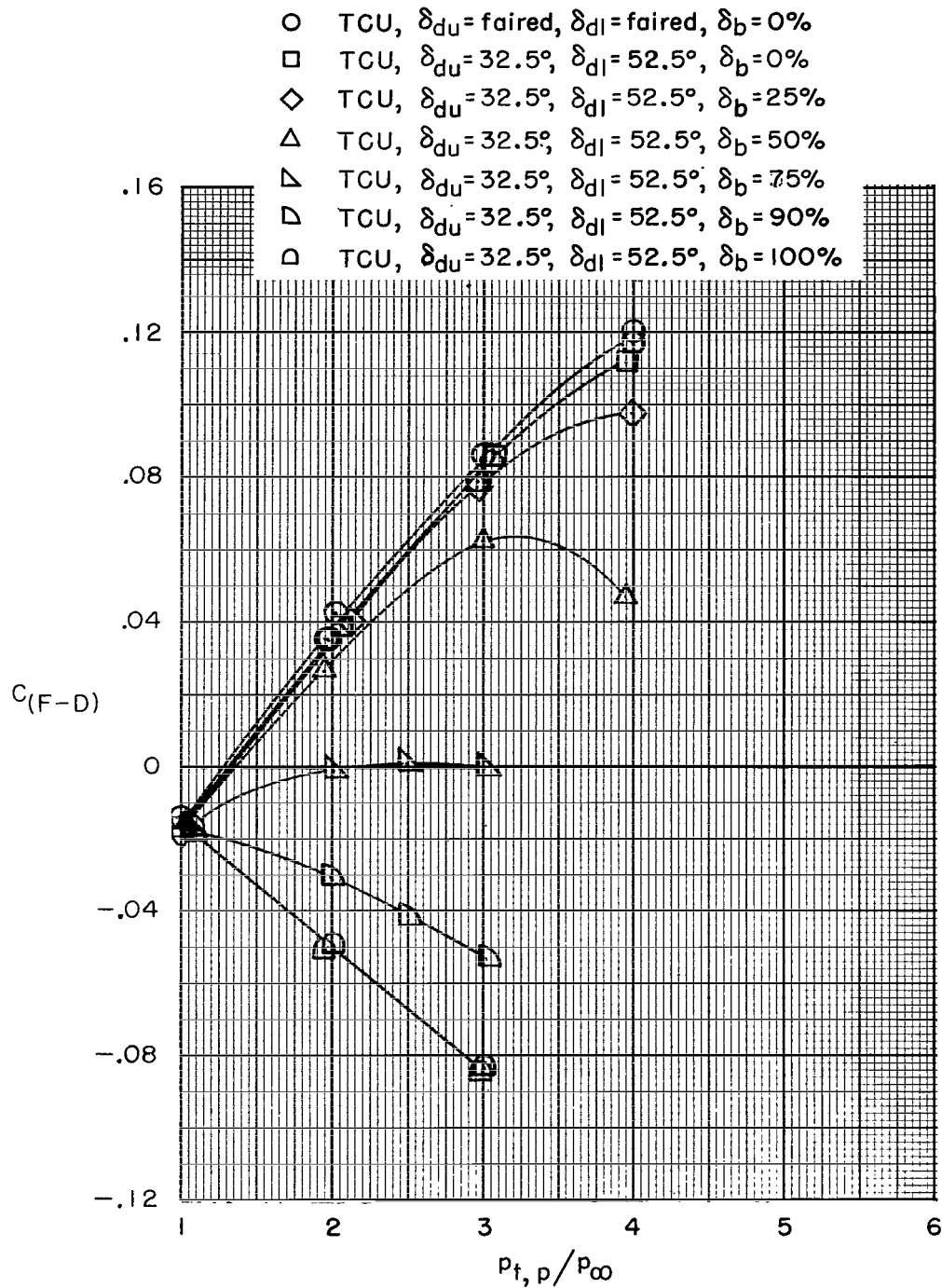
Figure 20.- Variation of thrust-minus-drag coefficient with pressure ratio and blocker-door position for several Mach numbers.

- TCU, $\delta_{du} = \text{faired}$, $\delta_{dl} = \text{faired}$, $\delta_b = 0\%$
- TCU, $\delta_{du} = 32.5^\circ$, $\delta_{dl} = 52.5^\circ$, $\delta_b = 0\%$
- ◇ TCU, $\delta_{du} = 32.5^\circ$, $\delta_{dl} = 52.5^\circ$, $\delta_b = 25\%$
- △ TCU, $\delta_{du} = 32.5^\circ$, $\delta_{dl} = 52.5^\circ$, $\delta_b = 50\%$
- ▽ TCU, $\delta_{du} = 32.5^\circ$, $\delta_{dl} = 52.5^\circ$, $\delta_b = 75\%$
- ▷ TCU, $\delta_{du} = 32.5^\circ$, $\delta_{dl} = 52.5^\circ$, $\delta_b = 90\%$
- ◻ TCU, $\delta_{du} = 32.5^\circ$, $\delta_{dl} = 52.5^\circ$, $\delta_b = 100\%$



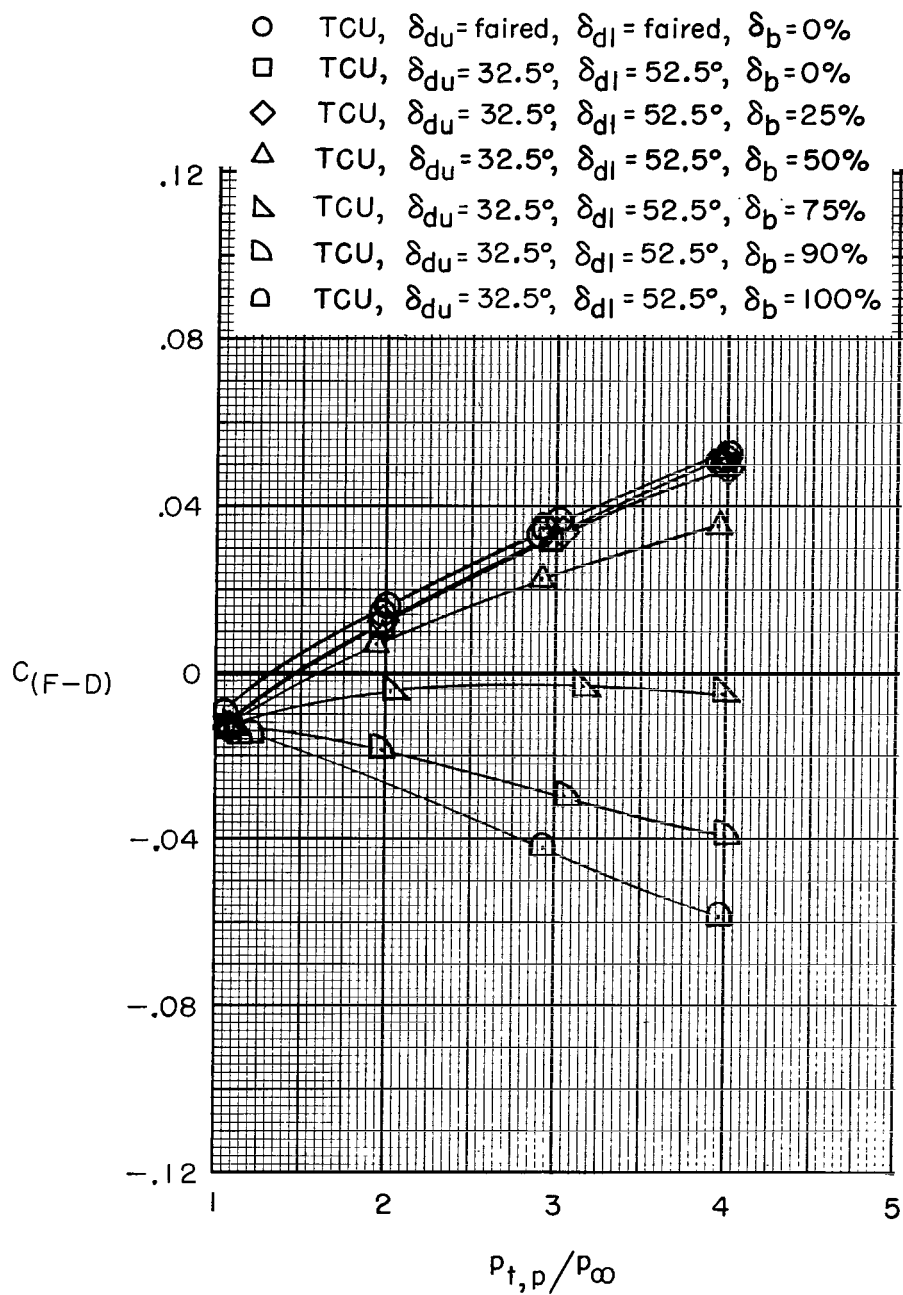
(b) $M = 0.34$; $\alpha = 6^\circ$.

Figure 20.- Continued.



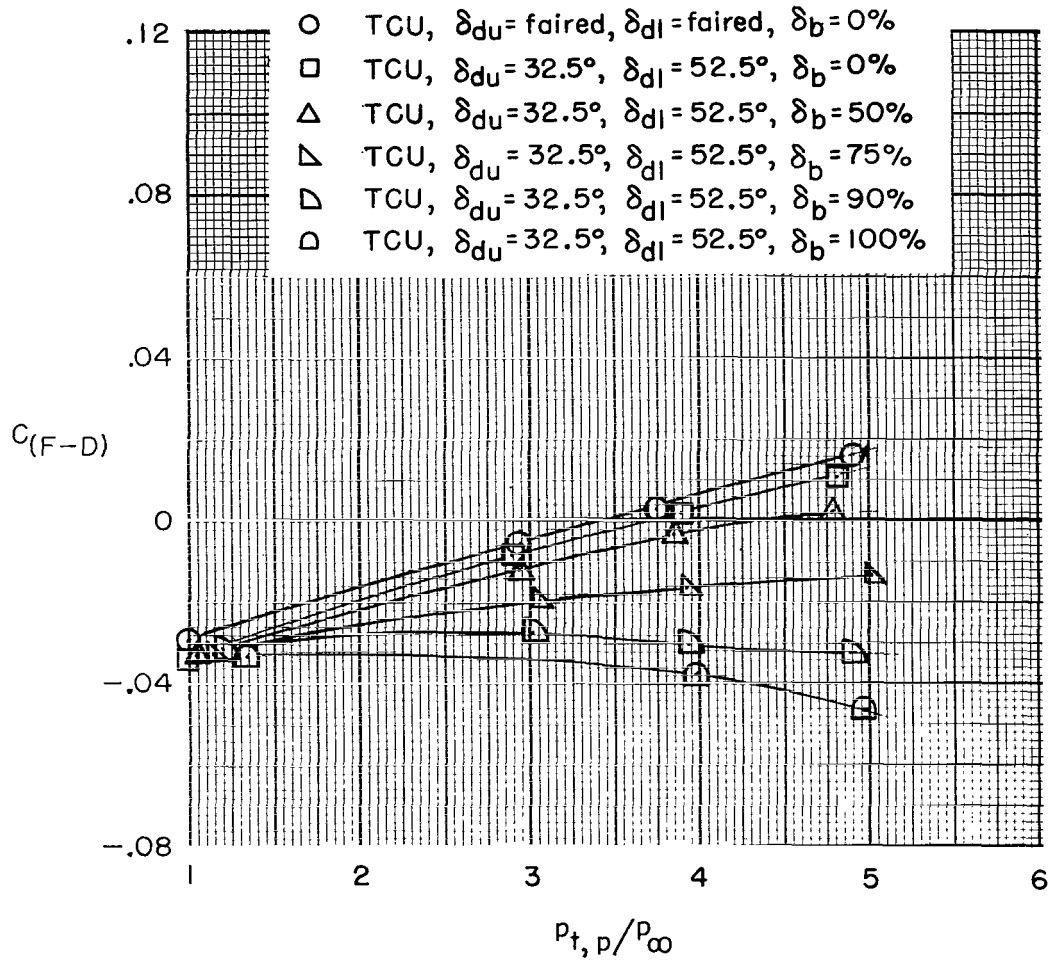
(c) $M = 0.60$; $\alpha = 3^\circ$.

Figure 20.- Continued.



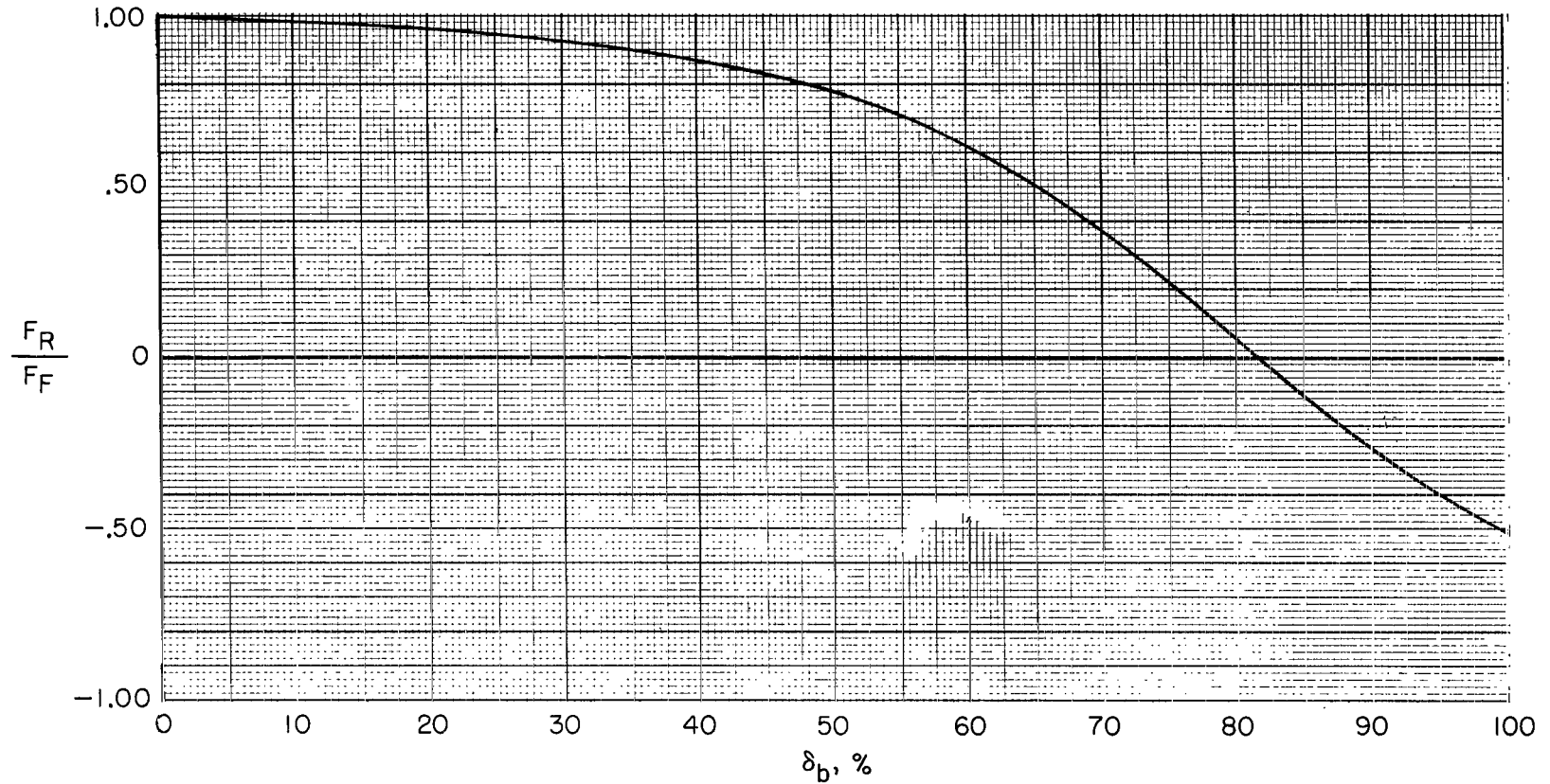
(d) $M = 0.90$; $\alpha = 0^\circ$.

Figure 20.- Continued.



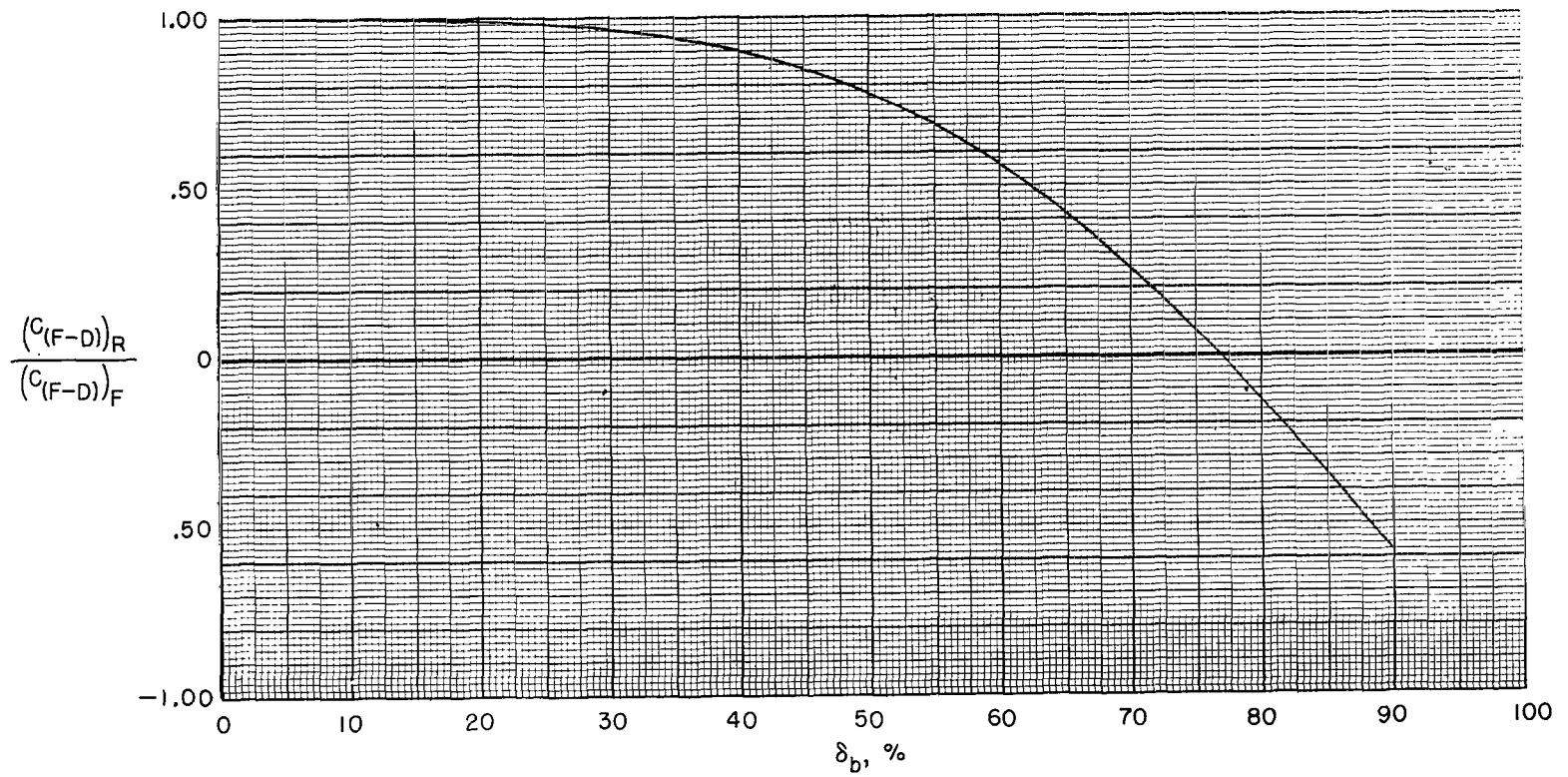
(e) $M = 1.30$; $\alpha = 0^\circ$.

Figure 20.- Concluded.



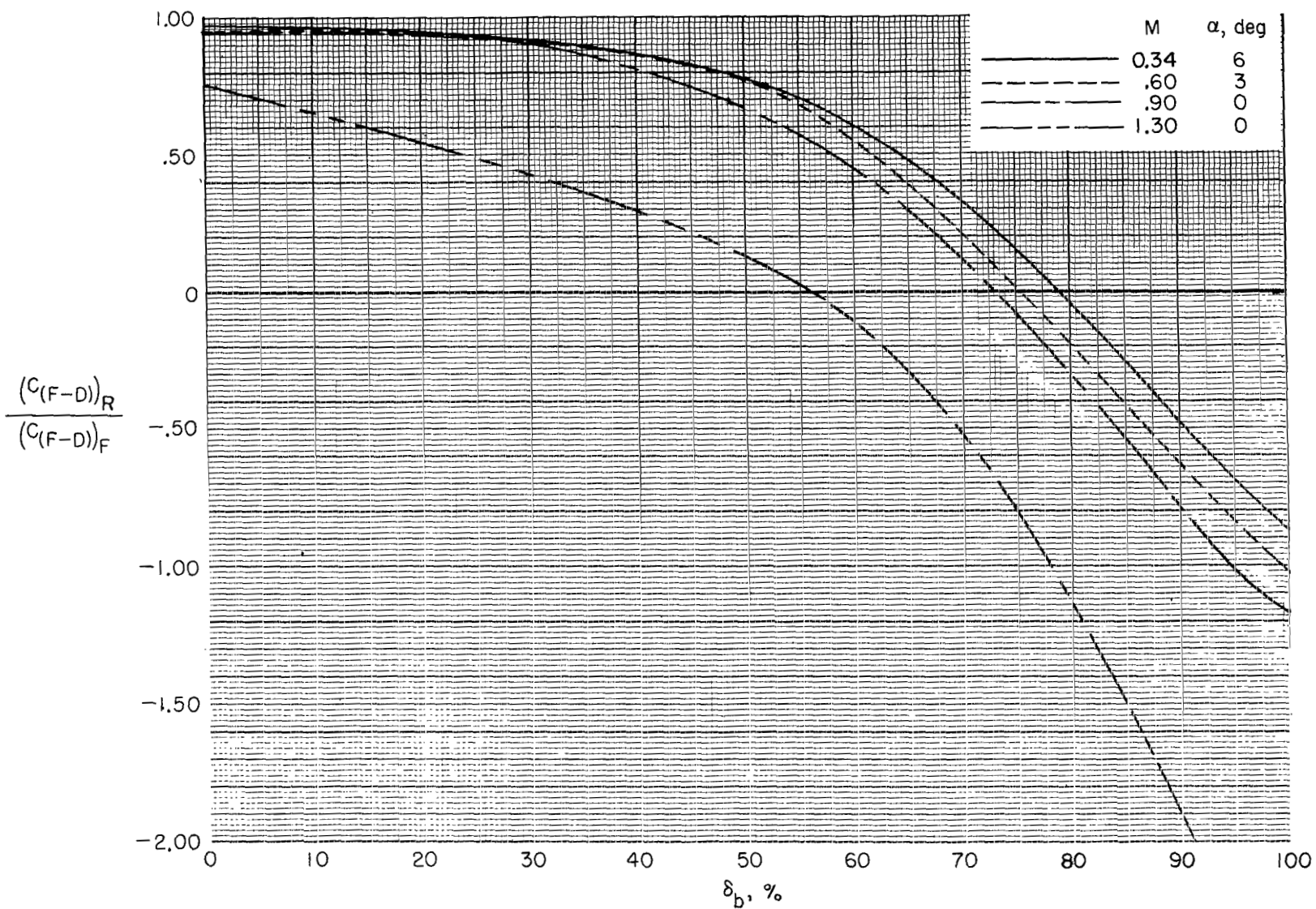
(a) $M = 0$; $\delta_{du} = 32.5^\circ$ and $\delta_{dl} = 52.5^\circ$ (both forward- and reverse-thrust mode); and $p_{t,p}/p_\infty = 2.0$.

Figure 21.- Thrust-modulation performance as a function of blocker-door position for the selected TCU at the estimated engine-operating pressure ratio and military power.



(b) $M = 0.23$; approach configuration; $\delta_{du} = 32.5^\circ$ and $\delta_{dl} = 52.5^\circ$ (both forward- and reverse-thrust mode);
 $\alpha = 12^\circ$; and $p_{t,p}/p_\infty = 2.25$.

Figure 21.- Continued.



(c) $\delta_{du} = \delta_{dl} = \text{Faired}$ (forward-thrust mode); $\delta_{du} = 32.5^\circ$ and $\delta_{dl} = 52.5^\circ$ (reverse-thrust mode).

Figure 21.- Concluded.

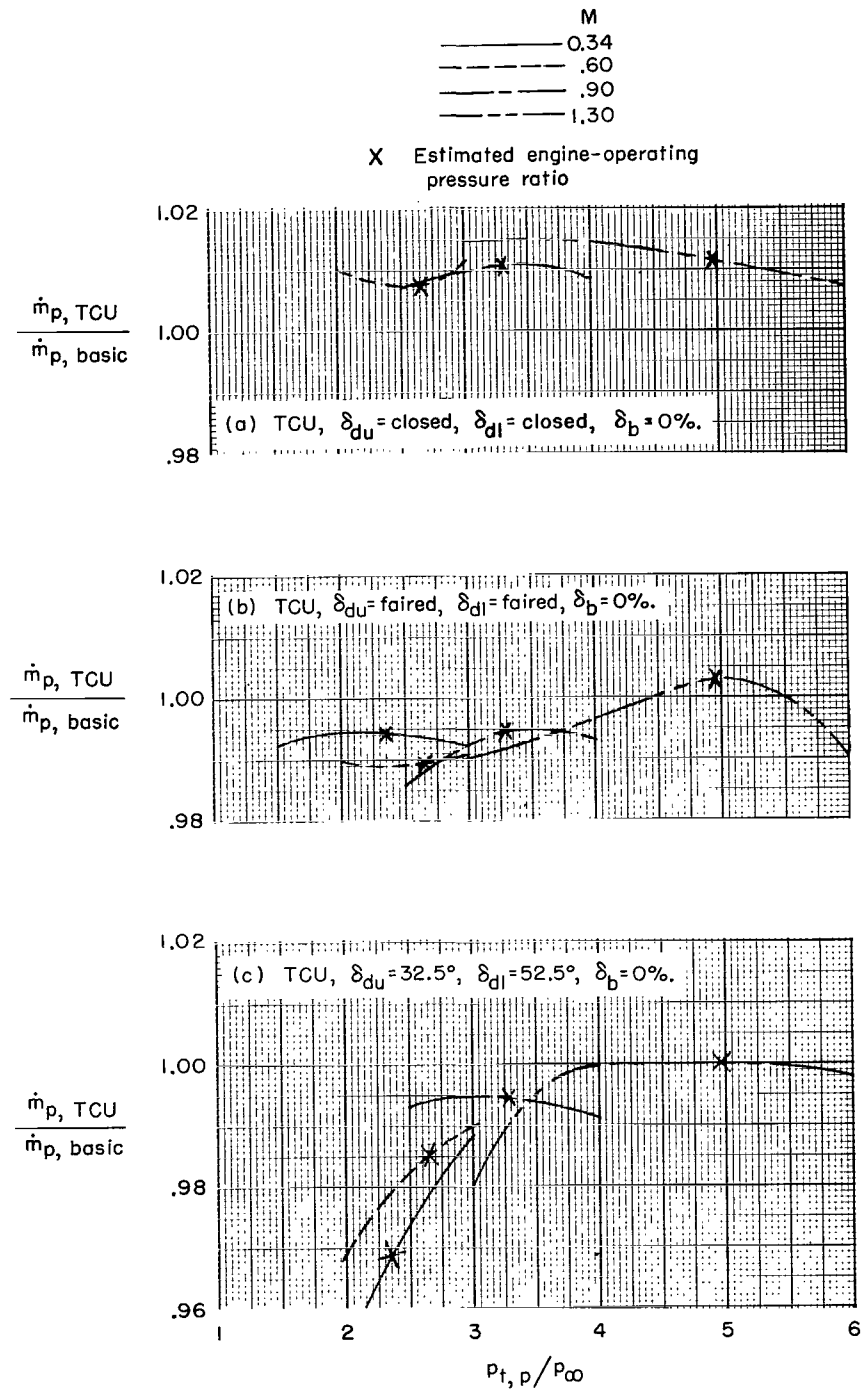


Figure 22.- Ratio of TCU primary-nozzle flow to basic primary-nozzle flow for military power in the forward-thrust mode.

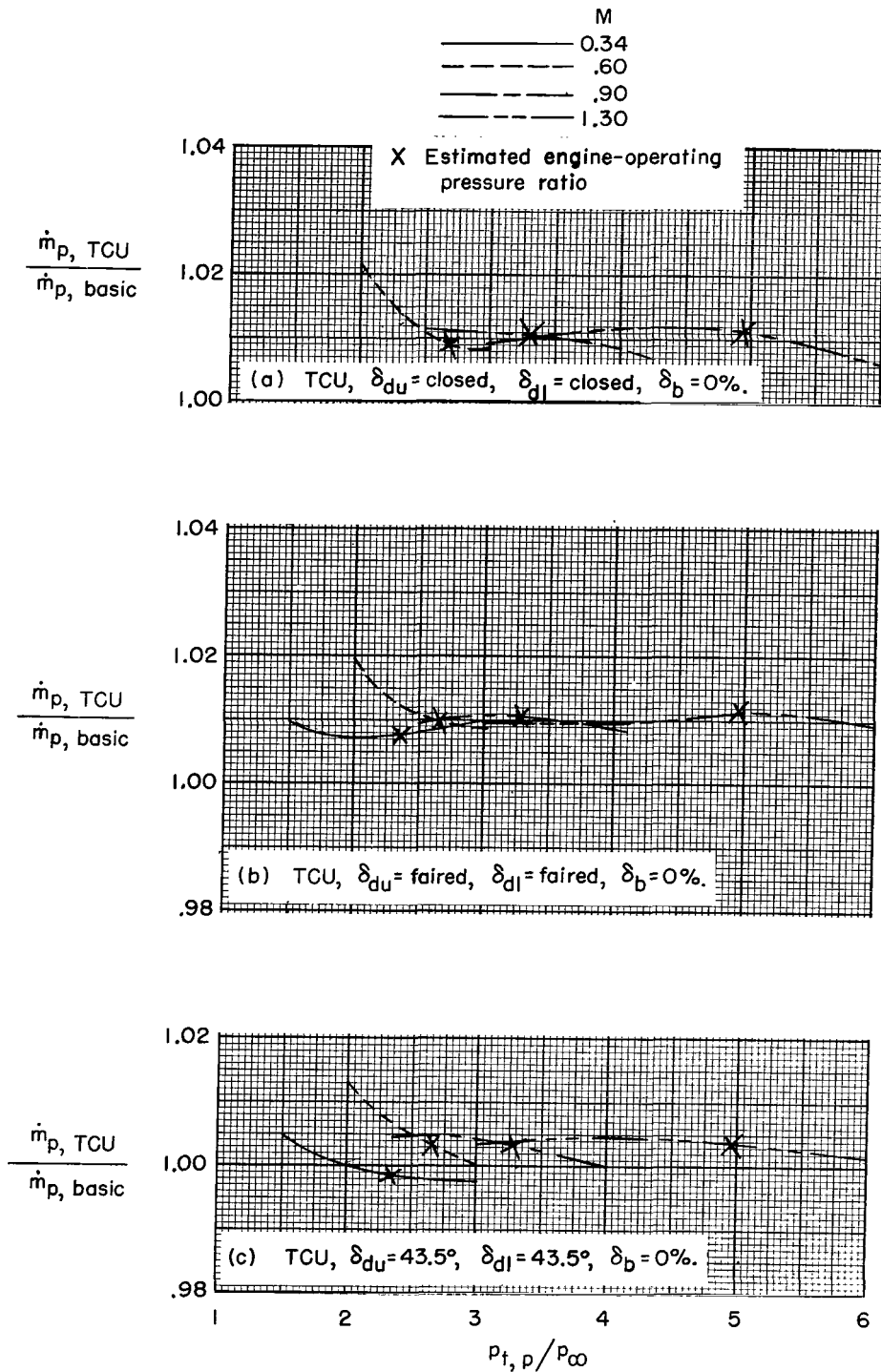


Figure 23.- Ratio of TCU primary-nozzle flow to basic primary-nozzle flow for afterburning power in the forward-thrust mode.

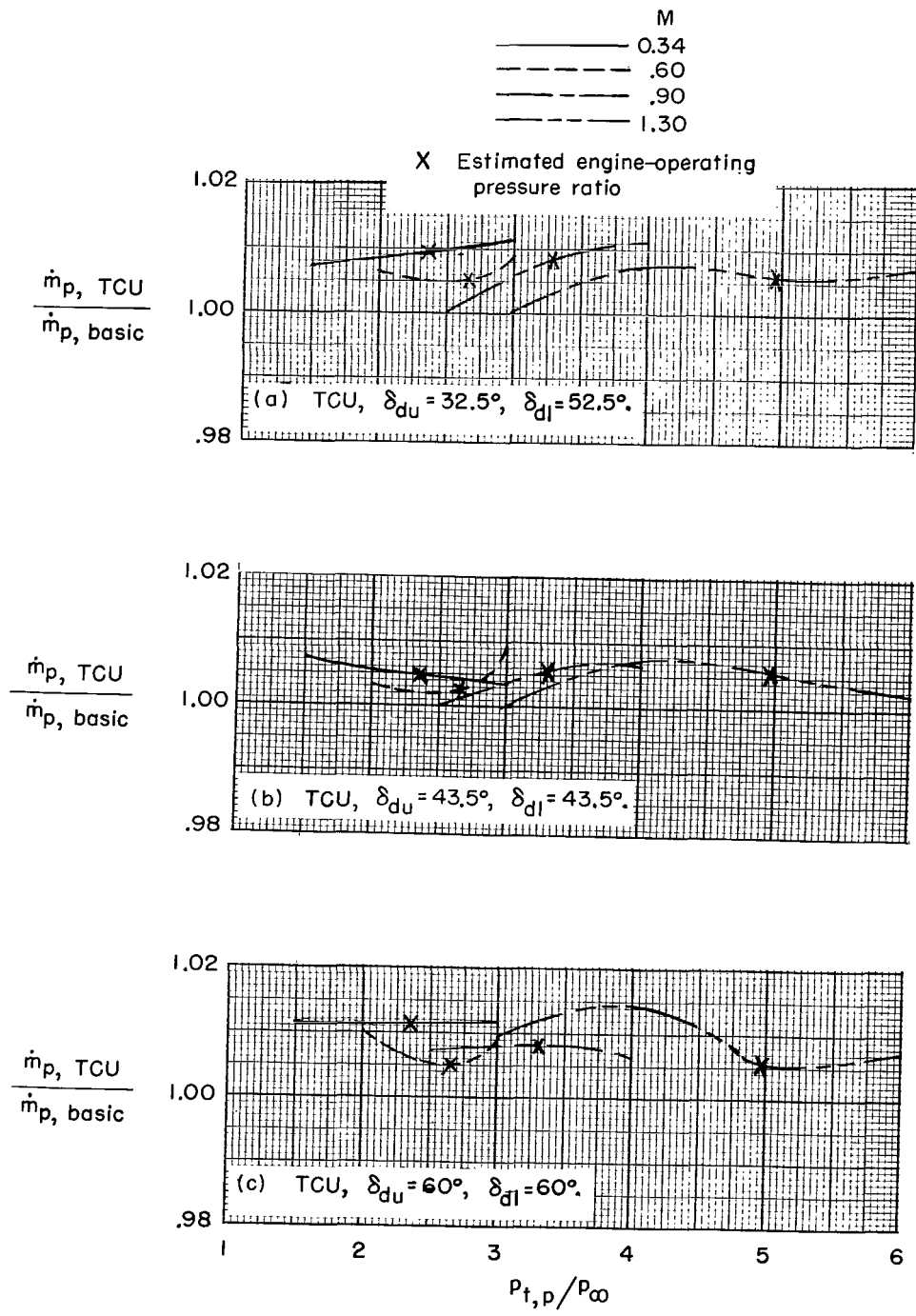
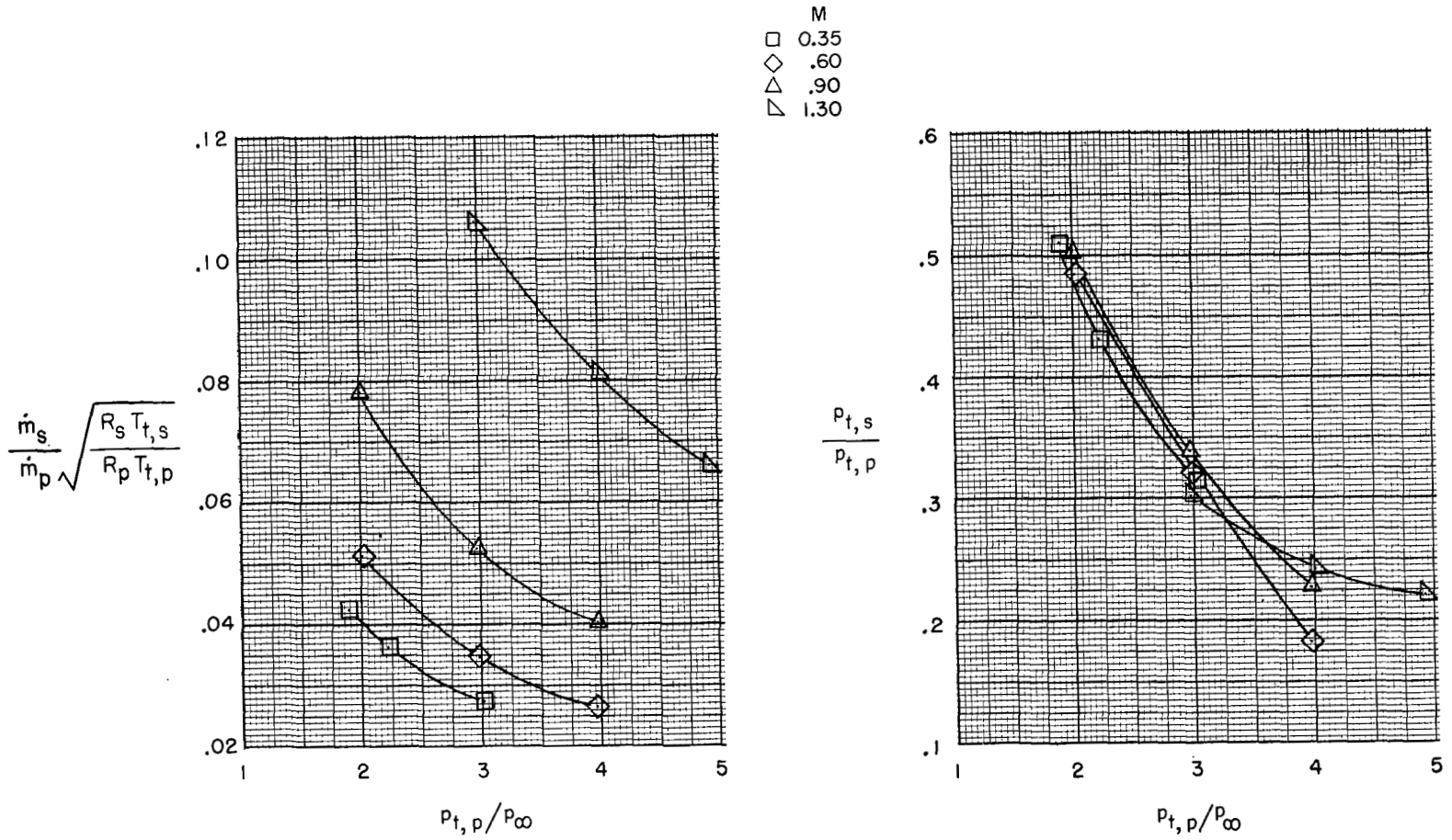
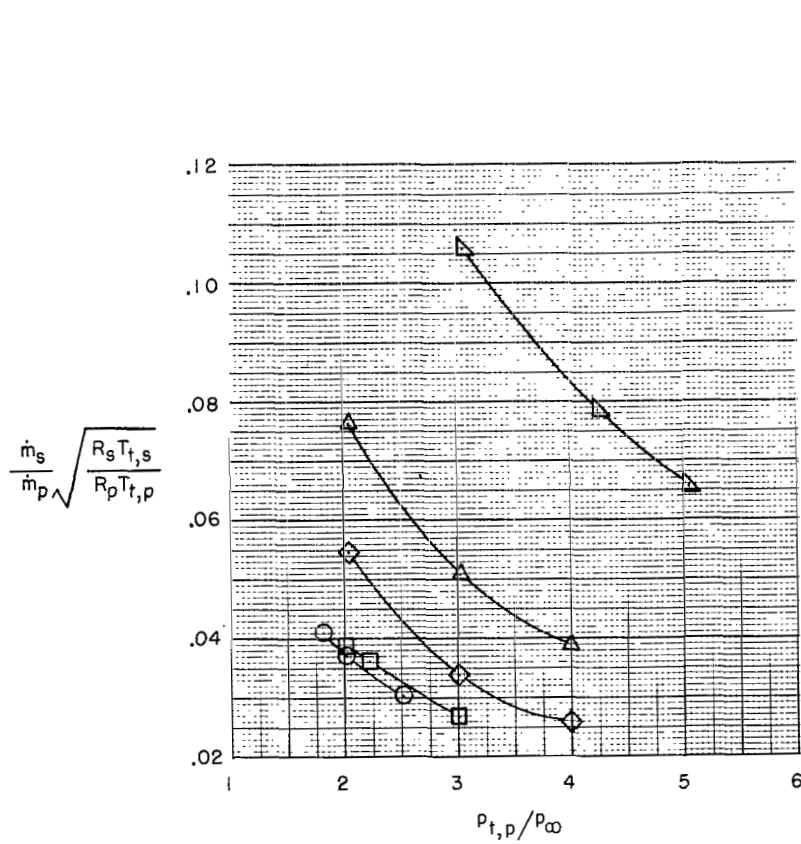


Figure 24.- Ratio of TCU primary-nozzle flow to primary-nozzle flow basic for military power in the full-reverse-thrust mode.

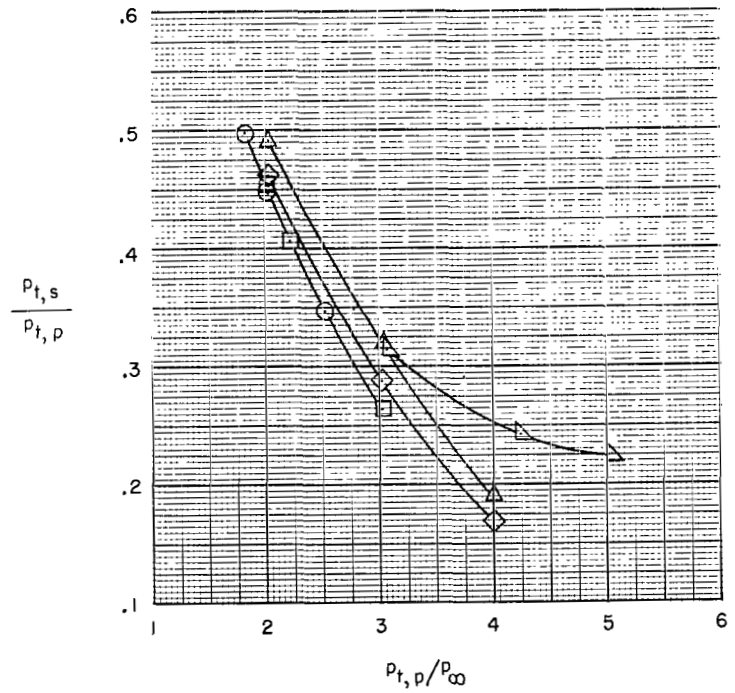


(a) Basic.

Figure 25.- Ejector pumping characteristics of various configurations for several Mach numbers at zero angle of attack and military power.

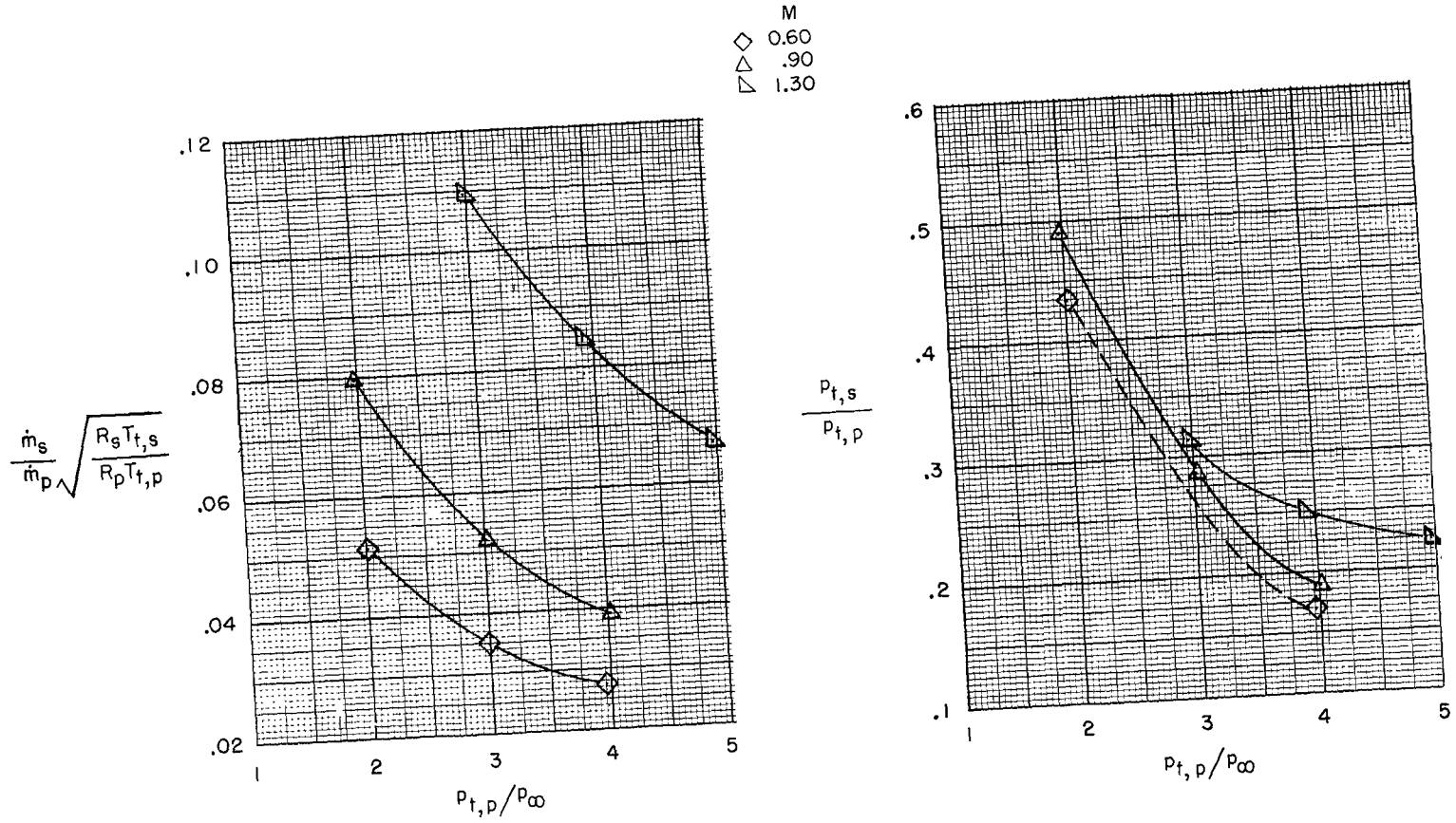


- M
 ○ 0.23
 □ 0.35
 ◇ 0.60
 △ 0.90
 ▽ 1.30



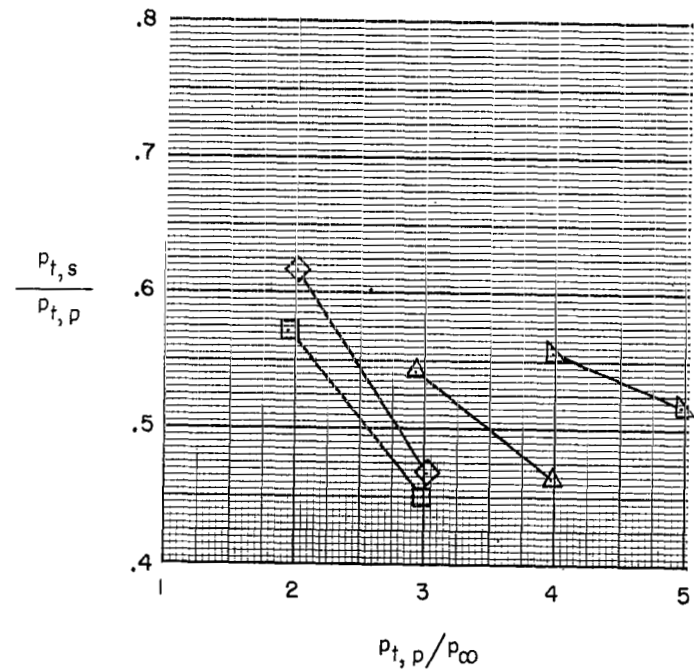
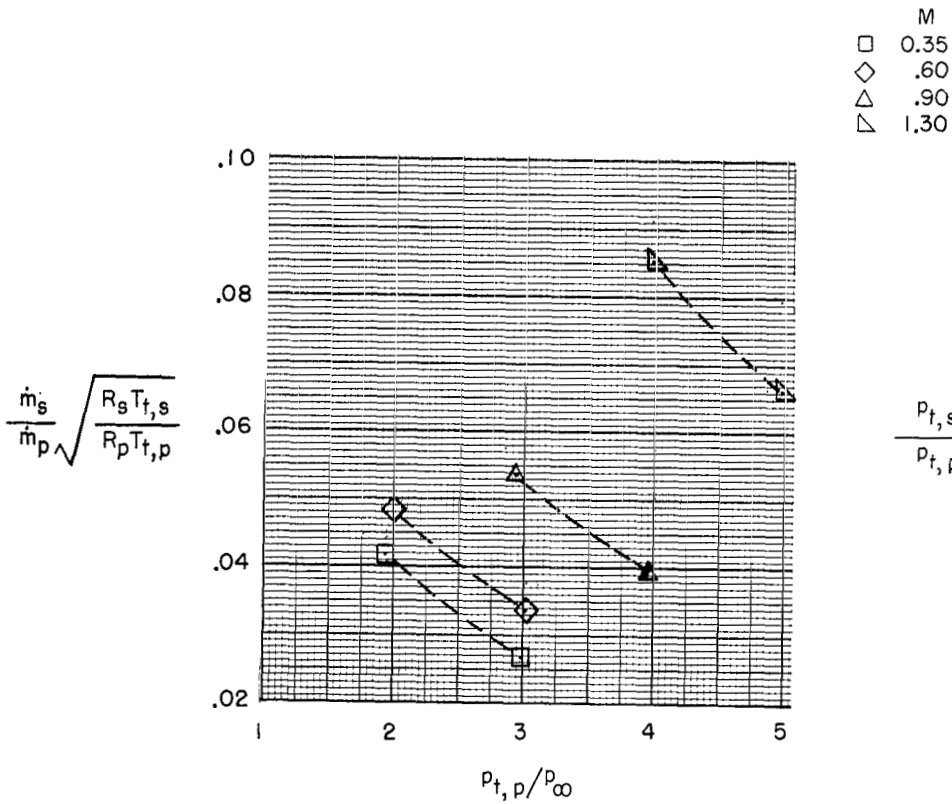
(b) TCU; $\delta_{du} = \text{Faired}$; $\delta_{dl} = \text{Faired}$; $\delta_b = 0\%$.

Figure 25.- Continued.



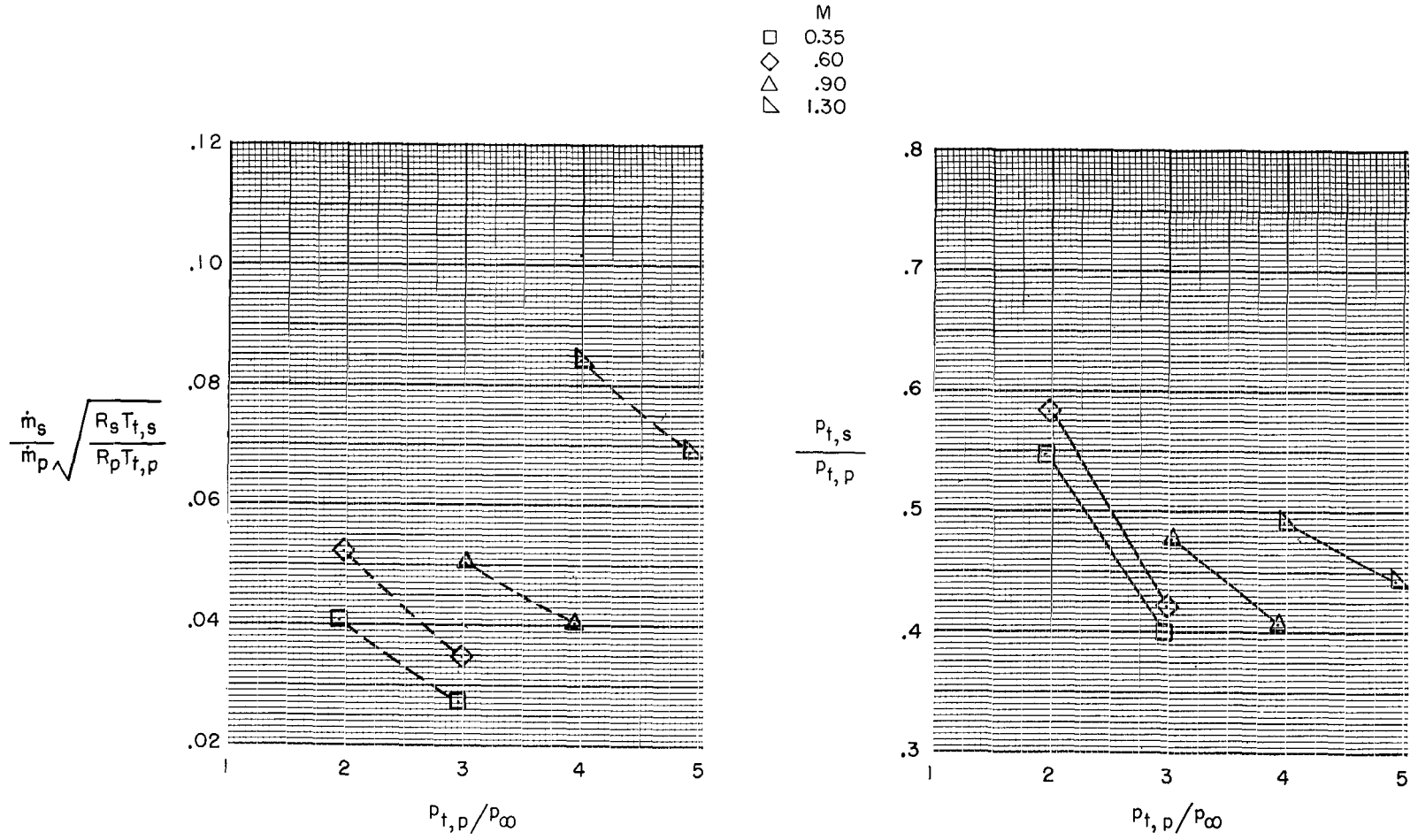
(c) TCU; $\delta_{du} = \text{Closed}$; $\delta_{dl} = \text{Closed}$; $\delta_b = 0\%$.

Figure 25.- Continued.



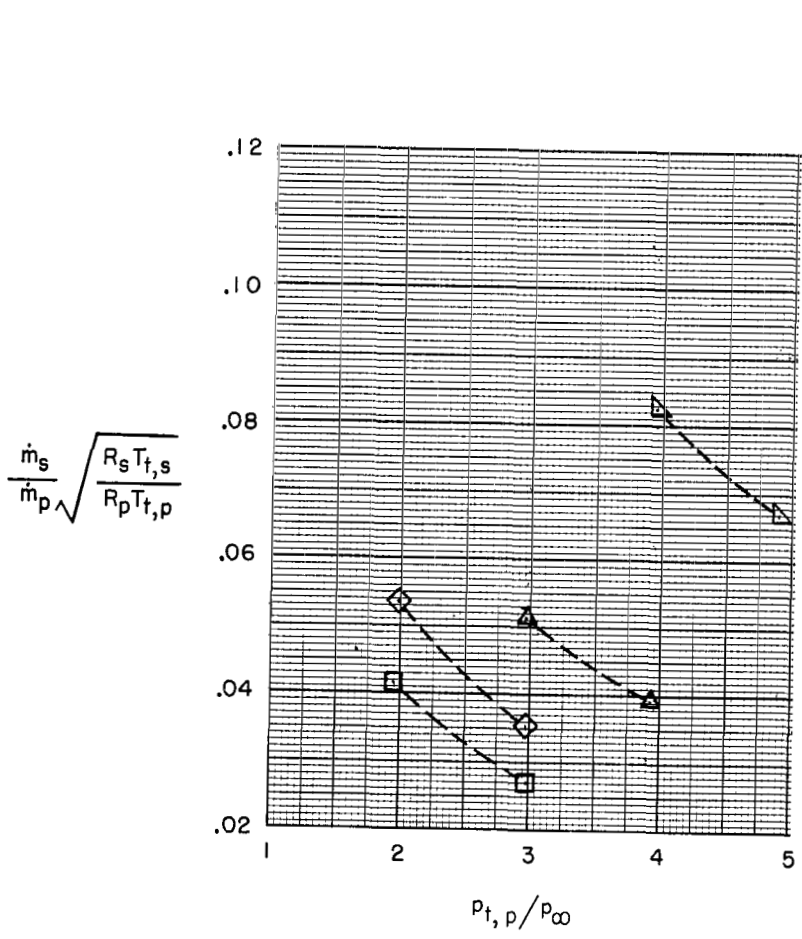
(d) TCU; $\delta_{du} = 32.5^\circ$; $\delta_{dl} = 52.5^\circ$; $\delta_b = 100\%$.

Figure 25.- Continued.

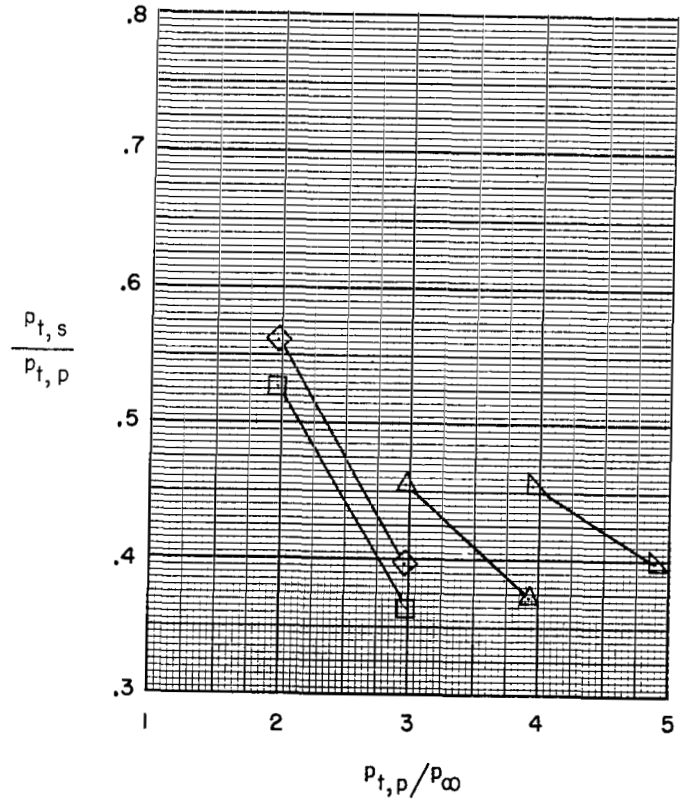


(e) TCU; $\delta_{du} = 43.5^{\circ}$; $\delta_{dl} = 43.5^{\circ}$; $\delta_p = 100\%$.

Figure 25.- Continued.

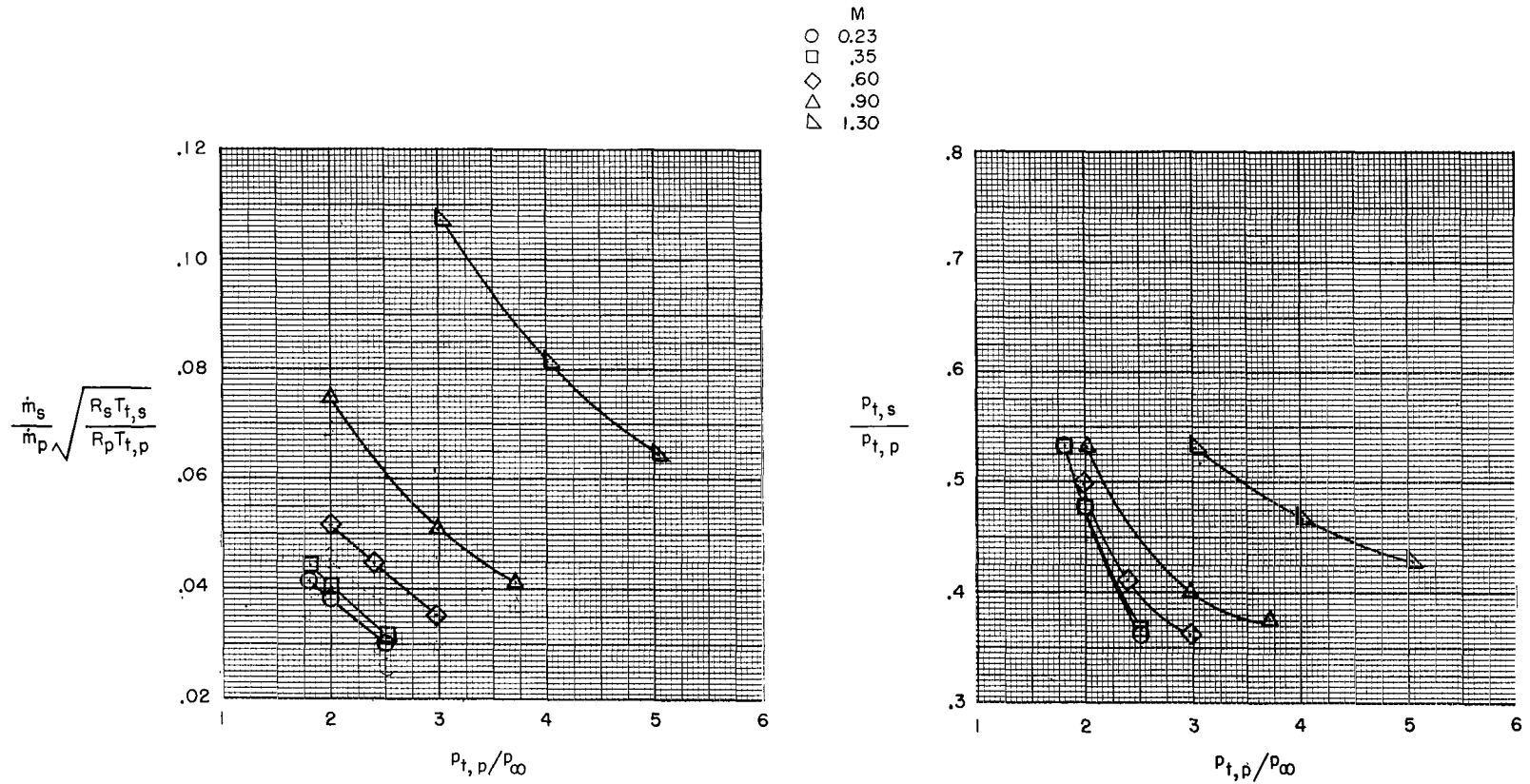


M
 □ 0.35
 ◇ .60
 △ .90
 ▽ 1.30



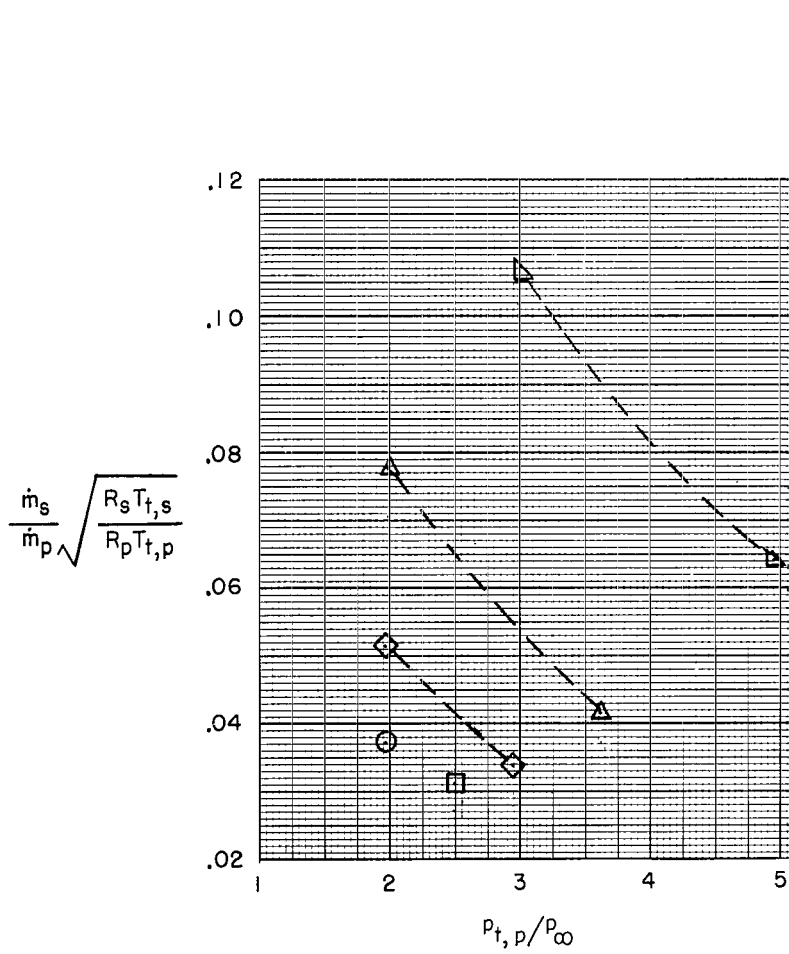
(f) TCU; $\delta_{du} = 60^\circ$; $\delta_{dl} = 60^\circ$; $\delta_b = 100\%$.

Figure 25.- Concluded.

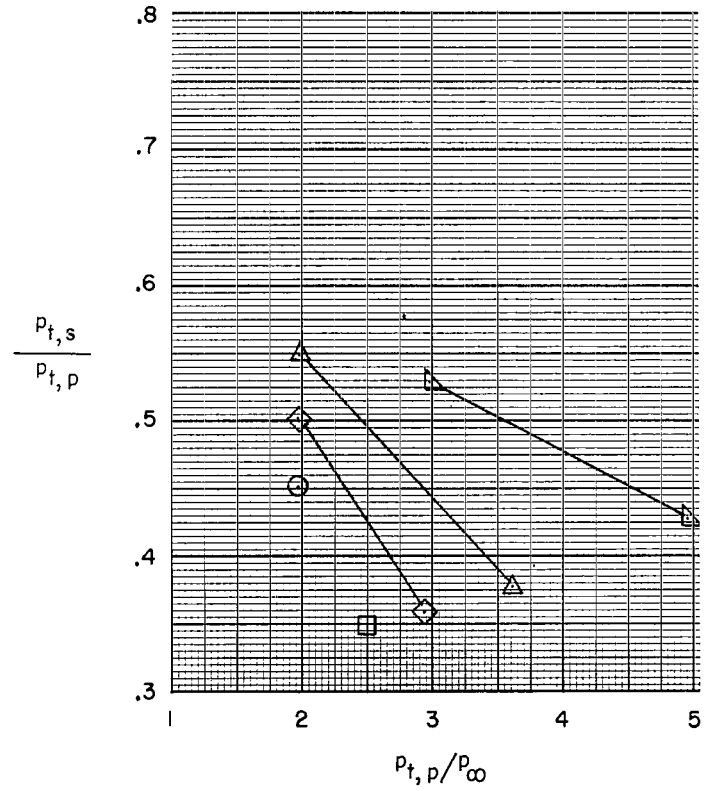


(a) Basic.

Figure 26.- Ejector pumping characteristics of various configurations for several Mach numbers at zero angle of attack and afterburning power.

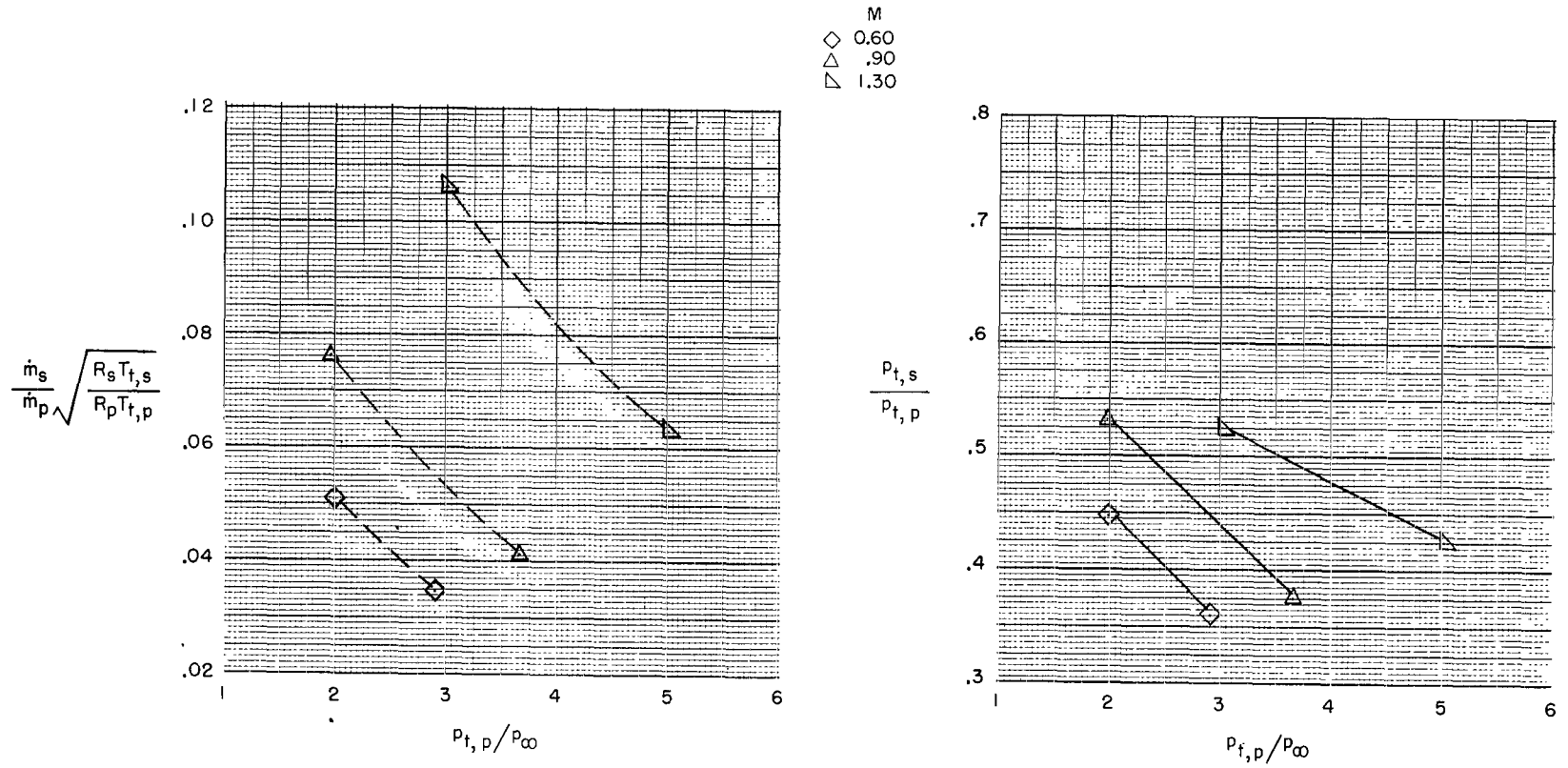


- M
 ○ 0.23
 □ .35
 ◇ .60
 △ .90
 ▽ 1.30



(b) TCU; $\delta_{du} = \text{Faired}$; $\delta_{dl} = \text{Faired}$; $\delta_b = 0\%$.

Figure 26.- Continued.



(c) TCU; δ_{du} = Closed; δ_{dl} = Closed; δ_b = 0%

Figure 26.- Concluded.

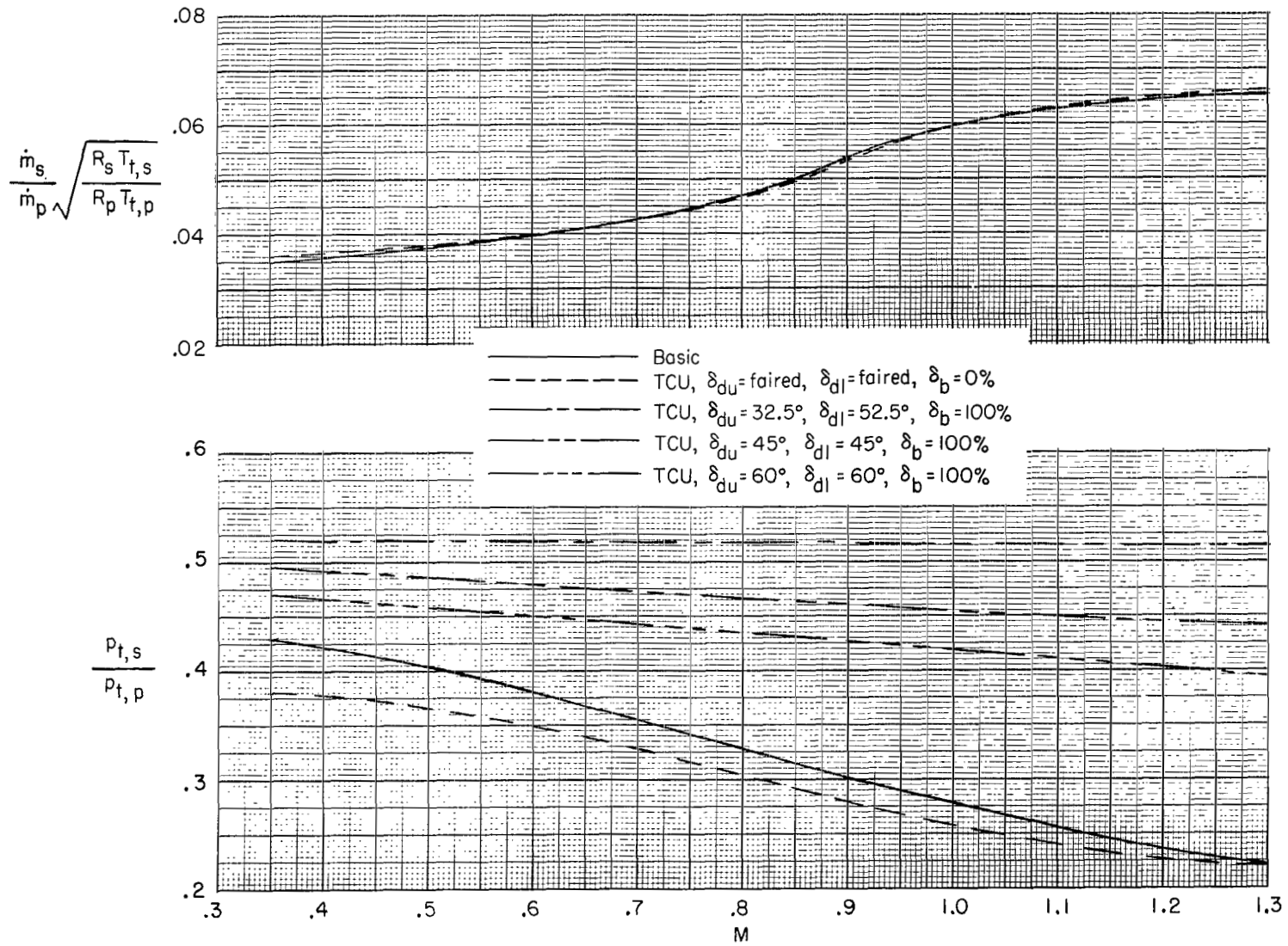
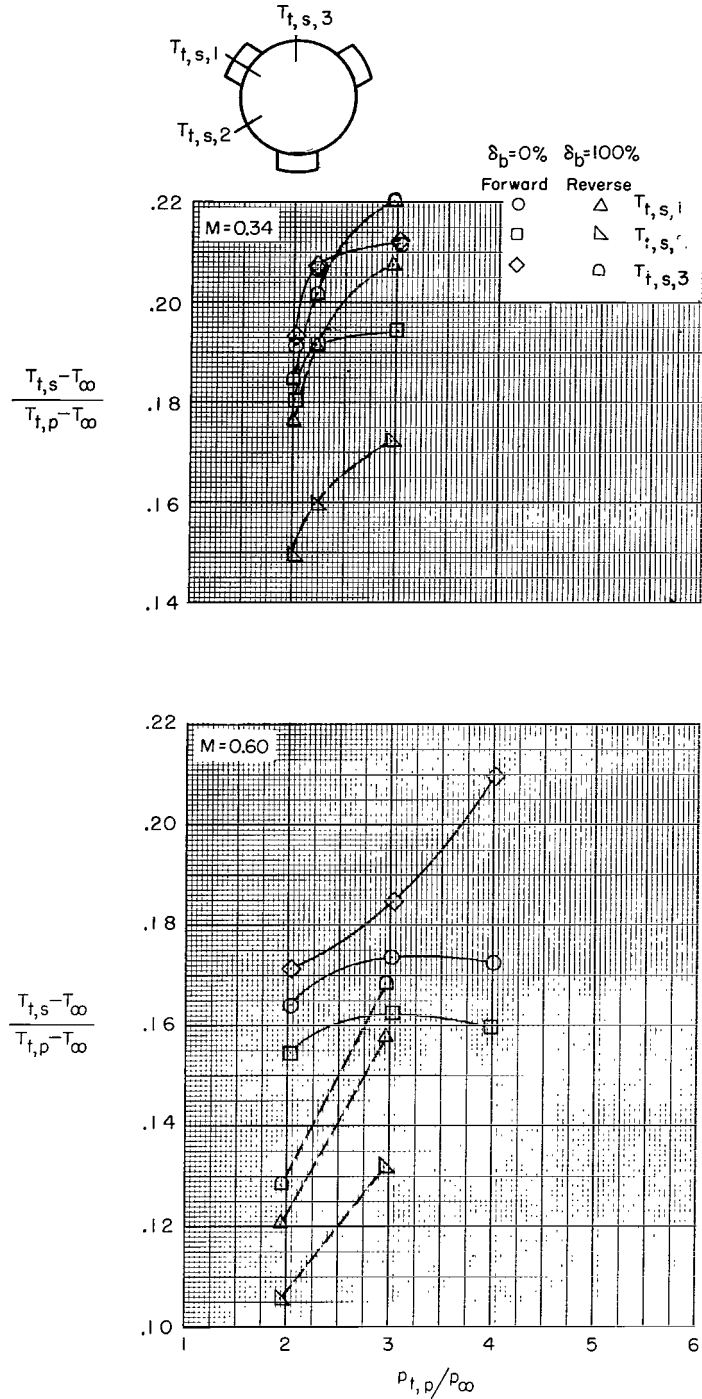
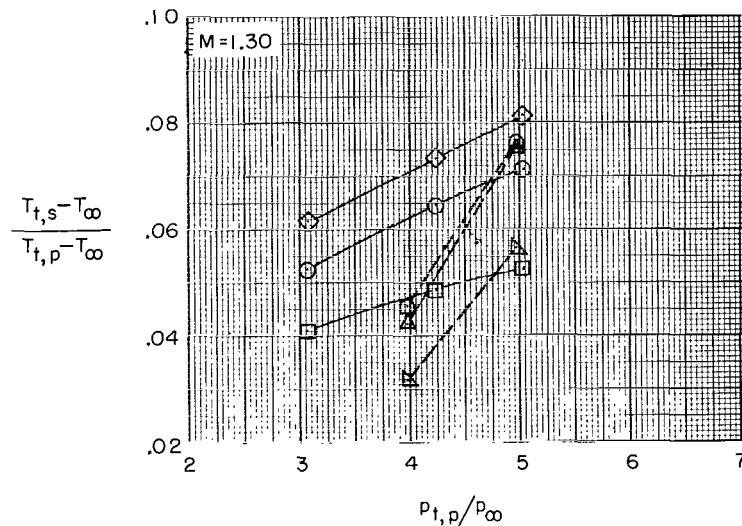
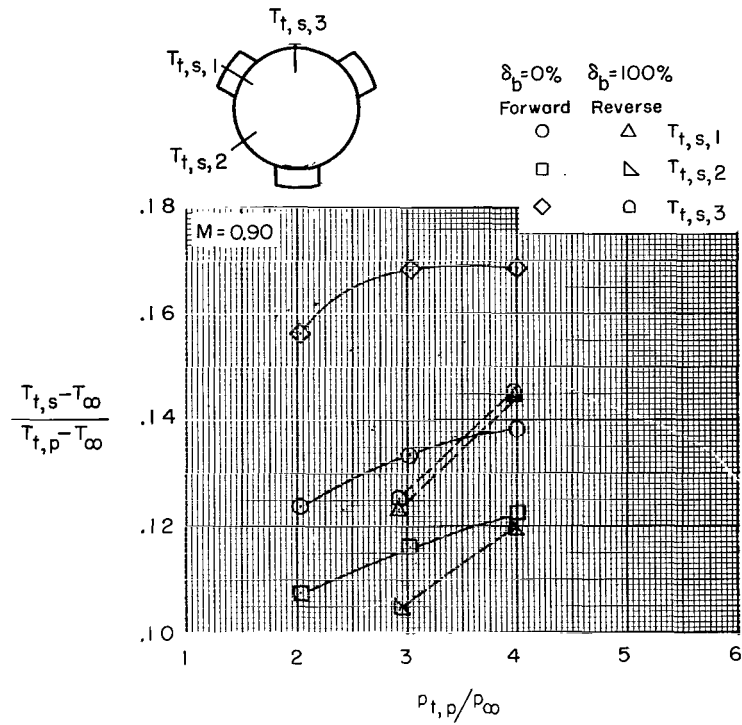


Figure 27.- Variation of ejector pumping characteristics with Mach number for estimated engine-operating pressure ratios as given in figure 11.



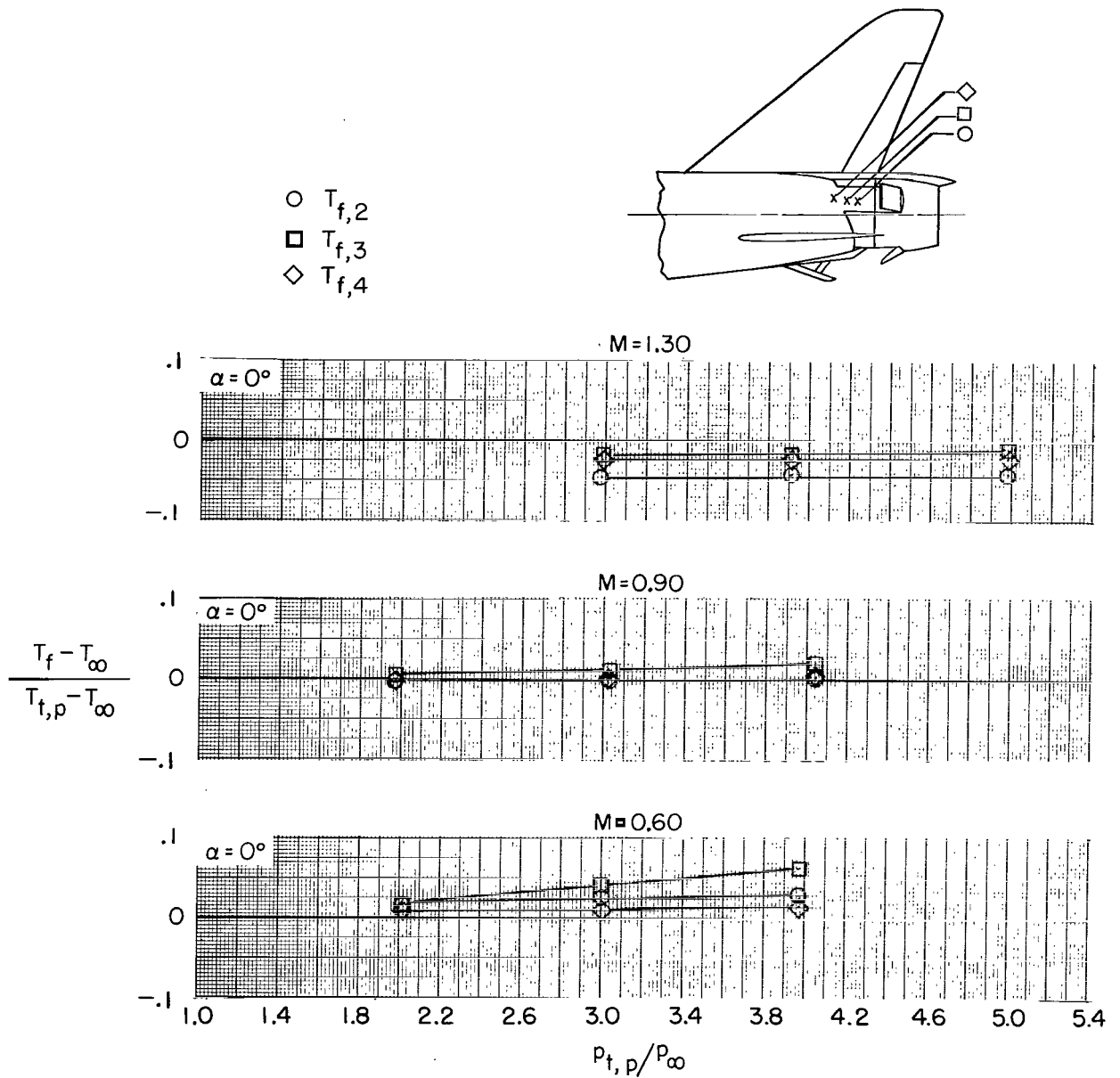
(a) $M = 0.34$ and 0.60 .

Figure 28.- Comparison of secondary-cooling-air temperature for forward- and reverse-thrust operation at $\alpha = 0^\circ$, $\delta_{du} = 32.5^\circ$, and $\delta_{dl} = 52.5^\circ$.



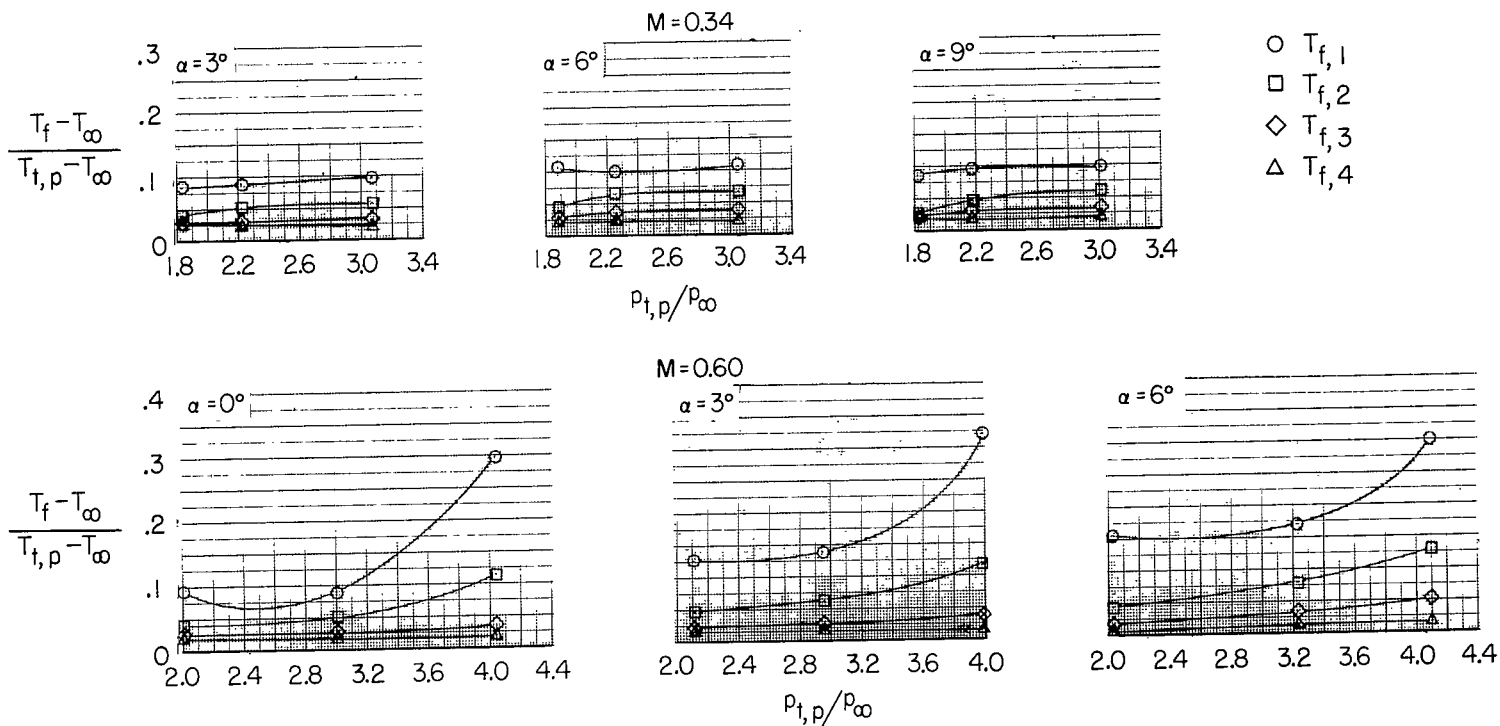
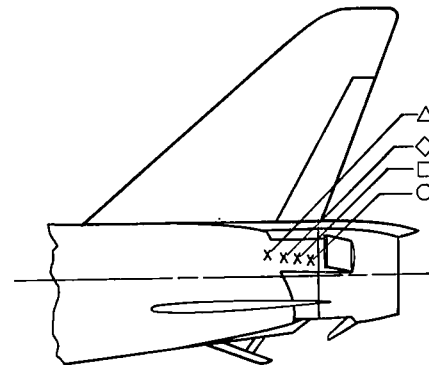
(b) $M = 0.90$ and 1.30 .

Figure 28.- Concluded.



(a) $\delta_{du} = \text{Faired}$; $\delta_{dl} = \text{Faired}$; $\delta_b = 0\%$.

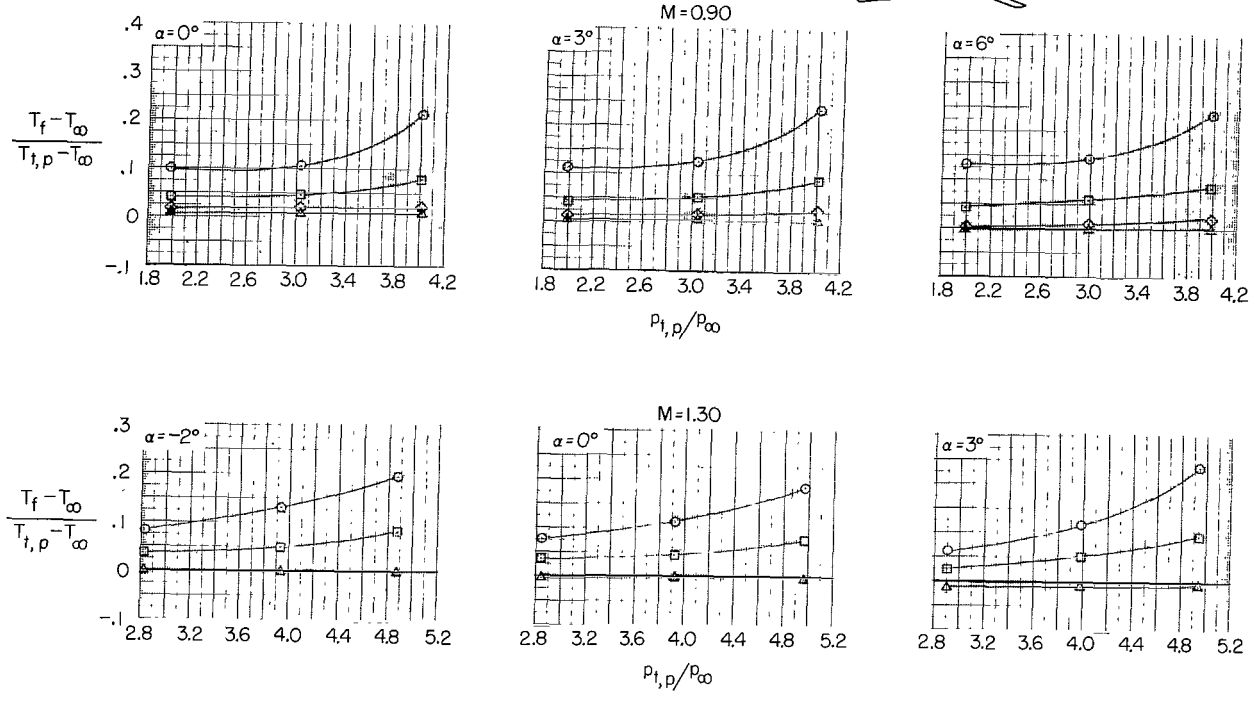
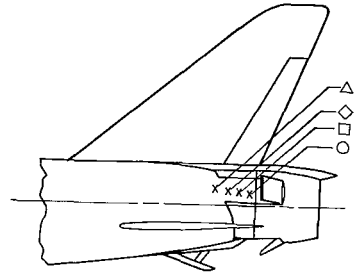
Figure 29.- Variation of local fuselage temperatures with primary-nozzle-jet total-pressure ratio for various TCU configurations.



(b) $\delta_{du} = 32.5^\circ$; $\delta_{dl} = 52.5^\circ$; $\delta_b = 25\%$.

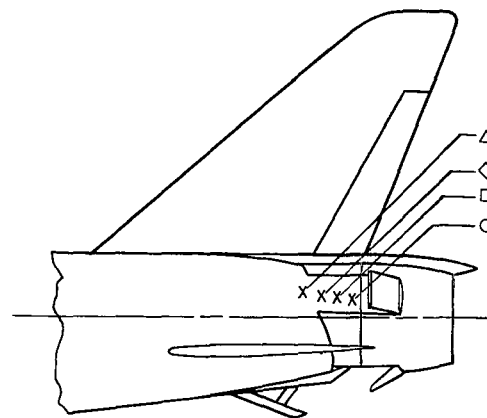
Figure 29.- Continued.

- $T_{f,1}$
- $T_{f,2}$
- ◇ $T_{f,3}$
- △ $T_{f,4}$

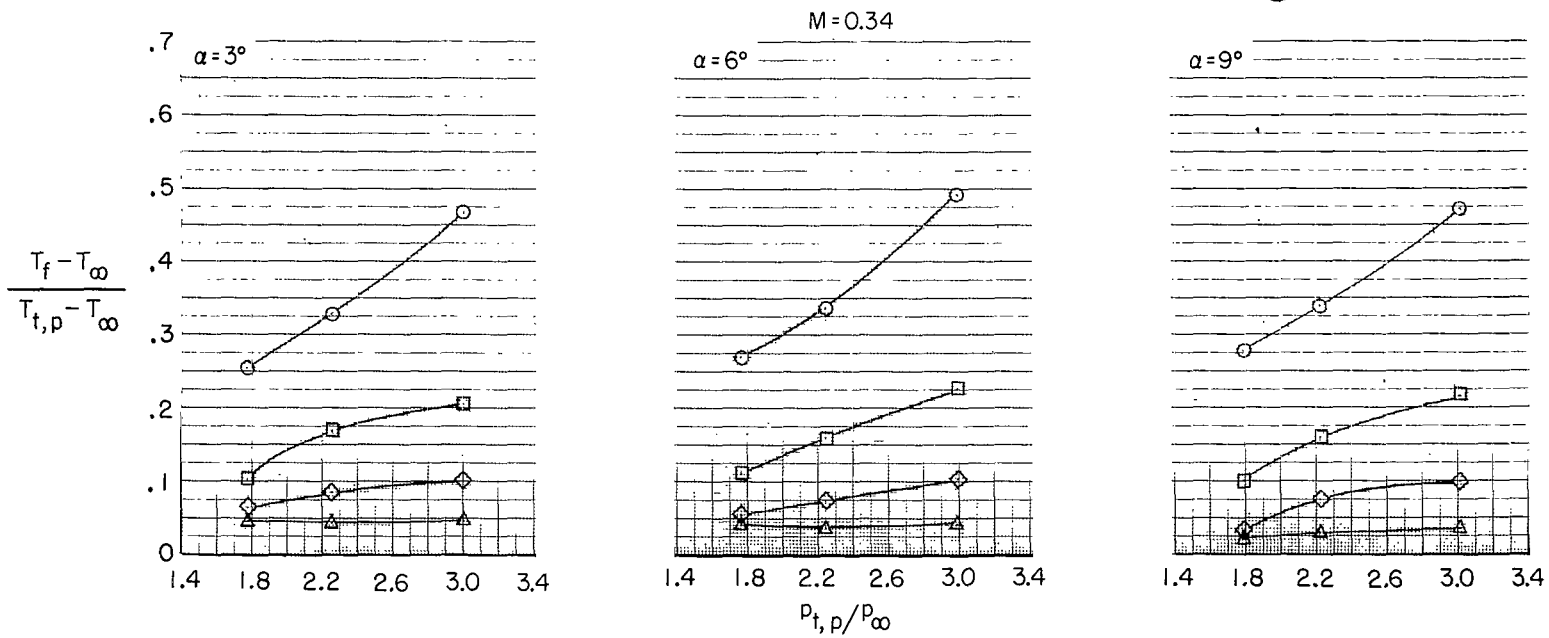


(b) Concluded.

Figure 29.- Continued.



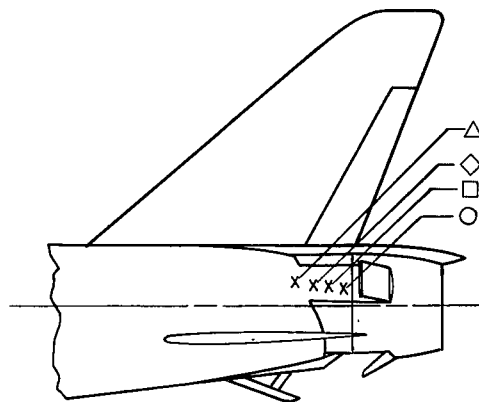
- $T_{f,1}$
- $T_{f,2}$
- ◇ $T_{f,3}$
- △ $T_{f,4}$



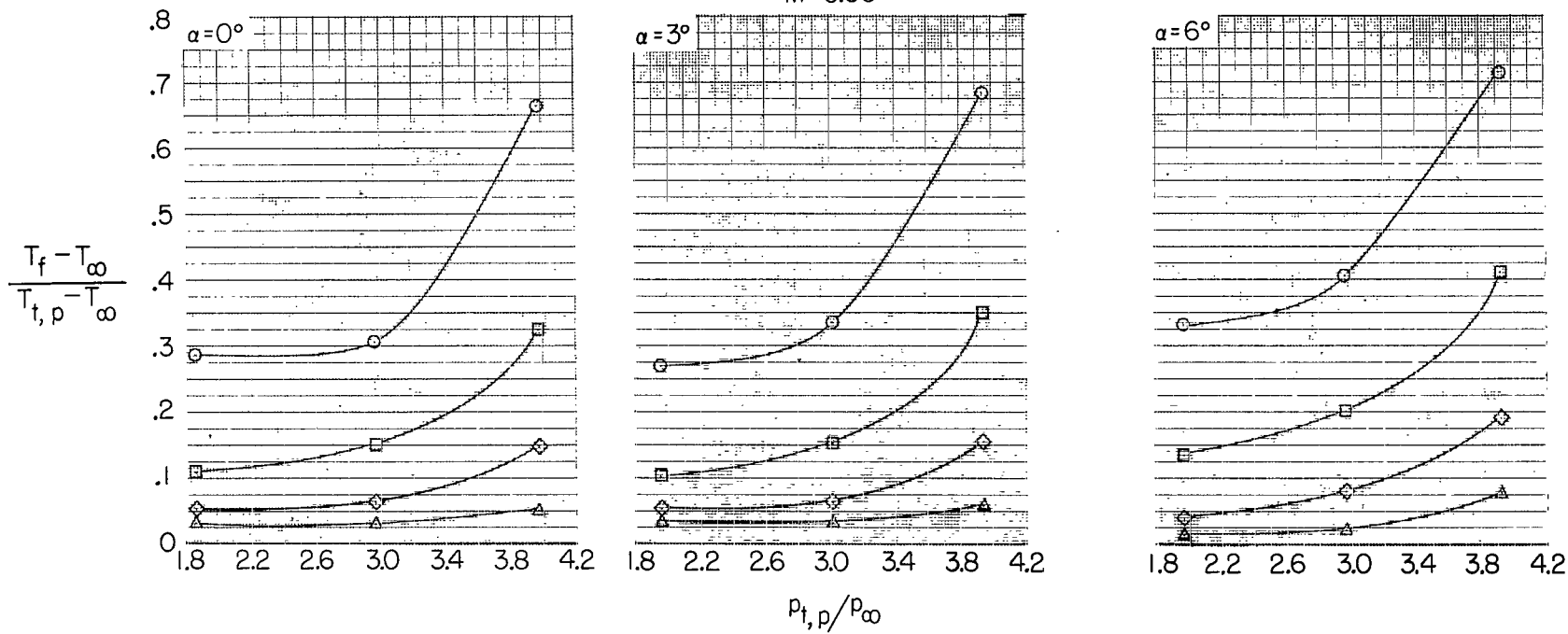
(c) $\delta_{du} = 32.5^\circ$; $\delta_{dl} = 52.5^\circ$; $\delta_b = 50\%$.

Figure 29.- Continued.

- $T_{f,1}$
- $T_{f,2}$
- ◇ $T_{f,3}$
- △ $T_{f,4}$



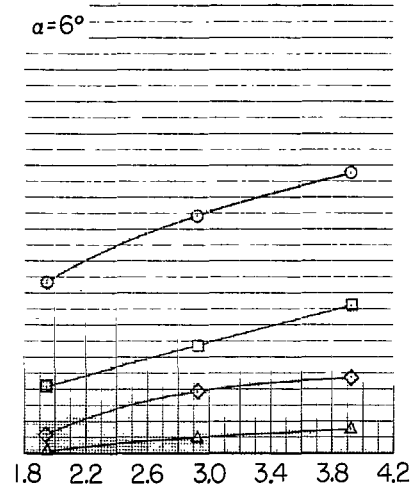
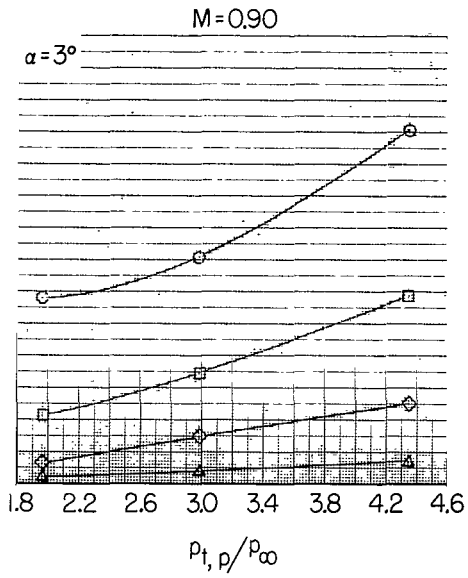
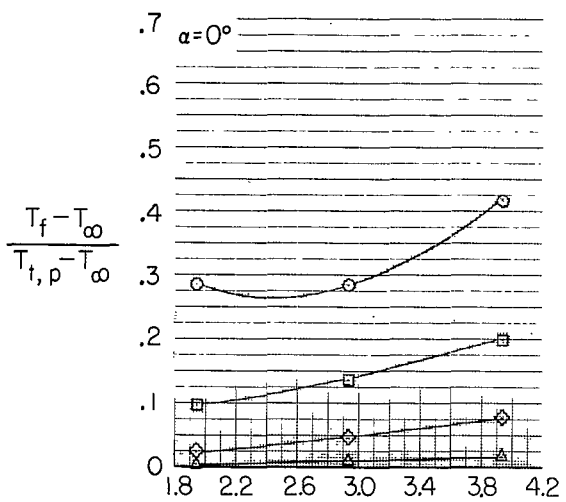
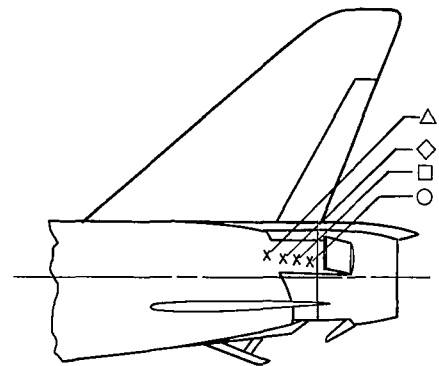
M=0.60



(c) Continued.

Figure 29.- Continued.

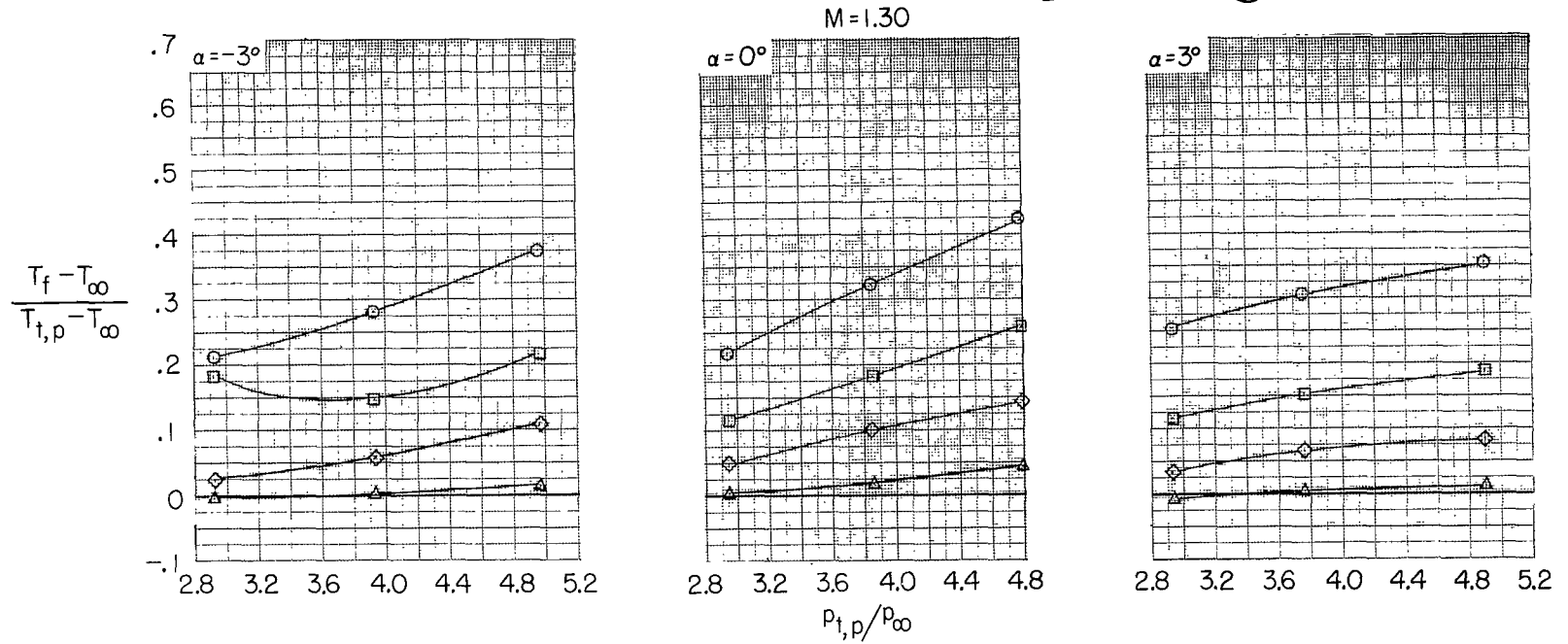
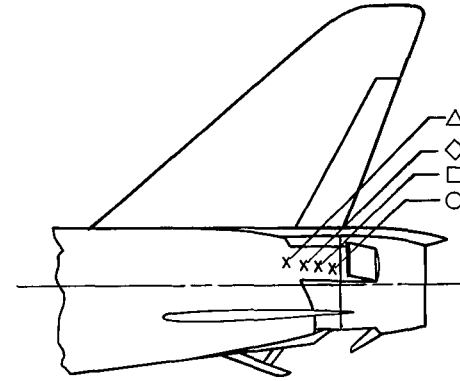
- $T_{f,1}$
- $T_{f,2}$
- ◇ $T_{f,3}$
- △ $T_{f,4}$



(c) Continued.

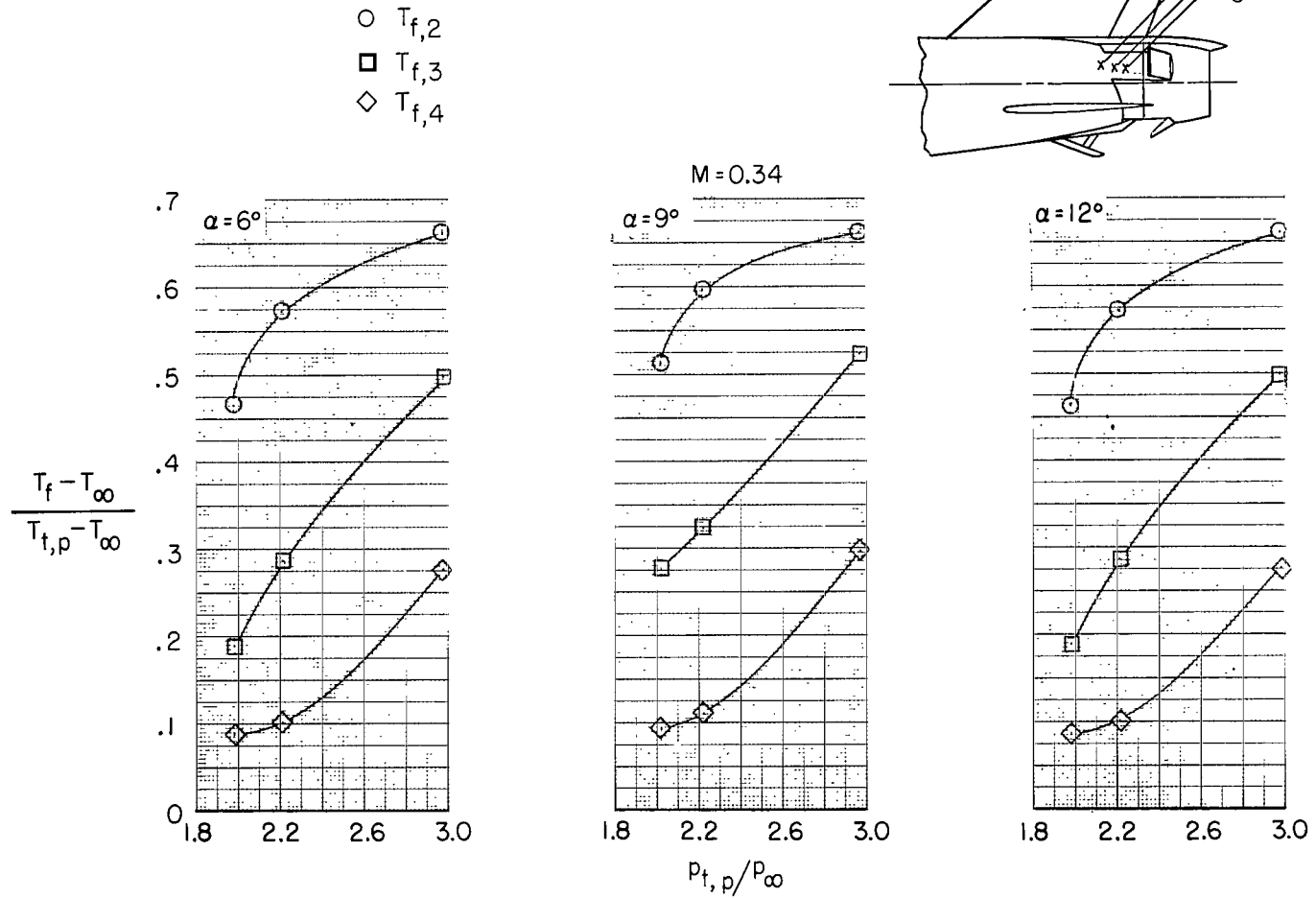
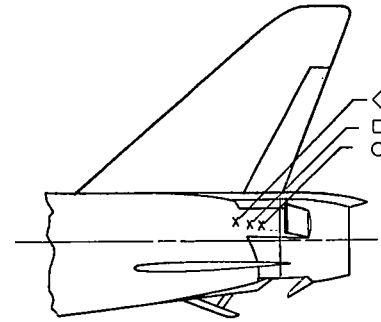
Figure 29.- Continued.

- $T_{f,1}$
- $T_{f,2}$
- ◇ $T_{f,3}$
- △ $T_{f,4}$



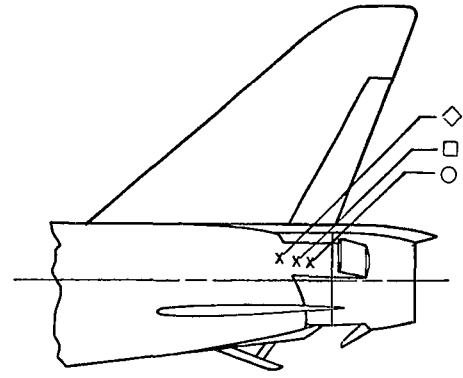
(c) Concluded.

Figure 29.- Continued.



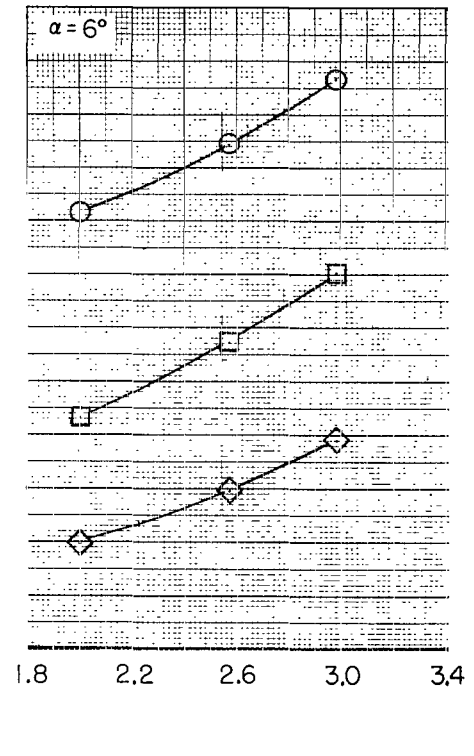
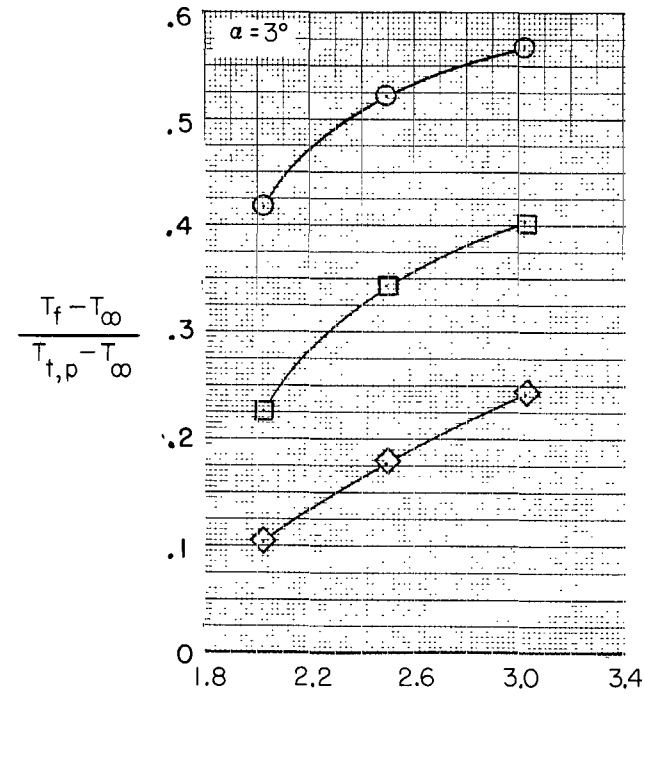
(d) $\delta_{du} = 32.5^\circ$; $\delta_{dl} = 52.5^\circ$; $\delta_b = 75\%$.

Figure 29.- Continued.



M=0.60

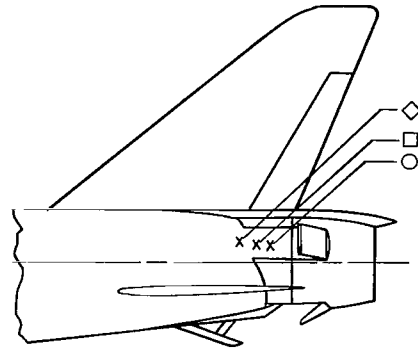
- $T_{f,2}$
- $T_{f,3}$
- ◇ $T_{f,4}$



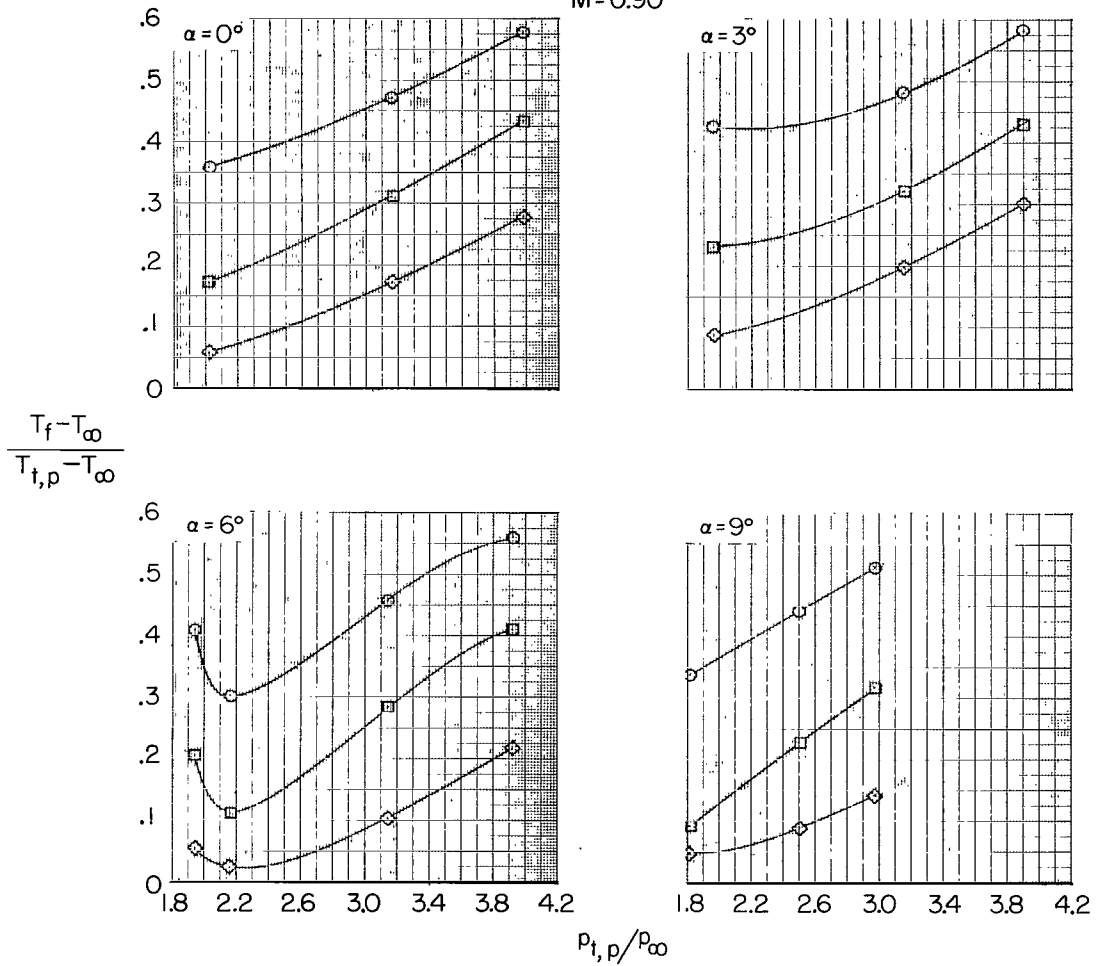
(d) Continued.

Figure 29.- Continued.

- $T_{f,2}$
- $T_{f,3}$
- ◇ $T_{f,4}$

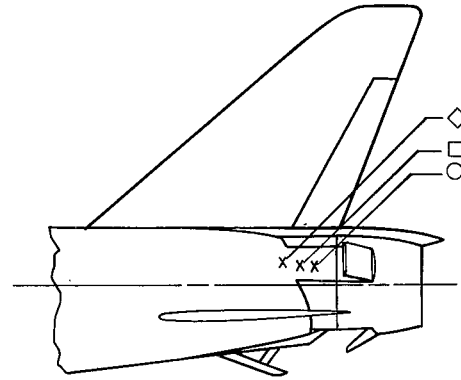
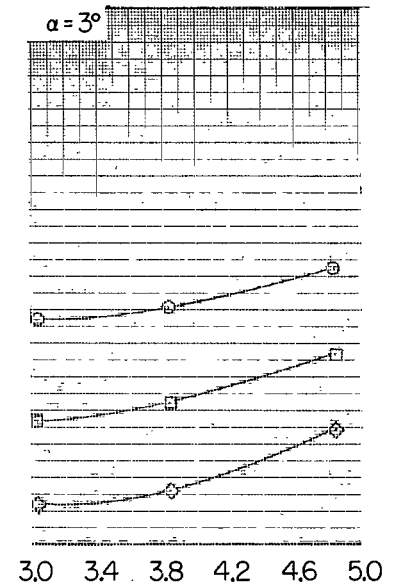
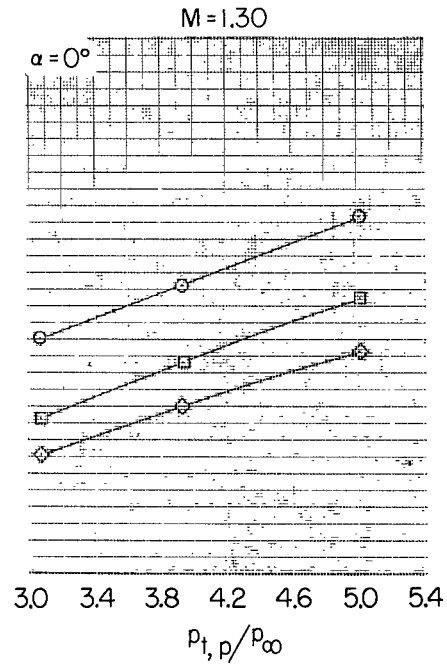
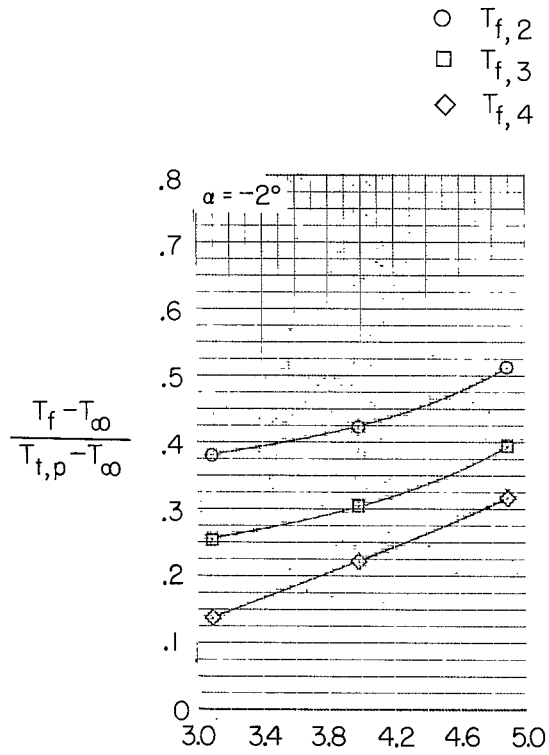


M=0.90



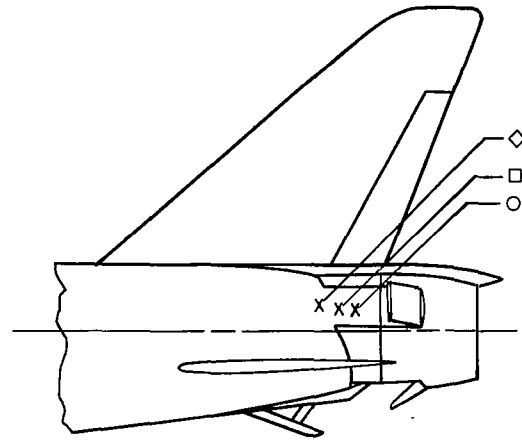
(d) Continued.

Figure 29.- Continued.

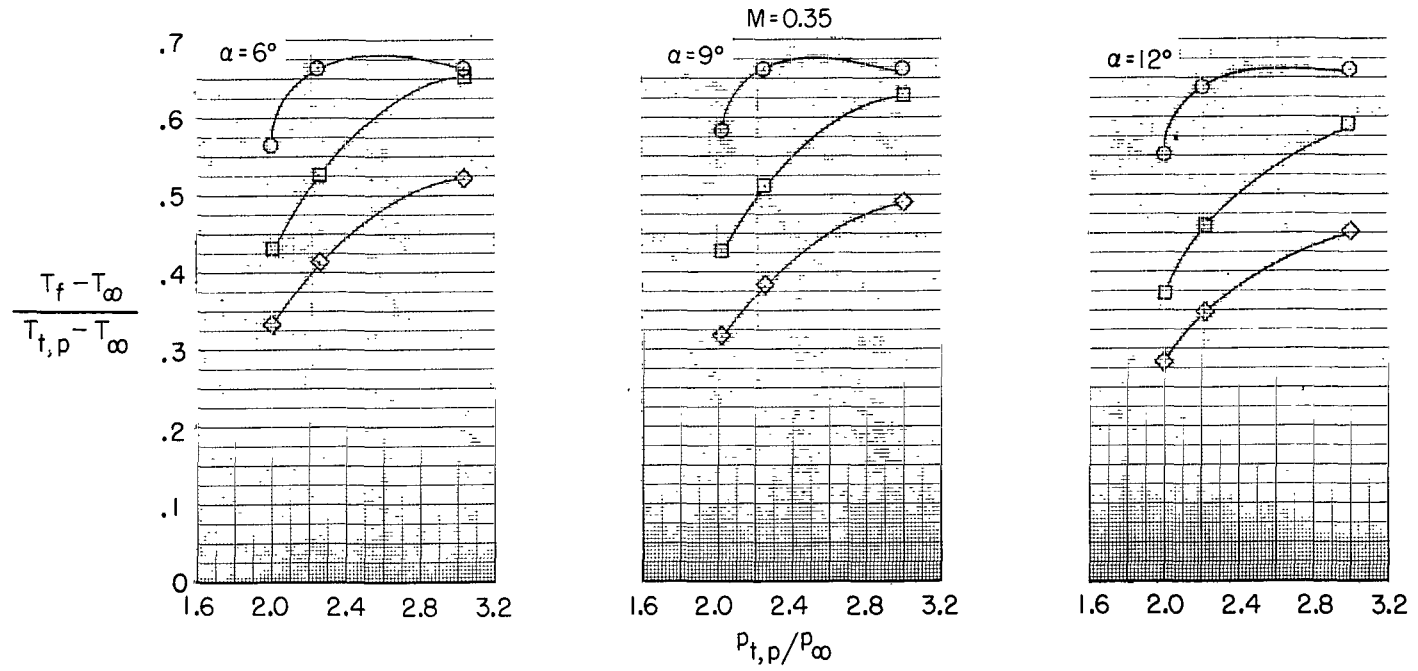


(d) Concluded.

Figure 29.- Continued.

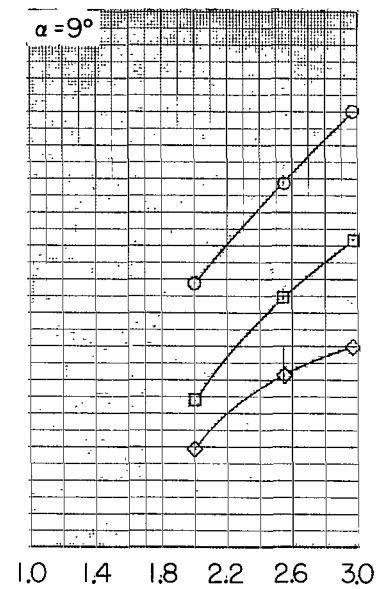
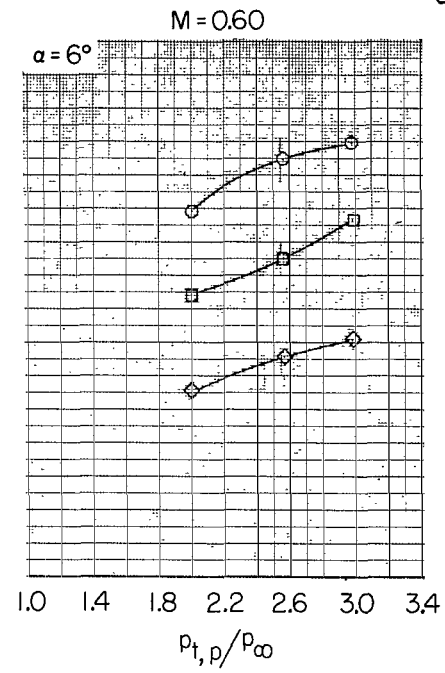
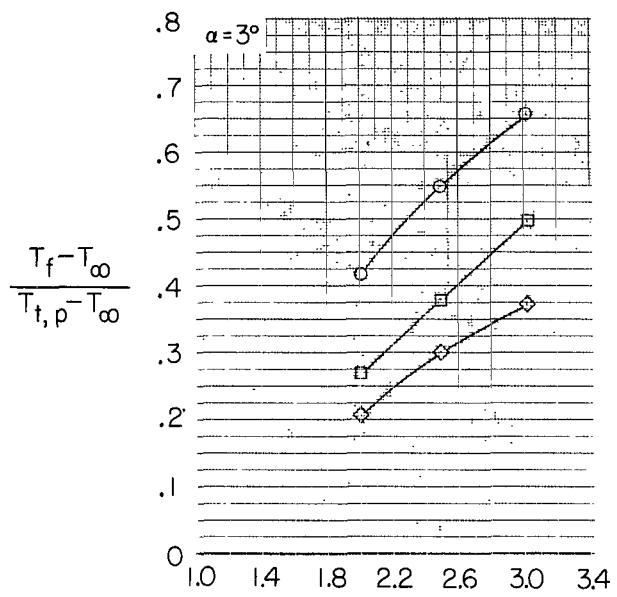
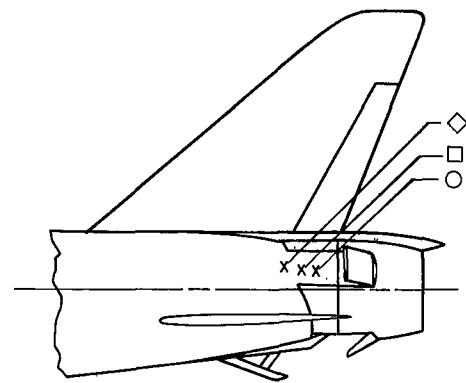


○ $T_{f,2}$
 □ $T_{f,3}$
 ◇ $T_{f,4}$



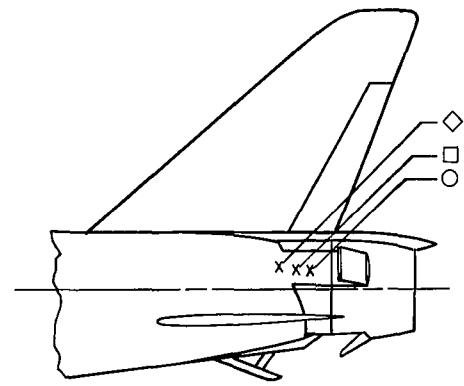
(e) $\delta_{du} = 32.5^\circ$; $\delta_{dl} = 52.5^\circ$; $\delta_b = 90\%$.

Figure 29.- Continued.

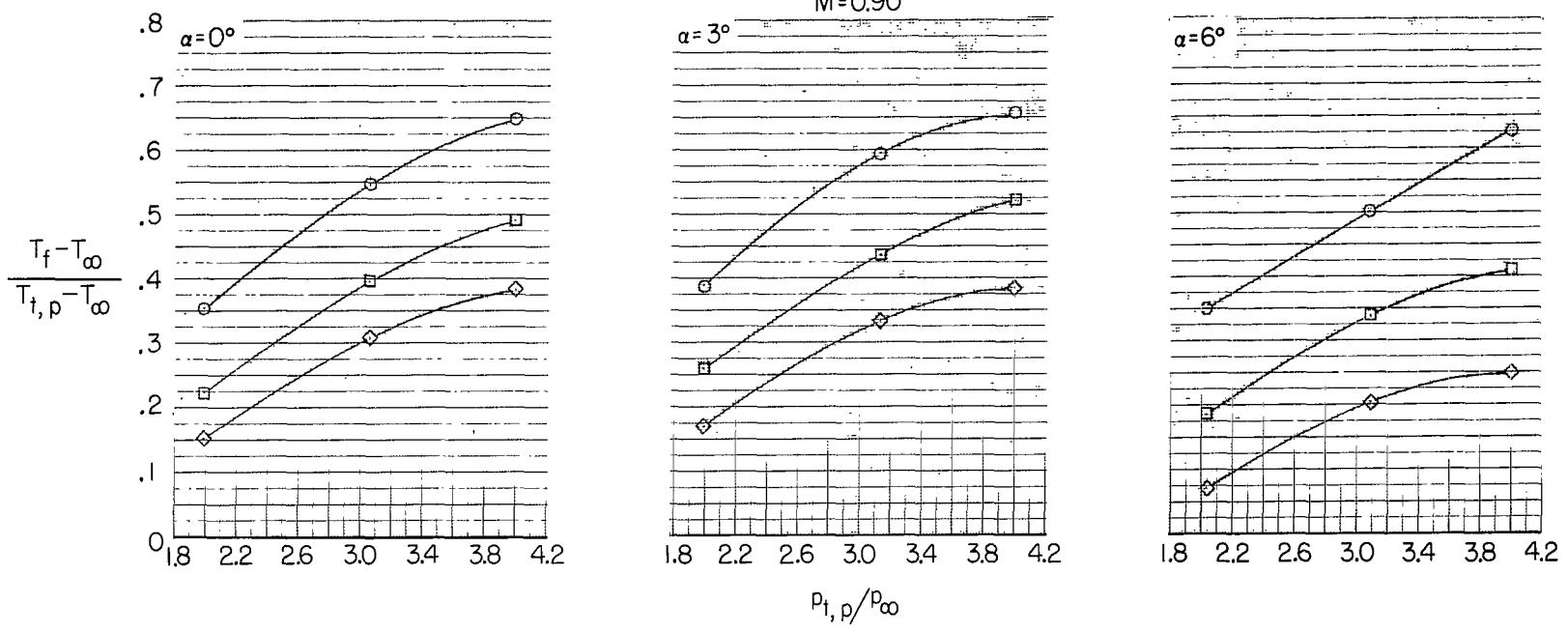


(e) Continued.

Figure 29.- Continued.

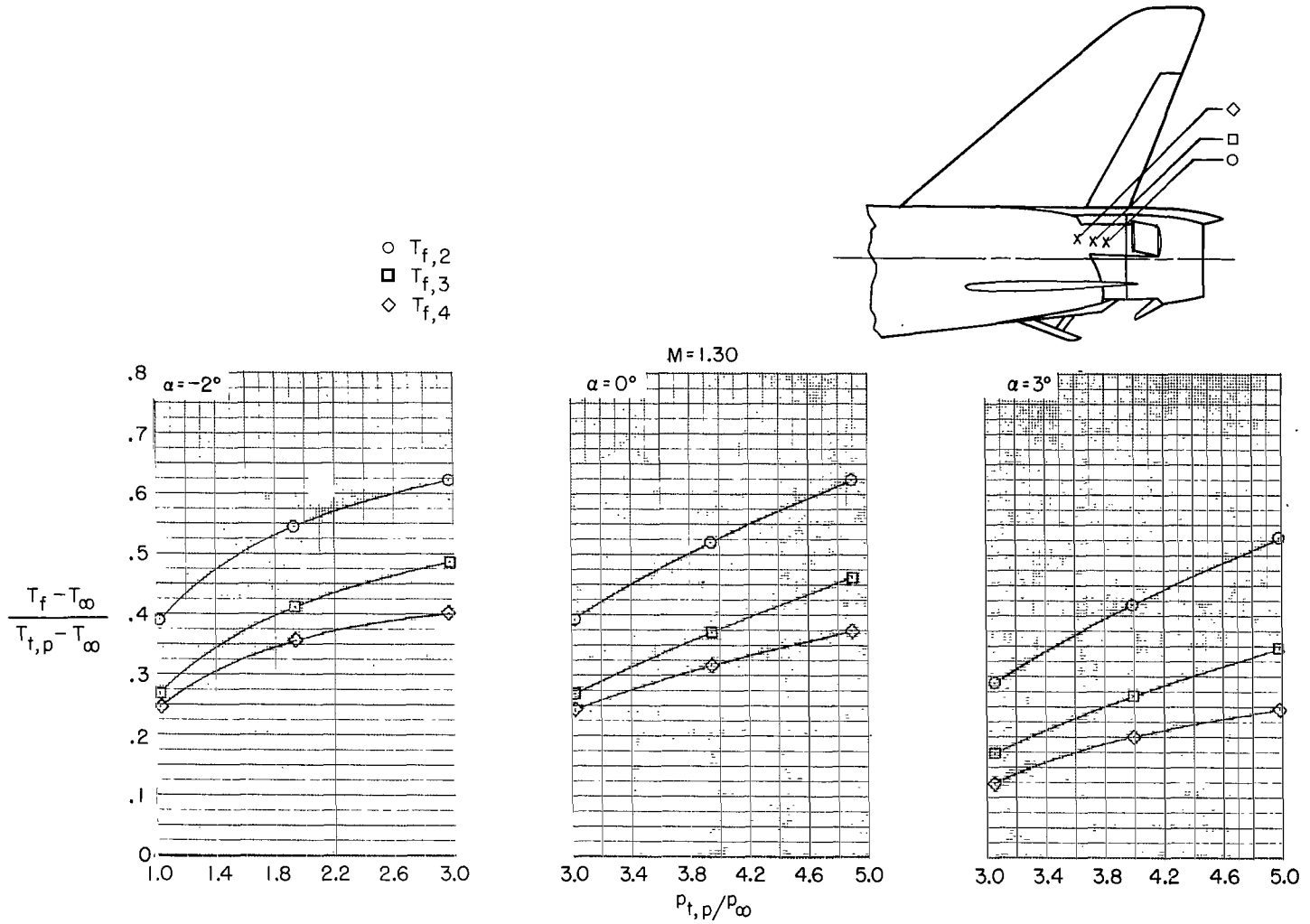


- T_{f,2}
- T_{f,3}
- ◇ T_{f,4}



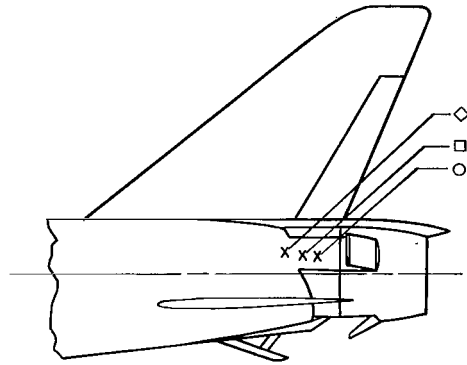
(e) Continued.

Figure 29.- Continued.



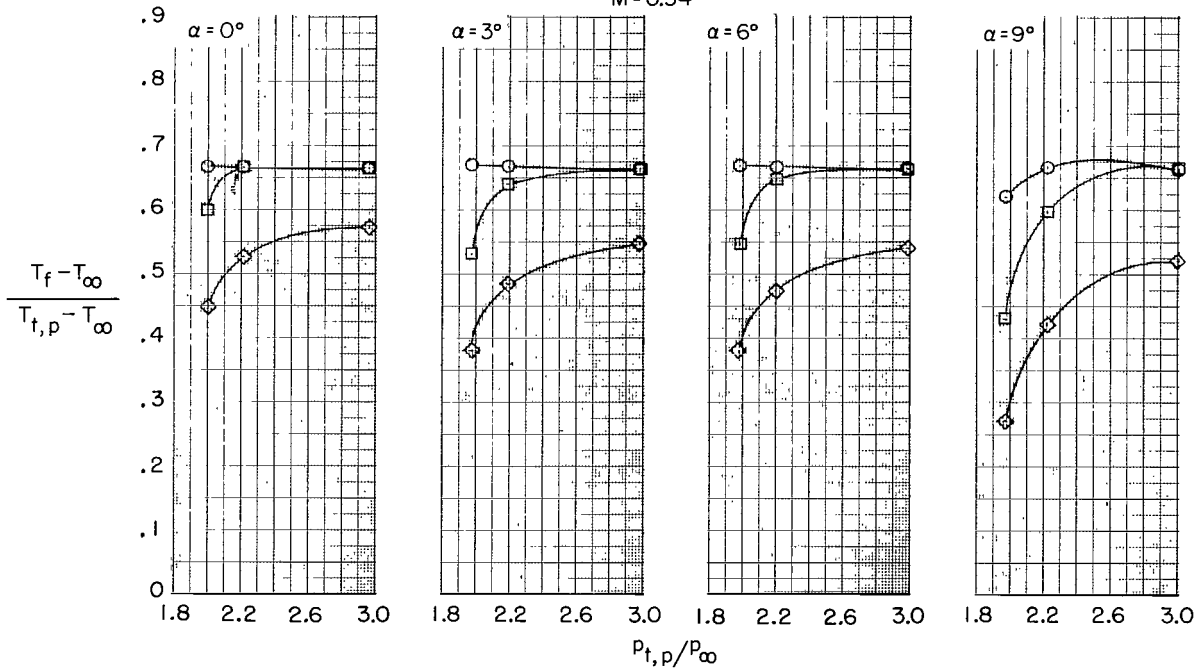
(e) Concluded.

Figure 29.- Continued.



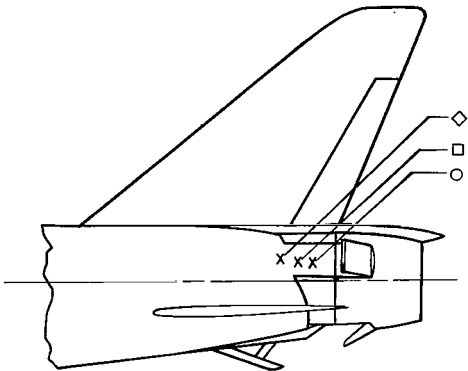
- $T_{f,2}$
- $T_{f,3}$
- ◇ $T_{f,4}$

M = 0.34

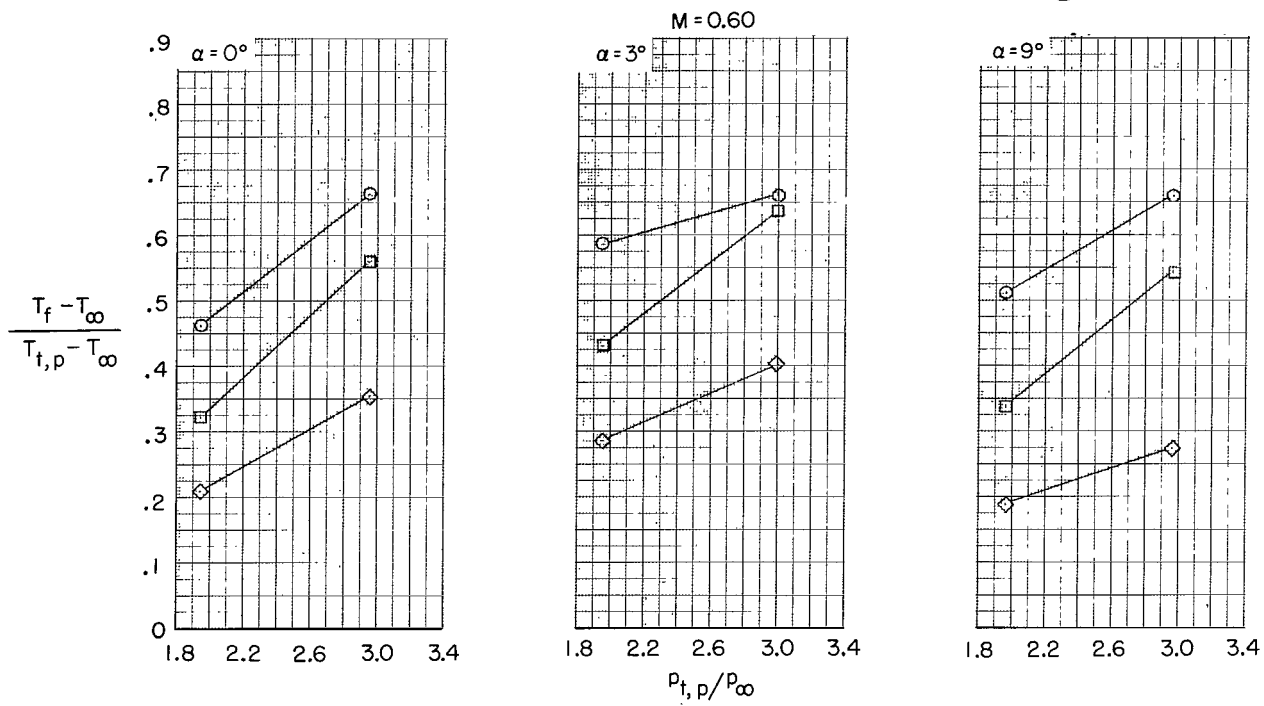


(f) $\delta_{du} = 32.5^\circ$; $\delta_{dl} = 52.5^\circ$; $\delta_b = 100\%$.

Figure 29.- Continued.

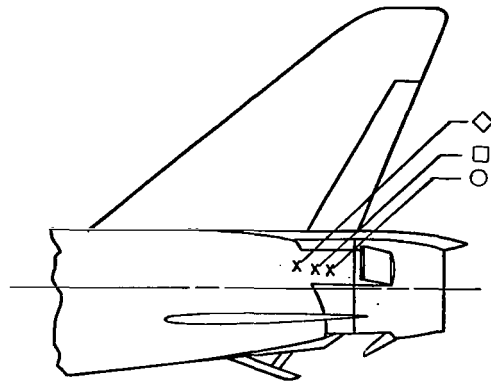


- $T_{f,2}$
- $T_{f,3}$
- ◇ $T_{f,4}$

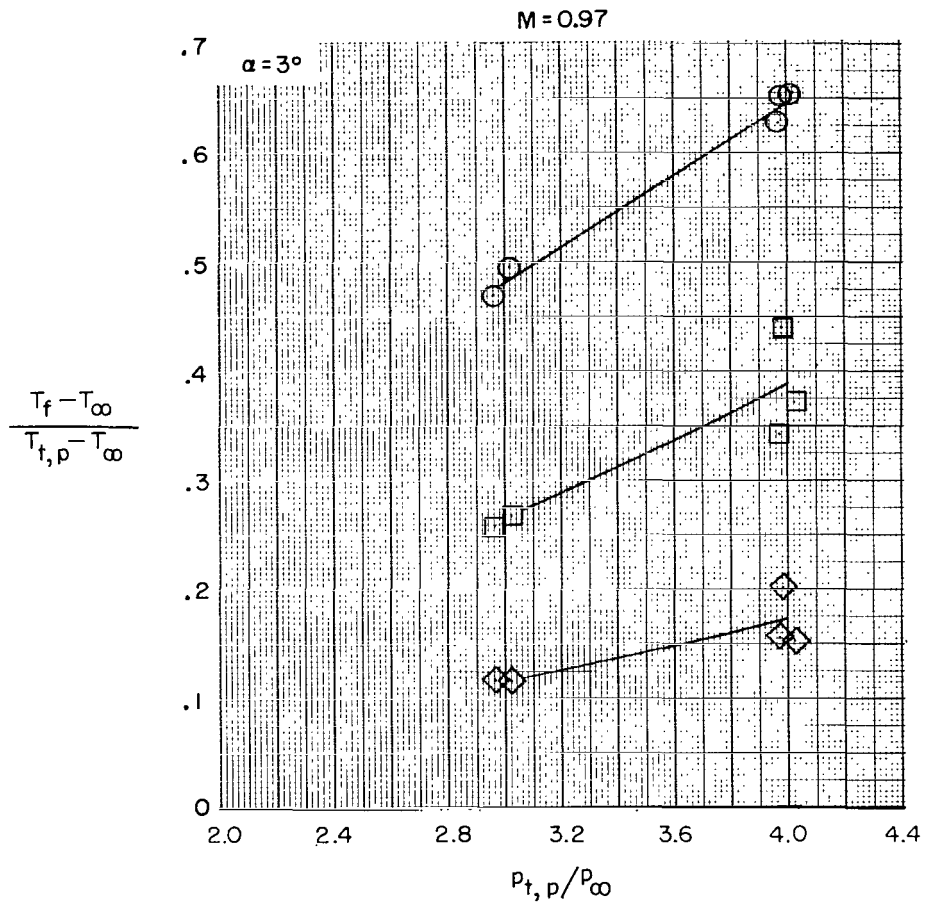


(f) Continued.

Figure 29. - Continued.



- $T_{f,2}$
- $T_{f,3}$
- ◇ $T_{f,4}$



(f) Concluded.

Figure 29.- Concluded.

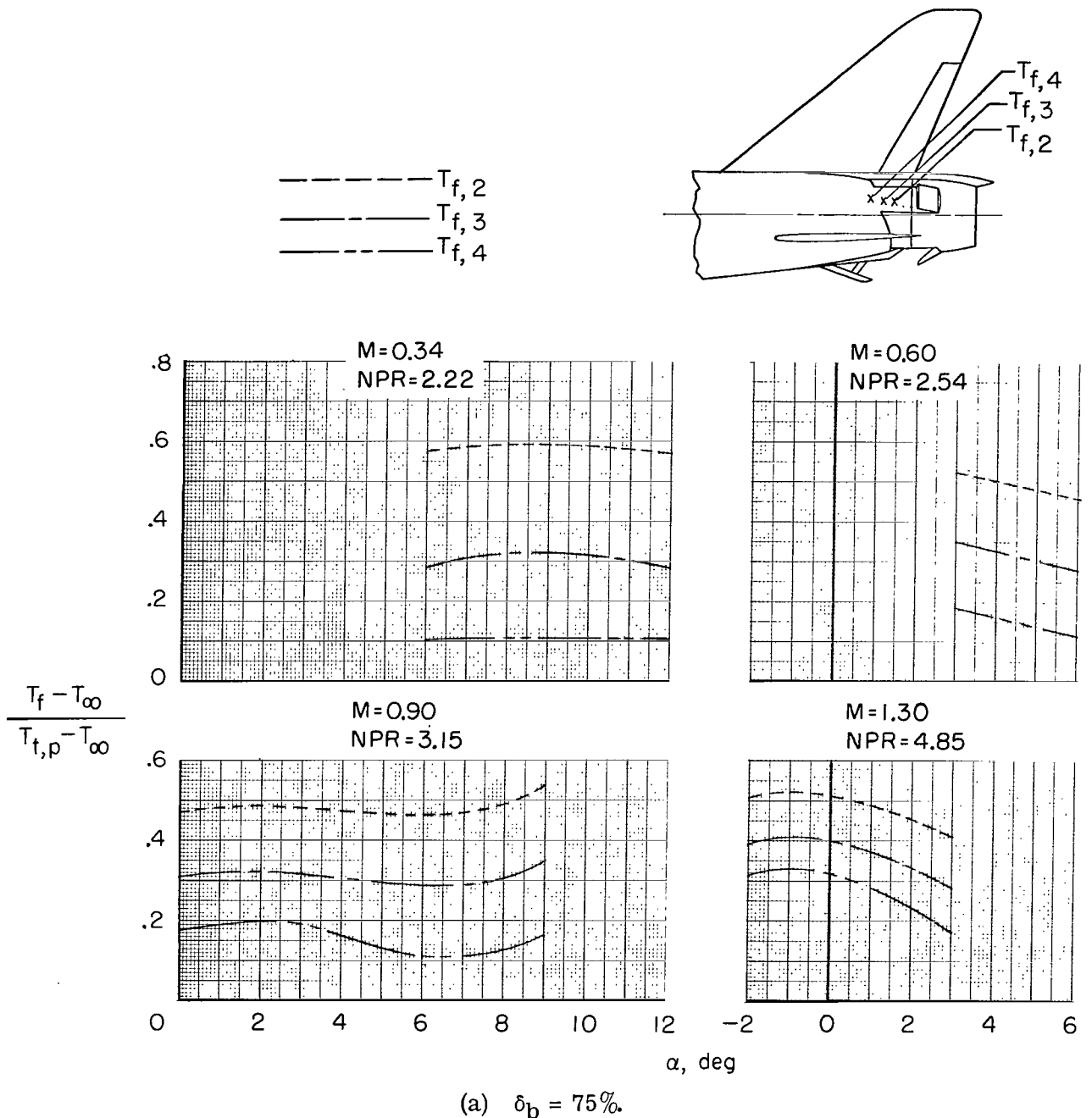
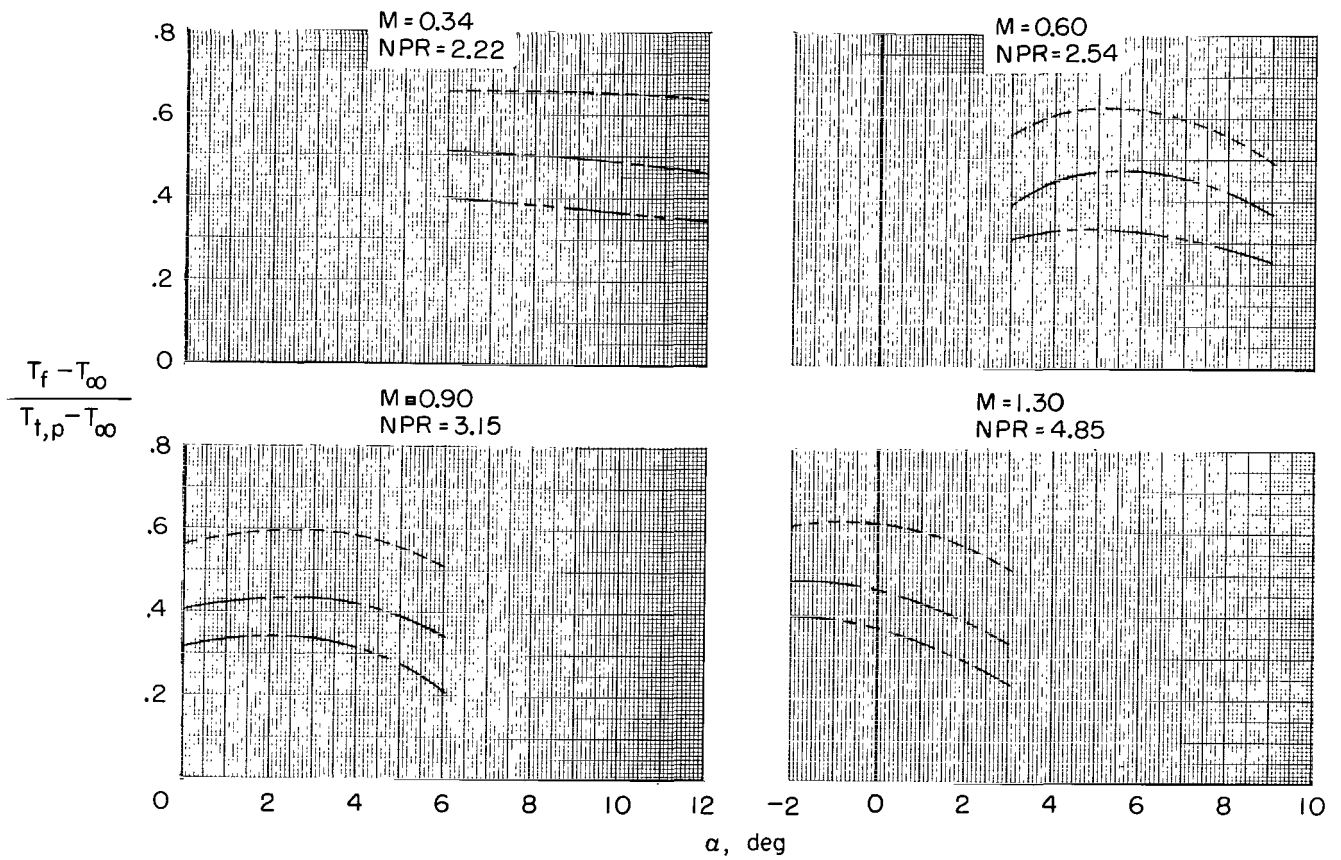
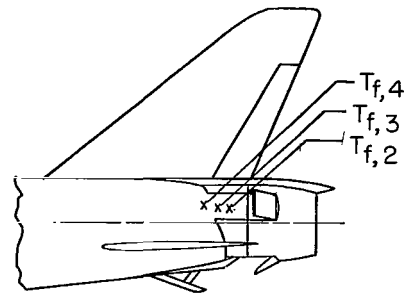


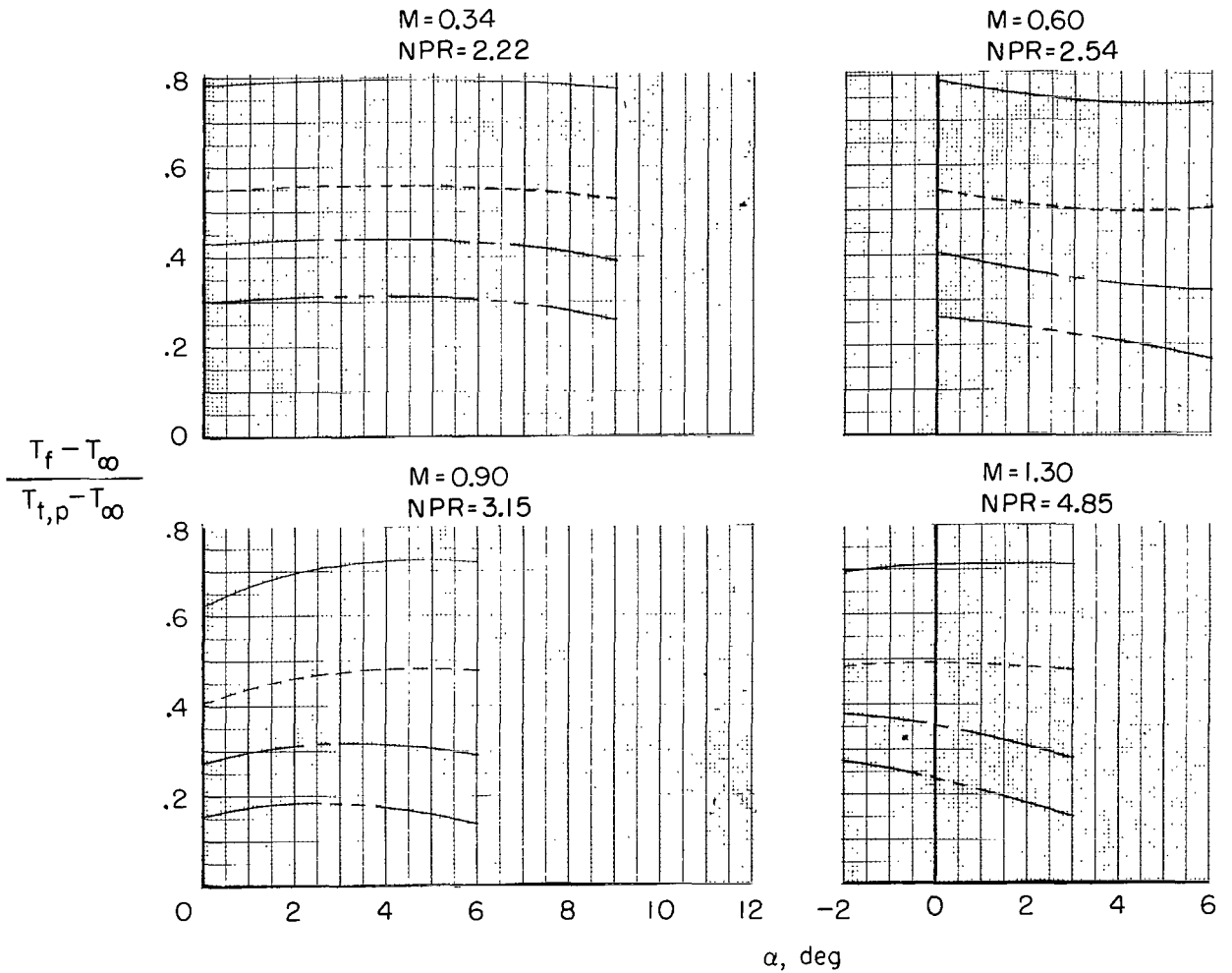
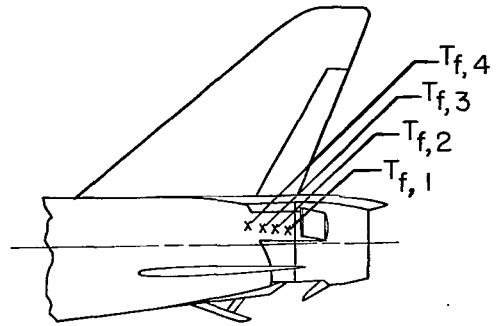
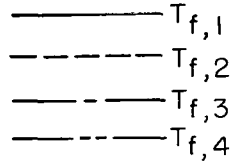
Figure 30.- Variation of local fuselage temperature with angle of attack at the maximum heating condition and representative primary-nozzle-jet total-pressure ratios for the selected deflector-door setting. $\delta_{du} = 32.5^\circ$; $\delta_{dl} = 52.5^\circ$.

- - - - - $T_{f,2}$
 - - - - - $T_{f,3}$
 - - - - - $T_{f,4}$



(b) $\delta_b = 90\%$.

Figure 30.- Continued.



(c) $\delta_b = 100\%$.

Figure 30.- Concluded.

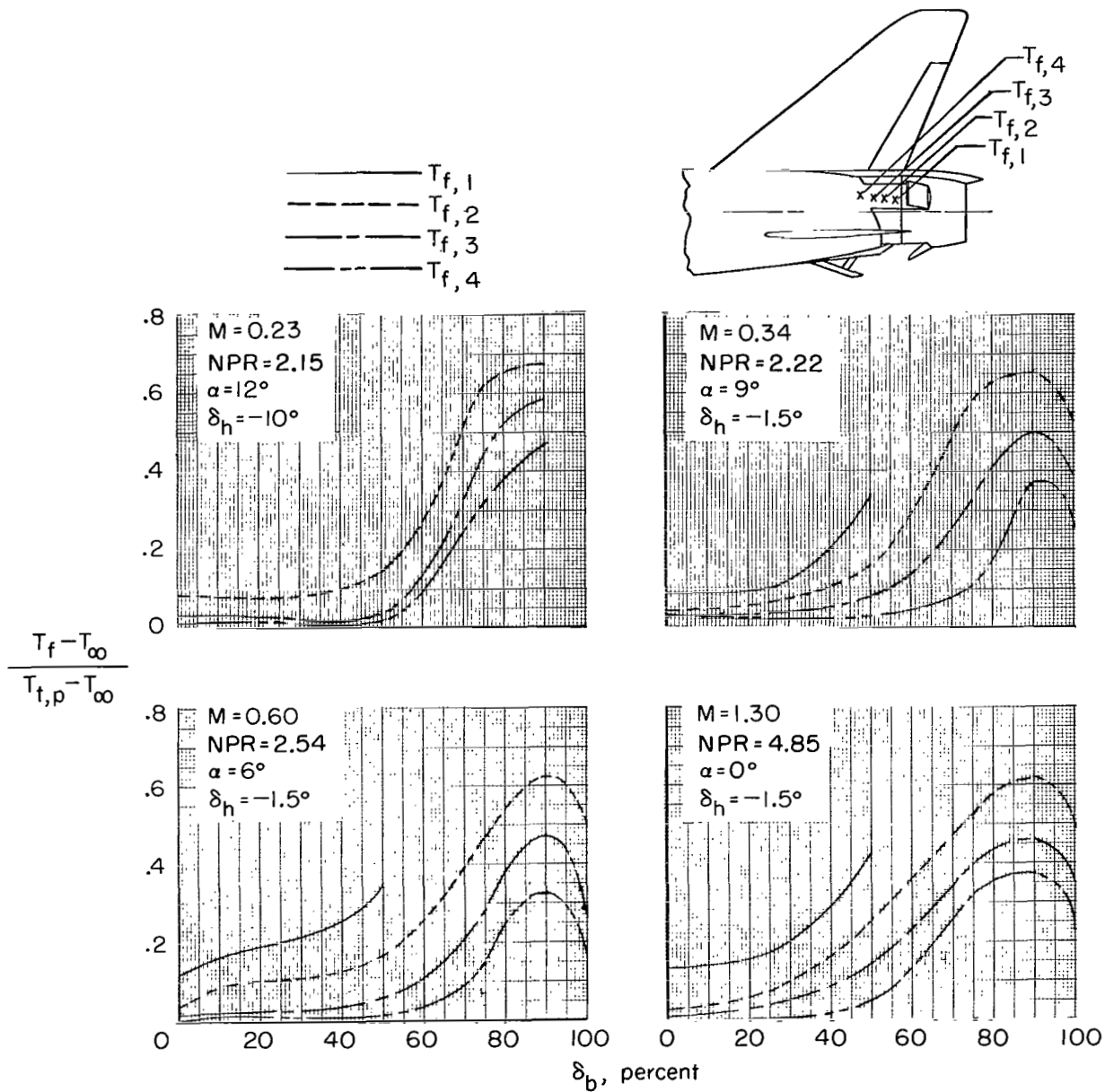
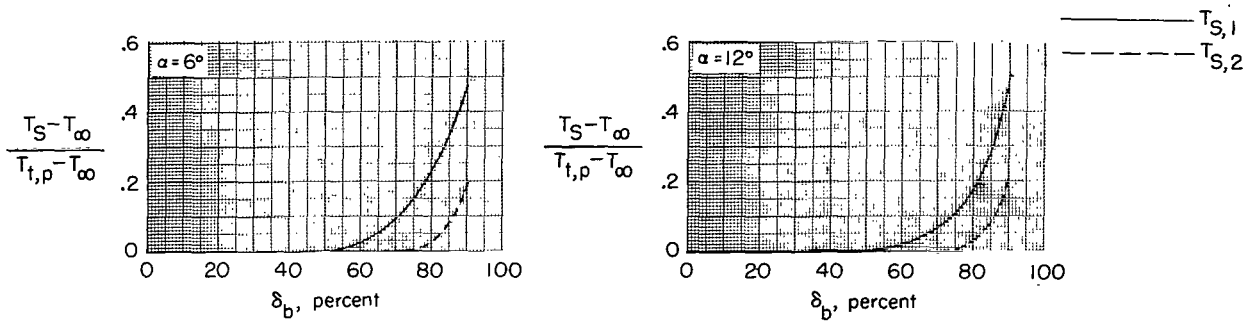
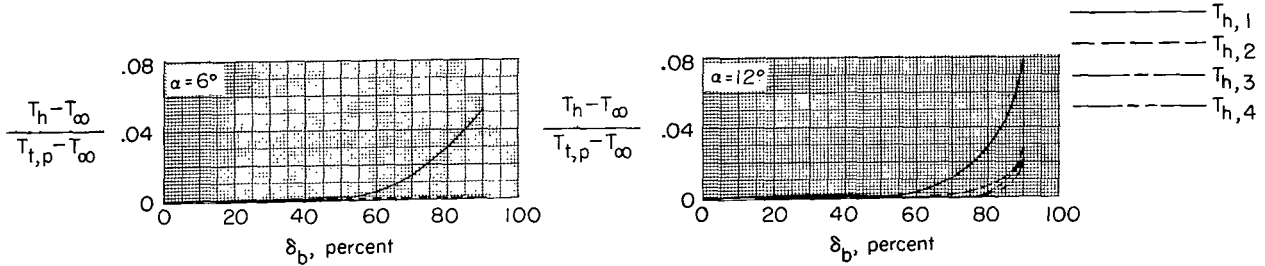


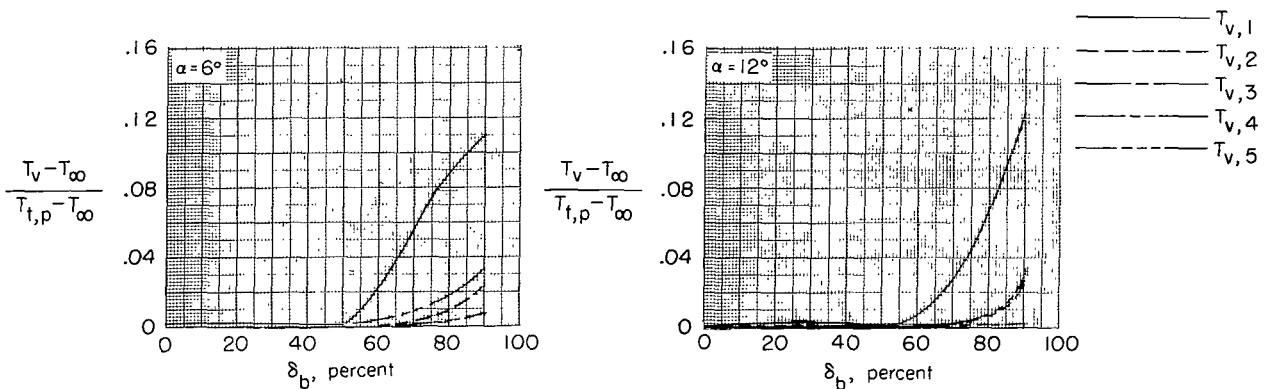
Figure 31.- Variation of local fuselage temperatures with blocker-door position for the selected deflector-door setting. $\delta_{du} = 32.5^\circ$; $\delta_{dl} = 52.5^\circ$.



(a) Skeg and tail-hook temperatures.

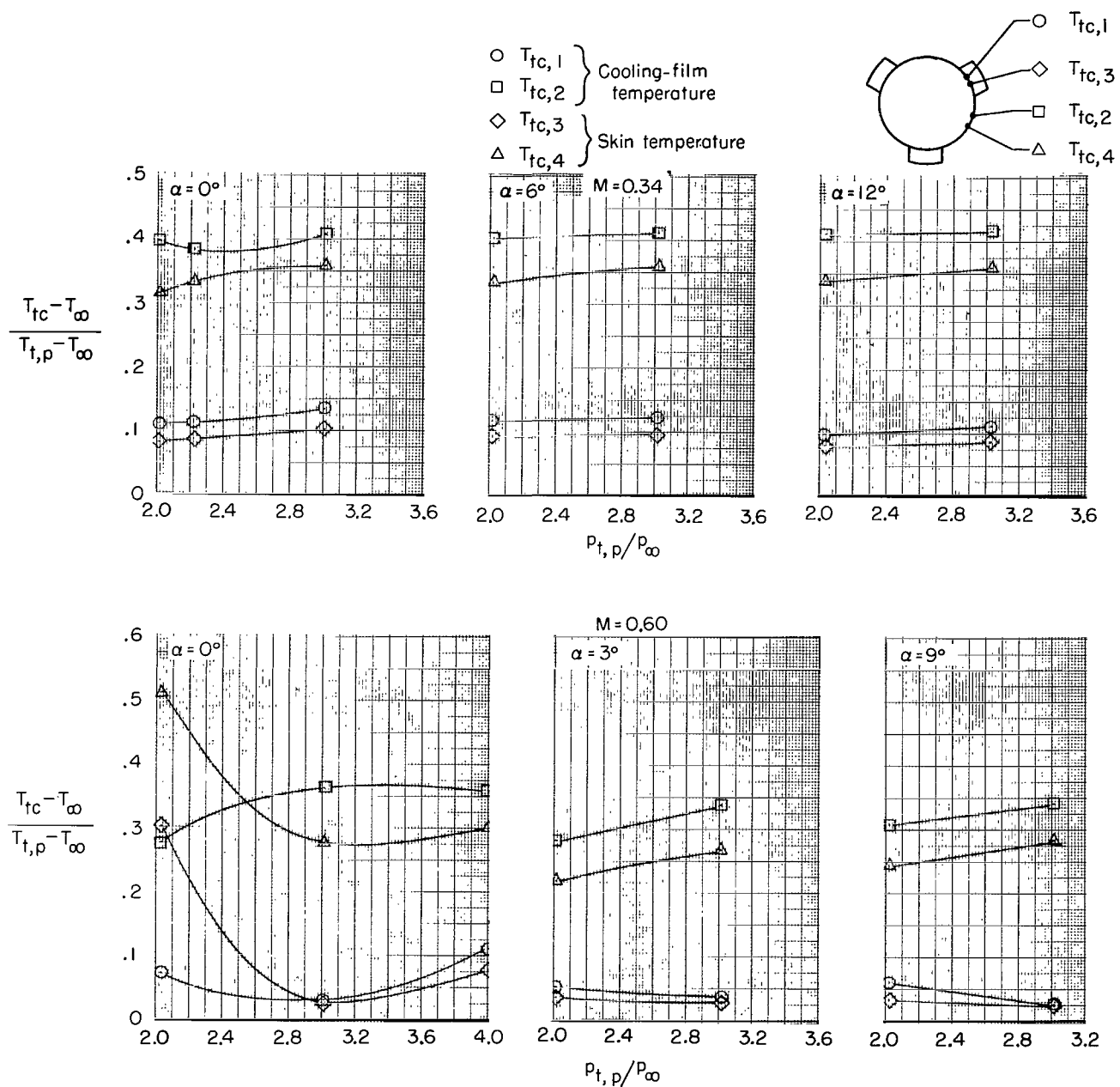


(b) Horizontal-tail temperatures.



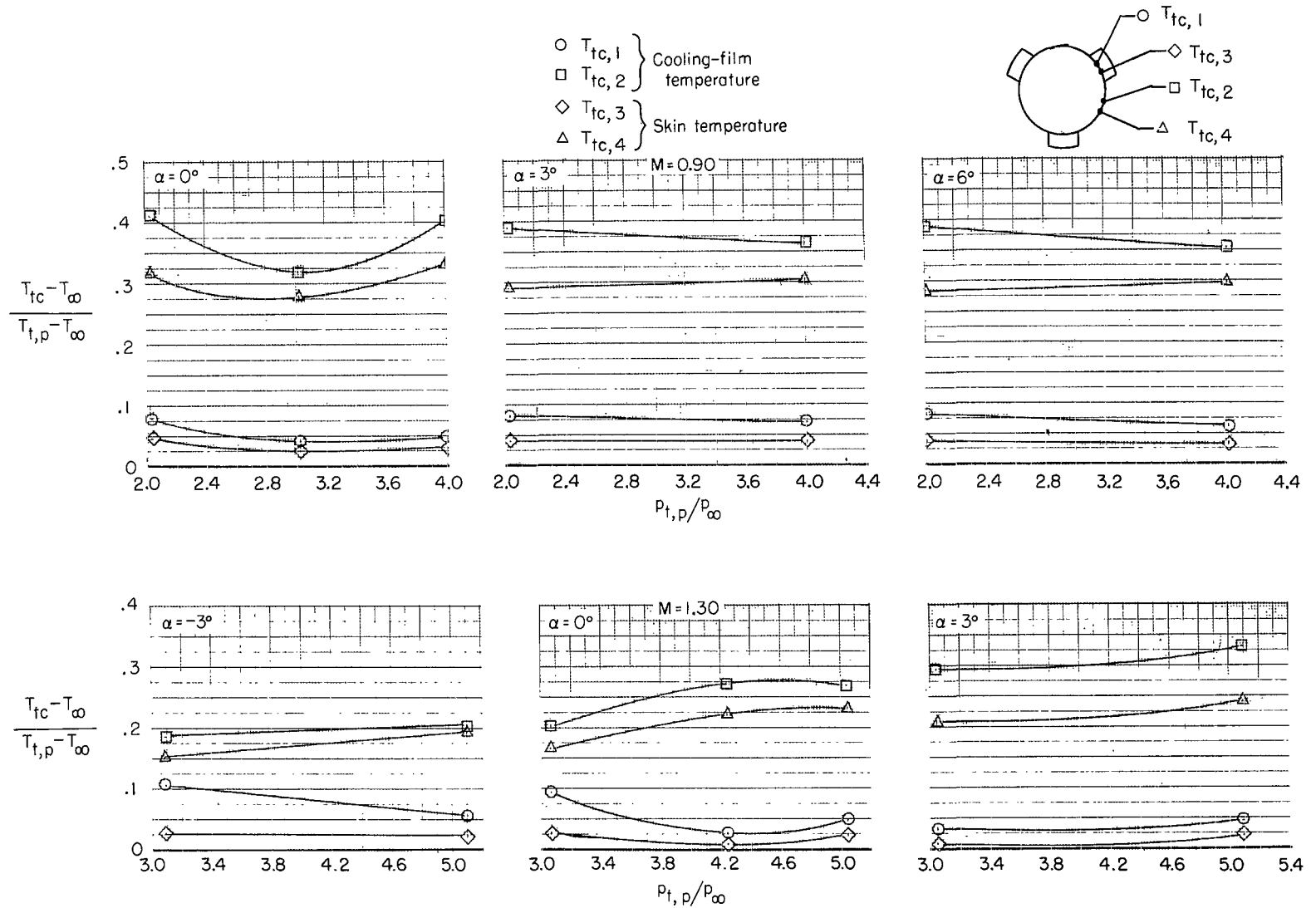
(c) Vertical-tail temperatures.

Figure 32.- Local-temperature variations with blocker-door position for the selected TCU ($\delta_{du} = 32.5^\circ$, $\delta_{dl} = 52.5^\circ$) in the landing-approach configuration. $M = 0.23$; $NPR = 2.15$; reverse-thrust mode. (See fig. 7 for thermocouple locations.)



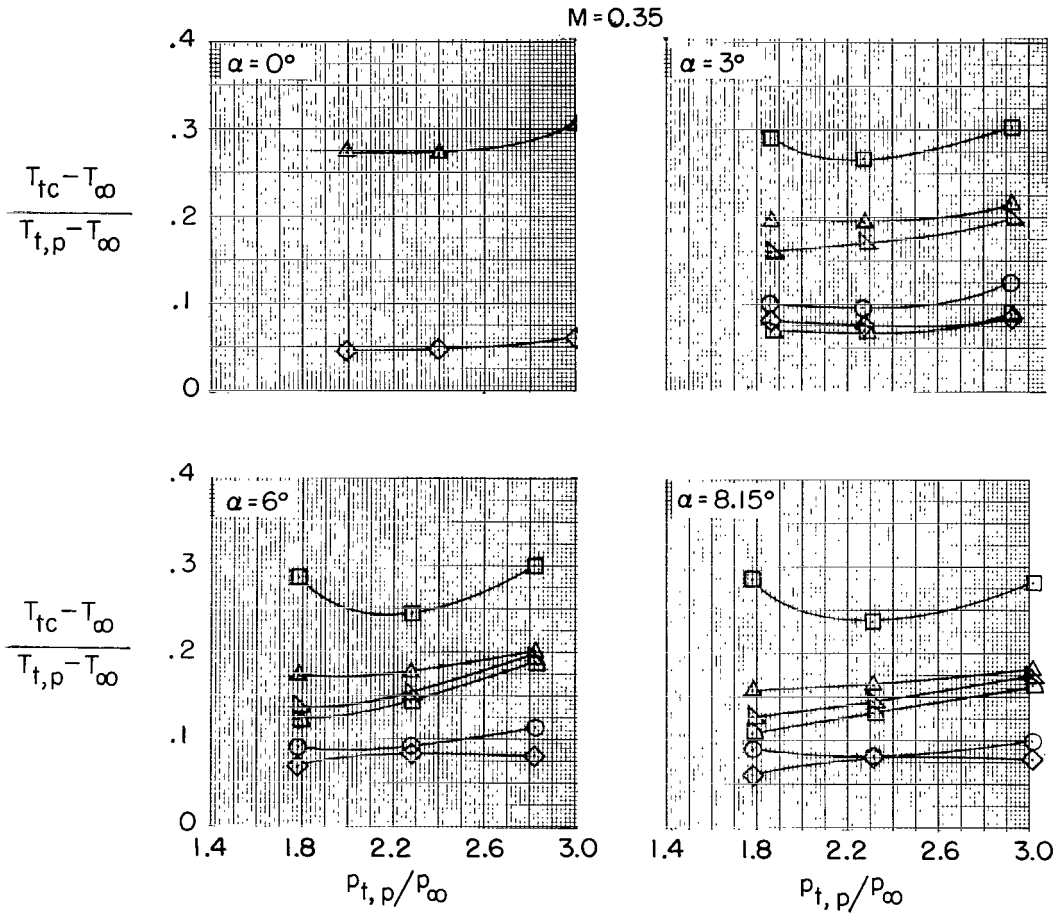
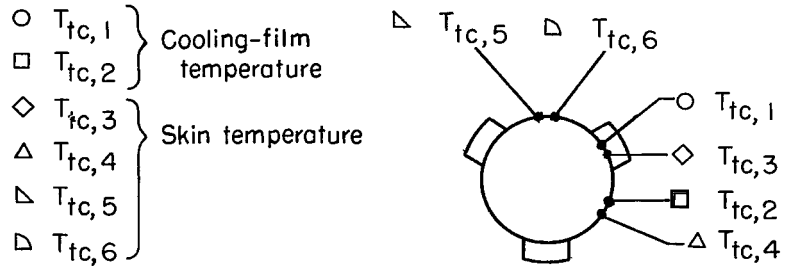
(a) $\delta_{du} = \text{Faired}$; $\delta_{dl} = \text{Faired}$; $\delta_b = 0\%$.

Figure 33.- Variation of TCU cooling-film and inner-skin temperature ratio at military power.



(a) Concluded.

Figure 33.- Continued.

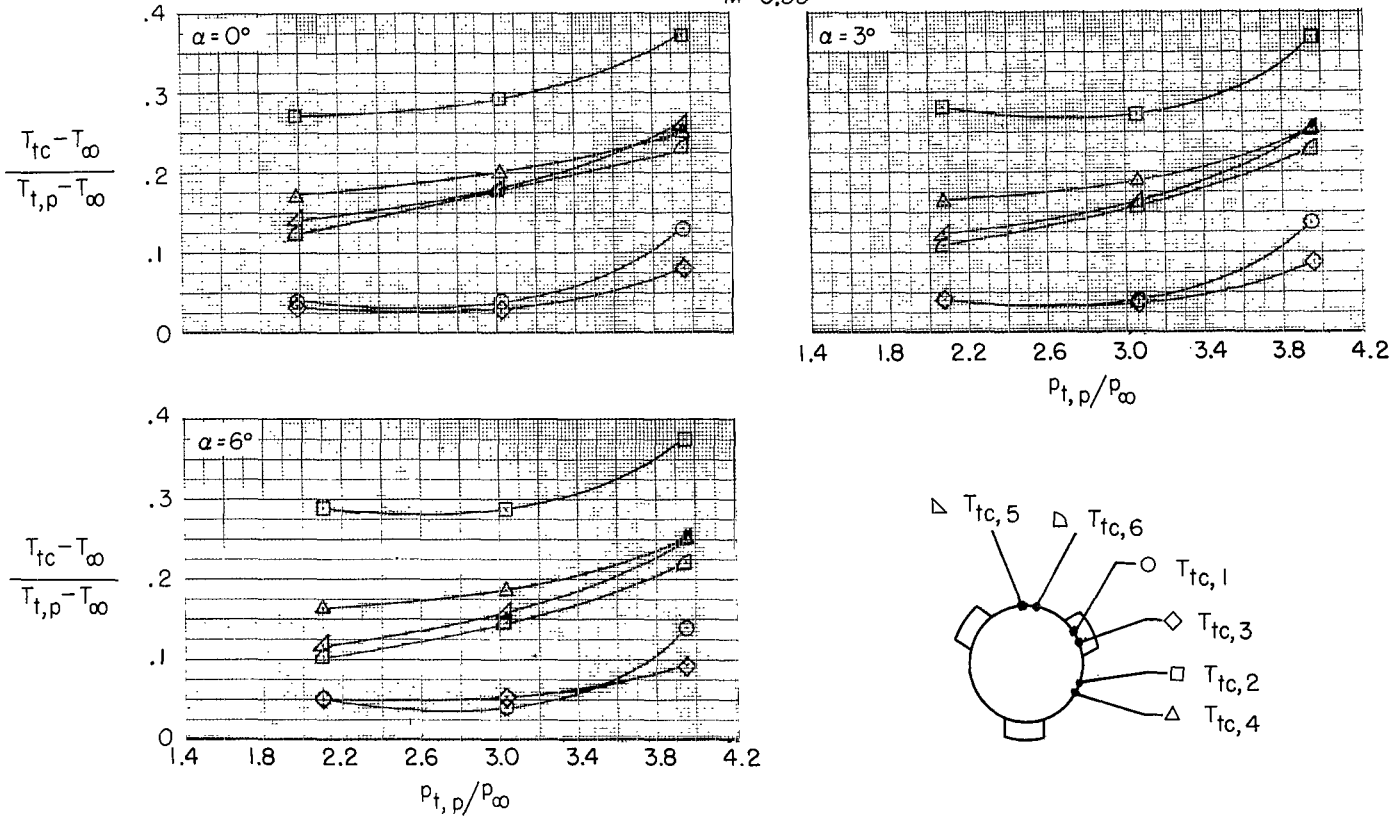


(b) $\delta_{du} = 32.5^{\circ}$; $\delta_{dl} = 52.5^{\circ}$; $\delta_b = 0\%$.

Figure 33.- Continued.

- $T_{tc,1}$ } Cooling-film temperature
- $T_{tc,2}$ }
- ◇ $T_{tc,3}$ } Skin temperature
- △ $T_{tc,4}$ }
- ▴ $T_{tc,5}$ }
- ◁ $T_{tc,6}$ }

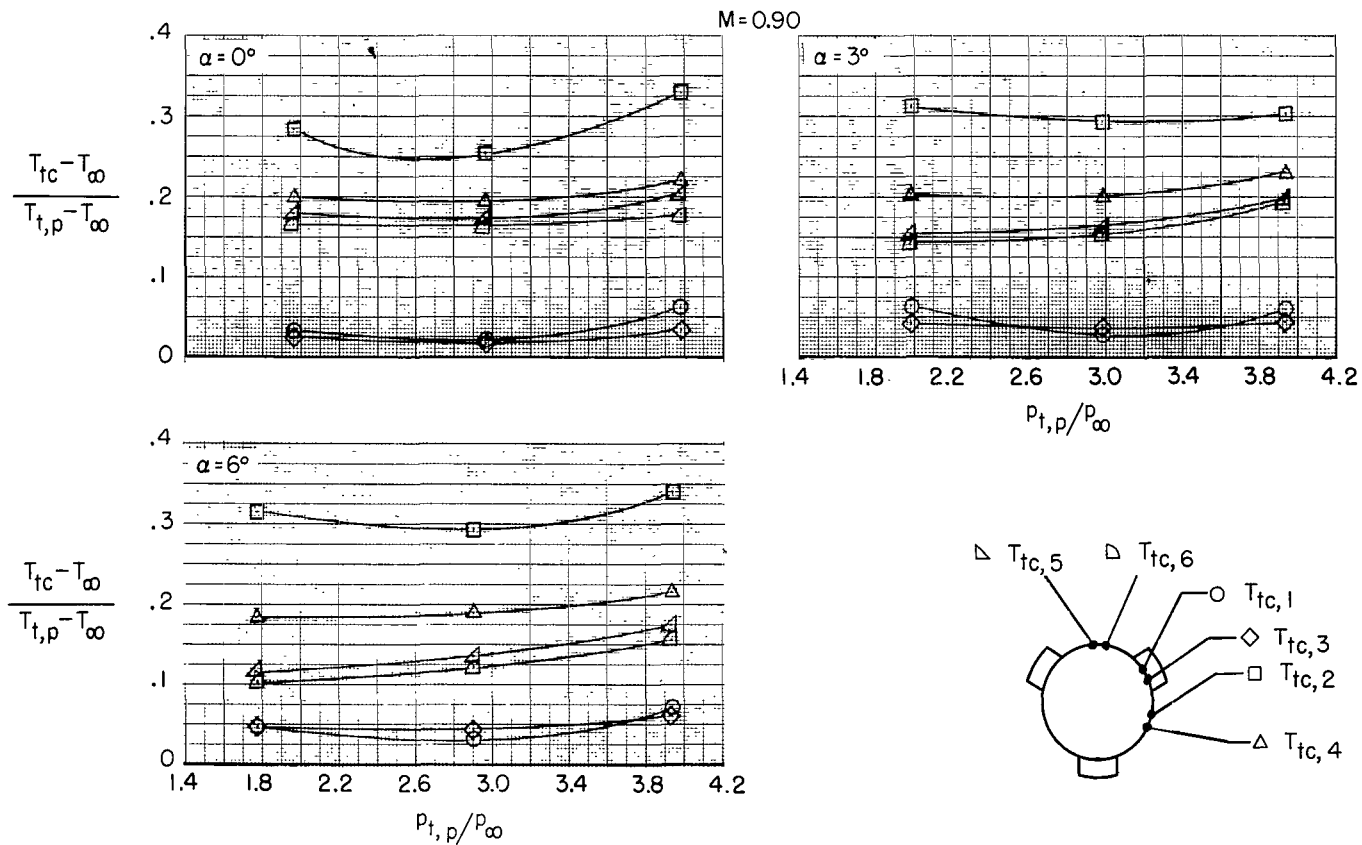
$M = 0.60$



(b) Continued.

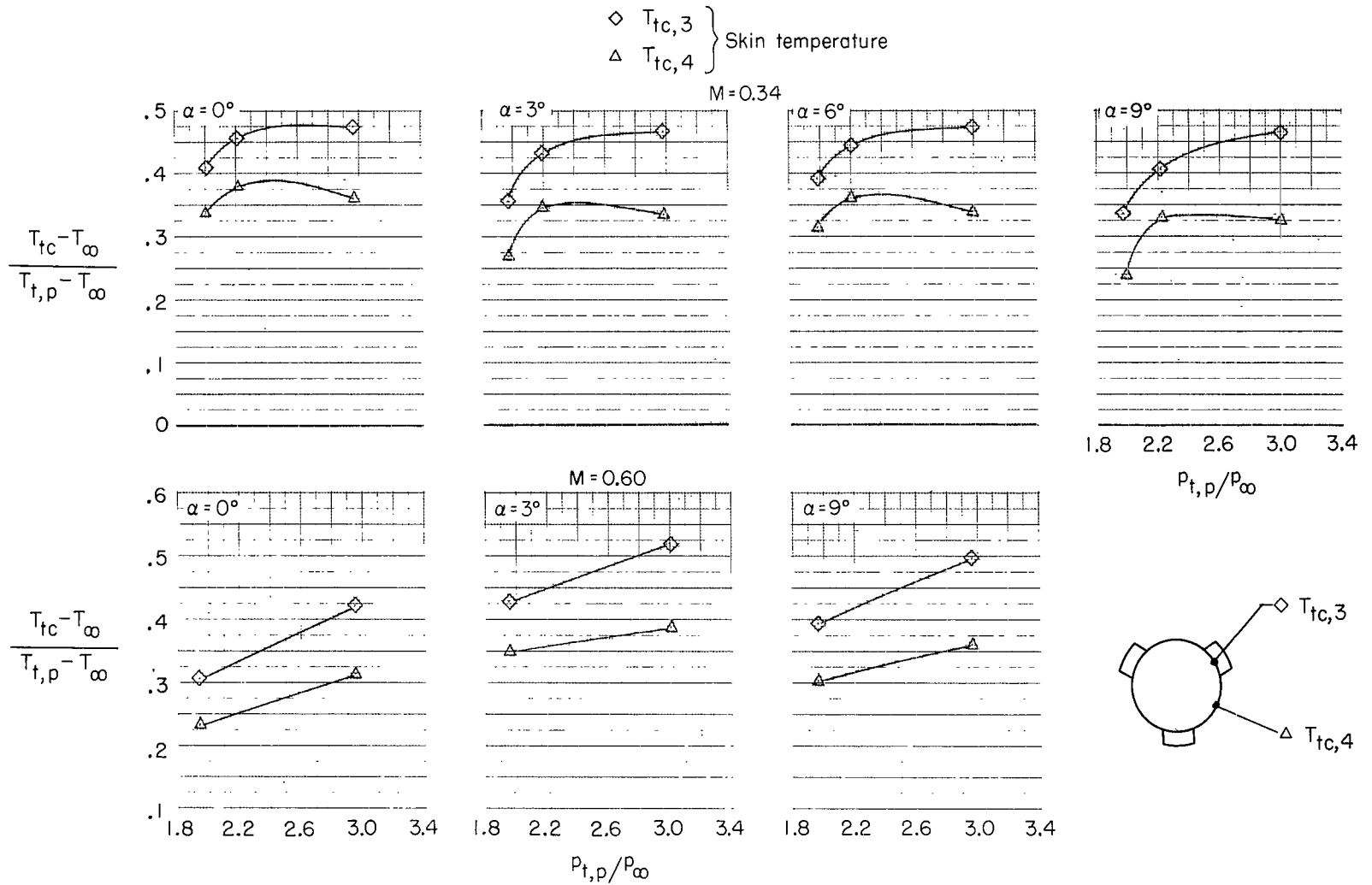
Figure 33.- Continued.

- $T_{tc,1}$
 - $T_{tc,2}$
 - ◇ $T_{tc,3}$
 - △ $T_{tc,4}$
 - ▽ $T_{tc,5}$
 - ◁ $T_{tc,6}$
- } Cooling-film temperature
- } Skin temperature



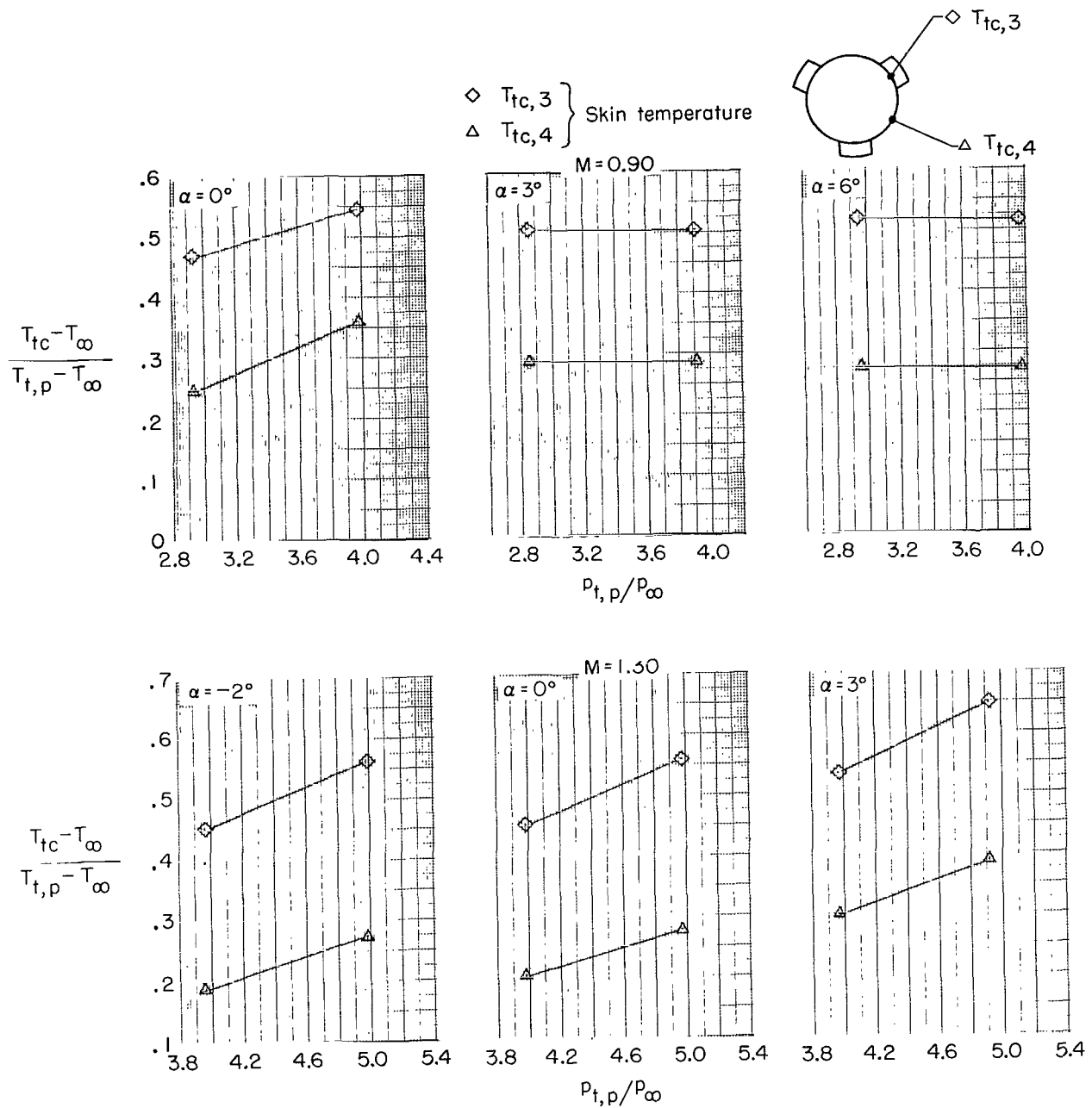
(b) Concluded.

Figure 33.- Continued.



(c) $\delta_{du} = 32.5^\circ$; $\delta_{dl} = 52.5^\circ$; $\delta_b = 100\%$.

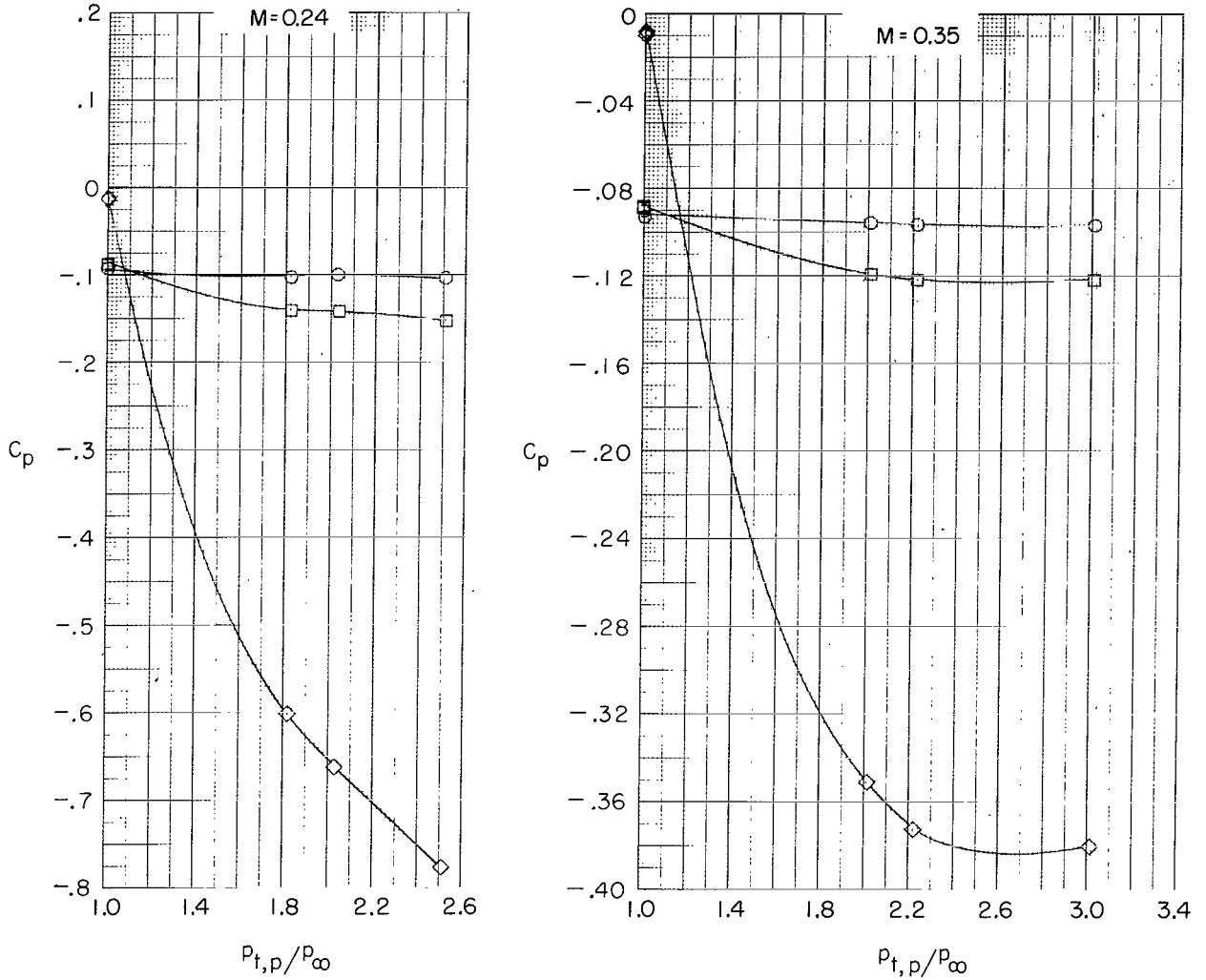
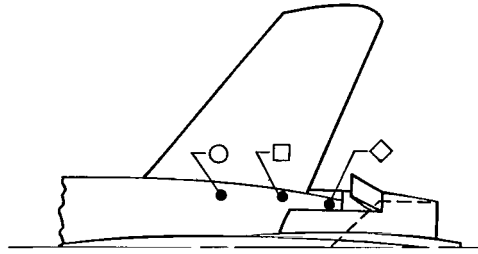
Figure 33.- Continued.



(c) Concluded.

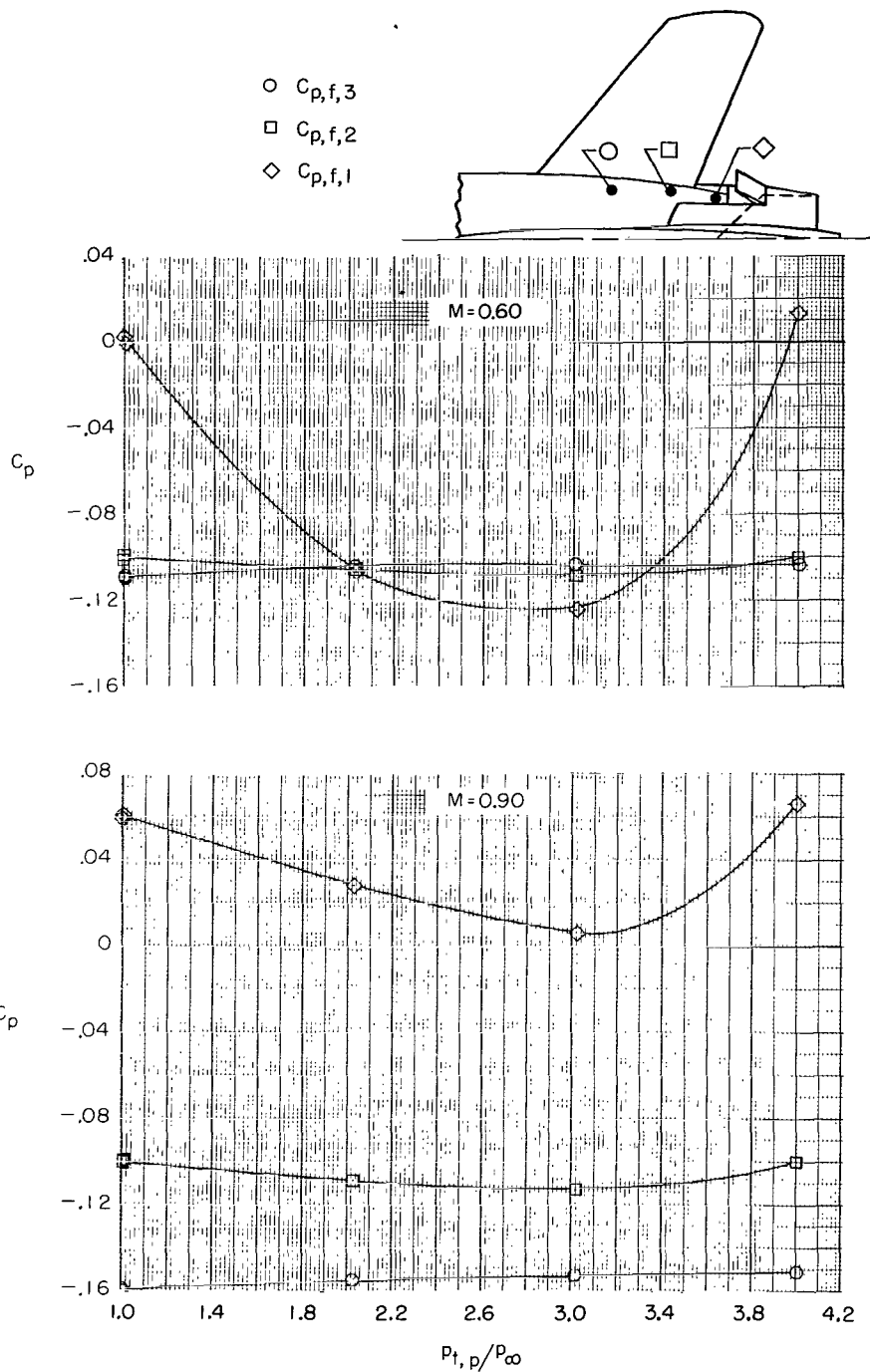
Figure 33.- Concluded.

- $C_{p,f,3}$
- $C_{p,f,2}$
- ◇ $C_{p,f,1}$



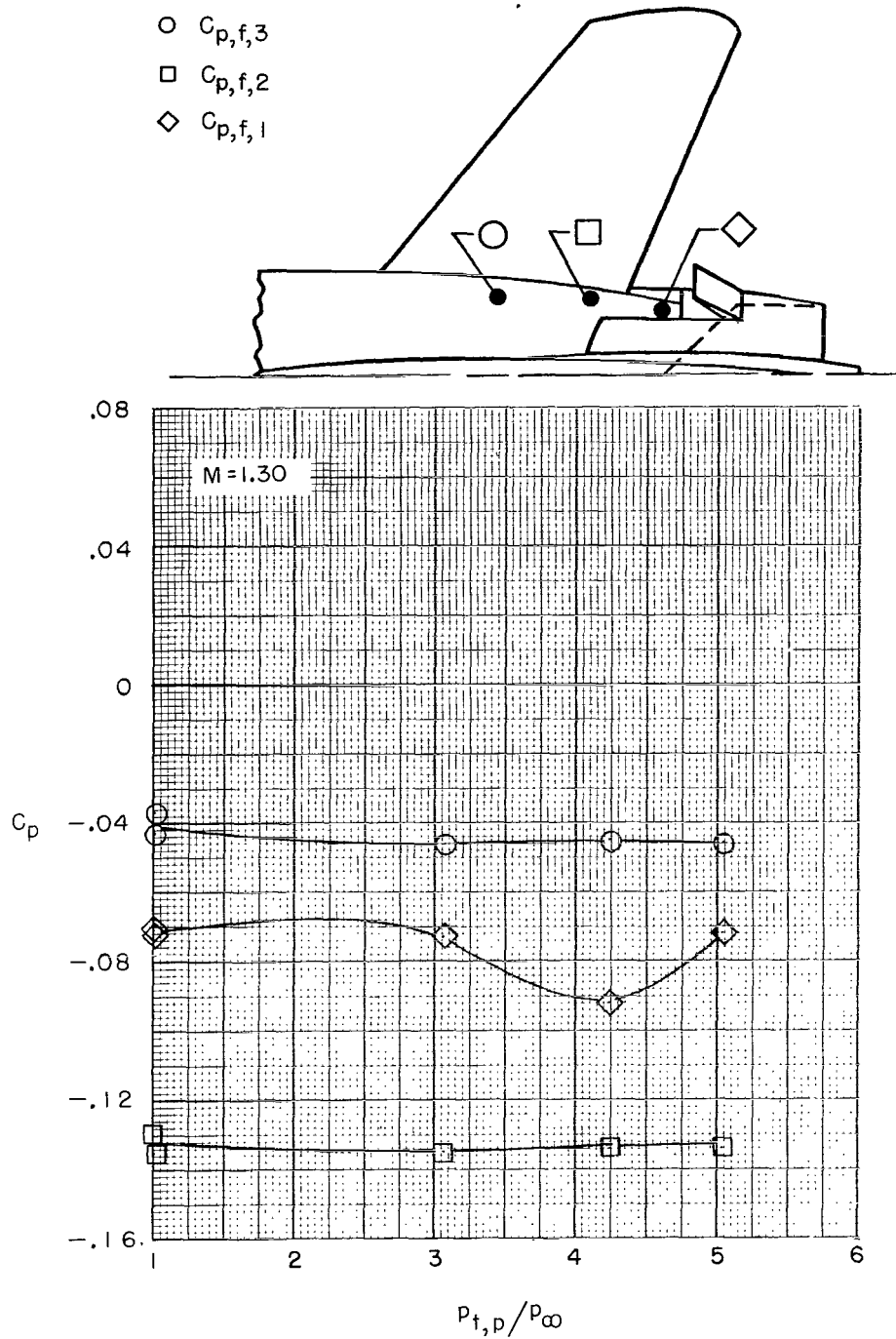
(a) $\delta_{du} = \text{Faired}$; $\delta_{dl} = \text{Faired}$; $\delta_b = 0\%$; military power.

Figure 34.- Variation of fuselage static-pressure coefficient with pressure ratio for several TCU configurations. $\alpha = 0^\circ$.



(a) Continued.

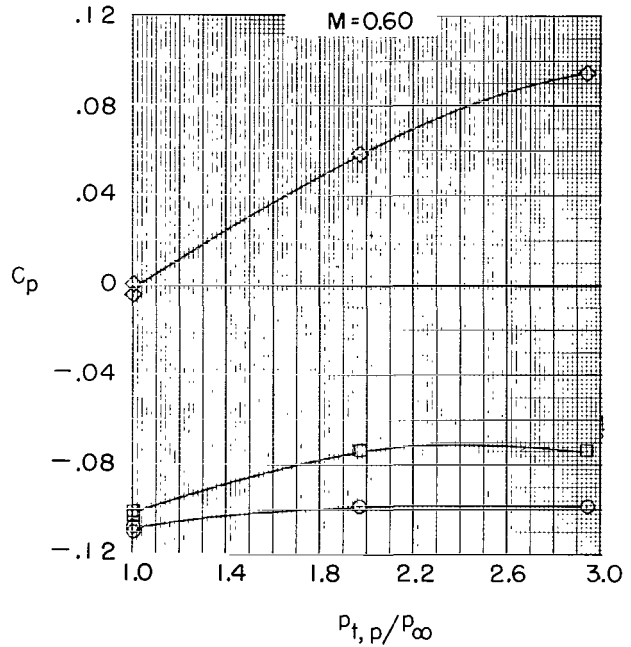
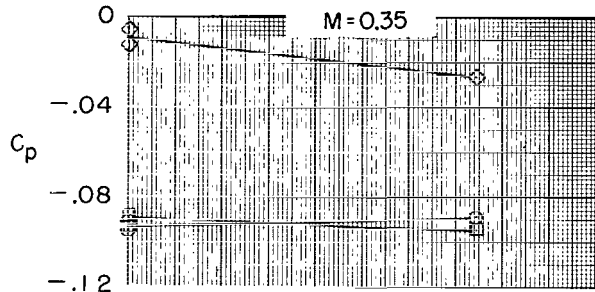
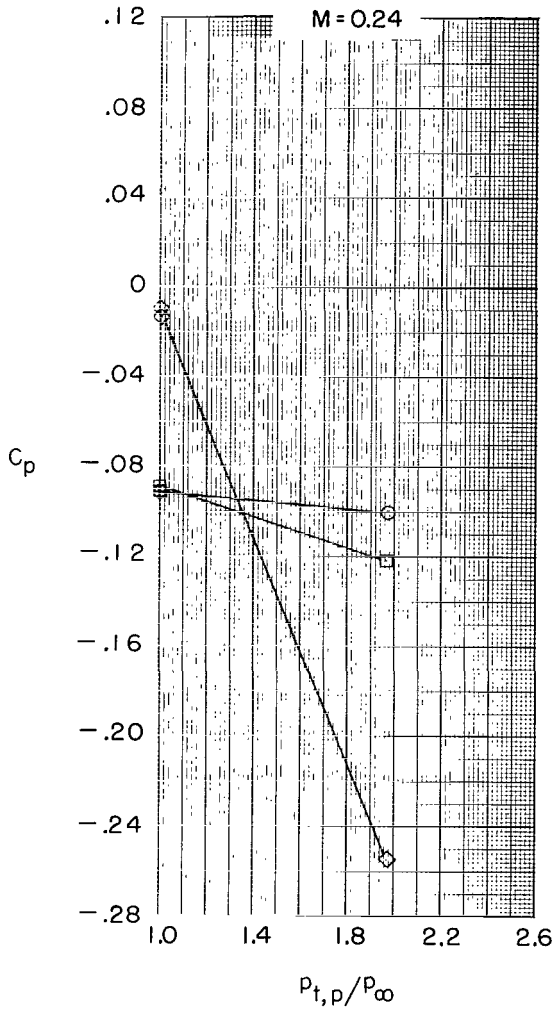
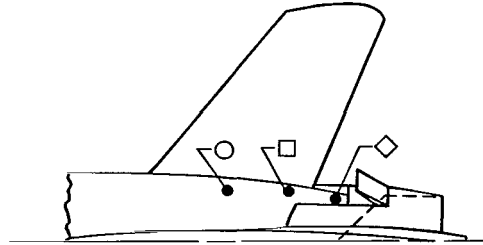
Figure 34.- Continued.



(a) Concluded.

Figure 34.- Continued.

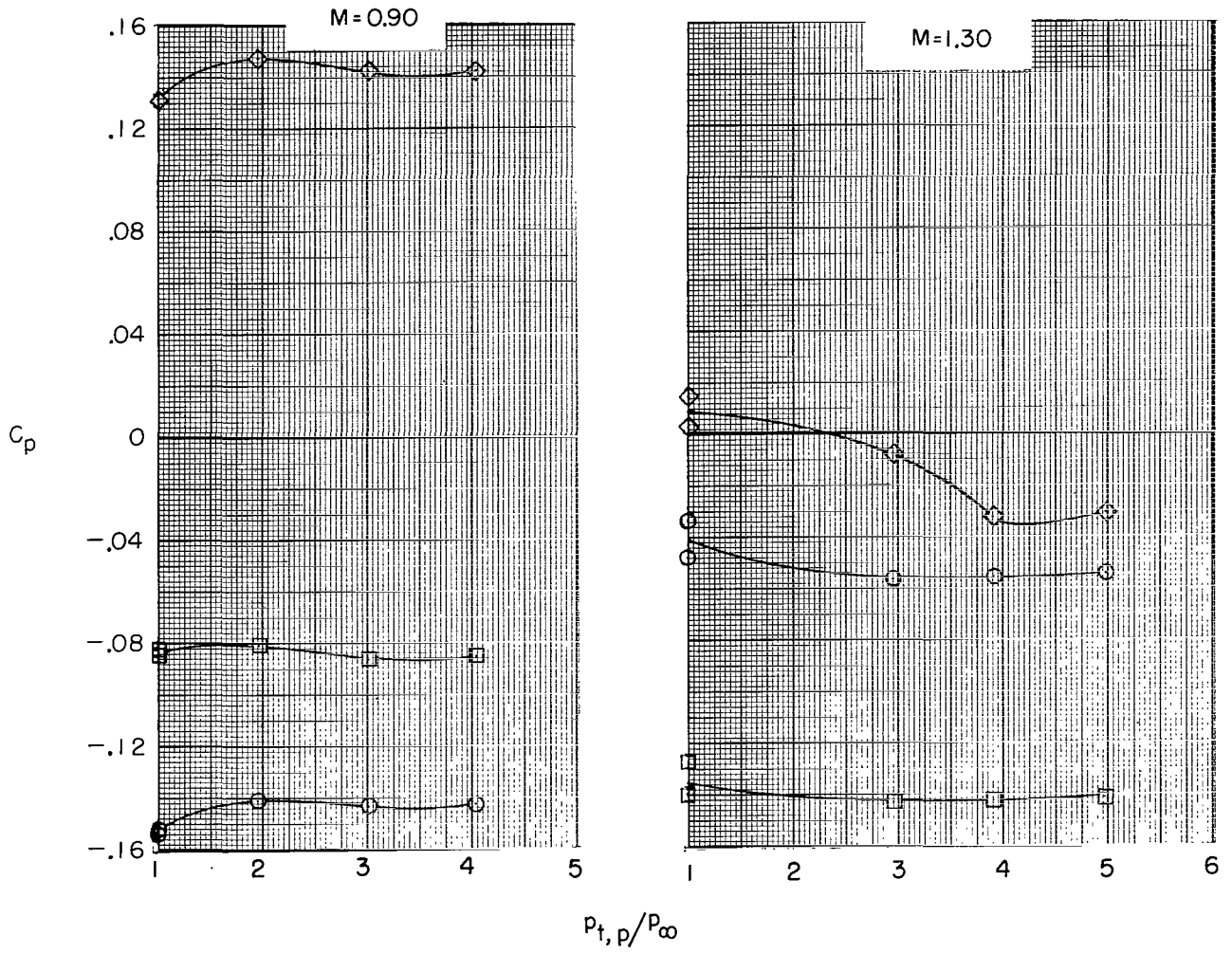
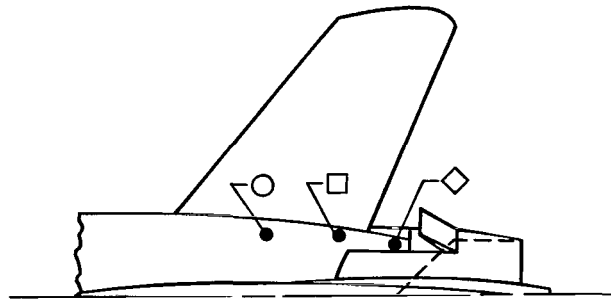
- $C_{p,f,3}$
- $C_{p,f,2}$
- ◇ $C_{p,f,1}$



(b) $\delta_{du} = \text{Faired}$; $\delta_{dl} = \text{Faired}$; $\delta_b = 0\%$; afterburning power.

Figure 34.- Continued.

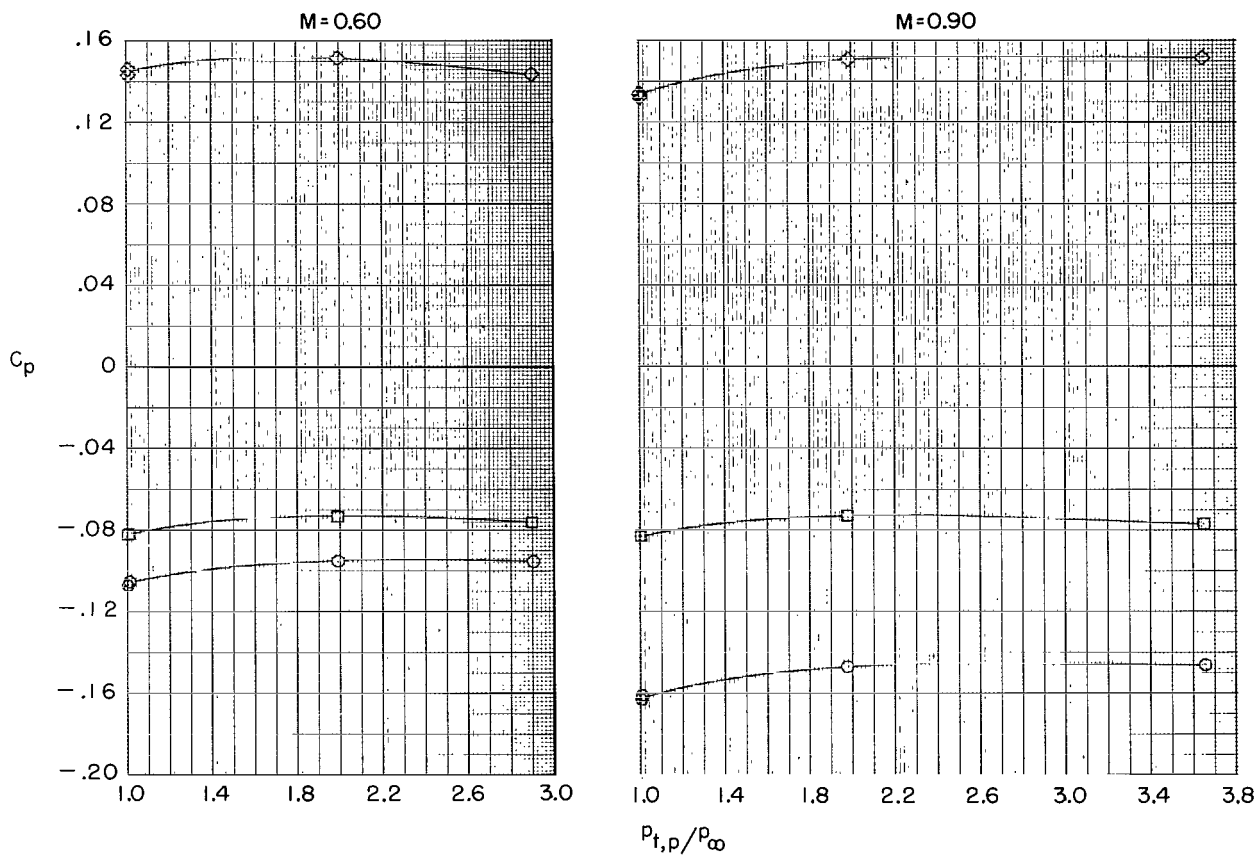
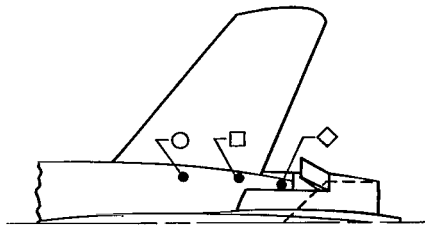
- $C_{p,f,3}$
- $C_{p,f,2}$
- ◇ $C_{p,f,1}$



(c) Concluded.

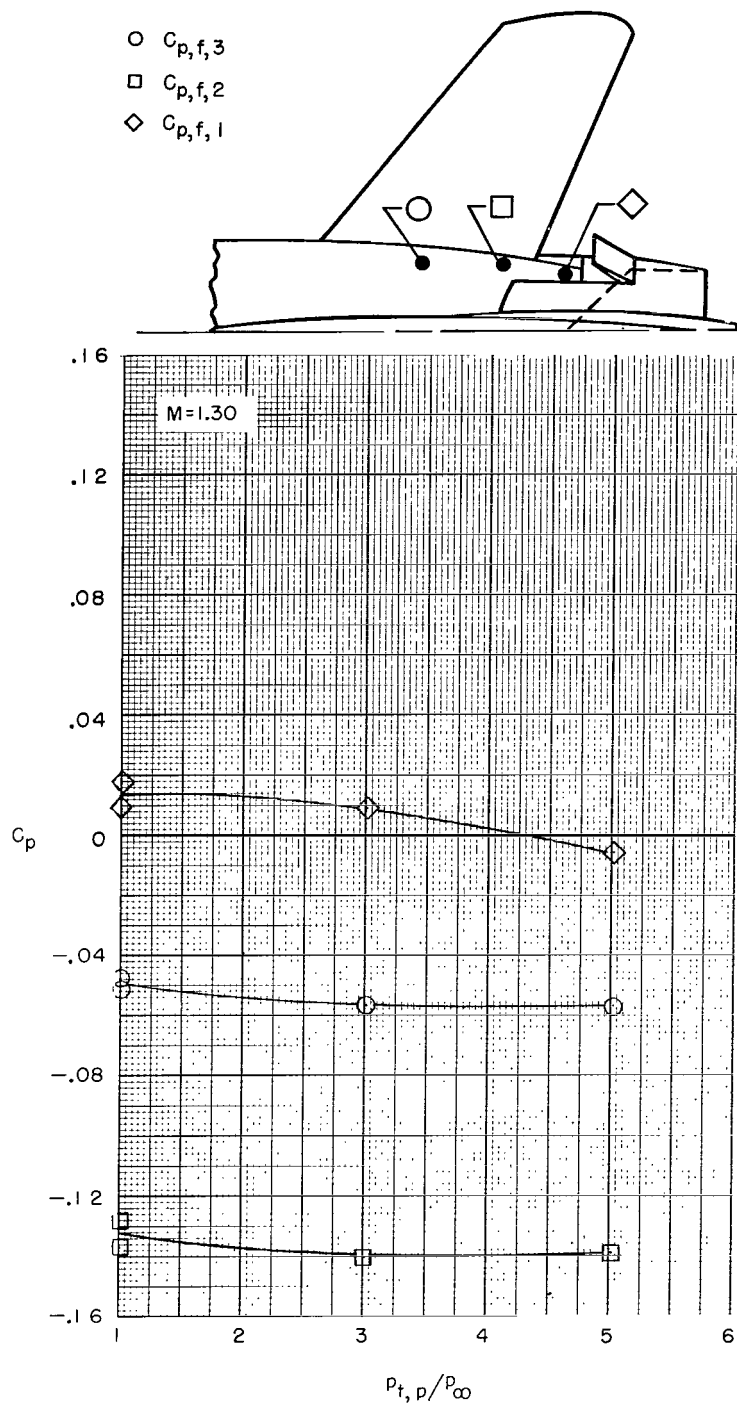
Figure 34.- Continued.

- $C_{p,f,3}$
- $C_{p,f,2}$
- ◇ $C_{p,f,1}$



(d) $\delta_{du} = \text{Closed}$; $\delta_{dl} = \text{Closed}$; $\delta_b = 0\%$; afterburning power.

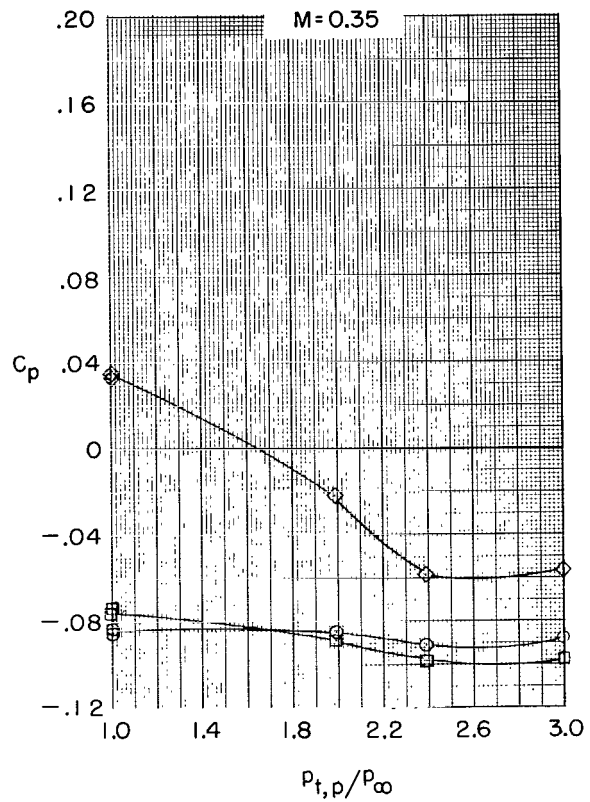
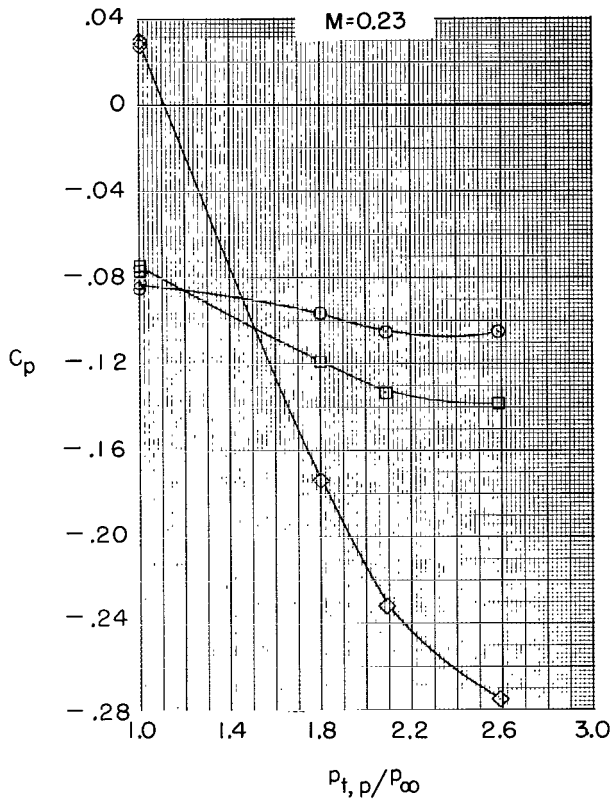
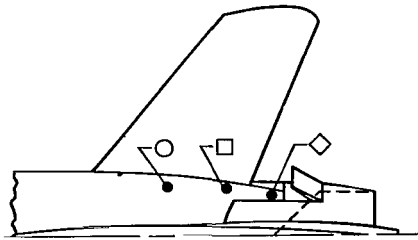
Figure 34.- Continued.



(d) Concluded.

Figure 34.- Continued.

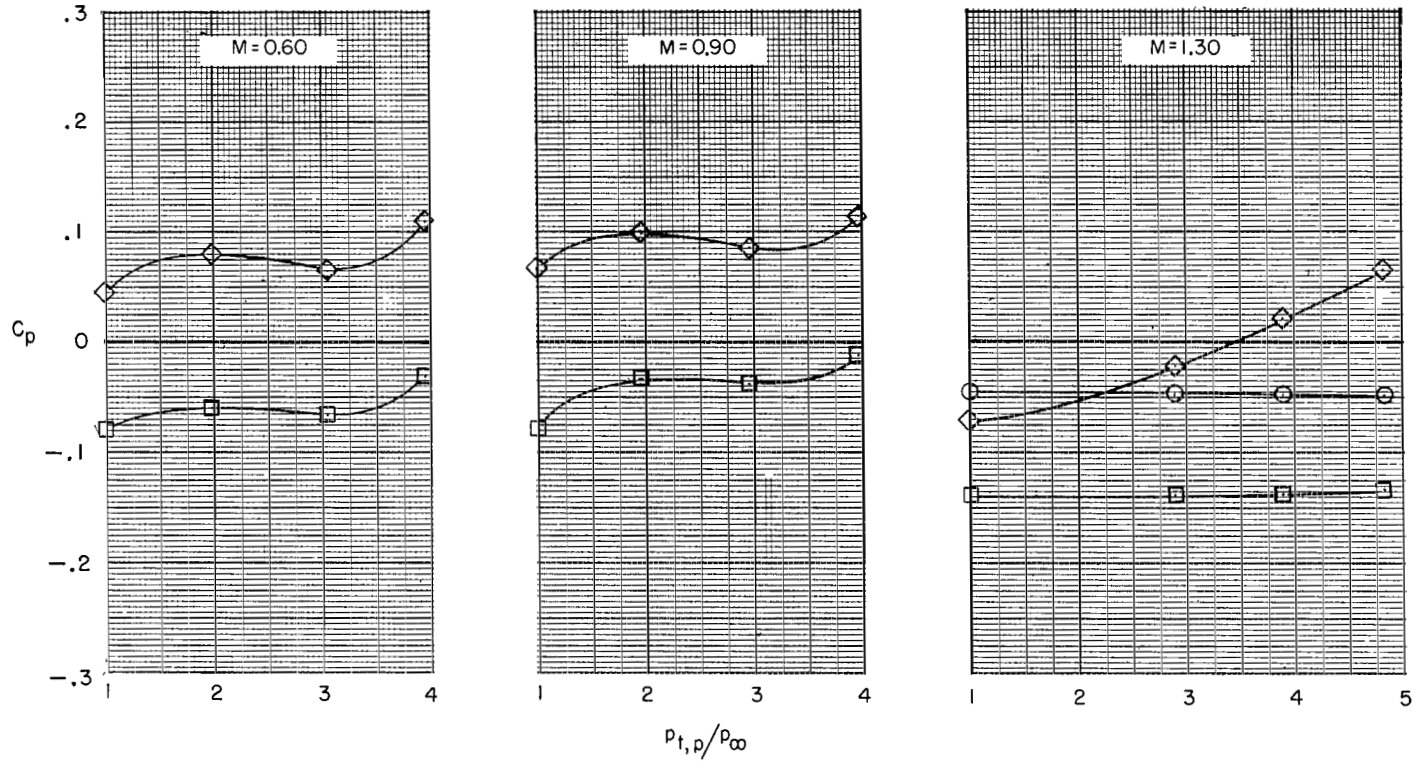
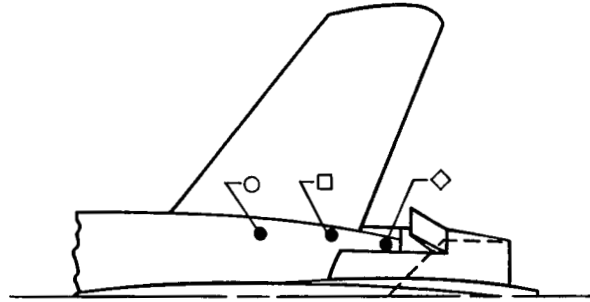
- $C_{p,f,3}$
- $C_{p,f,2}$
- ◇ $C_{p,f,1}$



(e) $\delta_{du} = 32.5^\circ$; $\delta_{dl} = 52.5^\circ$; $\delta_b = 0\%$; military power.

Figure 34.- Continued.

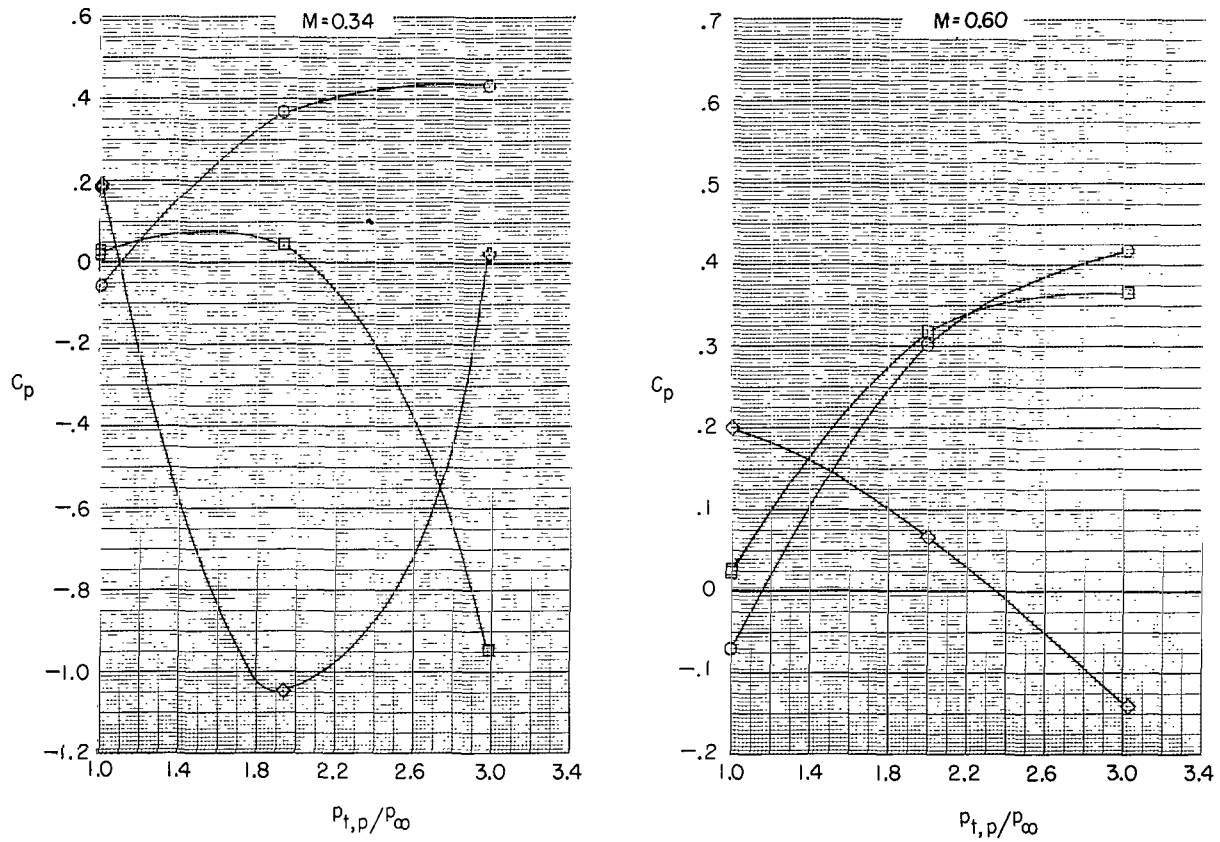
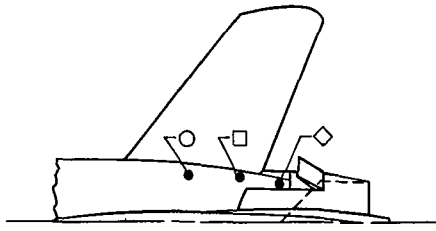
- $C_{p,f,3}$
- $C_{p,f,2}$
- ◇ $C_{p,f,1}$



(e) Concluded.

Figure 34.- Continued.

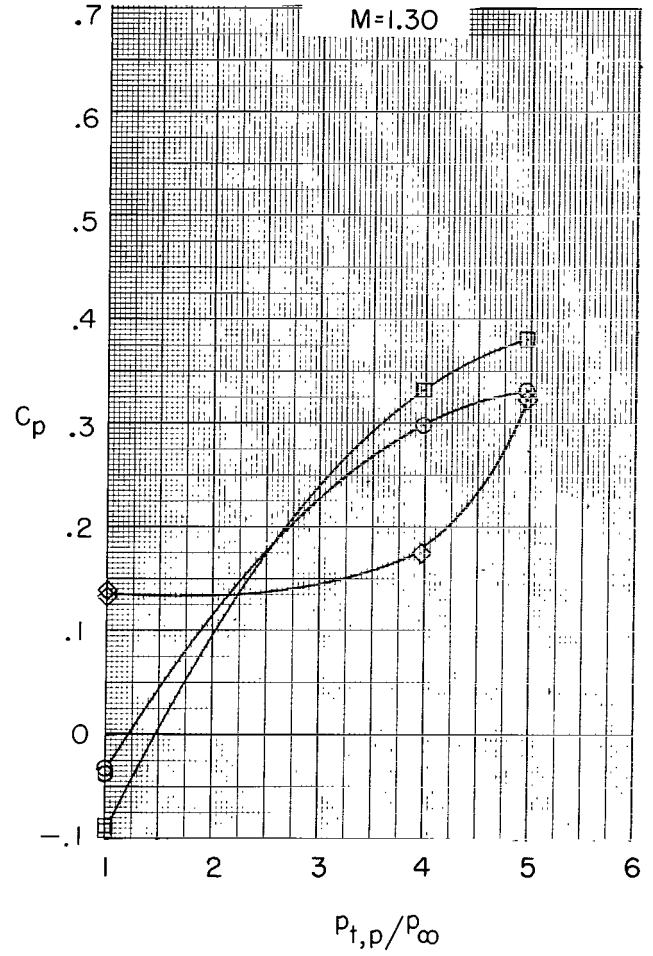
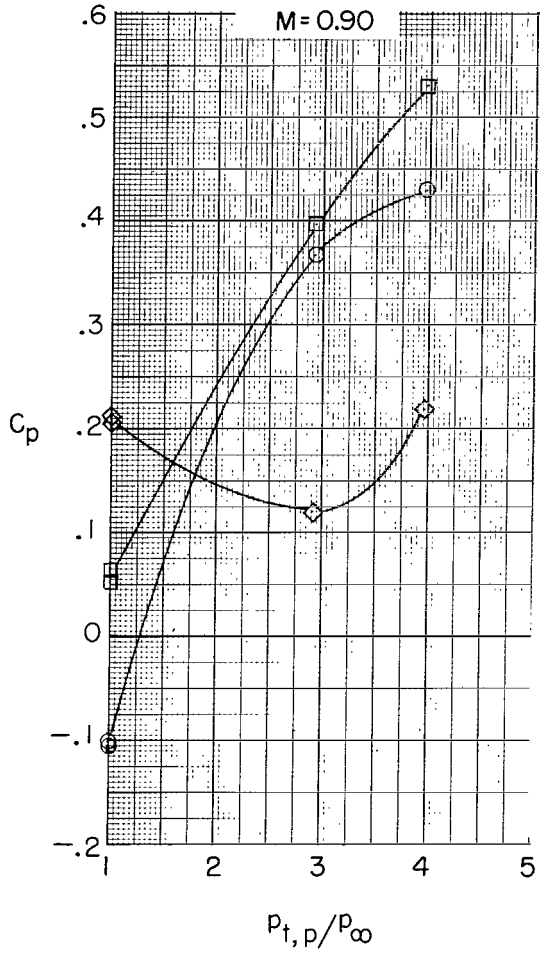
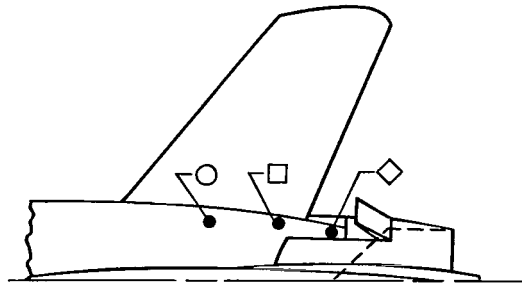
- $C_{p,f,3}$
- $C_{p,f,2}$
- ◇ $C_{p,f,1}$



(f) $\delta_{du} = 32.5^\circ$; $\delta_{dl} = 52.5^\circ$; $\delta_p = 100\%$; military power.

Figure 34.- Continued.

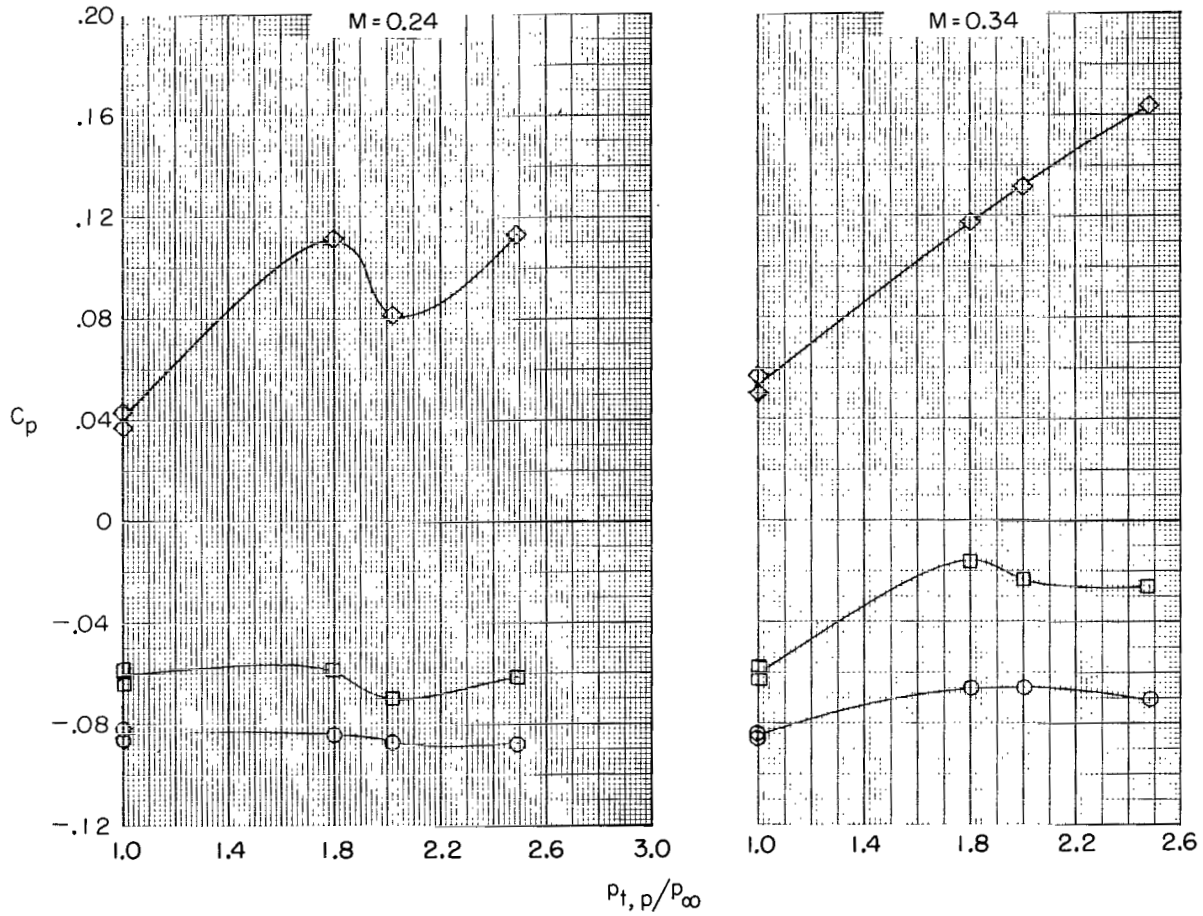
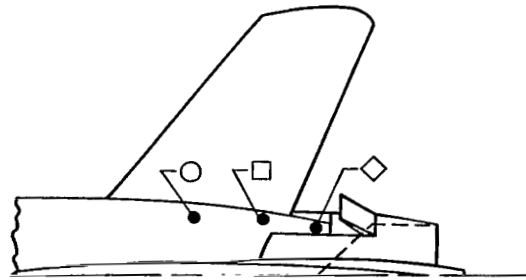
- $C_{p,f,3}$
- $C_{p,f,2}$
- ◇ $C_{p,f,1}$



(f) Concluded.

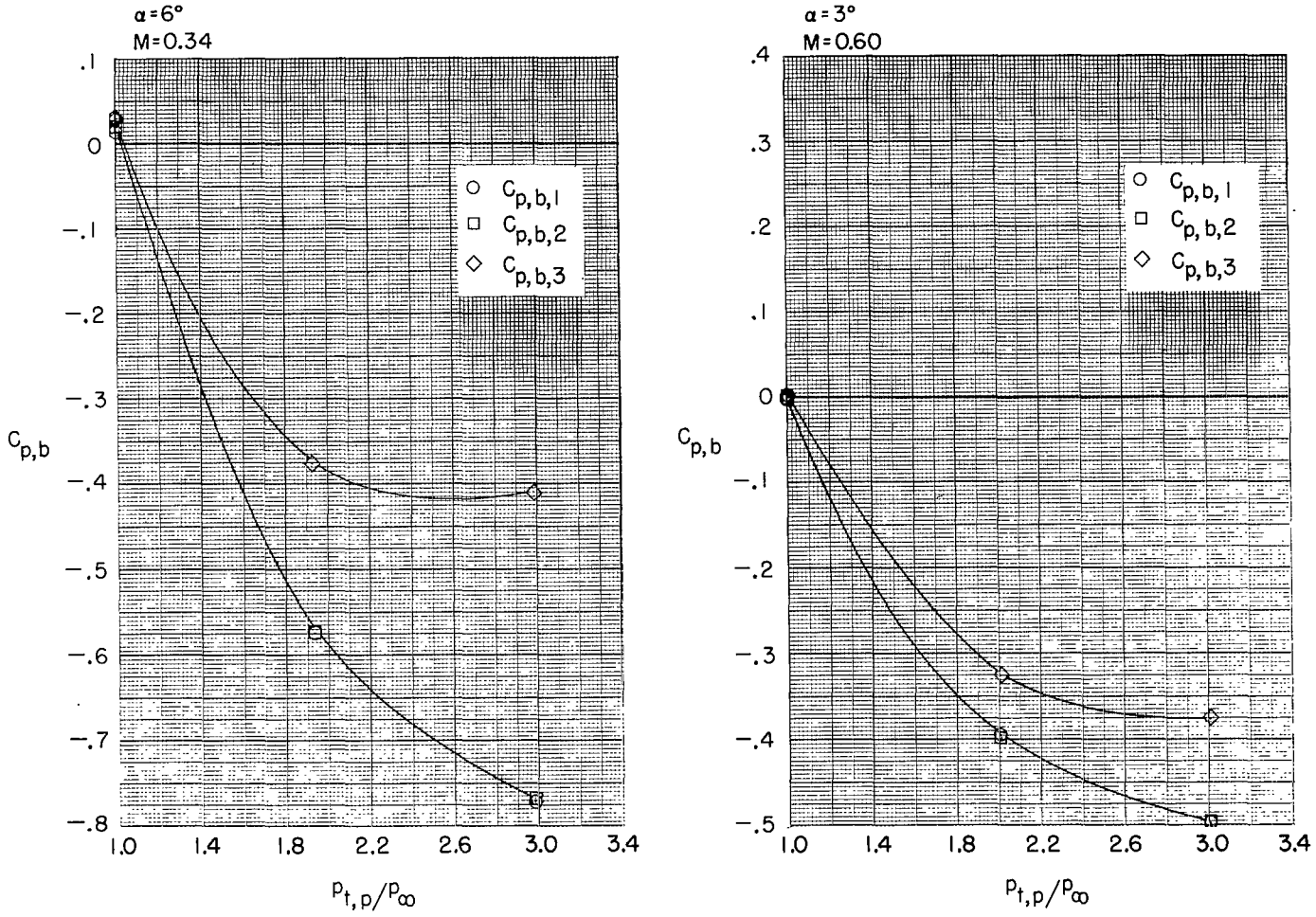
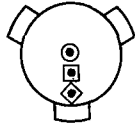
Figure 34.- Continued.

- $C_{p,f,3}$
- $C_{p,f,2}$
- ◇ $C_{p,f,1}$



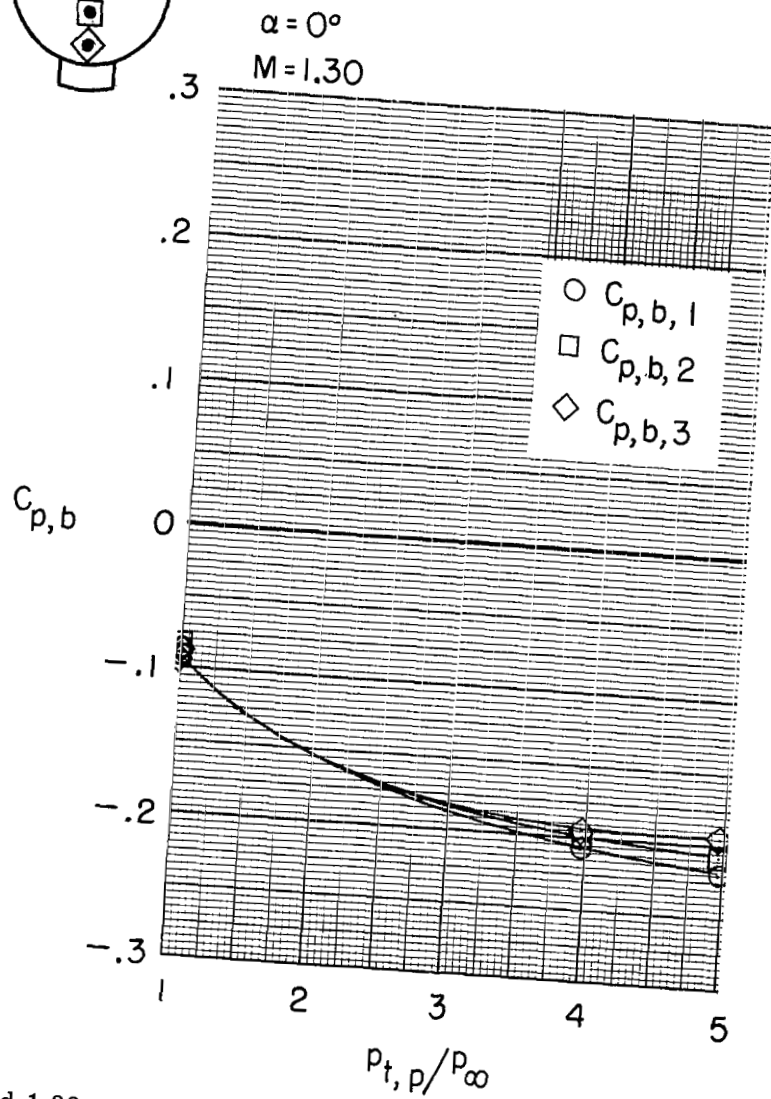
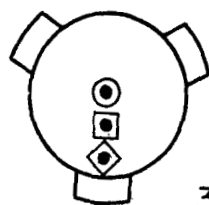
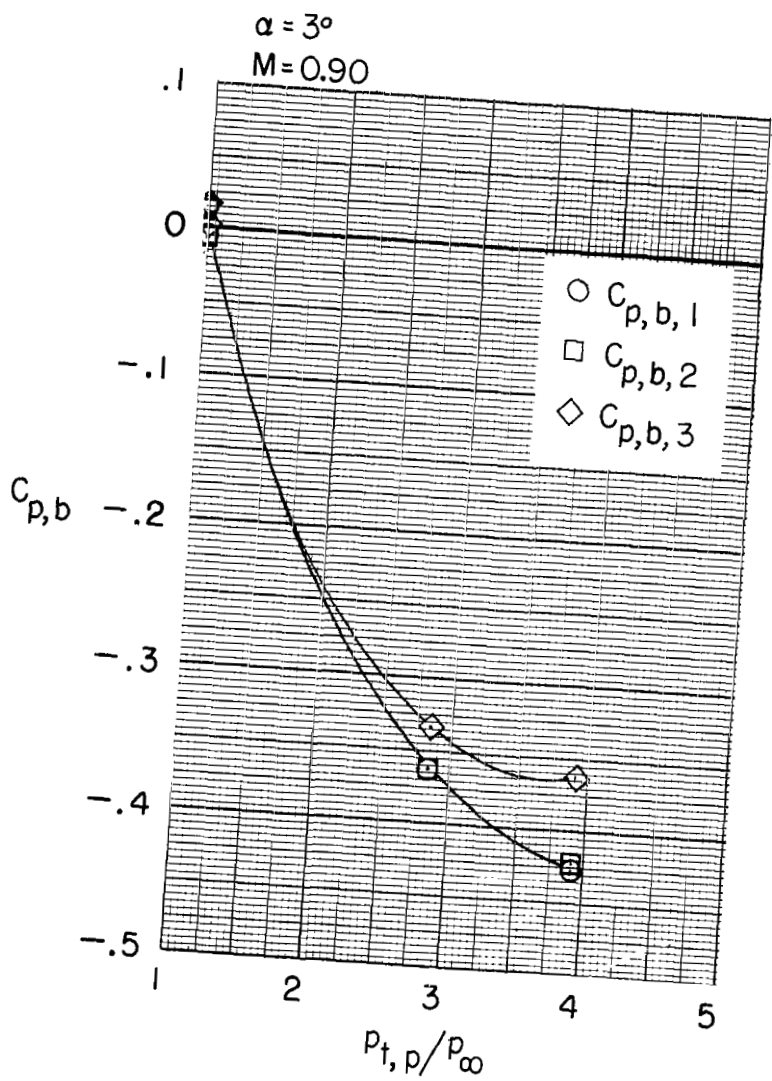
(g) $\delta_{du} = 43.5^\circ$; $\delta_{dl} = 43.5^\circ$; $\delta_b = 0\%$; afterburning power.

Figure 34.- Concluded.



(a) $M = 0.34$ and 0.60 .

Figure 35.- Variation of base pressure coefficient with primary-nozzle-jet total-pressure ratio.
 TCU; $\delta_{du} = 32.5^\circ$; $\delta_{dl} = 52.5^\circ$; $\delta_p = 100\%$; military power.



(b) $M = 0.90$ and 1.30 .

Figure 35.- Concluded.



013 001 C1 U 28 710902 S00903DS
DEPT OF THE AIR FORCE
AF SYSTEMS COMMAND
AF WEAPONS LAB (WLOL)
ATTN: E LOU BOWMAN, CHIEF TECH LIBRARY
KIRTLAND AFB NM 87117

POSTMASTER: If Undeliverable (Section 158
Postal Manual) Do Not Return

"The aeronautical and space activities of the United States shall be conducted so as to contribute . . . to the expansion of human knowledge of phenomena in the atmosphere and space. The Administration shall provide for the widest practicable and appropriate dissemination of information concerning its activities and the results thereof."

— NATIONAL AERONAUTICS AND SPACE ACT OF 1958

NASA SCIENTIFIC AND TECHNICAL PUBLICATIONS

TECHNICAL REPORTS: Scientific and technical information considered important, complete, and a lasting contribution to existing knowledge.

TECHNICAL NOTES: Information less broad in scope but nevertheless of importance as a contribution to existing knowledge.

TECHNICAL MEMORANDUMS: Information receiving limited distribution because of preliminary data, security classification, or other reasons.

CONTRACTOR REPORTS: Scientific and technical information generated under a NASA contract or grant and considered an important contribution to existing knowledge.

TECHNICAL TRANSLATIONS: Information published in a foreign language considered to merit NASA distribution in English.

SPECIAL PUBLICATIONS: Information derived from or of value to NASA activities. Publications include conference proceedings, monographs, data compilations, handbooks, sourcebooks, and special bibliographies.

TECHNOLOGY UTILIZATION PUBLICATIONS: Information on technology used by NASA that may be of particular interest in commercial and other non-aerospace applications. Publications include Tech Briefs, Technology Utilization Reports and Technology Surveys.

Details on the availability of these publications may be obtained from:

SCIENTIFIC AND TECHNICAL INFORMATION OFFICE

NATIONAL AERONAUTICS AND SPACE ADMINISTRATION
Washington, D.C. 20546